Published OnlineFirst March 13, 2017; DOI: 10.1158/1541-7786.MCR-16-0482

Signal Transduction

Molecular Cancer Research

Distinct Afatinib Resistance Mechanisms Identified in Lung Adenocarcinoma Harboring an EGFR Mutation

Toshimitsu Yamaoka[1], Tohru Ohmori[1], Motoi Ohba[1], Satoru Arata[1,2], Yasunori Murata[3], Sojiro Kusumoto[3], Koichi Ando[3], Hiroo Ishida[4], Tsukasa Ohnishi[3], and Yasutsuna Sasaki[4]

Abstract

EGFR tyrosine kinase inhibitors (TKI) are associated with significant responses in non–small cell lung cancer (NSCLC) patients harboring *EGFR*-activating mutations. However, acquired resistance to reversible EGFR-TKIs remains a major obstacle. In particular, although the second-generation irreversible EGFR-TKI afatinib is currently used for treating NSCLC patients, the mechanisms underlying acquired afatinib resistance remain poorly understood. Here, heterogeneous mechanisms of acquired resistance were identified following long-term exposure to increasing doses of afatinib in EGFR-mutant lung adenocarcinoma PC-9 cells. Notably, three resistant cell lines, PC-9AFR1, PC-9AFR2, and PC-9AFR3 (AFR1, AFR2, and AFR3, respectively) employed distinct mechanisms for avoiding EGFR inhibition, with increased *EGFR* expression being detected in all resistant cell lines. Moreover, an activating *EGFR* mutation was partially lost in AFR1 and AFR2 cells. AFR1 cells exhibited afatinib resistance as a result of wild-type KRAS amplification and overexpression; however, these cells showed a progressive decrease and eventual loss of the acquired KRAS dependence, as well as resensitization to afatinib, following a drug holiday. Meanwhile, AFR2 cells exhibited increased expression of insulin-like growth factor-binding protein 3 (IGFBP3), which promoted insulin-like growth factor 1 receptor (IGF1R) activity and subsequent AKT phosphorylation, thereby indicating a potential bypass signaling pathway associated with IGFR1. Finally, AFR3 cells harbored the secondary EGFR mutation T790M. Our findings constitute the first report showing acquired wild-type KRAS overexpression and attenuation of afatinib resistance following a drug holiday.

Implications: The heterogeneous mechanisms of afatinib resistance should facilitate the development of more effective therapeutic strategies for NSCLC patients. *Mol Cancer Res; 1–14. ©2017 AACR.*

Introduction

Administration of the EGFR tyrosine kinase inhibitors (TKI) gefitinib and erlotinib has been shown to result in dramatic tumor regression in non–small cell lung cancers (NSCLC) involving *EGFR*-activating mutations, including exon-19 deletions (dels) and the L858R point mutation (1). Notably, however, the tumors of many patients develop resistance to EGFR-TKIs within 9 to 15 months of treatment initiation (2, 3), and such acquired resistance constitutes a major difficulty in improving clinical outcomes. Intensive research has therefore focused on clarifying the mechanisms associated with acquired resistance to EGFR-targeted inhibitors (4, 5). The most common mechanism related to acquired resistance to first-generation EGFR-TKIs (i.e., the reversible ATP-competitive inhibitors gefitinib and erlotinib) involves the presence of the secondary mutation EGFR T790M, which was detected in >50% of tumors (6, 7). Other resistance mechanisms, including bypass signals to MET [also known as hepatocyte growth factor receptor (HGFR)], insulin-like growth factor 1 receptor (IGF1R), and HER2, transformation to SCLC, and induction of epithelial-to-mesenchymal transition (EMT), were reported in preclinical and clinical settings (8).

The second-generation EGFR-TKI afatinib is an irreversible drug that covalently binds to EGFR at Cys797 and was shown in preclinical studies to be more potent than first-generation EGFR-TKIs against all EGFR variants, including wild-type (WT), L858R, T790M, and those harboring exon-19 dels. In clinical studies on patients harboring *EGFR*-activating mutations (exon-19 del or L858R), afatinib was an effective first-line treatment and resulted in significantly prolonged survival rates compared with gefitinib treatment (9, 10). However, for patients with *EGFR*-mutant lung cancers that exhibit disease progression during treatment with gefitinib or erlotinib, the efficacy of treatment with afatinib was limited (11). Although the secondary EGFR

[1]Institute of Molecular Oncology, Showa University, Tokyo, Japan. [2]Center for Biotechnology, Showa University, Tokyo, Japan. [3]Division of Allergology and Respiratory Medicine, Department of Medicine, Showa University School of Medicine, Tokyo, Japan. [4]Division of Clinical Oncology, Department of Medicine, Showa University School of Medicine, Tokyo, Japan.

Note: Supplementary data for this article are available at Molecular Cancer Research Online (http://mcr.aacrjournals.org/).

Corresponding Author: Toshimitsu Yamaoka, Institute of Molecular Oncology, Showa University, 1-5-8 Hatanodai, Shinagawa-ku, Tokyo 142-8555, Japan. Phone: 81-33784-8146; Fax: 81-33784-2299; E-mail: yamaoka.t@med.showa-u.ac.jp

doi: 10.1158/1541-7786.MCR-16-0482

Published OnlineFirst March 13, 2017; DOI: 10.1158/1541-7786.MCR-16-0482

mutation T790M was frequently observed following the development of resistance to afatinib in clinical samples, other resistance mechanisms have yet to be fully confirmed (12, 13).

The emergence of acquired resistance remains a significant obstacle for afatinib-treated patients. *In vitro*, FGFR1 activation via a ligand of the FGF2-autocrine loop was reported as a bypass signal in the human lung cancer cell line PC-9, indicating that treatment with a combination of afatinib and an FGFR inhibitor resulted in drug resensitization (14). In addition, PC-9 cells that are resistant to dacomitinib (another irreversible EGFR-TKI) maintain PI3K/AKT signaling through activation of insulin-like growth factor 1 receptor (IGF1R) signaling, as mediated by downregulation of insulin-like growth factor-binding protein 3 (IGFBP3; ref. 15). Moreover, Eberlein and colleagues observed that PC-9 cells exhibit amplified KRAS or NRAS expression, resulting in afatinib resistance (16). These PC-9AR_1 cells subsequently exhibited significant decreases in ERK1/2 phosphorylation and cell proliferation following KRAS knockdown. However, the mechanisms associated with the development of acquired resistance to irreversible EGFR-TKIs remain uncharacterized.

Clinical reports suggest that retained sensitivity occurs upon gefitinib or erlotinib re-administration following disease progression (17, 18), and several studies have indicated that re-treatment with the EGFR-TKIs gefitinib or erlotinib might be effective following a drug holiday in certain patients (19, 20). Although the definitive rationale for the re-challenge of EGFR-TKIs remains unclear, it may constitute a promising therapeutic approach in NSCLC, particularly as subsequent lines of therapy remain undefined.

Here, we established three cell lines, PC-9AFR1, PC-9AFR2, and PC-9AFR3 (designated AFR1, AFR2, and AFR3, respectively), exhibiting resistance to long-term treatment with afatinib. Notably, although each of these cell lines displayed enhanced EGFR expression, this effect was mediated via three distinct mechanisms. Together, these results provide insight into the pharmacological basis underlying requirements for alternative treatment strategies.

Materials and Methods

Cell lines, antibodies, and reagents

The PC-9 human NSCLC cell line established from a previously untreated patient was donated by K. Hayata (Tokyo Medical College, Tokyo, Japan) during the 1980s and was cultured in RPMI1640 medium supplemented with 10% FBS, penicillin (100 U/mL), and streptomycin (100 μg/mL) in a 5% CO_2 incubator at 37°C. Cells were passaged for <4 months prior to renewal from the frozen stock. Cell lines used in this study were authenticated by short tandem-repeat analysis at the Japanese Collection of Research Bioresources cell bank in 2013. The following antibodies were purchased from Cell Signaling Technology: total EGFR antibody (#4267), phospho-EGFR (Y1068) antibody (#3777), EGFR (E746-A750del) antibody (#2085), total HER2 antibody (#4290), total ERBB3 antibody (#4754), total ERBB4 antibody (#4795), total IGF1R antibody (#3018), phospho-IGF1R antibody (#3024), total MET antibody (#8198), phospho-MET (Y1234/1235) antibody (#3077), total AKT antibody (#9272), phospho-AKT (S473) antibody (#9271), total ERK1/2 antibody (#9102), phospho-ERK1/2 antibody (#4370), phospho-MEK1/2 antibody (#2338), cleaved PARP antibody (#5625), β-actin antibody (#4970), and anti-rabbit IgG HRP-linked antibody (#7074). Meanwhile, antibodies specific to KRAS (sc-30), HRAS (sc-29), and NRAS (sc-31) were purchased from Santa Cruz Biotechnology. Gefitinib and afatinib were provided by AstraZeneca Pharmaceuticals and Boehringer-Ingelheim, respectively, and other inhibitors were obtained from Selleck Chemicals.

Establishment of PC-9 cells with acquired resistance to afatinib

To obtain cell lines with acquired resistance, PC-9 cells were exposed to increasing concentrations of afatinib in the growth medium. Starting with a dose that was nearly one tenth of the IC_{50}, the dosage was progressively increased over 6 to 9 months to 1 μmol/L afatinib. The three resulting PC-9 afatinib-resistant cell lines were designated AFR1, AFR2, and AFR3, and were maintained continuously in culture medium containing 1 μmol/L afatinib.

Cell proliferation assay

Cell proliferation was measured using the MTT assay (Promega), as previously described (21). Briefly, cells (5×10^2/well) were seeded in 96-well plates and incubated overnight, and assays were performed on days 0, 1, 2, 3, 5, and 7. To inhibit cell proliferation, 5×10^3 cells/well were seeded in 96-well plates and incubated overnight, followed by continuous exposure to the indicated concentrations of inhibitor for 72 hours. The optical density at 570 nm (OD_{570}) was then measured with a Powerscan HT microplate reader (BioTek) and expressed as a percentage of the value obtained from the control cells. We prepared 6 to 12 replicates, and the experiments were repeated at least three times. Data were graphically displayed using GraphPad Prism version 5.0 software (GraphPad, Inc.).

Western blot analysis

Treated cells were washed twice with ice-cold PBS and lysed with modified RIPA buffer consisting of 50 mmol/L Tris (pH 7.4), 150 mmol/L NaCl, 1 mmol/L EDTA, 1% Nonidet P-40, 0.25% sodium deoxycholate, 0.1% SDS, and 1.0% protease- and phosphatase-inhibitor cocktails (Sigma-Aldrich). Cell suspensions were centrifuged for 5 minutes at 1,200 rpm at 4°C, and protein concentrations were determined using the bicinchoninic acid assay (Sigma-Aldrich). Equal amounts of protein were mixed and boiled in Laemmli buffer, and samples were separated by 8% to 12% SDS-PAGE and transferred to polyvinylidene difluoride (PVDF) membranes. Membranes were probed using the appropriate primary and secondary antibodies (diluted according to the manufacturers' instructions, 1:1,000–2,000), and were subsequently treated with enhanced chemiluminescence solution and exposed to film. β-Actin and at least one additional protein were used as loading controls. All experiments were performed in triplicate.

RAS pull-down assay

Pull-down assays were performed using a glutathione S-transferase fusion protein corresponding to the human RAS-binding domain of RAF-1, which specifically binds to the GTP-bound form of RAS (EMD Millipore). Western blots were developed using an anti-KRAS antibody (F234; Santa Cruz Biotechnology).

RNA interference

Nontargeting (N/T) siRNA (controls) and SMARTpool siRNAs targeting EGFR (M003114), IGF1R (M003012), KRAS

Published OnlineFirst March 13, 2017; DOI: 10.1158/1541-7786.MCR-16-0482

(M005069), and IGFBP3 (M004777) respectively, were purchased from Dharmacon. Cells were seeded in 6-well plates in RPMI1640 medium supplemented with 10% FBS but no antibiotics. The following day, cells were transfected with 100 pmol/well siRNA using Lipofectamine 2000 reagent (Life Technologies), according to the manufacturer's instructions, and were analyzed at 72-hour posttransfection.

Real-time RT-PCR

Total RNA was isolated from cells using an RNeasy Mini kit (Qiagen) according to the manufacturer's instructions. cDNA was then synthesized from each isolated RNA sample using random 6-mers and an RT-PCR Kit (Takara Bio). Meanwhile, genomic DNA (gDNA) was extracted from cells using a QIAamp DNA Mini Kit (Qiagen). cDNA and genomic DNA samples were amplified and analyzed using Power SYBR Green PCR master mix (Applied Biosystems) and a fluorescence-based RT-PCR-detection system (GeneAmp 5700; Applied Biosystems). Specific primer sets are shown in Supplementary Table S1.

EGFR- and *KRAS*-sequence analysis

Exons 19 to 21 of the *EGFR* gene and exons 2 to 4 of the *KRAS* gene were amplified from genomic DNA via PCR. Products were purified and sequenced by FASMAC. The primers used for PCR and sequencing analysis are shown in Supplementary Table S1.

PCR analysis of *EGFR* exon 19

To analyze WT *EGFR* and the 15-bp deletion mutation in exon 19, the *EGFR* gene was amplified using the following PCR primers: WT, 5′-CCGTCGCTATCAAGGAATTAAG-3′; mutant, 5′-TCCCGTCGCTATCAAAACATC-3′; both WT and mutant, 5′-ATGTGGCACCATCTCACAATTGCC-3′; reverse primer 5′-CCACACAGCAAAGCAGAAACTCAC-3′. Amplification was performed using TaKaRa ExTaq polymerase (22).

EGFR allele quantification by digital PCR analysis

Droplet digital PCR was performed using an LBx Probe for the *EGFR* exon-19 del or T790M mutation, and samples were quantified using a QX200 droplet reader (Bio-Rad Laboratories). Distribution of the WT, exon-19 del, and/or T790M alleles was determined by Riken Genesis.

Xenograft mouse studies

A suspension of 5×10^6 cells was injected subcutaneously into the flanks of 6- to-8-week-old female SCID mice. The care and treatment of experimental animals were in accordance with institutional guidelines. Mice were randomized ($n = 5$) once the mean tumor volume reached ∼230 to 300 mm^3. Drugs were administered once daily by oral gavage. Afatinib (6 mg/kg) was suspended in 0.5% 2-hydroxyethyl cellulose/H_2O. Tumors were measured twice weekly using calipers, and tumor volume was calculated using the following formula: length × length × width × 0.5. According to institutional guidelines, mice were sacrificed when their tumor volume reached 2,000 mm^3.

Statistical analysis

Data are presented as means ± SEM and were analyzed using GraphPad Prism version 5.0 software (GraphPad, Inc.). Statistical significance was evaluated by two-tailed Student *t* test and, unless otherwise noted, $P < 0.05$ was considered statistically significant.

Results

Characteristics of PC-9–derived cell lines with acquired resistance to the irreversible EGFR-TKI afatinib

We established three afatinib-resistant PC-9 cell lines via dose escalation of afatinib (up to 1 μmol/L) over 6 to 9 months (Fig. 1A). Notably, unlike the parental PC-9 cells, none of the three cell lines exhibited inhibition of cell proliferation following afatinib treatment, as determined by MTT assay (Fig. 1B). However, the proliferation rates of the three cell lines were slower than that observed in parental PC-9 cells (Fig. 1C). Moreover, the afatinib-resistant cell lines exhibited increased EGFR gene copy numbers and protein expression, compared with the parental control cells (Fig. 1D and E).

Allelic distribution analyses using WT and mutant (E746–A750del) allele-specific PCR primers (22) detected a higher proportion of mutant *EGFR* alleles than WT alleles in parental PC-9 cells; a similar ratio was also observed in AFR3 cells. Conversely, AFR1 and AFR2 cells exhibited significantly higher proportions of WT *EGFR* alleles, compared with the parental PC-9 cells (Fig. 1F). Moreover, subsequent digital PCR analysis for quantification of these distribution data detected significant decreases in both the number of mutant *EGFR* alleles and their corresponding protein expression levels in AFR1 and AFR2, compared with those observed in parental PC-9 cells (Fig. 1E and G).

To determine the homoduplex (WT/WT or mutant/mutant) or heteroduplex (WT/mutant) status of *EGFR* exon 19, this region was amplified using specific primers. Notably, AFR1 and AFR2 primarily harbored WT/WT homoduplexes in the *EGFR* gene, whereas PC-9 and AFR3 cells contained both mutant/mutant homoduplexes and WT/mutant heteroduplexes (Fig. 1H). Although afatinib-resistant cell lines exhibited both increased copy numbers of *EGFR* and increased protein expression, there were remarkable decreases in the number of *EGFR* exon-19 del alleles in AFR1 and AFR2 cells, compared with the control cells. Conversely, the copy number of this allele was sustained in AFR3 cells.

Direct sequencing reveals no EGFR E746–A750 deletion in AFR1 and AFR2 cells and a T790M point mutation in AFR3 cells

Direct sequencing analysis detected a deletion, encompassing residues E746 to A750, within *EGFR* exon 19 in both PC-9 and AFR3 cells; however, this particular activating mutation was not evident in AFR1 or AFR2 cells. Indeed, these two strains harbored WT *EGFR* alleles (Fig. 2A). Previous studies reported the complete loss of alleles containing *EGFR*-activating mutations in gefitinib- or erlotinib-resistant cell lines (22, 23), and demonstrated that these resistant cells evaded EGFR inhibition by initiating formation of an ERBB receptor through HER2 and ERBB3 dimerization for survival or induction of EMT features. In addition, the AFR3 cell line harbored a T790M mutation in *EGFR* exon 20, which was not detected in PC-9, AFR1, or AFR2 cells (Fig. 2A). The EGFR T790M mutation represents the most frequent mutation associated with resistance to afatinib (12). Because parental PC-9 cells did not harbor this mutation (Fig. 2B), the presence of EGFR T790M in AFR3 cells might be presumed to have emerged through an as yet unclear evolutionary process, as has been observed previously (24).

Third-generation EGFR-TKIs effectively suppress AFR3 cell proliferation

AFR3 cells were sensitive to the third-generation EGFR-TKIs osimertinib and rociletinib, which target EGFR-activating mutations and the EGFR T790M mutation that confers drug resistance (Fig. 2C;

Published OnlineFirst March 13, 2017; DOI: 10.1158/1541-7786.MCR-16-0482

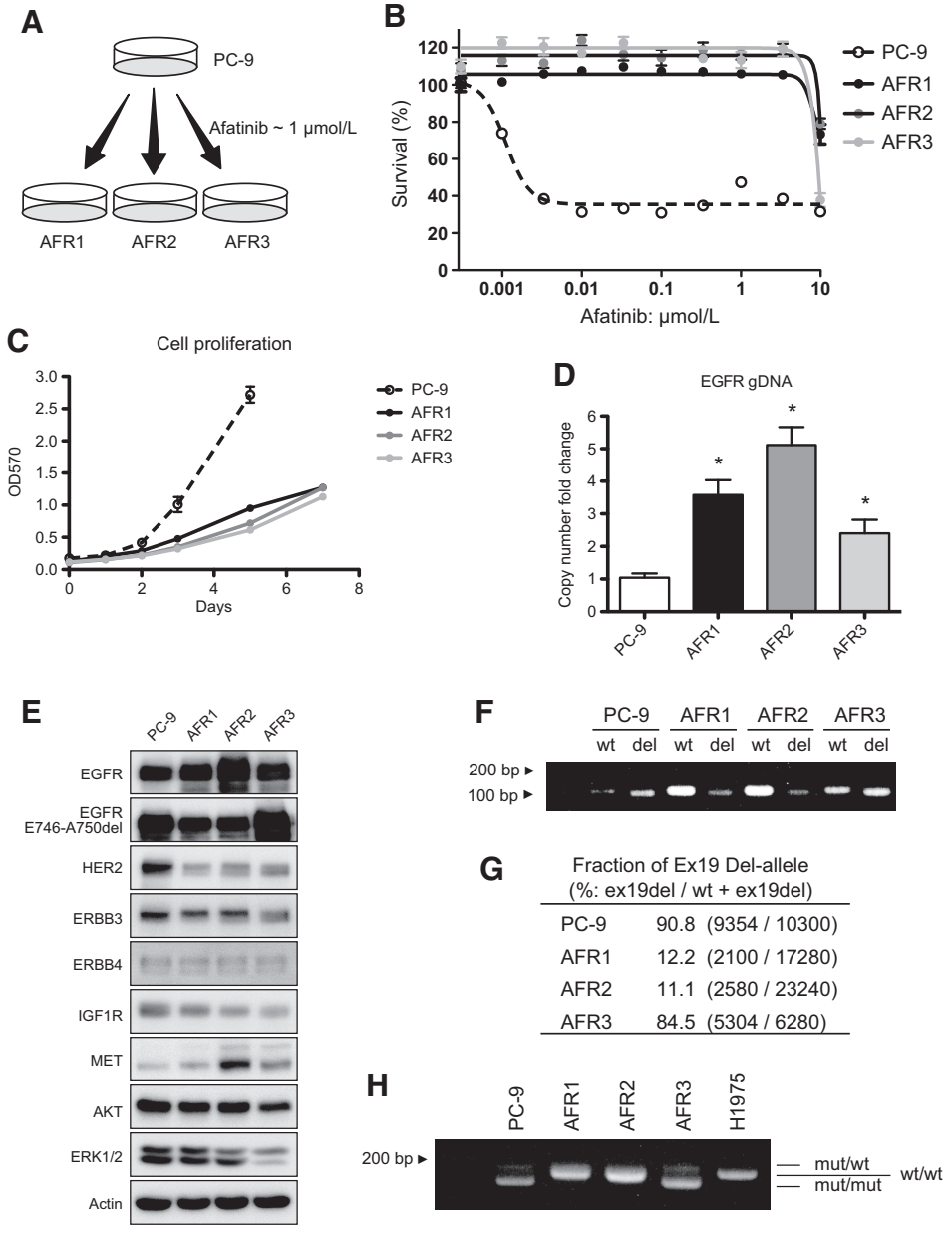

Figure 1.
Establishment of afatinib-resistant cell lines from PC-9 cells. **A,** Schematic model describing the process of generating afatinib-resistant cell lines from PC-9 cells. **B,** Cells were seeded into 96-well plates at 5×10^3 cells/50 μL growth media/well, preincubated overnight, and treated with afatinib at the indicated concentrations for 72 hours. An MTT assay was then performed, and OD_{570} values were obtained. Data represent means ± SEM of data obtained from 6 to 12 replicate wells. **C,** Cells were seeded into 96-well plates at 5×10^2 cells/100 μL/well. Following MTT assays, OD_{570} values were obtained on days 0, 1, 2, 3, 5, and 7. **D,** Elevation of *EGFR* gene copy number was measured by quantitative PCR analysis of genomic DNA extracted from PC-9, AFR1, AFR2, and AFR3 cells; *, $P < 0.01$. **E,** Western blot analysis of basal levels of EGFR, EGFR exon-19 deletion (E746–A750del), HER2, ERBB3, ERBB4, IGF1R, MET, AKT, and ERK1/2 expression in PC-9, AFR1, AFR2, and AFR3 cells. β-Actin was included as a loading control. **F,** Detection of WT and mutated sequences using specific primers. **G,** The proportion of *EGFR* exon-19 del alleles, as measured by digital PCR analysis. **H,** Proportions of heteroduplexes (mut/WT) and homoduplexes (mut/mut and WT/WT) in *EGFR* among PC-9, AFR1, AFR2, and AFR3 cells, as determined by PCR analysis. H1975 cells harbored a WT exon-19 variant, an L858R mutation in exon 21, and a mutation in exon 20 resulting in EGFR T790M.

refs. 25, 26). Indeed, we observed complete inhibition of EGFR phosphorylation in AFR3 cells treated with 1 μmol/L osimertinib or rociletinib, but not in cells treated with 1 μmol/L gefitinib or afatinib, resulting in suppression of AKT and ERK1/2 phosphorylation and induction of apoptosis (Fig. 2D and Supplementary Fig. S1). Moreover, co-administration of cetuximab, a chimeric monoclonal antibody targeting EGFR, and afatinib also led to drug sensitivity in AFR3 cells, according to MTT assay results and as previously reported (Fig. 2E; ref. 27). These data indicate that survival of AFR3 cells remains dependent on the EGFR signaling pathway.

Enhanced expression of WT *KRAS* promotes afatinib resistance in AFR1 cells

Afatinib was administered to AFR1 cells at increasing concentrations, leading to dose-dependent inhibition of EGFR phosphorylation and attenuation of downstream AKT and ERK1/2 phosphorylation. However, this suppression of AKT and ERK1/2 phosphorylation was modest (Fig. 3A) as compared with the levels observed following administration of 0.01 μmol/L afatinib to parental PC-9 cells, which resulted in complete inhibition of EGFR, AKT, and ERK1/2 phosphorylation (Fig. 3B). In addition, we observed elevated *KRAS* gene copy numbers and KRAS protein expression levels in AFR1 cells, but not in PC-9, AFR2, or AFR3 cells. Meanwhile, each of the cell lines exhibited similar levels of NRAS and HRAS protein expression (Fig. 3C and D). Together these data indicate that EGFR inhibition did not affect KRAS, NRAS, or HRAS expression in the parental cells or in the AFR2 and AFR3 cell lines. Meanwhile, pull-down assay analyses detected elevated KRAS activity in AFR1 cells (Fig. 3E) but not constitutive mutational

Published OnlineFirst March 13, 2017; DOI: 10.1158/1541-7786.MCR-16-0482

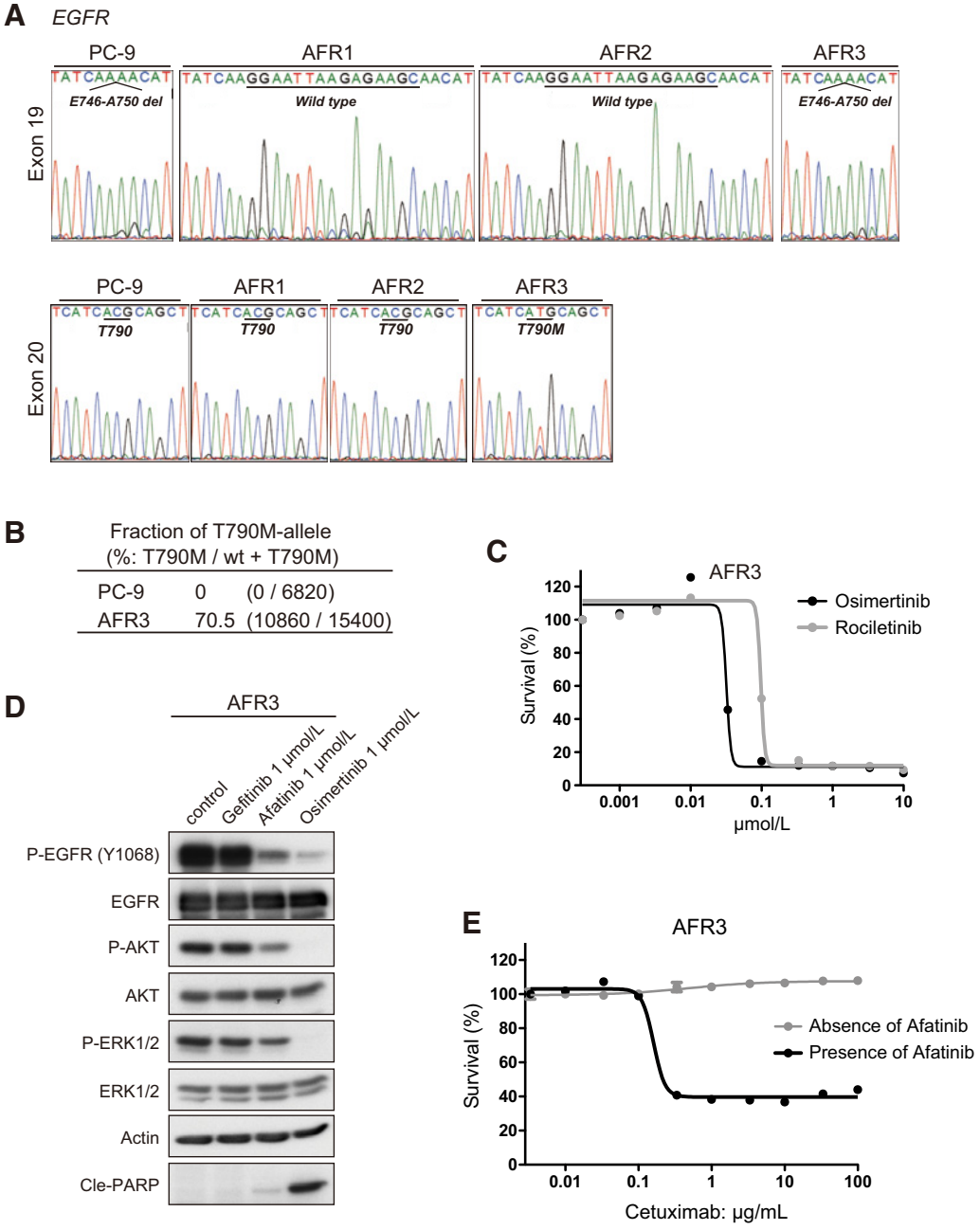

Figure 2.

Loss of exon-19 deletion (dels) in AFR1 and AFR2 cells and appearance of EGFR T790M mutation in an exon-20 of AFR3 cells. **A,** DNA sequence reads in *EGFR* exons 19 and 20. **B,** The proportion of *EGFR* T790M alleles in each group, as measured by digital PCR analysis. **C,** AFR3 cells were seeded into 96-well plates at 5×10^3 cells/50 μL growth media/well, preincubated overnight, and treated with osimertinib or rociletinib at the indicated concentrations for 72 hours. An MTT assay was then performed, and OD_{570} values were obtained. Data represent the means ± SEM of the data obtained from 6 to 12 replicate wells. **D,** AFR3 cells were exposed to 1 μmol/L of gefitinib, afatinib, or osimertinib for 24 hours, and cell lysates were subjected to Western blot analysis using antibodies specific to phosphorylated (Y1068) EGFR (P-EGFR)/EGFR, P-AKT (Ser473)/AKT, and P-ERK1/2/ERK1/2. β-Actin was included as a loading control. Immunoblot analysis of PARP cleavage was used to screen for the induction of apoptosis. Blots are representative of three independent experiments. **E,** AFR3 cells were seeded into 96-well plates, preincubated overnight, and treated with 1 μmol/L afatinib in the presence or absence of the indicated concentrations of cetuximab for 72 hours. An MTT assay was then performed, and the OD_{570} values were obtained. Data represent the means ± SEM for 6 to 12 wells.

activation of KRAS, which is indicative of a wild-type *KRAS* exon 2 (ref. 28; Fig. 3F). In human cancers, mutations in RAS genes occur primarily at residues G12, G13, or Q61. In lung cancer, *KRAS* mutations occur primarily at codon 12 or 13. Notably, such mutations are associated with a lack of response to EGFR-TKIs (29). In this study, xenograft model mice

Published OnlineFirst March 13, 2017; DOI: 10.1158/1541-7786.MCR-16-0482

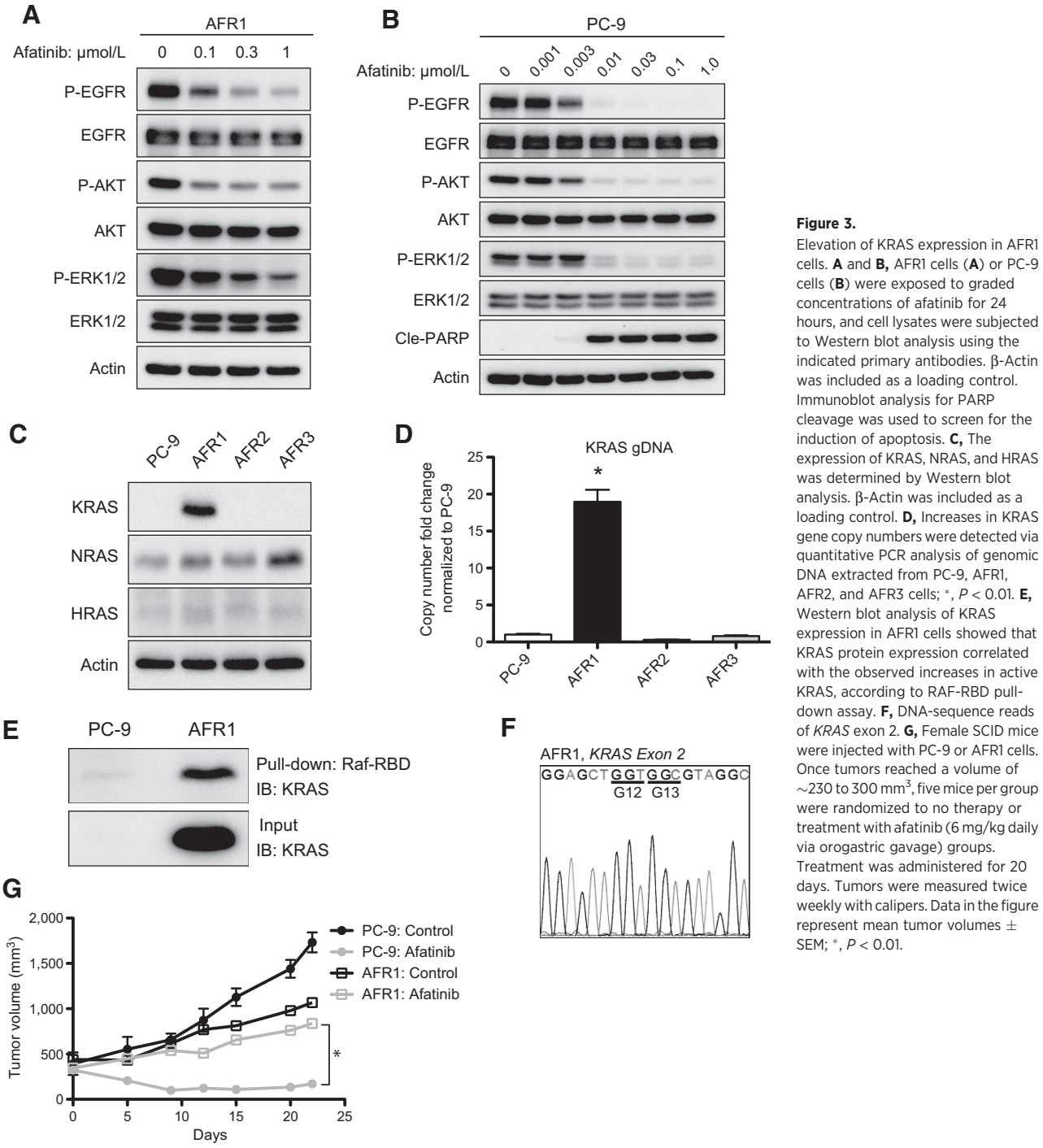

Figure 3.
Elevation of KRAS expression in AFR1 cells. **A** and **B,** AFR1 cells (**A**) or PC-9 cells (**B**) were exposed to graded concentrations of afatinib for 24 hours, and cell lysates were subjected to Western blot analysis using the indicated primary antibodies. β-Actin was included as a loading control. Immunoblot analysis for PARP cleavage was used to screen for the induction of apoptosis. **C,** The expression of KRAS, NRAS, and HRAS was determined by Western blot analysis. β-Actin was included as a loading control. **D,** Increases in KRAS gene copy numbers were detected via quantitative PCR analysis of genomic DNA extracted from PC-9, AFR1, AFR2, and AFR3 cells; *, $P < 0.01$. **E,** Western blot analysis of KRAS expression in AFR1 cells showed that KRAS protein expression correlated with the observed increases in active KRAS, according to RAF-RBD pull-down assay. **F,** DNA-sequence reads of *KRAS* exon 2. **G,** Female SCID mice were injected with PC-9 or AFR1 cells. Once tumors reached a volume of ~230 to 300 mm^3, five mice per group were randomized to no therapy or treatment with afatinib (6 mg/kg daily via orogastric gavage) groups. Treatment was administered for 20 days. Tumors were measured twice weekly with calipers. Data in the figure represent mean tumor volumes ± SEM; *, $P < 0.01$.

transplanted with AFR1 cells exhibited slower tumor growth than those transplanted with PC-9 cells. Interestingly, although administration of 6 mg/kg afatinib resulted in significant suppression of parental PC-9-tumor growth, AFR1 tumors were resistant to this treatment (Fig. 3G). These data are therefore consistent with a previous report of increased WT-*KRAS* expression upon acquisition of afatinib resistance in PC-9 cells (16). The elevated WT-KRAS activity dissociates EGFR from the down-stream of ERK1/2 and AKT in AFR1 cells.

IGF1R activation serves as an alternative survival pathway in AFR1 cells exhibiting increased expression of *KRAS*.

To characterize the mechanisms of afatinib resistance in AFR1 cells exhibiting increased *KRAS* expression, cells were treated with KRAS-specific siRNA. Because KRAS is involved in the MAPK pathway, KRAS silencing significantly attenuated ERK1/2 phosphorylation, but only modestly inhibited AKT phosphorylation (Fig. 4A). Previously, Cepero and colleagues reported that enhanced *KRAS* expression mediated the acquisition of resistance

Published OnlineFirst March 13, 2017; DOI: 10.1158/1541-7786.MCR-16-0482

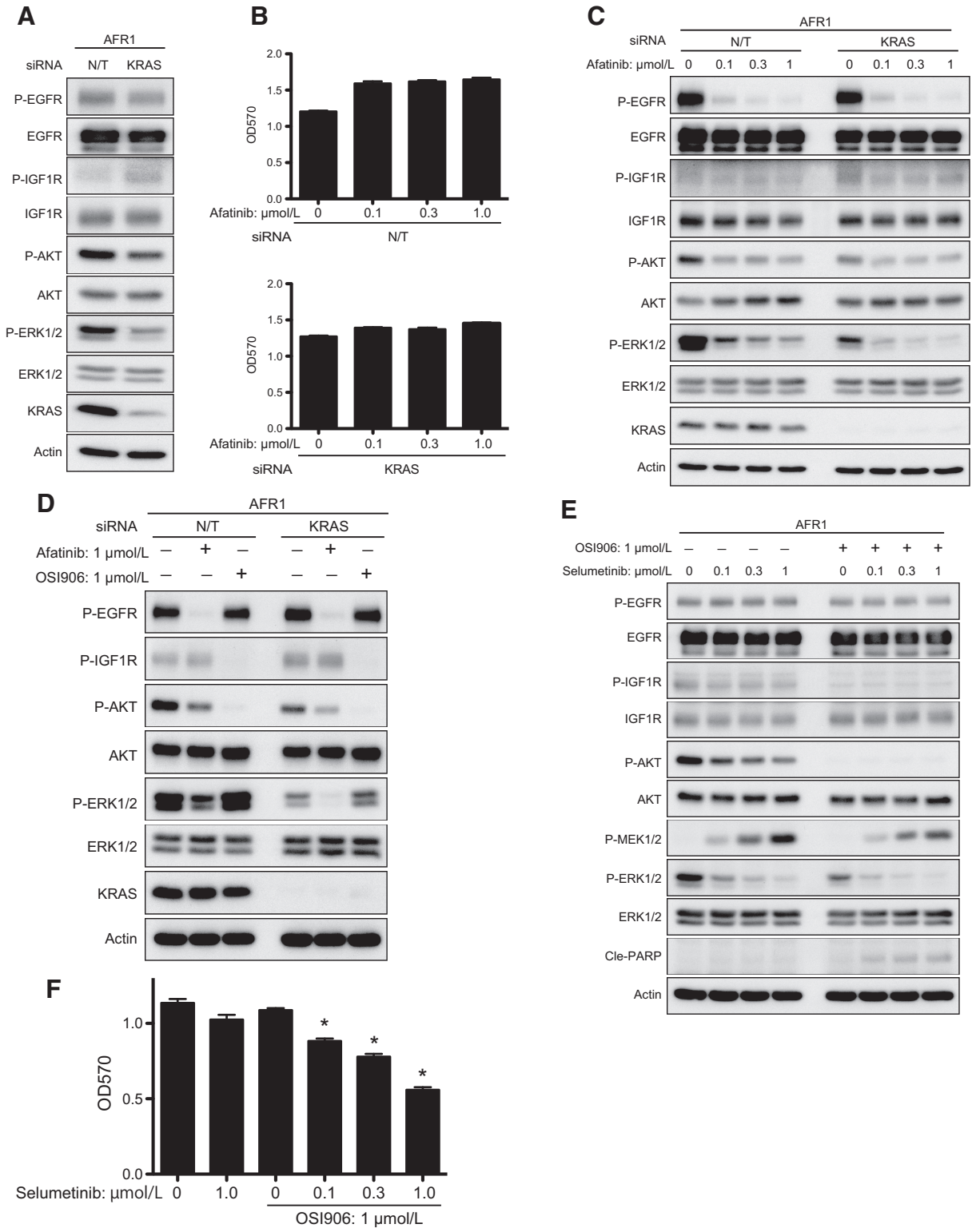

Figure 4.

AFR1 cells are sensitive to cotreatment with MEK inhibitor and IGF1R inhibitor. **A,** AFR1 cells were transfected with N/T siRNA or siRNA directed against KRAS, and KRAS knockdown was determined by Western blot analysis. Lysates were then subjected to immunoblot analysis using the indicated primary antibodies; β-actin was included as a loading control. Blots are representative of three independent experiments. **B,** Transfected cells were reseeded in the presence or absence of the indicated concentrations of afatinib. Following a 72-hour incubation, an MTT assay was performed and OD_{570} values were obtained. Data represent the means ± SEM of the data obtained from six replicate wells. (*Continued on the following page.*)

Published OnlineFirst March 13, 2017; DOI: 10.1158/1541-7786.MCR-16-0482

to MET-TKI PHA665752 in gastric cancer cell lines, and that short hairpin (sh)RNA-mediated silencing of *KRAS* resulted in decreased cell viability (30). Although knockdown of *KRAS* expression did not suppress cell proliferation in this study, even in the presence of afatinib cotreatment (Fig. 4B), Western blot analysis revealed that KRAS knockdown led to downregulation of ERK1/2 phosphorylation, and that cotreatment with afatinib resulted in complete inhibition of ERK1/2 phosphorylation. Conversely, we detected no inhibition of AKT phosphorylation in siRNA-treated cells, even following afatinib treatment (Fig. 4C), which may have been due to the increase in IGF1R phosphorylation observed following KRAS silencing (Fig. 4A and C).

To determine the role of EGFR and IGF1R in AFR1 cells, cells were treated with afatinib or the IGF1R inhibitor OSI906 in the presence or absence of *KRAS* attenuation. Afatinib treatment inhibited EGFR phosphorylation and partially inhibited ERK1/2 phosphorylation, with further inhibition of ERK1/2 phosphorylation observed in KRAS-silenced AFR1 cells. Notably, although no change in AKT phosphorylation was distinguished upon KRAS attenuation, even following afatinib treatment, administration of OSI906 resulted in complete inhibition of AKT phosphorylation, but not of ERK1/2 phosphorylation, regardless of KRAS status (Fig. 4D). These results indicate that ERK1/2 phosphorylation is regulated by EGFR-KRAS signaling and that AKT phosphorylation is regulated by IGF1R in AFR1 cells, whereas EGFR-KRAS signaling only partially affects AKT activation.

Molina-Arcas and colleagues reported that inhibition of both IGF1R and MEK activation in *KRAS* mutant lung cancer cell lines resulted in marked decreases in cell proliferation (31). Therefore, we treated AFR1 cells with increasing concentrations of the MEK inhibitor selumetinib (0.1–1.0 μmol/L) in the presence or absence of 1 μmol/L OSI906. Selumetinib treatment alone inhibited ERK1/2 phosphorylation in a dose-dependent manner, whereas OSI906 treatment alone inhibited AKT phosphorylation. Cotreatment of AFR1 cells with selumetinib and OSI906 resulted in induction of apoptosis and suppression of cell proliferation (Fig. 4E and F). These results indicate that cotreatment with both a MEK and IGF1R inhibitor could be used to effectively suppress AFR1 cell proliferation, as observed in KRAS-mutant cells.

Attenuation of enhanced *KRAS* expression following cessation of afatinib treatment

AFR1 cells were cultured in afatinib-free media for 2 weeks (F2W), 1 month (F1M), and 2 months (F2M), and then evaluated for alterations in *KRAS* expression. We observed gradual attenuation of *KRAS* expression in F2M cells to levels comparable with those detected in parental PC-9 cells (Fig. 5A and B). Although *KRAS* expression was attenuated following removal of afatinib treatment, we did not observe an increase in the prevalence of the *EGFR* exon-19 del allele; WT *EGFR* remained the predominant allele according to mutant-specific PCR, Western blot analysis, and digital PCR analysis (Fig. 5C and Supplementary Fig. S2A and S2B). In addition, F2W, F1M, and F2M cells each exhibited significantly higher *EGFR* copy numbers than PC-9 cells (Fig. 5D). F2M cells exhibiting levels of *KRAS* expression similar to those of PC-9 cells showed renewed sensitivity to afatinib, with treatment leading to inhibition of EGFR phosphorylation, suppression of AKT and ERK1/2 phosphorylation, and induction of apoptosis (Fig. 5E and F). Treatment of F2M cells with gefitinib also suppressed cell proliferation, but to a lesser degree than that observed upon treatment of PC-9 cells with gefitinib (Supplementary Fig. S2C). In addition, although gefitinib treatment also suppressed EGFR, AKT, and ERK1/2 phosphorylation and induced apoptosis in F2M cells, these alterations occurred to lesser degrees than those observed following afatinib treatment (Supplementary Fig. S2D).

To determine the role of IGF1R in AKT phosphorylation, F2M cells were transfected with siRNA against EGFR or IGF1R. Although AKT phosphorylation was inhibited by IGF1R knockdown in AFR1 cells, this activity was not inhibited in F2M cells, indicating that IGF1R signaling was dissociated with AKT in F2M cells. Thus, phosphorylation of both AKT and ERK1/2 was inhibited by EGFR knockdown and resulted in induction of apoptosis in F2M cells. Meanwhile, AFR1 cells exhibiting enhanced levels of WT *KRAS* expression required IGF1R to initiate AKT phosphorylation (Fig. 5G). These results indicate that, regardless of *EGFR* allelic distribution, the observed increase in *KRAS* expression was attenuated following cessation of afatinib treatment. Furthermore, the subsequent resensitization of cells to afatinib suggests that enhanced *KRAS* expression resulted in afatinib resistance in AFR1 cells.

Increased expression of IGFBP3 is required for IGF1R activation as a bypass signaling pathway in AFR2 cells

As previously reported, PC-9 cells develop resistance to the irreversible EGFR-TKI dacomitinib following continuous exposure, and the resulting dacomitinib-resistant cells exhibited activation of IGF1R signaling as a bypass signaling pathway in response to IGFBP3 downregulation (15). IGFBP3 is involved in transporting IGF1 and IGF2 ligands within cells and modulating IGF bioavailability and signaling (32). Compared with the parental PC-9 cells, AFR2 cells exhibited significant upregulation of IGFPB3 mRNA expression, as well as increased levels of IGFBP3 protein within both cell lysates and conditioned media samples (Fig. 6A and Supplementary Fig. S3A). In addition, MET expression was elevated in AFR2 cells relative to levels observed in PC-9

(*Continued.*) **C,** AFR1 cells were transfected with N/T siRNA or siRNA directed against KRAS for 48 hours and then treated with the indicated concentrations of afatinib for 24 hours. KRAS knockdown was determined by Western blot analysis. Lysates were subjected to immunoblot analysis using the indicated primary antibodies. β-Actin was included as a loading control. **D,** AFR1 cells were transfected with N/T siRNA or siRNA directed against KRAS for 48 hours and then treated with 1 μmol/L of afatinib or OSI906 for 24 hours. KRAS knockdown was determined by Western blot analysis. Lysates were subjected to immunoblot analysis using the indicated primary antibodies. β-Actin was included as a loading control. **E,** AFR1 cells were exposed to graded concentrations of selumetinib in the presence or absence of 1 μmol/L OSI906 for 24 hours, and cell lysates were generated and subjected to immunoblot analysis using the indicated primary antibodies. Immunoblot analysis of PARP cleavage was used to screen for the induction of apoptosis. β-Actin was included as a loading control. **F,** AFR1 cells were seeded into 96-well plates at 5×10^3 cells/50 μL growth media/well, preincubated overnight, and treated with selumetinib at the indicated concentrations in the presence or absence of 1 μmol/L OSI906 for 72 hours. An MTT assay was performed, and OD_{570} values were measured. Data represent the means ± SEM for 6 to 12 wells.

Published OnlineFirst March 13, 2017; DOI: 10.1158/1541-7786.MCR-16-0482

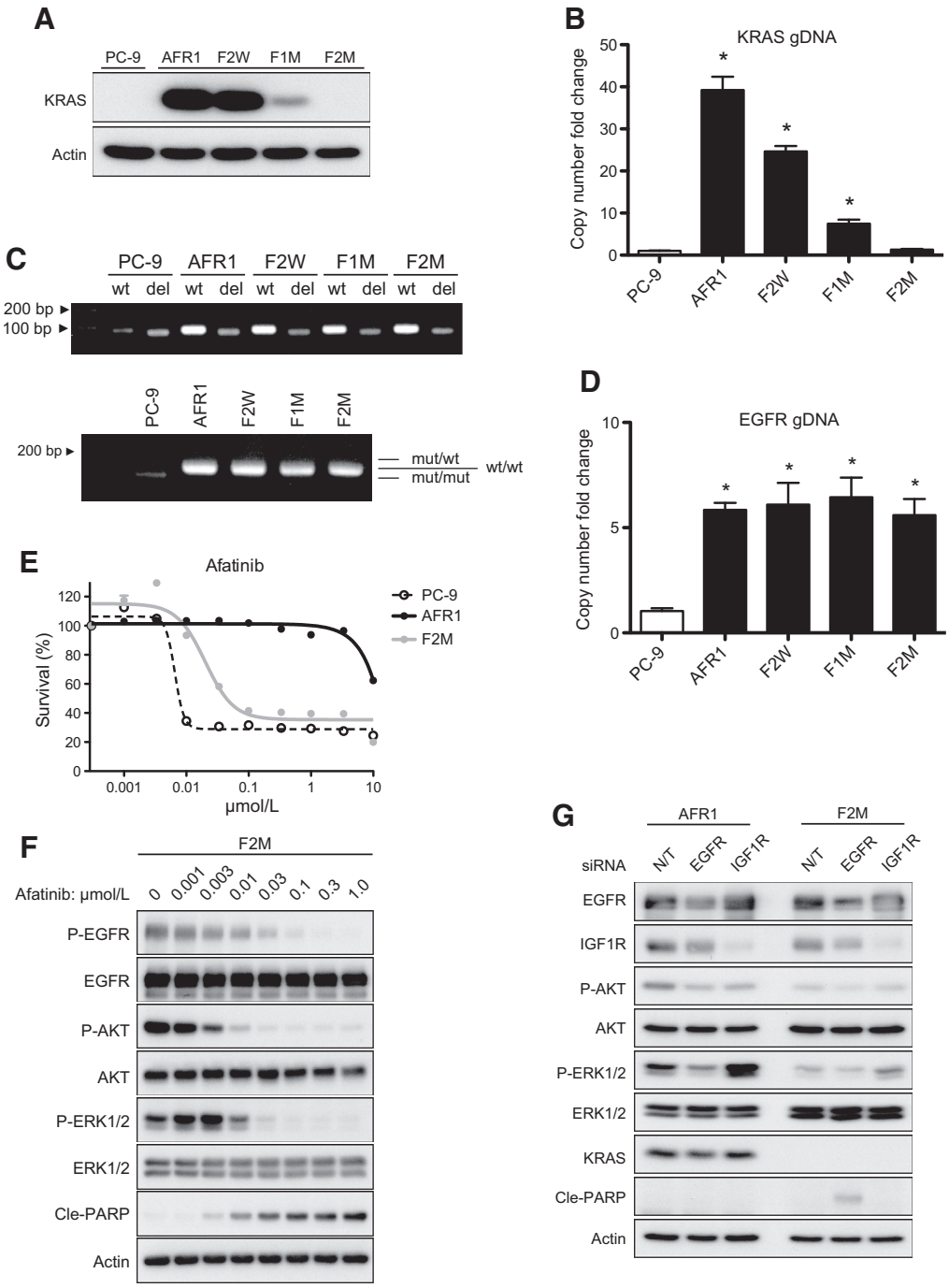

Figure 5.

Acquired increases in KRAS expression are attenuated following removal of afatinib. **A,** AFR1 cells were cultured in the absence of afatinib for 2 weeks (F2W), for 1 month (F1M), and for 2 months (F2M), and lysates were generated and subjected to Western blot analysis of KRAS protein expression. β-Actin was included as a loading control. **B,** *KRAS* copy numbers were evaluated in PC-9, AFR1, F2W, F1M, and F2M cells by real-time PCR analysis; *, $P < 0.01$. **C,** Detection of WT and mutant sequences using specific primers (top). Heteroduplexes (mut/WT) and homoduplexes (mut/mut and WT/WT) of the *EGFR* gene were detected by PCR analysis (bottom). **D,** Elevated *EGFR* gene copy numbers were detected by quantitative PCR analysis of genomic DNA from PC-9, AFR1, F2W, F1M, and F2M cells; *, $P < 0.01$. **E,** Cells were seeded into 96-well plates at 5×10^3 cells/50 μL growth media/well, preincubated overnight, and treated with afatinib at the indicated concentrations for 72 hours. An MTT assay was performed, and OD_{570} values were measured. Data represent the means ± SEM of the data obtained from 6 to 12 replicate wells. **F,** F2M cells were exposed to graded concentrations of afatinib for 24 hours, and cell lysates were subjected to immunoblot analysis using the indicated primary antibodies. β-Actin was included as a loading control. Immunoblot analysis of PARP cleavage was used to screen for the induction of apoptosis. **G,** AFR1 and F2M cells were transfected with N/T siRNA or siRNA directed against EGFR or IGF1R, and knockdown of EGFR and IGF1R expression was determined by Western blot analysis. Lysates were generated and subjected to immunoblot analysis using the indicated primary antibodies, and PARP cleavage was used to screen for the induction of apoptosis. Blots are representative of three independent experiments.

Published OnlineFirst March 13, 2017; DOI: 10.1158/1541-7786.MCR-16-0482

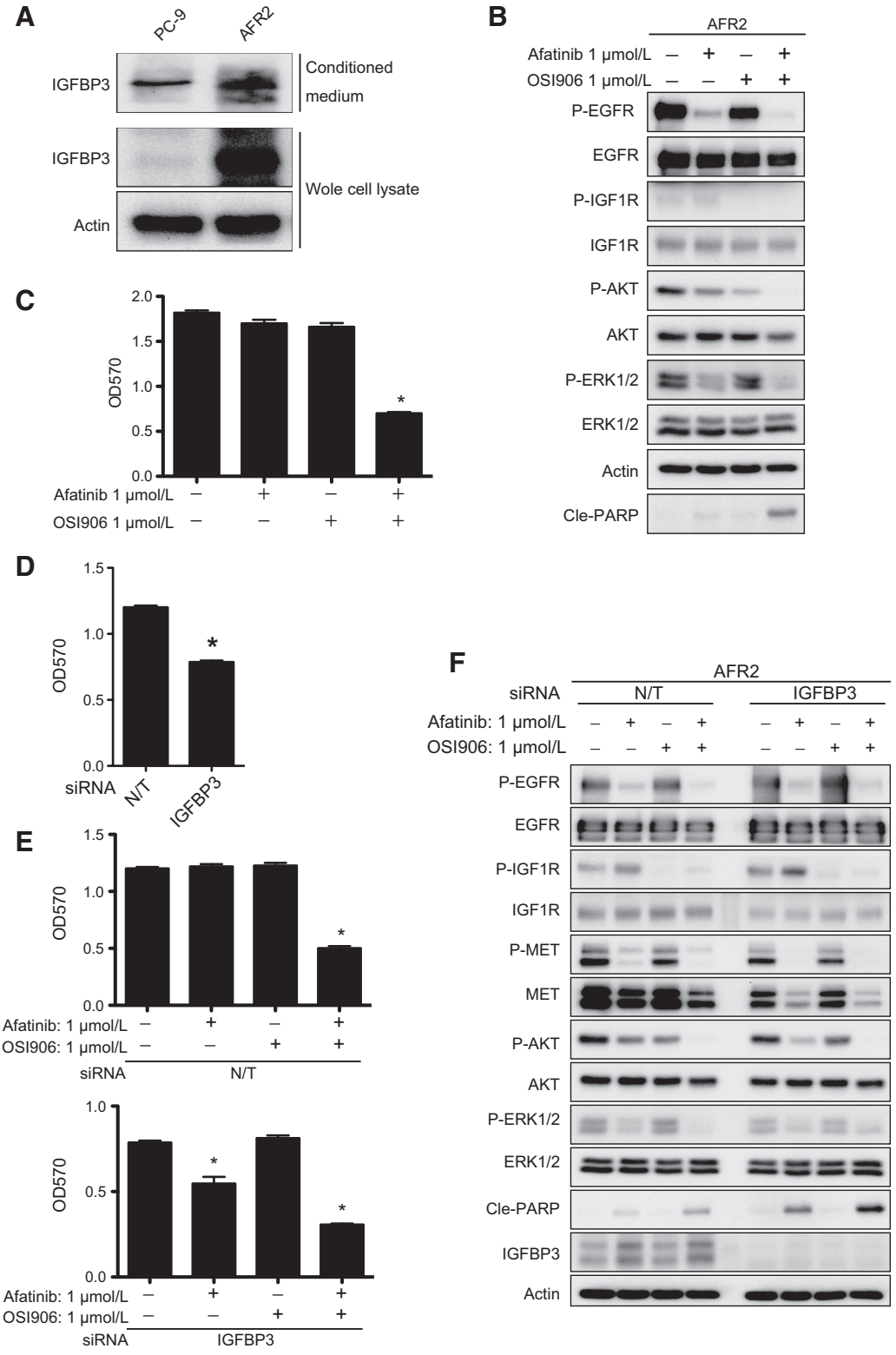

Figure 6.

IGFBP3 upregulation leads to increased IGF1R activation and AKT phosphorylation, resulting in afatinib resistance via bypass signaling by IGF1R in AFR2 cells. **A,** Conditioned media samples from 2×10^6 PC-9 or AFR2 cells were collected after incubation for 24 hours and concentrated 20-fold by ultrafiltration. Conditioned media samples or 20 μg whole-cell lysate proteins were subjected to immunoblotting with IGFBP3 or β-actin antibodies. (*Continued on the following page.*)

Published OnlineFirst March 13, 2017; DOI: 10.1158/1541-7786.MCR-16-0482

cells (Fig. 1E). We previously reported that increased IGFBP3 expression enhances MET expression and promotes partial resistance to the MET inhibitor PHA665752 in DR4 cells, resulting in their dual resistance to gefitinib and PHA665752. Following establishment of an IGF1R bypass signal, however, cotreatment with the MET-TKI PHA665752 and an IGF1R inhibitor effectively suppressed cell proliferation (33). In this study, AFR2 cells were administered afatinib and/or the IGF1R inhibitor OSI906 to assess alterations in AKT and ERK1/2 phosphorylation. We observed that ERK1/2 phosphorylation was inhibited following afatinib treatment; however, AKT phosphorylation was only partially suppressed following treatment with either afatinib or OSI906. Moreover, cotreatment with afatinib and OSI906 completely abrogated AKT phosphorylation, inhibited cell proliferation, and induced apoptosis (Fig. 6B and C).

Given that IGF1R signaling in AFR2 cells might constitute a mechanism for escaping EGFR inhibition via maintenance of AKT phosphorylation, we determined the role of IGFBP3 in AFR2 cells by siRNA-targeted silencing of IGFBP3. We observed partial inhibition of cell proliferation in IGFBP3-silenced AFR2 cells, which also exhibited recovery of afatinib sensitivity based on further inhibition of cell proliferation following cotreatment with afatinib and OSI906 (Fig. 6D and E). Afatinib treatment alone partially inhibited AKT and ERK1/2 phosphorylation and induced apoptosis in IGFBP3-silenced AFR2 cells, whereas cotreatment with afatinib and OSI906 completely inhibited AKT phosphorylation and enhanced apoptosis (Fig. 6F). Increased IGFBP3 expression resulted in enhanced MET expression and ERK1/2 phosphorylation; however, treatment with the MET inhibitor PHA665752 did not suppress downstream signals associated with AKT and ERK1/2 phosphorylation (Supplementary Fig. S3B), indicating that, in AFR2 cells, IGFBP3 promotes afatinib resistance by sustaining AKT phosphorylation. These results indicate that IGFBP3 attenuation enhances afatinib sensitivity; however, the precise mechanisms associated with IGF1R activation related to afatinib resistance remain unknown. Further studies, including an assessment of IGFBP3-stimulated IGF1R activity, are needed to adequately define the role(s) of IGFBP3 in EGFR-TKI resistance.

Discussion

In this study, we identified three distinct mechanisms of acquired resistance to the irreversible EGFR-TKI afatinib. First, we detected enhanced expression of WT *KRAS* in AFR1 cells, which results in dissociation of signal transduction between EGFR and the downstream effectors ERK1/2 or AKT. Notably, however, there was a steady decrease in this enhanced expression upon removal of afatinib from the culture medium, with *KRAS* expression levels reaching that of the parental PC-9 cells within 2 months of cultivation in afatinib-free medium. Moreover, these cells exhibited resensitization to afatinib after this time period. Second, we detected the utilization of an IGF1R bypass signaling pathway along with increased IGFBP3 expression in AFR2 cells. Specifically, IGFBP3 upregulation resulted in partial resistance to afatinib and enhanced IGF1R activity, which was sufficient to sustain AKT phosphorylation. Finally, AFR3 cells were found to harbor a secondary T790M mutation in *EGFR* exon 20. Our results provide evidence of heterogeneity among drug-resistant cell lines and reflect the variable nature of clinical resistance.

The afatinib-resistant PC-9 cell lines AFR1 and AFR2 partially lost the mutant-*EGFR* allele, which also served as the driver oncogene; therefore, cell proliferation might be expected to be lower in these cells, compared with that observed in the parental population (Fig. 1C). Although PCR screening for EGFR mutations did not provide information regarding the number of EGFR-mutation alleles, a partial loss of the mutant-*EGFR* allele was detected by direct sequencing and digital PCR analysis (Figs. 1G and 2A; Supplementary Table S2). Given that the target of EGFR-TKI treatment is an *EGFR* activating mutation, it might be necessary to monitor the target of this therapy. Similar results were reported upon the loss of mutant alleles from gefitinib- and erlotinib-resistant PC-9, HCC827, and 11–18 cells, which involved bypass signals to HER2, ERBB3, or IGF1R or the induction of EMT with stem cell-like properties (22, 23). Furthermore, in clinical samples from refractory patients administered EGFR-TKI, loss of activating mutations in the *EGFR* gene was observed (22). Here, however, the AFR1 and AFR2 cell lines expressed significantly higher levels of EGFR than the parental PC-9 cells and did not show EMT-like features, including decreased E-cadherin and increased Vimentin expression (Supplementary Fig. S4). Interestingly, AFR1 cells with enhanced WT *KRAS* expression exhibited increased *EGFR* copy numbers, compared with the parental control cells. However, although the expression of WT *KRAS* decreased following cessation of afatinib treatment in AFR1 cells, there were no changes in *EGFR* copy number or EGFR protein expression in these cells, and the ratio of mutant and WT *EGFR* alleles remained unchanged (Fig. 5A–D; Supplementary Fig. S2A). These findings might indicate that an acquired elevation in WT *KRAS* expression is separately regulated by the loss of a mutant *EGFR* allele.

Oncogenic mutations in the *KRAS* gene occur in ∼26% and ∼11% of NSCLC adenocarcinomas in Western and Asian

(*Continued.*) **B,** AFR2 cells were exposed to 1 μmol/L afatinib and/or OSI906 for 24 hours, and cell lysates were subjected to immunoblot analysis using the indicated antibodies. β-Actin was included as a loading control. Immunoblot analysis of PARP cleavage was used to screen for the induction of apoptosis. Blots are representative of three independent experiments. **C,** AFR2 cells were seeded into 96-well plates at 5×10^3 cells/50 μL growth media/well, pre-incubated overnight, and treated with 1 μmol/L gefitinib and/or 1 μmol/L OSI906 for 72 hours. An MTT assay was then performed, and OD_{570} values were obtained. Data represent the means ± SEM of the data obtained from 6 to 12 replicate wells; *, $P < 0.01$, compared with the control value. **D,** AFR2 cells were transfected with N/T siRNA or siRNA directed against IGFBP3, and transfected cells were re-seeded. After a 72-hour incubation, an MTT assay was performed and OD_{570} values were obtained. Data represent the means ± SEM for six replicate wells; *, $P < 0.01$, compared with the control value. **E,** AFR2 cells were transfected with N/T siRNA or siRNA directed against IGFBP3, and the transfected cells were reseeded in the presence or absence of 1 μmol/L afatinib and/or OSI906. After a 72-hour incubation, an MTT assay was performed and OD_{570} values were obtained. Data represent the means ± SEM for six replicate wells; *, $P < 0.01$, compared with the control value. **F,** AFR2 cells were transfected with N/T siRNA or siRNA directed against IGFBP3. After a 48-hour transfection, AFR2 cells were treated with 1 μmol/L afatinib or OSI906 for 24 hours, and IGFBP3 knockdown was determined by Western blot analysis. Lysates were subjected to immunoblot analysis using the indicated primary antibodies. Immunoblot analysis for PARP cleavage was used to screen for the induction of apoptosis. β-Actin was included as a loading control.

Published OnlineFirst March 13, 2017; DOI: 10.1158/1541-7786.MCR-16-0482

populations, respectively, and are associated with poor prognosis (34). Moreover, *KRAS* mutations are predictive of a lack of response to EGFR inhibition in lung and colorectal cancers (35, 36). In this study, AFR1 cells exhibited elevated WT *KRAS* copy numbers, leading to increased expression and activation of the KRAS protein (Fig. 3C–F). Few reports have described *KRAS* amplification in malignant tumors (30, 37, 38). Cepero and colleagues reported that WT *KRAS* amplification leads to MET-TKI resistance with *MET* amplification, and that elevated KRAS and MET levels were decreased following cessation of MET-TKI PHA665752 treatment in the gastric cancer cell line GTL16 (30). Meanwhile, PHA665752-resistant GTL16 cells showed dose-dependent increases in *MET* and *KRAS* expression, suggesting that amplification of *MET* and *KRAS* expression constituted an adaptive process in response to the MET inhibitor. In AFR1 cells, although the *KRAS* copy number decreased under afatinib-free conditions, partial loss of the mutant *EGFR* allele and sustainment of the ratio of WT to mutant *EGFR* alleles was observed during this period. Therefore, these results suggested that AFR1 cells were not selected from preexisting clones, and that genetic alterations occurred during the course of inhibitor treatment. The mechanism underlying this rapid loss of KRAS copy number remains unclear. However, it is conceivable that removal of the inhibitor results in excessive signal transduction, which can lead to cellular stress and loss of extrachromosomal DNA, including amplified *KRAS* gene copies, which are typically extrachromosomal. Cells that have lost *KRAS* would subsequently be at an advantage and predominate in the absence of afatinib (39, 40).

We discovered that IGF1R activation maintained AKT phosphorylation in WT *KRAS*-amplified AFR1 cells (Fig. 4A and C). The specific inhibitors for mutant *KRAS* showed little clinical efficacy; therefore, it was necessary to target this downstream *KRAS* effector protein, which is involved in the MAPK pathway. Notably, however, MEK inhibitors have limited activity in patients with *KRAS*-mutant lung cancer (41). Because lung and colorectal cancer cells harboring *KRAS* mutations exhibit increased dependence on IGF1R signaling, cotreatment with a MEK inhibitor and an IGF1R inhibitor enhances cell death (31). Consistent with previous reports, treatment of AFR1 cells exhibiting enhanced WT *KRAS* expression with the MEK inhibitor selumetinib resulted in dose-dependent suppression of ERK1/2 phosphorylation, but no changes in AKT phosphorylation (Fig. 4E). Conversely, siRNA-mediated KRAS knockdown resulted in partial suppression of both AKT and ERK1/2 phosphorylation, as well as slight increases in IGF1R phosphorylation (Fig. 4A and C). Despite the phenotypic differences observed between cells harboring KRAS mutations or amplified *KRAS* expression, cotreatment with selumetinib and the IGF1R inhibitor OSI906 induced apoptosis and suppressed cell proliferation in AFR1 cells (Fig. 4E and F). In previous studies, WT KRAS-amplified resistant cell lines (e.g., PC-9AR_1 and resistant GTL16 cells) exhibited reduced viability only after attenuation of KRAS expression (16, 29). Meanwhile, in this study, IGF1R signaling led to PI3K/AKT activation in AFR1 cells. Therefore, in these cells, only KRAS knockdown failed to suppress proliferation.

This is the first report elucidating the mechanisms associated with effective EGFR-TKI re-challenge following acquisition of resistance. Our findings suggest that this process involves drug-holiday-mediated tumor resensitization to afatinib through KRAS attenuation. Small-scale clinical trials and case reports indicated that retreatment with EGFR-TKIs might benefit limited numbers of patients that had previously undergone EGFR-TKI treatment (e.g., gefitinib or erlotinib; refs. 17, 20, 42). However, the particular characteristics of these patients and the duration of the drug holiday were unknown. Here, our results indicate that *KRAS*-amplified AFR1 cells recovered sensitivity to afatinib within 2 months following decrease of *KRAS* expression to levels comparable with those of parental PC-9 cells (Fig. 5A and B). Repeated biopsy is required for clinical definitions of acquired resistance to EGFR-TKIs in NSCLC. Therefore, comprehensive research using clinical samples derived from patients who regained sensitivity after exhibiting EGFR-TKI resistance is needed to confirm our hypothesis.

IGF bioavailability is regulated by a family of six IGFBPs, of which IGFBP3 is the major IGF-carrier protein in serum. Although IGFBP3 can exert stimulatory or inhibitory effects on IGF bioactivity, little is known regarding these biological switches. Regarding the mechanism associated with EGFR-TKI resistance, down-regulation of IGFBP3 leads to IGF1R activation through enhancement of ligand-related activity as a bypass signaling pathway (15, 43). Upregulation of IGFBP3 also potentiates IGF bioactivity. Similar studies of fibroblasts and mammary epithelial cells indicated that IGFBP3 possibly potentiates IGF activity through modulation of IGF1R activation and AKT-signaling pathways (44, 45). In afatinib-resistant AFR2 cells, IGFBP3 expression significantly increased, according to mRNA and protein levels, resulting in IGF1R activation as a bypass signaling pathway (Fig. 6A and Supplementary Fig. S3A). IGFBP3-mediated IGF1R activation as a bypass signal constitutes a novel mechanism for EGFR-TKI resistance. Furthermore, NSCLC tumor tissues exhibiting elevated expression of IGFBP3 show significant activation of IGF1R (46). However, the precise mechanisms related to IGF activation in the presence of increased IGFBP3 levels remain unclear. Previously, we reported that increased IGFBP3 expression stimulates IGF1R activation as a bypass signal in PC-9 cells resistant to both MET-TKI PHA665752 and the EGFR-TKI gefitinib (33). Moreover, in the current study, siRNA silencing of IGFBP3 in AFR2 cells resulted in inhibition of AKT phosphorylation and cell proliferation and induction of apoptosis following afatinib administration (Fig. 6E and F). These results suggest that increased IGFBP3 levels prevent afatinib-mediated inhibition of PI3K/AKT and sustain AKT phosphorylation through an IGF1R activity. However, further studies are required to elucidate the mechanisms associated with IGFBP3 potentiation of IGF1R activity in EGFR-TKI-resistant cells.

In summary, we elucidated novel mechanisms related to afatinib resistance using lung adenocarcinoma PC-9 cells. Three afatinib-resistant cell lines, AFR1, AFR2, and AFR3, exhibiting different mechanisms of resistance were generated, implying that afatinib resistance observed in patients might be heterogeneous in nature. AFR1 cells exhibited enhanced expression of WT *KRAS*, which was reversible following a drug holiday. Subsequent recovery of afatinib sensitivity provides a rationale for EGFR-TKI rechallenge. Moreover, we observed that the bypass signaling pathway associated with IGF1R was dependent upon IGFBP3 expression. In AFR2 cells, increased IGFBP3 levels modulated IGF1R and sustained AKT phosphorylation, resulting in recovery of afatinib sensitivity via IGFBP3 silencing. These novel resistance mechanisms should be evaluated in clinical samples following reacquisition of sensitivity to afatinib or other EGFR-TKIs. Finally, a secondary mutation, EGFR T790M, was detected in AFR3 cells, which was sensitive to third-generation EGFR-TKIs and to

cotreatment with afatinib and cetuximab. Together, our findings provide insight into next-generation therapeutics for patients with NSCLC harboring EGFR-activating mutations (Supplementary Fig. S5).

Disclosure of Potential Conflicts of Interest

No potential conflicts of interest were disclosed.

Authors' Contributions

Conception and design: T. Yamaoka, T. Ohmori, S. Kusumoto
Development of methodology: T. Yamaoka, S. Arata
Acquisition of data (provided animals, acquired and managed patients, provided facilities, etc.): T. Yamaoka, T. Ohmori, S. Arata, Y. Murata
Analysis and interpretation of data (e.g., statistical analysis, biostatistics, computational analysis): T. Yamaoka, T. Ohmori, S. Kusumoto
Writing, review, and/or revision of the manuscript: T. Yamaoka, T. Ohmori, M. Ohba, S. Kusumoto, H. Ishida
Administrative, technical, or material support (i.e., reporting or organizing data, constructing databases): T. Yamaoka, T. Ohmori, M. Ohba, K. Ando, Y. Sasaki
Studysupervision: T. Yamaoka, S. Kusumoto, T. Ohnishi, Y. Sasaki

Acknowledgments

The authors thank the members of the Institute of Molecular Oncology for their thoughtful discussions and helpful advice, and Editage for their assistance with English-language editing. This work was supported by the MEXT-supported Program for the Strategic Research Foundation at Private Universities (2012–2016) from the Ministry of Education, Culture, Sports, Science, and Technology of Japan.

Grant Support

This work was supported by the MEXT-Supported Program for the Strategic Research Foundation at Private Universities (2012–2016) from the Ministry of Education, Culture, Sports, Science, and Technology of Japan. (T. Yamaoka, T. Ohmori, and M. Ohba received this grant.)

The costs of publication of this article were defrayed in part by the payment of page charges. This article must therefore be hereby marked *advertisement* in accordance with 18 U.S.C. Section 1734 solely to indicate this fact.

Received December 22, 2016; revised December 21, 2016; accepted March 7, 2017; published OnlineFirst March 13, 2017.

References

1. Maemondo M, Inoue A, Kobayashi K, Sugawara S, Oizumi S, Isobe H, et al. Gefitinib or chemotherapy for non-small-cell lung cancer with mutated EGFR. N Engl J Med 2010;362:2380–8.
2. Mok TS, Wu YL, Thongprasert S, Yang CH, Chu DT, Saijo N, et al. Gefitinib or carboplatin-paclitaxel in pulmonary adenocarcinoma. N Engl J Med 2009;361:947–57.
3. Rosell R, Carcereny E, Gervais R, Vergnenegre A, Massuti B, Felip E, et al. Erlotinib versus standard chemotherapy as first-line treatment for European patients with advanced EGFR mutation-positive non-small-cell lung cancer (EURTAC): a multicentre, open-label, randomised phase 3 trial. Lancet Oncol 2012;13:239–46.
4. Garraway LA, Janne PA. Circumventing cancer drug resistance in the era of personalized medicine. Cancer Discov 2012;2:214–26.
5. Ellis LM, Hicklin DJ. Resistance to targeted therapies: refining anticancer therapy in the era of molecular oncology. Clin Cancer Res 2009;15:7471–8.
6. Arcila ME, Oxnard GR, Nafa K, Riely GJ, Solomon SB, Zakowski MF, et al. Rebiopsy of lung cancer patients with acquired resistance to EGFR inhibitors and enhanced detection of the T790M mutation using a locked nucleic acid-based assay. Clin Cancer Res 2011;17:1169–80.
7. Pao W, Miller VA, Politi KA, Riely GJ, Somwar R, Zakowski MF, et al. Acquired resistance of lung adenocarcinomas to gefitinib or erlotinib is associated with a second mutation in the EGFR kinase domain. PLoS Med 2005;2:e73.
8. Chong CR, Janne PA. The quest to overcome resistance to EGFR-targeted therapies in cancer. Nat Med 2013;19:1389–400.
9. Sequist LV, Yang JC, Yamamoto N, O'Byrne K, Hirsh V, Mok T, et al. Phase III study of afatinib or cisplatin plus pemetrexed in patients with metastatic lung adenocarcinoma with EGFR mutations. J Clin Oncol 2013;31:3327–34.
10. Park K, Tan EH, O'Byrne K, Zhang L, Boyer M, Mok T, et al. Afatinib versus gefitinib as first-line treatment of patients with EGFR mutation-positive non-small-cell lung cancer (LUX-Lung 7): a phase 2B, open-label, randomised controlled trial. Lancet Oncol 2016;17:577–89.
11. Katakami N, Atagi S, Goto K, Hida T, Horai T, Inoue A, et al. LUX-Lung 4: a phase II trial of afatinib in patients with advanced non-small-cell lung cancer who progressed during prior treatment with erlotinib, gefitinib, or both. J Clin Oncol 2013;31:3335–41.
12. Wu SG, Liu YN, Tsai MF, Chang YL, Yu CJ, Yang PC, et al. The mechanism of acquired resistance to irreversible EGFR tyrosine kinase inhibitor-afatinib in lung adenocarcinoma patients. Oncotarget 2016;7:12404–13.
13. Kim Y, Ko J, Cui Z, Abolhoda A, Ahn JS, Ou SH, et al. The EGFR T790M mutation in acquired resistance to an irreversible second-generation EGFR inhibitor. Mol Cancer Ther 2012;11:784–91.
14. Azuma K, Kawahara A, Sonoda K, Nakashima K, Tashiro K, Watari K, et al. FGFR1 activation is an escape mechanism in human lung cancer cells resistant to afatinib, a pan-EGFR family kinase inhibitor. Oncotarget 2014;5:5908–19.
15. Cortot AB, Repellin CE, Shimamura T, Capelletti M, Zejnullahu K, Ercan D, et al. Resistance to irreversible EGF receptor tyrosine kinase inhibitors through a multistep mechanism involving the IGF1R pathway. Cancer Res 2013;73:834–43.
16. Eberlein CA, Stetson D, Markovets AA, Al-Kadhimi KJ, Lai Z, Fisher PR, et al. Acquired resistance to the mutant-selective EGFR inhibitor AZD9291 is associated with increased dependence on RAS signaling in preclinical models. Cancer Res 2015;75:2489–500.
17. Kurata T, Tamura K, Kaneda H, Nogami T, Uejima H, Asai Go Go, et al. Effect of re-treatment with gefitinib ('Iressa', ZD1839) after acquisition of resistance. Ann Oncol 2004;15:173–4.
18. Wong AS, Seto KY, Chin TM, Soo RA. Lung cancer response to gefitinib, then erlotinib, then gefitinib again. J Thorac Oncol 2008;3:1077–8.
19. Watanabe S, Tanaka J, Ota T, Kondo R, Tanaka H, Kagamu H, et al. Clinical responses to EGFR-tyrosine kinase inhibitor retreatment in non-small cell lung cancer patients who benefited from prior effective gefitinib therapy: a retrospective analysis. BMC Cancer 2011;11:1.
20. Becker A, Crombag L, Heideman DA, Thunnissen FB, van Wijk AW, Postmus PE, et al. Retreatment with erlotinib: Regain of TKI sensitivity following a drug holiday for patients with NSCLC who initially responded to EGFR-TKI treatment. Eur J Cancer 2011;47:2603–6.
21. Ando K, Ohmori T, Inoue F, Kadofuku T, Hosaka T, Ishida H, et al. Enhancement of sensitivity to tumor necrosis factor alpha in non-small cell lung cancer cells with acquired resistance to gefitinib. Clin Cancer Res 2005;11:8872–9.
22. Tabara K, Kanda R, Sonoda K, Kubo T, Murakami Y, Kawahara A, et al. Loss of activating EGFR mutant gene contributes to acquired resistance to EGFR tyrosine kinase inhibitors in lung cancer cells. PLoS One 2012;7:e41017.
23. Shien K, Toyooka S, Yamamoto H, Soh J, Jida M, Thu KL, et al. Acquired resistance to EGFR inhibitors is associated with a manifestation of stem cell-like properties in cancer cells. Cancer Res 2013;73:3051–61.
24. Hata AN, Niederst MJ, Archibald HL, Gomez-Caraballo M, Siddiqui FM, Mulvey HE, et al. Tumor cells can follow distinct evolutionary paths to become resistant to epidermal growth factor receptor inhibition. Nat Med 2016;22:262–9.
25. Janne PA, Yang JC, Kim DW, Planchard D, Ohe Y, Ramalingam SS, et al. AZD9291 in EGFR inhibitor-resistant non-small-cell lung cancer. N Engl J Med 2015;372:1689–99.

Published OnlineFirst March 13, 2017; DOI: 10.1158/1541-7786.MCR-16-0482

26. Sequist LV, Soria JC, Goldman JW, Wakelee HA, Gadgeel SM, Varga A, et al. Rociletinib in EGFR-mutated non-small-cell lung cancer. N Engl J Med 2015;372:1700–9.
27. Janjigian YY, Smit EF, Groen HJ, Horn L, Gettinger S, Camidge DR, et al. Dual inhibition of EGFR with afatinib and cetuximab in kinase inhibitor-resistant EGFR-mutant lung cancer with and without T790M mutations. Cancer Discov 2014;4:1036–45.
28. Roberts PJ, Stinchcombe TE. KRAS mutation: should we test for it, and does it matter? J Clin Oncol 2013;31:1112–21.
29. Linardou H, Dahabreh IJ, Kanaloupiti D, Siannis F, Bafaloukos D, Kosmidis P, et al. Assessment of somatic k-RAS mutations as a mechanism associated with resistance to EGFR-targeted agents: a systematic review and meta-analysis of studies in advanced non-small-cell lung cancer and metastatic colorectal cancer. Lancet Oncol 2008;9:962–72.
30. Cepero V, Sierra JR, Corso S, Ghiso E, Casorzo L, Perera T, et al. MET and KRAS gene amplification mediates acquired resistance to MET tyrosine kinase inhibitors. Cancer Res 2010;70:7580–90.
31. Molina-Arcas M, Hancock DC, Sheridan C, Kumar MS, Downward J. Coordinate direct input of both KRAS and IGF1 receptor to activation of PI3 kinase in KRAS-mutant lung cancer. Cancer Discov 2013;3:548–63.
32. Baxter RC. IGF binding proteins in cancer: mechanistic and clinical insights. Nat Rev Cancer 2014;14:329–41.
33. Yamaoka T, Ohmori T, Ohba M, Arata S, Kishino Y, Murata Y, et al. Acquired resistance mechanisms to combination Met-TKI/EGFR-TKI exposure in Met-amplified EGFR-TKI resistant lung adenocarcinoma harboring an activating EGFR mutation. Mol Cancer Ther 2016;15:3040–54.
34. Dearden S, Stevens J, Wu YL, Blowers D. Mutation incidence and coincidence in non-small-cell lung cancer: meta-analyses by ethnicity and histology (mutMap). Ann Oncol 2013;24:2371–6.
35. Lievre A, Bachet JB, Boige V, Cayre A, Le Corre D, Buc E, et al. KRAS mutations as an independent prognostic factor in patients with advanced colorectal cancer treated with cetuximab. J Clin Oncol 2008; 26:374–9.
36. Roberts PJ, Stinchcombe TE, Der CJ, Socinski MA. Personalized medicine in non-small-cell lung cancer: is KRAS a useful marker in selecting patients for epidermal growth factor receptor-targeted therapy? J Clin Oncol 2010; 28:4769–77.
37. Sasaki H, Hikosaka Y, Kawano O, Moriyama S, Yano M, Fujii Y. Evaluation of Kras gene mutation and copy number gain in non-small cell lung cancer. J Thorac Oncol 2011;6:15–20.
38. Hoa M, Davis SL, Ames SJ, Spanjaard RA. Amplification of wild-type K-ras promotes growth of head and neck squamous cell carcinoma. Cancer Res 2002;62:7154–6.
39. Durkin SG, Ragland RL, Arlt MF, Mulle JG, Warren ST, Glover TW. Replication stress induces tumor-like microdeletions in FHIT/FRA3B. Proc Natl Acad Sci U S A 2008;105:246–51.
40. Nathanson DA, Gini B, Mottahedeh J, Visnyei K, Koga T, Gomez G, et al. Targeted therapy resistance mediated by dynamic regulation of extrachromosomal mutant EGFR DNA. Science 2014;343:72–6.
41. Infante JR, Fecher LA, Falchook GS, Nallapareddy S, Gordon MS, Becerra C, et al. Safety, pharmacokinetic, pharmacodynamic, and efficacy data for the oral MEK inhibitor trametinib: a phase 1 dose-escalation trial. Lancet Oncol 2012;13:773–81.
42. Jackman D, Pao W, Riely GJ, Engelman JA, Kris MG, Janne PA, et al. Clinical definition of acquired resistance to epidermal growth factor receptor tyrosine kinase inhibitors in non-small-cell lung cancer. J Clin Oncol 2010;28:357–60.
43. Guix M, Faber AC, Wang SE, Olivares MG, Song Y, Qu S, et al. Acquired resistance to EGFR tyrosine kinase inhibitors in cancer cells is mediated by loss of IGF-binding proteins. J Clin Invest 2008;118:2609–19.
44. Grill CJ, Cohick WS. Insulin-like growth factor binding protein-3 mediates IGF-I action in a bovine mammary epithelial cell line independent of an IGF interaction. J Cell Physiol 2000;183:273–83.
45. De Mellow JS, Baxter RC. Growth hormone-dependent insulin-like growth factor (IGF) binding protein both inhibits and potentiates IGF-I-stimulated DNA synthesis in human skin fibroblasts. Biochem Biophys Res Commun 1988;156:199–204.
46. Kim WY, Kim MJ, Moon H, Yuan P, Kim JS, Woo JK, et al. Differential impacts of insulin-like growth factor-binding protein-3 (IGFBP-3) in epithelial IGF-induced lung cancer development. Endocrinology 2011; 152:2164–73.

AACR American Association for Cancer Research

Molecular Cancer Research

Distinct Afatinib Resistance Mechanisms Identified in Lung Adenocarcinoma Harboring an EGFR Mutation

Toshimitsu Yamaoka, Tohru Ohmori, Motoi Ohba, et al.

Mol Cancer Res Published OnlineFirst March 13, 2017.

Published OnlineFirst September 9, 2016; DOI: 10.1158/1535-7163.MCT-16-0313

Cancer Biology and Signal Transduction

Molecular Cancer Therapeutics

Acquired Resistance Mechanisms to Combination Met-TKI/EGFR-TKI Exposure in Met-Amplified EGFR-TKI–Resistant Lung Adenocarcinoma Harboring an Activating EGFR Mutation

Toshimitsu Yamaoka[1], Tohru Ohmori[1], Motoi Ohba[1], Satoru Arata[1,2], Yasunari Kishino[3], Yasunori Murata[3], Sojiro Kusumoto[3], Hiroo Ishida[4], Takao Shirai[3], Takashi Hirose[3], Tsukasa Ohnishi[3], and Yasutsuna Sasaki[4]

Abstract

Met-amplified EGFR-tyrosine kinase inhibitor (TKI)-resistant non–small cell lung cancer (NSCLC) harboring an activating EGFR mutation is responsive to concurrent EGFR-TKI and Met-TKI treatment in a preclinical model. Here, we determined that Met-amplified gefitinib-resistant cells acquire dual resistance to inhibition of EGFR and Met tyrosine kinase activities. PC-9 lung adenocarcinoma cells harboring 15-bp deletions (Del E746_A750) in *EGFR* exon 19 were treated with increasing concentrations of the Met-TKI PHA665752 and 1 μmol/L gefitinib for 1 year; three resistant clones were established via Met amplification. The three dual-resistance cell lines (PC-9DR2, PC-9DR4, and PC-9DR6, designated as DR2, DR4, and DR6, respectively) exhibited different mechanisms for evading both EGFR and Met inhibition. None of the clones harbored a secondary mutation of *EGFR* T790M or a *Met* mutation. Insulin-like growth factor (IGF)/IGF1 receptor activation in DR2 and DR4 cells acted as a bypass signaling pathway. Met expression was attenuated to a greater extent in DR2 than in PC-9 cells, but was maintained in DR4 cells by overexpression of IGF-binding protein 3. In DR6 cells, Met was further amplified by association with HSP90, which protected Met from degradation and induced SET and MYND domain-containing 3 (SMYD3)-mediated *Met* transcription. This is the first report describing the acquisition of dual resistance mechanisms in NSCLC harboring an activating EGFR mutation to Met-TKI and EGFR-TKI following previous EGFR-TKI treatment. These results might inform the development of more effective therapeutic strategies for NSCLC treatment. *Mol Cancer Ther; 15(12); 3040–54. ©2016 AACR.*

Introduction

EGFR-tyrosine kinase inhibitors (EGFR-TKI) such as gefitinib, erlotinib, and afatinib are highly effective in patients with non–small cell lung cancer (NSCLC) harboring activating *EGFR* mutations in exons 19 and 21 (1). However, nearly all of these patients exhibit tumor regrowth within a year as a result of acquired resistance to EGFR-TKI. Several resistance mechanisms have been proposed including acquisition of a T790M mutation in *EGFR* exon 20, transformation to SCLC, and the emergence of bypass signaling pathways such as Met, HER2 (also known as erbB-2), insulin-like growth factor 1 receptor (IGF1R), and Axl (2–4).

Secondary T790M mutation and Met amplification are the two major causes of EGFR-TKI resistance. Several drugs targeting EGFR T790M are currently being tested in clinical trials for their ability to overcome this resistance (5, 6). A drug that can overcome Met amplification–associated resistance is also being tested clinically in combination with EGFR-TKI and Met-TKI in patients with NSCLC and acquired resistance to EGFR-TKI treatment (ClinicalTrials.gov identifier NCT02468661). It is not known whether NSCLC can acquire resistance to the combination of EGFR-TKI and Met-TKI in Met-amplified, EGFR-TKI–resistant NSCLC.

The expression of Met, a receptor tyrosine kinase (RTK) for hepatocyte growth factor, is dysregulated in many tumors; as such, Met is a major target for cancer therapy. Met amplification is observed in lung, breast, prostate, renal, esophageal, and gastric cancers (7), and Met-amplified cancer cells, which proliferate in the absence of ligand, are dependent on Met signaling for survival; their proliferation is therefore effectively suppressed by Met-TKI treatment (8–11). However, some preclinical studies have reported acquired resistance to initial Met-TKI treatment. EGFR activation (which functions as a bypass signaling mechanism that acts via aberrant TGFα expression) and the emergence of a Met Y1230H mutation (which increases Met activity and reduces its affinity for

[1]Institute of Molecular Oncology, Showa University, Tokyo, Japan. [2]Center for Biotechnology, Showa University, Tokyo, Japan. [3]Division of Allergology and Respiratory Medicine, Department of Medicine, Showa University School of Medicine, Tokyo, Japan. [4]Division of Medical Oncology, Department of Medicine, Showa University School of Medicine, Tokyo, Japan.

Note: Supplementary data for this article are available at Molecular Cancer Therapeutics Online (http://mct.aacrjournals.org/).

Corresponding Author: Toshimitsu Yamaoka, Institute of Molecular Oncology, Showa University, 1-5-8 Hatanodai, Shinagawa-ku, Tokyo 142-8555, Japan. Phone: 81-3-3784-8146; Fax: 81-3-3784-2299; E-mail: yamaoka.t@med.showa-u.ac.jp

doi: 10.1158/1535-7163.MCT-16-0313

Published OnlineFirst September 9, 2016; DOI: 10.1158/1535-7163.MCT-16-0313

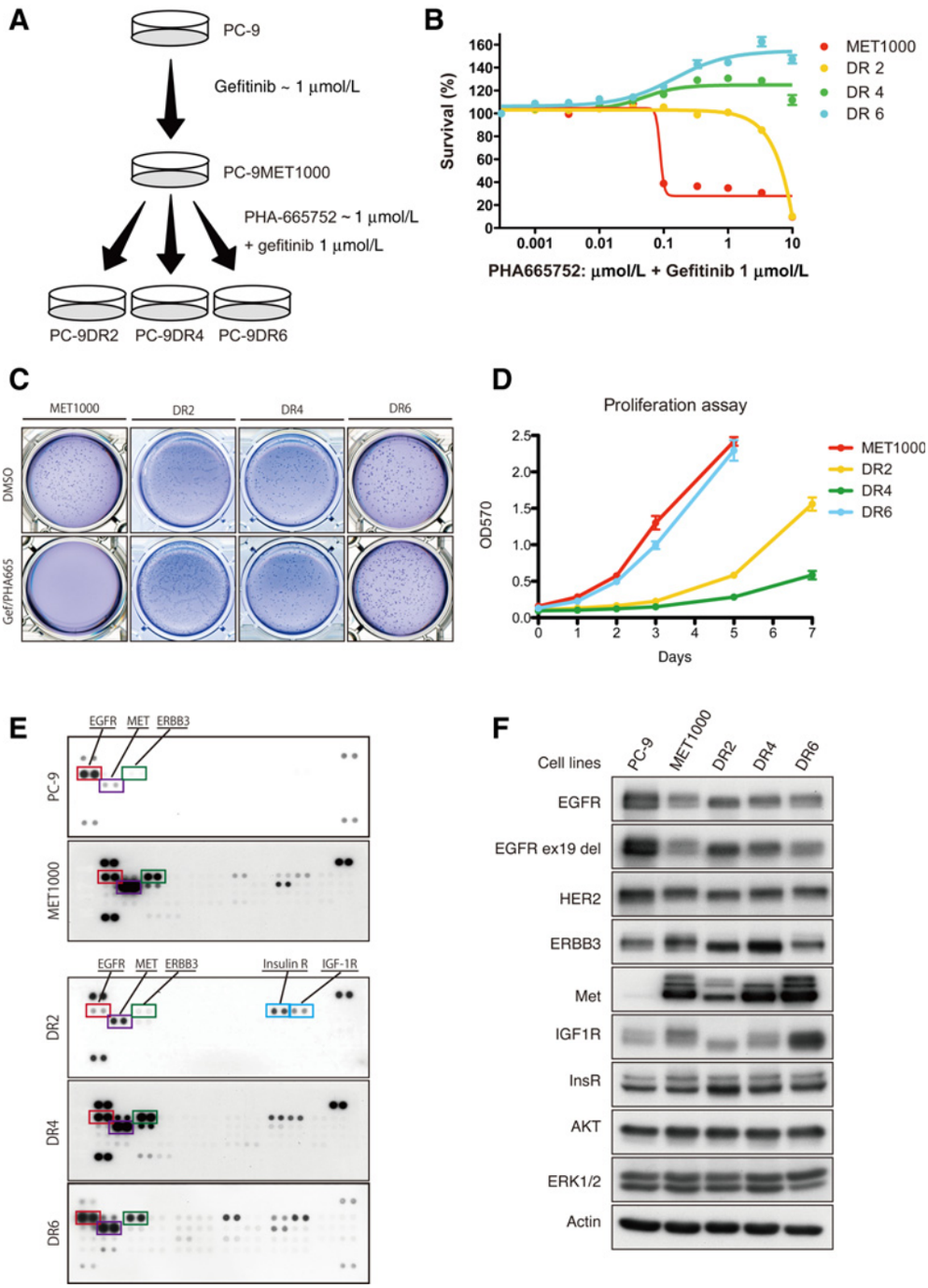

Figure 1.

PC-9MET1000 cells were treated with increasing concentrations of Met-TKI PHA665752 in combination with 1 μmol/L gefitinib to establish dual-resistant clones. **A,** Schema of generating dual-resistance: DR clones from PC-9MET1000 cells. **B,** Cells were seeded into 96-well plates at 5×10^3 cells/50 μL growth media/well, then preincubated overnight and treated with PHA665752 at the indicated concentrations under 1 μmol/L gefitinib exposure for 72 hours. An MTT assay was performed and the OD570 measured. Data are the means ± SEM for 6–12 wells. **C,** Anchorage-independent proliferation in soft agar. Cells (1×10^4) resuspended with 0.3% agar containing 10% FBS were seeded into 6-well plates precoated with 0.6% soft agar. The following day, cells were treated with gefitinib and PHA665752 and then incubated for 14–21 days. Colonies were stained with 0.005% crystal violet for 1 hour. **D,** Cells were seeded into 96-well plates at 5×10^2 cells/100 μL/well. Following an MTT assay, the OD570 was measured at days 0, 1, 2, 3, 5, and 7. **E,** A human phospho-RTK array was used to determine the candidates for bypass pathways by comparison of PC-9, MET100, DR2, DR4, and DR6 cell lysates. **F,** In PC-9, MET1000, DR2, DR4, and DR6 cells, the basal expression of EGFR, EGFR ex19 del, HER2, ERBB3, Met, IGF1R, Insulin receptor (InsR), AKT, and ERK1/2 was determined by Western blot analysis. β-Actin was included as a loading control.

Published OnlineFirst September 9, 2016; DOI: 10.1158/1535-7163.MCT-16-0313

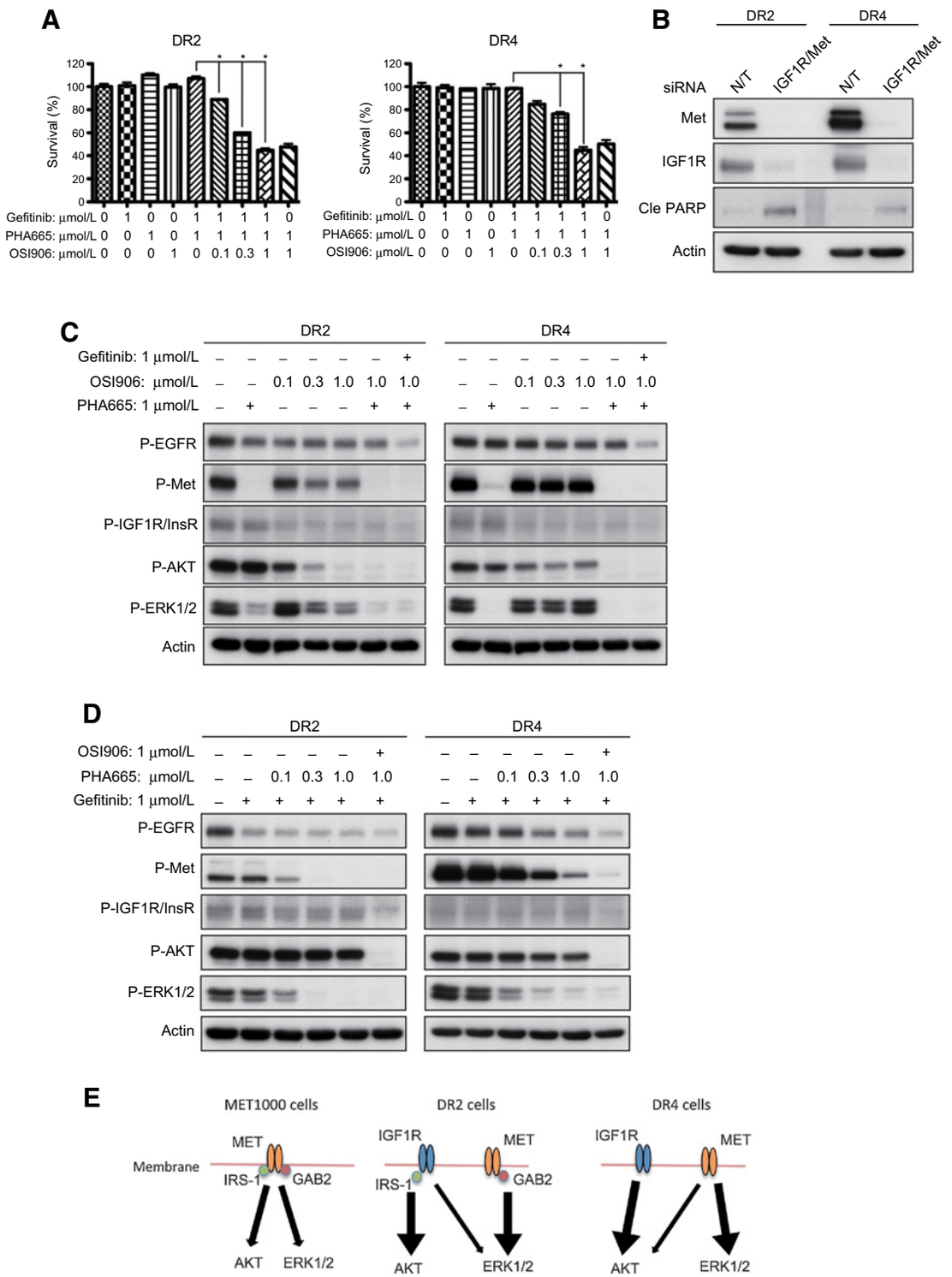

Figure 2.

IGF1R phosphorylation protects DR2 and DR4 cells from apoptosis under gefitinib and PHA665752 exposure. **A,** DR2 and DR4 cells were seeded into 96-well plates at 5×10^3 cells/50 μL of growth media/well, then preincubated overnight and treated with gefitinib, PHA665752 (PHA665), and/or OSI906 with the indicated concentrations for 72 hours. An MTT assay was performed and the OD570 measured. Data are the means ± SEM for 6–12 wells. *, $P < 0.01$ for comparison of the indicated pairs. **B,** DR2 and DR4 cells were transfected with nontargeting (N/T) siRNA or siRNA directed against Met and IGF1R. Met and IGF1R knockdown was determined by Western blot analysis. (*Continued on the following page.*)

Published OnlineFirst September 9, 2016; DOI: 10.1158/1535-7163.MCT-16-0313

PHA665752) have been observed in SNU638 gastric cancer cells (12). In addition, *Met* gene amplification resulted in resistance to Met-TKIs (PHA665752 and JNJ38877605) along with wild-type *KRAS* amplification in GTL-16 gastric cancer cells (13).

The combination of Met-TKI and EGFR-TKI has been shown to overcome Met-amplified EGFR-TKI resistance in HCC827GR cells (14, 15). HCC827EPR cells developed by treating HCC827 cells with increasing concentrations of erlotinib and 1 μmol/L PHA665752 and harboring an activating EGFR mutation in exon 19 resulted in EGFR T790M mutation without *Met* gene amplification, whereas erlotinib-resistant HCC827 (HCC827ER) cells exhibited a gain in *Met* gene copy number (16). However, there have been no reports of dual resistance to sequential EGFR-TKI and Met-TKI treatment (i.e., EGFR-TKI followed by Met-TKI plus EGFR-TKI) in conjunction with Met amplification.

We previously reported that PC-9 lung adenocarcinoma cells, which harbor a 15-bp deletion (Del E746_A750) in exon 19 of *EGFR*, developed gefitinib resistance caused by Met amplification with continuous dose escalation up to 1 μmol/L gefitinib for a year; this cell line was designated as PC-9MET1000 (or simply MET1000; ref. 17). Cell proliferation was suppressed in these cells upon concurrent treatment with Met-TKI and EGFR-TKI.

In this study, we established the independent dual resistance clones PC-9DR2, PC-9DR4, and PC-9DR6 (designated as DR2, DR4, and DR6, respectively) from MET1000 cells using increasing concentrations of Met-TKI PHA665752 with concurrent 1 μmol/L gefitinib treatment. None of the clones had secondary mutation of EGFR T790M or a mutation in Met, and harbored only the original 15-bp deletion in EGFR exon 19. The dual resistance mechanisms were of two types. The IGF/IGF1R pathway was activated as bypass signaling in DR2 and DR4 cells, as evidenced by IGF-binding protein (IGFBP) down- and upregulation, respectively. In addition, overamplification of Met in association with HSP90 was detected in DR6 cells. These findings provide insight into the development of acquired resistance induced by EGFR and Met inhibition, and are expected to serve as a basis for improved therapeutic strategies. This is also the first report of acquired resistance to concurrent treatment with Met-TKI and EGFR-TKI in Met-amplified NSCLC with acquired resistance to previous EGFR-TKI treatment.

Materials and Methods

Cell lines, antibodies, and reagents

The PC-9 human NSCLC cell line established from a previously untreated patient was donated by K. Hayata (Tokyo Medical College, Tokyo, Japan) during the 1980s and cultured in RPMI1640 medium supplemented with 10% FBS, penicillin (100 U/mL), and streptomycin (100 μg/mL) in a 5% CO_2 incubator at 37°C. The gefitinib-resistant PC-9MET1000 cell line was established in our laboratory (17). A recombinant mouse cell line expressing human IGF1R was provided by Dr. Vigneri in 2015 (University of Catania, Catania, Italy; ref. 18). Cells were passaged for less than 4 months before renewal from the frozen stock. Cell lines used in this study were authenticated by short tandem repeat analysis at the Japanese Collection of Research Bioresources (JCRB) cell bank in 2013. All antibodies were purchased from Cell Signaling Technology with the exception of antibodies against IGFBP2, IGFBP3, IGFBP4, and HSP90 (Santa Cruz Biotechnology). Gefitinib and BI836845 were provided by AstraZeneca Pharmaceuticals and Boehringer-Ingelheim, respectively, and other inhibitors were obtained from Selleck Chemicals.

Establishment of PC-9MET1000 clones with acquired resistance to the Met-TKI PHA665752 under 1 μmol/L gefitinib exposure

To obtain clones with acquired resistance, MET1000 cells were exposed to increasing concentrations of the Met-TKI PHA665752 in growth medium containing 1 μmol/L gefitinib. Starting with a dose that was approximately 1/10 of the half-maximal inhibitory concentration (IC_{50}), the dose was progressively increased over 1 year to 1 μmol/L PHA665752. Three PC-9 dual-resistant (PC-9DR) clones were obtained and designated as DR2, DR4, and DR6. The established resistant cell lines were maintained in continuous culture medium containing the achieved dose of inhibitor.

Cell proliferation and soft agar colony formation assays

Cell proliferation was measured with the 3-(4,5-dimethylthiazol-2-yl)-2,5-diphenyltetrazolium bromide (MTT) assay (Promega) as described previously (17). Cells (5×10^2/well) were seeded in 96-well plates and incubated overnight, and the assay was carried out on days 0, 1, 2, 3, 5, and 7. To inhibit cell proliferation, 5×10^3 cells/well were seeded in 96-well plates and incubated overnight, and then continuously exposed to the indicated concentrations of inhibitor for 72 hours. The optical density at 570 nm (OD_{570}) was measured with a Powerscan HT microplate reader (BioTek) and is expressed as a percentage of the value of control cells. We prepared 6–12 replicates and the experiments were repeated at least three times. Data were graphically displayed using GraphPad Prism v.5.0 software (GraphPad Inc.). For the soft agar colony formation assay, 1×10^4 cells resuspended in 0.3% agar containing 10% FBS were seeded in 6-well plates precoated with 0.6% soft agar. The following day, cells were treated with the indicated inhibitors for 14–21 days; colonies were stained with crystal violet.

Phospho-RTK profiling

The Human Phospho-RTK Array (R&D Systems) was used to measure relative levels RTK tyrosine phosphorylation. Membranes contained spotted antibodies corresponding to 49 distinct

(*Continued.*) Immunoblot analysis for PARP cleavage demonstrates the induction of apoptosis. Blots are representative of three independent experiments. β-Actin was included as a loading control. **C** and **D,** DR2 and DR4 cells were exposed to graded concentrations (0.1–1.0 μmol/L) of OSI906 (**C**) or PHA665752 (**D**) for 24 hours and cell lysates were immunoblotted for phosphorylated Y 1068 EGFR (P-EGFR), phosphorylated Y1234/1235 Met (P-Met), phosphorylated Y 1135/1136 IGF1R/insulin receptor-β (tyr1150/1151; P-IGF1R/InsR), phosphorylated AKT (Ser473; P-AKT), and phosphorylated ERK1/2 (P-ERK1/2). **E,** Schematic of the signaling in MET1000, DR2, and DR4 cells with respect to the association of the receptors (Met and IGF1R) and their downstream targets (ERK1/2 and AKT).

Published OnlineFirst September 9, 2016; DOI: 10.1158/1535-7163.MCT-16-0313

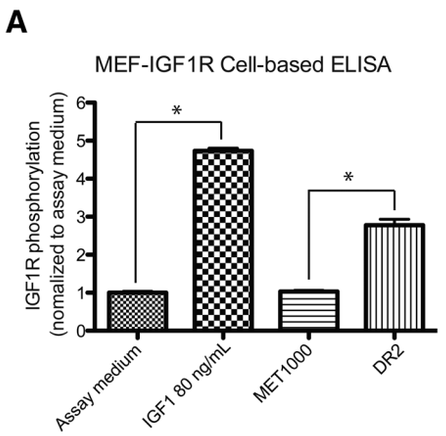

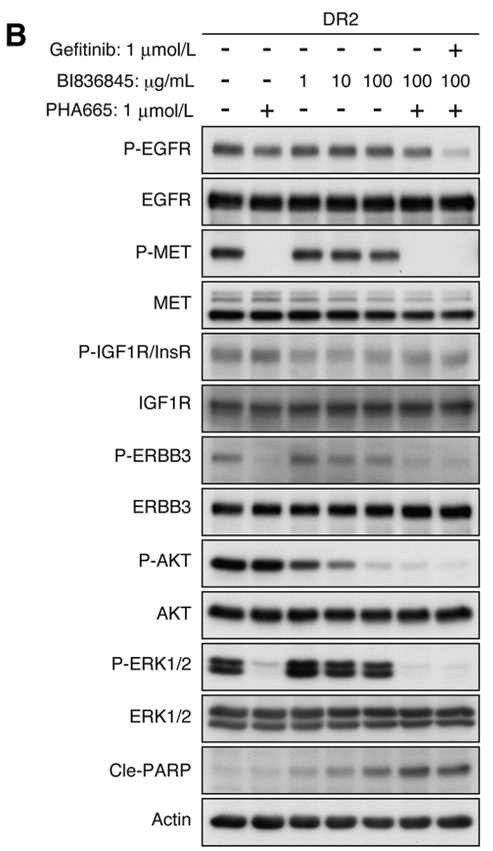

C

	MET1000	DR2	*P*
Igf1r	1.0 ± 0.04	0.7 ± 0.1	0.02
Igf2r	1.0 ± 0.07	2.1 ± 0.1	< 0.0001
Ins r	1.0 ± 0.05	2.1 ± 0.1	< 0.0001
Igf-1	1.1 ± 0.1	1.2 ± 0.2	0.13
Igf-2	1.0 ± 0.08	0.1 ± 0.01	< 0.0001
Igfbp1	1.0 ± 0.1	1.8 ± 0.2	0.001
Igfbp2	1.1 ± 0.2	0.3 ± 0.06	0.002
Igfbp3	1.0 ± 0.08	1.2 ± 0.1	0.03
Igfbp4	1.1 ± 0.2	0.7 ± 0.06	0.02
Igfbp5	1.1 ± 0.2	0.1 ± 0.01	0.002
Igfbp6	1.1 ± 0.2	0.9 ± 0.1	0.12

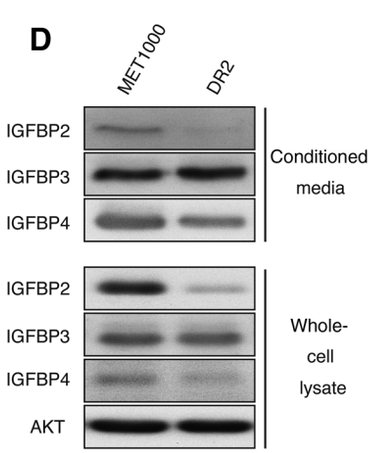

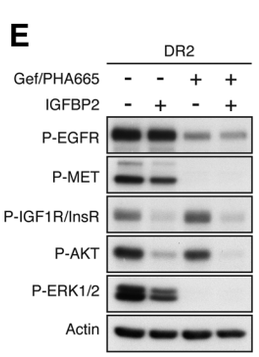

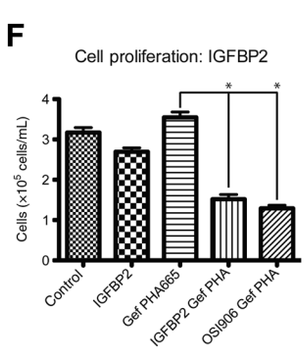

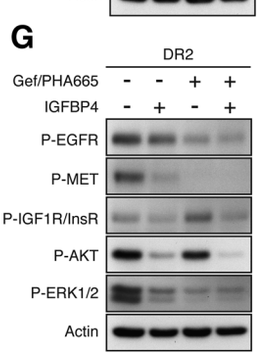

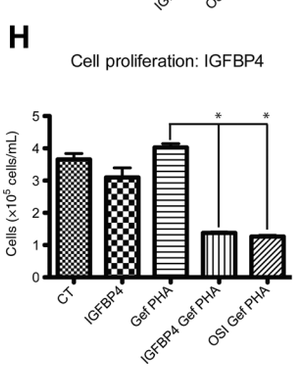

Published OnlineFirst September 9, 2016; DOI: 10.1158/1535-7163.MCT-16-0313

RTKs as well as positive and negative controls. Cell lines were cultured to subconfluence and protein was then isolated according to the manufacturer's protocol.

Western blot analysis

Treated cells were washed twice with ice-cold PBS and lysed with modified radioimmunoprecipitation assay (RIPA) buffer consisting of 50 mmol/L Tris (pH 7.4), 150 mmol/L NaCl, 1 mmol/L EDTA, 1% Nonidet P-40, 0.25% sodium deoxycholate, 0.1% SDS, and 1.0% protease and phosphatase inhibitor cocktails (Sigma-Aldrich). Cell suspensions were centrifuged and protein concentration was determined using the DC Protein assay (Bio-Rad). Equal amounts of protein were mixed and boiled in Laemmli buffer. Samples were separated by 8%–10% SDS-PAGE, blotted on a polyvinylidene difluoride membrane, treated with enhanced chemiluminescence solution, and exposed to film. β-Actin and at least one additional protein were used as loading controls. All experiments were repeated three times.

RNA interference

Nontargeting siRNA (controls) and SMARTpool siRNAs targeting EGFR, ERBB3, Met, IGF1R, insulin receptor (InsR), IGFBP3, dual specificity phosphatase (DUSP)4, and SET and MYND domain–containing (SMYD)3 were purchased from Dharmacon. Cells were seeded in 6-well plates with RPMI1640 medium supplemented with 10% FBS without antibiotics. The following day, the cells were transfected with 100 pmol/well siRNA using Lipofectamine 2000 (Life Technologies) according to the manufacturer's instructions, and then analyzed 72 hours later.

Cell-based IGF1R phosphorylation assay

IGF bioactivity was measured using mouse embryonic fibroblasts (MEF) derived from IGF1R-deficient mice and engineered to overexpress human IGF1R (MEF-IGF1R). MEFs were maintained in DMEM supplemented with 10% FBS, 1 mmol/L sodium pyruvate, 0.075% sodium bicarbonate, nonessential amino acids (Gibco/Life Technologies), and 0.3 μg/mL puromycin at 37°C and 5% CO_2. MEF-IGF1R cells (1×10^4) were seeded in 96-well plates and incubated for 24 hours, starved in medium containing 0.5% FBS overnight, then exposed to either IGF1 (80 ng/mL) as a positive control, or MET1000 or DR2 cell culture medium for 30 minutes at 37°C. MEF-IGF1R cells were fixed in 4% formaldehyde, quenched by treatment with 1.2 wt% hydrogen peroxide, blocked with 5% BSA, and then incubated with phospho-IGF1R-β (Tyr1135/1136)/insulin receptor-β (Tyr1150/1151) antibody overnight, followed by secondary antibody and tetramethylbenzidine solution. The reaction was terminated by adding 1 mol/L phosphoric acid, and the absorbance at OD_{450} was measured with a Powerscan HT microplate reader.

Reverse transcription real-time PCR

Total RNA was isolated via the guanidium isothiocyanate method using the RNeasy Mini kit (Qiagen) according to the manufacturer's instructions, and used to prepare cDNA with random 6-mers and a reverse transcription PCR kit (TaKaRa Bio). *EGFR*, *ERBB3*, *Met*, *IGF1R*, *IGF2R*, *InsR*, *IGF1*, *IGF2*, and *IGFBP1–6* mRNA levels were quantified with a fluorescence-based RT-PCR detection system (GeneAmp 5700; Applied Biosystems) using the primer sets shown in Supplementary Table S1A. *GAPDH* was used as an internal control.

EGFR and *Met* sequence analysis

Exons 14–21 of the *Met* gene were amplified from genomic DNA by PCR. The products were purified and sequenced by FASMAC. Cycleave PCR (19) was carried out by SRL to detect *EGFR* mutations including G719X, deletion of exon 19, T790M, L858R, and L861Q. The primers used for PCR and sequencing are shown in Supplementary Table S1B.

Dual-luciferase reporter assay

Cells were seeded in a 6-well plate and transfected with 4 μg Met promoter-luciferase plasmid (pGL4-phMET; Riken BRC DNA Bank) and 0.2 μg *Renilla* luciferase. After 24 hours, the HSP90 inhibitor AUY992 (0.01–0.1 μmol/L) was added to the cells for 24 hours. Luciferase activity was evaluated using the Dual-Luciferase Reporter assay system (Promega) according to the manufacturer's instructions. Data are shown as the means ± SEM of 6 wells, and $P < 0.01$ relative to the control value was considered statistically significant. Data are representative of three independent experiments.

Figure 3.

IGFBP downregulation leads to increased bioactivity of IGF1R ligands (IGF-1 or IGF-2) and induces IGF1R activation as acquired resistance to gefitinib and PHA665752 in DR2 cells. **A,** In mouse embryonic fibroblasts (MEF) engineered to express human IGF1R (MEF-IGF1R), IGF1 (80 ng/mL) effectively phosphorylated human IGF1R and was thus used as a positive control, whereas the assay medium (0.5% FBS) did not and was used as a negative control. MET1000 and DR2 cells were seeded at 2×10^5 cells/well and incubated for 48 hours, whereupon the medium was collected. The conditioned culture medium was then exposed to MRF-IGF1R cells and the stimulation of IGF1R phosphorylation was determined by ELISA. *, $P < 0.01$ for comparison of the indicated pairs. Results presented are representative of three independent experiments. **B,** DR2 cells were exposed to graded concentrations of BI836845, a humanized mAb for IGF1 and IGF2, in the presence or absence of gefitinib and/or PHA665752 for 24 hours and cell lysates were immunoblotted for the indicated primary antibodies. β-Actin was included as a loading control. **C,** MET1000 and DR2 cellular mRNA transcripts were quantified by real-time RT-PCR and normalized to *GAPDH*. Data are presented relative to MET1000 values, as means ± SEM ($n = 8$). **D,** The conditioned medium from 2×10^6 cells was collected after 24-hour incubation and concentrated 20-fold by ultrafiltration. Conditioned media or whole-cell lysate proteins were subjected to immunoblotting with IGFBP2, IGFBP3, IGFBP4, or AKT antibodies. **E** and **G,** DR2 cells were exposed to human recombinant IGFBP2 (1 μg/mL) or IGFBP4 (1 μg/mL) in the presence or absence of 1 μmol/L gefitinib and 1 μmol/L PHA665752 for 24 hours. β-Actin was included as a loading control. **F** and **H,** DR2 cells were seeded into 96-well plates at 5×10^3 cells/50-μL growth media/well, then preincubated overnight and treated with 1 μg/mL IGFBP2 or IGFBP4 in the presence or absence of 1 μmol/L gefitinib and 1 μmol/L PHA665752 for 72 hours. The number of cells was counted by a TC10 automated cell counter (Bio-Rad). Data are the means ± SEM for 6–12 wells. *, $P < 0.01$ for comparison of the indicated pairs.

Published OnlineFirst September 9, 2016; DOI: 10.1158/1535-7163.MCT-16-0313

A

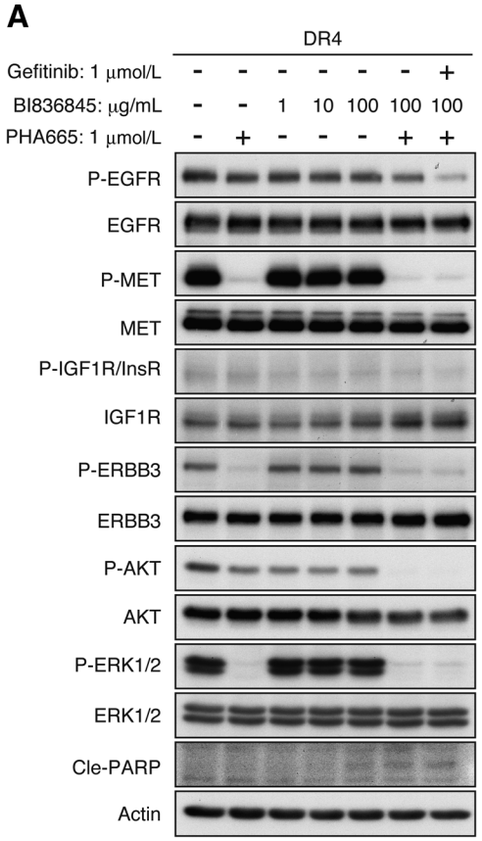

B

	MET1000	DR4	*P*
Egfr	1.0 ± 0.05	1.2 ± 0.04	0.0003
Erbb3	1.0 ± 0.07	1.3 ± 0.04	0.002
Met	1.0 ± 0.1	1.5 ± 0.1	0.02
Igf1r	1.0 ± 0.04	0.89 ± 0.03	0.002
Igf2r	1.0 ± 0.07	1.7 ± 0.07	< 0.0001
Insr	1.0 ± 0.05	2.0 ± 0.2	0.001
Igf1	1.1 ± 0.1	2.5 ± 0.4	0.009
Igf2	1.0 ± 0.08	0.86 ± 0.1	0.1
Igfbp1	1.0 ± 0.1	2.6 ± 0.3	0.0009
Igfbp2	1.2 ± 0.2	1.0 ± 0.2	0.1
Igfbp3	1.0 ± 0.08	88.7 ± 4.0	< 0.0001
Igfbp4	1.1 ± 0.2	0.8 ± 0.1	< 0.0001
Igfbp5	1.1 ± 0.2	0.1 ± 0.02	0.001
Igfbp6	1.1 ± 0.2	2.3 ± 0.5	0.005

C1

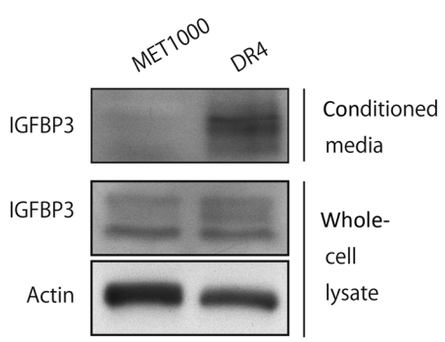

C2

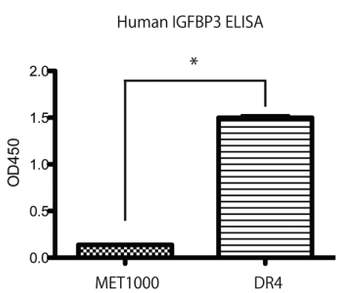

D

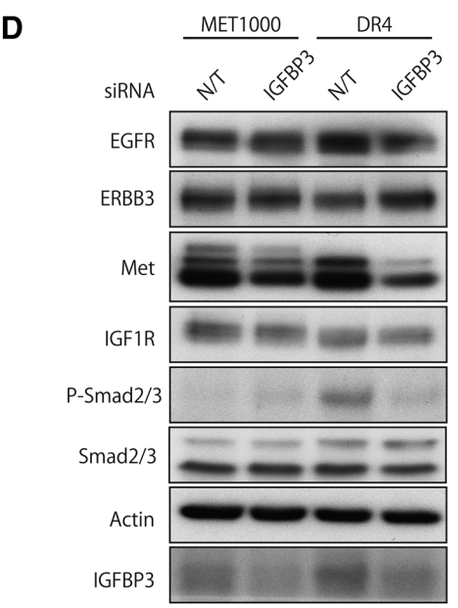

E

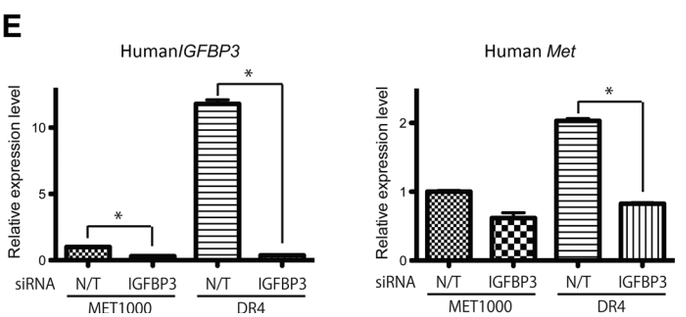

Published OnlineFirst September 9, 2016; DOI: 10.1158/1535-7163.MCT-16-0313

IGFBP levels in cell culture supernatants

Serum-free conditioned medium from 2×10^6 cells grown for 24 hours was concentrated using centrifugal filter devices (Millipore) and analyzed by Western blotting using antibodies against IGFBP2, IGFBP3, and IGFBP4. The IGFBP3 level in the culture medium was measured by ELISA (Abcam).

Statistical analysis

Data are presented as the means ± SEM and were analyzed using GraphPad Prism v.5.0 software. Statistical significance was evaluated with the two-tailed Student *t* test, and unless otherwise noted, a $P < 0.05$ was considered statistically significant.

Results

Characteristics of PC-9MET1000 clones with acquired resistance to the Met-TKI PHA665752 under 1 μmol/L gefitinib exposure

We established gefitinib-resistant PC-9 cells (designated as MET1000). This cell line showed Met amplification instead of a T790M secondary mutation in *EGFR* exon 20 (Fig. 1F; Supplementary Table S2A). Other groups have reported that PC-9 cells invariably develop the T790M mutation during acquisition of EGFR-TKI resistance (20–24). The discrepancy between these previously reported findings and our results, which both incorporated PC-9 cells, is unclear. In cases of EGFR-TKI resistance owing to Met amplification, the combination of EGFR-TKI and Met-TKI was effective in overcoming this resistance. To identify mechanisms of extreme resistance, we treated MET1000 cells with increasing concentrations of the Met-TKI PHA665752 up to a concentration of 1 μmol/L under 1 μmol/L gefitinib for 1 year. Three independent cell lines designated as DR2, DR4, and DR6 were established (Fig. 1A), which were resistant to a combination of gefitinib and PHA665752, as determined by the MTT and colony formation assays (Fig. 1B and C). The proliferation rate of DR6 cells was similar to that of parental MET1000 cells; however, growth was slower in DR2 and DR4 cells (Fig. 1D). A mutation analysis of *EGFR* and *Met* by direct sequencing and cycleave PCR found no acquired mutations in any of the cell lines (Supplementary Table S2A and S2B), leading us to speculate that a bypass signaling mechanism was activated. Indeed, a phospho-RTK array revealed activation of IGF1R and InsR under gefitinib and PHA665752 treatment in DR2 and DR4 cells (quantitated by densitometric analysis; Supplementary Fig. S1A), whereas RTK phosphorylation patterns were similar between MET1000 and DR6 cells (Fig. 1E). Met expression was downregulated and that of EGFR was upregulated relative to baseline in DR2 cells. The levels of these receptors were comparable with and higher than those in MET1000 in DR4 and DR6 cells, respectively (Fig. 1F).

Activation of IGF/IGF1R signaling is required for the survival of DR2 and DR4 cells under EGFR-TKI and Met-TKI treatment

The phospho-RTK array indicated that the activation of IGF1R and/or InsR signaling is required for DR2 and DR4 cell survival (Fig. 1E and Supplementary Fig. S1A). To confirm this possibility, the cells were treated with OSI906, a TKI that targets IGF1R and InsR, in the presence of 1 μmol/L gefitinib and 1 μmol/L PHA665752. DR2 and DR4 cell proliferation was suppressed by this treatment (Fig. 2A), but not by the combination of 1 μmol/L gefitinib and other Met-TKIs (Supplementary Fig. S1B). Both the *IGF1R* and *InsR* genes are expressed in many cancers and this tyrosine kinase class of membrane receptors forms homo- and heterodimers, then activates downstream signals. We then investigated whether IGF1R or InsR is required for bypass signaling by siRNA-mediated knockdown. Loss of *IGF1R* but not *InsR* resulted in AKT dephosphorylation in both DR2 and DR4 cells, suggesting that IGF1R was activated as a bypass signal (Supplementary Fig. S1C and S1D). Apoptosis was induced upon the suppression of IGF1R and Met in DR2 and DR4 cells (Fig. 2B). To clarify the association between these receptors and downstream AKT and extracellular signal-regulated kinase (ERK)1/2 signaling, MET1000 and DR2 cells were exposed to PHA665752 and/or OSI906 in the presence or absence of gefitinib. In MET1000 cells, PHA665752 inhibited the phosphorylation of Met, EGFR, and ERBB3 and inhibited AKT and ERK1/2 (Supplementary Fig. S2A and S2B). DR2 and DR4 cells were next exposed to increasing concentrations of PHA665752 and/or OSI906. IGF1R phosphorylation was attenuated in a dose-dependent manner by OSI906 treatment, resulting in the inhibition of AKT in DR2 and DR4 cells. Furthermore, ERK1/2 activation was partly suppressed by OSI906 in DR2 cells (Fig. 2C). Met phosphorylation was decreased in a dose-dependent matter, whereas ERK1/2 was inhibited by PHA665752 treatment, although AKT remained activated in both DR2 and DR4 cells (Fig. 2D). These results suggest that two distinct signaling pathways, Met-ERK1/2 and IGF1R-AKT, function in DR2 and DR4 cells (Fig. 2E).

Total Met expression was decreased, whereas EGFR expression was increased in DR2 cells (Fig. 1F). Upon treatment with PHA665752, Met and ERBB3 phosphorylation was attenuated, resulting in decreased ERK1/2 activation via growth factor

Figure 4.

IGFBP3 upregulation leads to increased Met expression via Smad2/3 activation and results in Met-TKI resistance accompanying bypass signaling of IGF1R in DR4 cells. **A,** DR4 cells were exposed to graded concentrations of BI836845, a humanized mAb for IGF1 and IGF2, in the presence or absence of gefitinib and/or PHA665752 for 24 hours and the cell lysates immunoblotted for the indicated primary antibodies. β-Actin was included as a loading control. **B,** MET1000 and DR4 cellular mRNA transcripts were quantified by real-time RT-PCR and normalized to *GAPDH*. Data are presented relative to MET1000 values, as means ± SEM ($n = 8$). **C,** The conditioned medium from 2×10^6 MET1000 or DR4 cells was collected after 24-hour incubation and concentrated 20-fold by ultrafiltration. These conditioned media or 20-μg whole-cell lysate proteins were subjected to immunoblotting with IGFBP3 or β-actin antibodies (1). 2, Human IGFBP3 ELISA was performed with MET1000 and DR4 cell culture medium. *, $P < 0.01$ for comparison of the indicated pairs. **D,** MET1000 and DR4 cells were transfected with nontargeting (N/T) siRNA or siRNA directed against IGFBP3. IGFBP3 knockdown was determined by Western blot analysis. Immunoblot analysis for EGFR, ERBB3, Met, IGF1R, Smad2/3, and phosphorylated Smad2/3 is shown. β-Actin was included as a loading control. Blots are representative of three independent experiments. **E,** MET1000 and DR4 cellular *IGFBP3* and *Met* mRNA transcripts were quantified by real-time RT-PCR and normalized to *GAPDH*. Data are presented relative to MET1000 values as means ± SEM ($n = 8$).

Published OnlineFirst September 9, 2016; DOI: 10.1158/1535-7163.MCT-16-0313

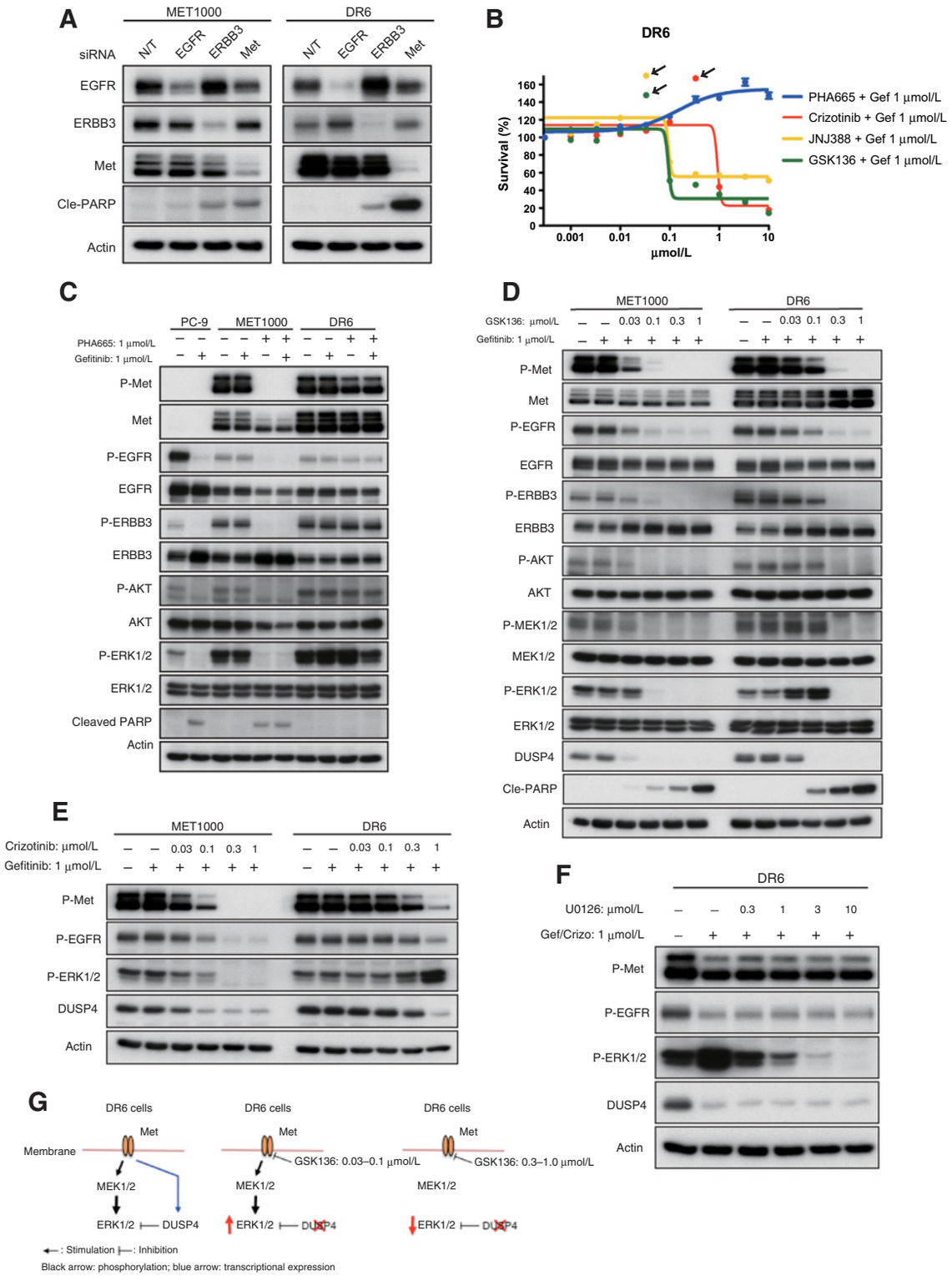

Figure 5.

Expression of overamplified *Met* leads to Met-TKI resistance in DR6 cells. **A,** MET1000 and DR6 cells were transfected with nontargeting (N/T) siRNA or siRNA directed against EGFR, ERBB3, or Met. Knockdown of EGFR, ERBB3, and Met was determined by Western blot analysis. Immunoblot analysis for PARP cleavage demonstrates the induction of apoptosis. Blots are representative of three independent experiments. **B,** DR6 cells were seeded into 96-well plates at 5×10^3 cells/50-µL growth media/well, then preincubated overnight and treated with PHA665752 (PHA665), crizotinib, JNJ38877605 (JNJ388), or GSK1363089 (GSK136) at the indicated concentrations under 1 µmol/L gefitinib exposure for 72 hours. (*Continued on the following page.*)

Published OnlineFirst September 9, 2016; DOI: 10.1158/1535-7163.MCT-16-0313

receptor-binding protein 2-associated binding protein (GAB)2, a scaffolding protein that mediates interactions with downstream effectors such as Src homology domain (SH) protein 2, p85, phospholipase C-γ, SH2-containing transforming protein, and SH2-containing inositol phosphatase (25). GAB2 plays a critical role in signal transduction to MAPK and PI3K-AKT pathways. Moreover, OSI906 inhibited IGF1R phosphorylation and suppressed AKT activation via the adaptor protein insulin receptor substrate (IRS)1 (Supplementary Fig. S2A and S2B), resulting in PI3K binding and activation. This indicated that Met-ERK1/2 and IGF1R-AKT act via GAB2 and IRS1, respectively, in the acquisition of EGFR and Met inhibitor resistance (Fig. 2E).

In DR4 cells, AKT and ERK1/2 activation was suppressed by concurrent treatment with PHA665752 and OSI906 (Fig. 2C and D). Because Met expression was not attenuated, Met phosphorylation was difficult to suppress with PHA665752; thus, AKT and ERK1/2 were not fully inhibited up to the concurrent treatment of 1μmol/L each of PHA665752 and OSI906. At that point, the cells remained partly resistant to Met and IGF1R inhibition compared with DR2 cells (Fig. 2A, C, and D).

IGFBP2 and IGFBP4 suppression is required for IGF/IGF1R bypass signaling in DR2 cells

To clarify the mechanism of IGF1R activation in DR2 cells, we first measured the bioactivity of IGF1R in the culture medium of DR2 as compared with MET1000 cells with the cell-based IGF1R phosphorylation assay using MEF-IGF1R, for which IGF1R phosphorylation can be quantified by ELISA (26). The culture medium of DR2 cells phosphorylated IGF1R to a greater degree than that of MET1000 cells (Fig. 3A). When the IGF1R ligands IGF1 and IGF2 were neutralized by treatment with the humanized mAb BI836845 (26), IGF1R phosphorylation and AKT activation were attenuated in a dose-dependent manner. Furthermore, apoptosis was induced by a combination of BI836845 and PHA665752 (Fig. 3B). These results indicate that the increased bioactivity of IGF1 and/or IGF2 lead to IGF1R phosphorylation to bypass Met and EGFR inhibition. Although *IGF1* and *IGF2* mRNA levels were not higher in DR2 than in MET1000 cells, *IGFBP2*, *IGFBP4*, and *IGFBP5* expression was downregulated, as determined by RT-PCR (Fig. 3C). Moreover, IGFBP2 and IGFBP4 protein expression was markedly decreased in the cell lysate and culture medium of DR2 as compared with MET1000 cells (Fig. 3D). IGFBPs transport IGF1 and IGF2 in the circulation and within cells and modulate IGF bioavailability and signaling (27). When DR2 cells were treated with human recombinant IGFBP2 or IGFBP4, IGF1R phosphorylation was inhibited, leading to suppression of AKT. In addition, combined treatment with PHA665752 and IGFBP2 or IGFBP4 blocked AKT and ERK1/2 activation and cell proliferation (Fig. 3E–H).

Increased IGFBP3 enhances Met expression via Smad2/3 activation, leading to partial Met-TKI resistance in DR4 cells

As in DR2 cells, combined treatment of DR4 cells with BI836845 and PHA665752 inhibited AKT and ERK1/2 activation, thereby decreasing cell proliferation and the induction of apoptosis; this indicated that IGF/IGF1R was activated as a bypass signal (Fig. 4A). However, in contrast to DR2 cells, Met expression was not attenuated to a greater degree than in MET1000 cells, and a higher concentration of PHA665752 was required to inhibit Met phosphorylation and downstream signaling (Fig. 2C and D). Therefore, we assessed the mRNA expression of factors that potentially modulate IGF/IGF1R activity, such as ligands, receptors, and IGFBPs. *IGF1* and *IGFBP3* mRNA expression was upregulated in DR4 cells (Fig. 4B), whereas *IGFBP3* levels were increased in cell lysates and conditioned medium (Fig. 4C, 1 and 2). IGFBP3 reportedly activates TGFβ-Smad2/3 signaling independent of IGF/IGF1R (28), and the *Met* promoter region contains putative Smad2/3-binding sites (29). This suggests that increased IGFBP3 expression might stimulate TGFβ-Smad2/3 signaling and enhance Met expression. siRNA-mediated knockdown of IGFBP3 expression suppressed Smad2/3 activation and Met expression in DR4 cells, and moreover Smad2/3 knockdown also attenuated Met expression (Supplementary Fig. S3A), suggesting that IGFBP3–Smad2/3 signaling regulates Met expression and leads to acquisition of partial Met resistance (Fig. 4D). Furthermore, *Met* mRNA (Fig. 4E) but not EGFR or IGF1R mRNA and protein (Fig. 4D and Supplementary Fig. S3B and S3C) expression was attenuated by *IGFBP3* knockdown.

Overamplified Met expression leads to Met-TKI resistance and ERK1/2 activation through negative feedback via DUSP4-induced proliferation in DR6 cells

Met expression was upregulated in DR6 and MET1000 cells relative to PC-9 cells (Fig. 1F). A phospho-RTK array revealed activation of Met, IGF1R, and InsR; this phosphorylation pattern was similar to that observed in MET1000 cells (Fig. 1E). To determine whether Met activation is required for cell survival, *Met* expression was knocked down by siRNA in MET1000 and DR6 cells. This led to a marked induction of apoptosis in DR6 as compared with MET1000 cells (Fig. 5A), indicating a further requirement for Met expression in cell survival. To overcome Met overamplification, we treated cells with various Met inhibitors including crizotinib, GSK1363089, and JNJ38877605. Proliferation of DR6 cells was enhanced by combined treatment with PHA665752 and gefitinib; however, it was inhibited by crizotinib, a Met/ALK-TKI, at concentrations over 1 μmol/L, and completely suppressed by GSK1363089 and JNJ38877605 even at lower concentrations (Fig. 5B). No additional mutations in the Met kinase domain involving the Met activation loop were identified in DR6 cells that might account for the selective resistance to PHA665752 (Supplementary Fig. S4A;

(*Continued.*) An MTT assay was performed and the OD570 measured. Arrows indicate the peak of proliferation for each treatment. **C–F,** PC-9, MET1000, and DR6 cells were exposed to 1 μmol/L gefitinib and/or 1 μmol/L PHA665752 (**C**), DR6 cells were exposed to graded concentrations of GSK1363089 (GSK136) in the presence of 1 μmol/L gefitinib (**D**), MET1000 and DR6 cells were exposed to graded concentrations of crizotinib in the presence of 1 μmol/L gefitinib (**E**), and DR6 cells were pretreated to graded concentrations of U0126 for 30 minutes and then treated with 1 μmol/L gefitinib and crizotinib (**F**) for 8–12 hours and cell lysates were immunoblotted for the indicated primary antibodies. β-Actin was included as a loading control. **G,** Schematic of the signaling in DR6 cells illustrating the action of negative feedback on ERK1/2 activation via DUSP4 (left) following partial (0.03–0.1 μmol/L GSK136; center) or complete (0.3–1.0 μmol/L GSK136; right) Met dephosphorylation.

Published OnlineFirst September 9, 2016; DOI: 10.1158/1535-7163.MCT-16-0313

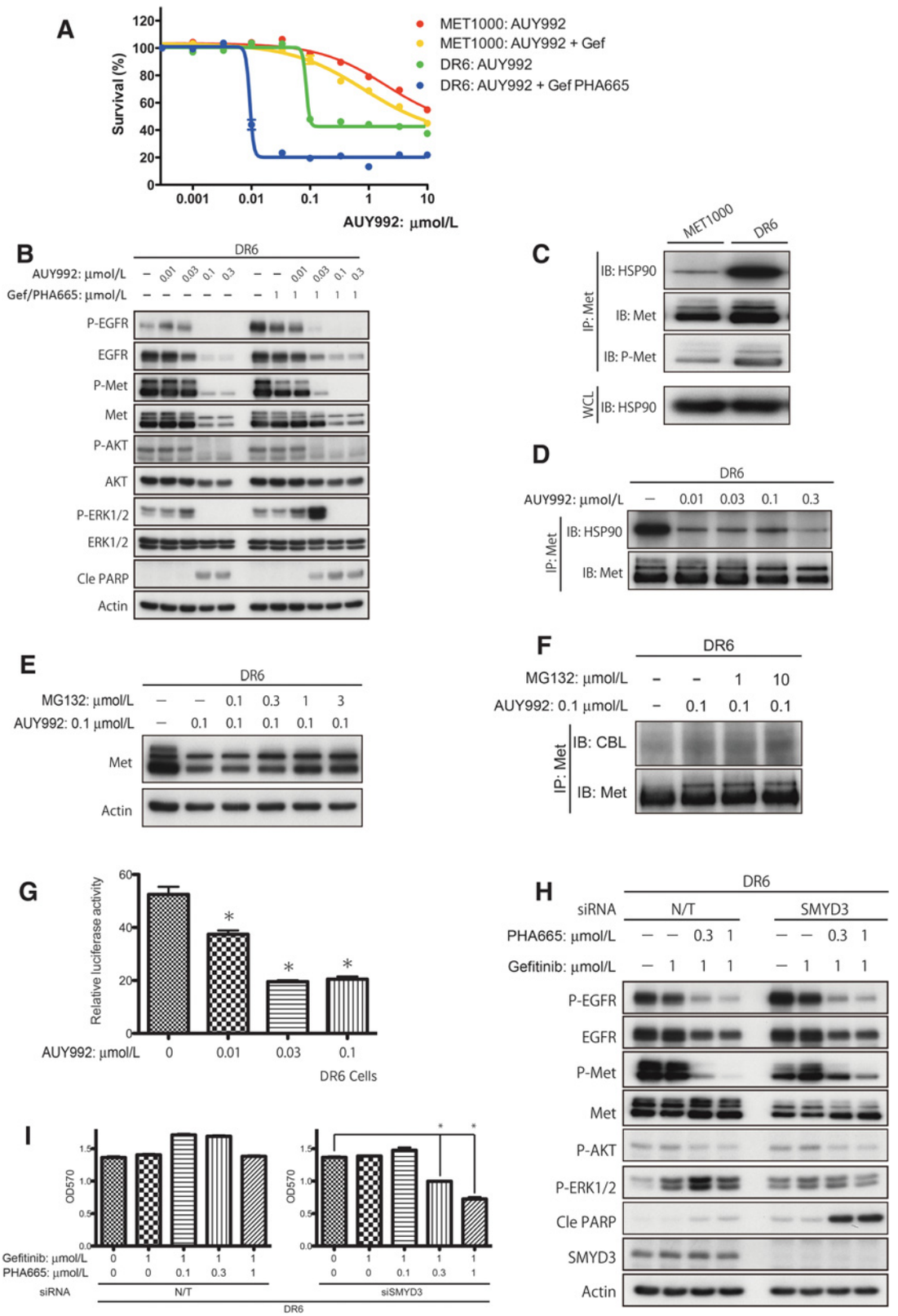

Published OnlineFirst September 9, 2016; DOI: 10.1158/1535-7163.MCT-16-0313

Supplementary Table S2). In MET1000 cells, PHA665752 inhibited the phosphorylation of Met as well as that of EGFR and ERBB3, thereby blocking AKT and ERK1/2 activation and inducing apoptosis (Fig. 5C). However, the combination of PHA665752 and gefitinib did not inhibit Met, EGFR, and ERBB3 phosphorylation in DR6 cells (Fig. 5C). On the other hand, GSK1363089 treatment inhibited the phosphorylation of all three proteins in a dose-dependent manner, thereby suppressing the downstream activation of AKT and ERK1/2 (Fig. 5D). Notably, ERK1/2, but not MEK1/2, which is upstream of ERK1/2, was activated by treatment with 0.03–0.1 μmol/L GSK1363089 (to decrease Met phosphorylation by degrees). As DUSPs are known to inhibit ERK (30), this result suggested the presence of negative feedback regulation of ERK1/2 via the DUSP4 induced by suppression of Met phosphorylation (Fig. 5D). Consistent with this model, reduction of DUSP4 expression was shown to occur upon Met inhibition followed by further activation of ERK1/2 in gastric cancer cells (31). Accordingly, the reduction of DUSP4 expression in DR6 cells treated with 1 μmol/L crizotinib and gefitinib resulted in ERK1/2 phosphorylation (Fig. 5E). On the other hand, ERK1/2 phosphorylation was blocked by treatment with the MEK inhibitor U0126 (Fig. 5F). Furthermore, ERK1/2 activation via reduction of DUSP4 enhanced DR6 cell proliferation (Fig. 5B, indicated by arrows). However, because GSK1363089 treatment from 0.3–1 μmol/L led to complete inhibition of MEK1/2 phosphorylation in addition to DUSP4 downregulation (loss of negative feedback), ERK1/2 was completely inhibited, leading to the induction of apoptosis in DR6 cells (Fig. 5D and G). This suggested that the negative feedback-mediated ERK1/2 activation via DUSP4 is likely inferior to the signals of MEK1/2 to ERK1/2 and might be insufficient to promote resistance to Met-TKI.

Met overexpression is mediated by HSP90 via Met stabilization and SMYD3-associated transcriptional regulation in DR6 cells

It was previously reported that *Met* gene amplification mediates Met inhibitor resistance (known as inhibitor addiction) in GSK-45, EBC-1, and GTL16 cancer cell lines (13, 32), although the precise mechanisms of *Met* amplification are unclear. In the current study, DR6 cells exhibited *Met* gene amplification (Supplementary Fig. S4B). HSP90 is a molecular chaperone that regulates the stability of various oncogenic kinases (33). Upon exposure to increasing concentrations of the HSP90 inhibitor AUY992, proliferation was suppressed in DR6 cells in the presence of PHA665752 and gefitinib, although the effect was modest in MET1000 cells even in the presence of gefitinib (Fig. 6A). Treatment of MET1000 cells with increasing concentrations of AUY992 in the presence or absence of 1 μmol/L gefitinib slightly attenuated EGFR and Met expression and phosphorylation but had no effect on AKT and ERK1/2 signaling or induction of apoptosis (Supplementary Fig. S5A). In contrast, in DR6 cells, treatment with 0.1 μmol/L AUY992 attenuated EGFR and Met expression and phosphorylation, thereby decreasing AKT and ERK1/2 activation and inducing apoptosis. Moreover, in the presence of gefitinib and PHA665752, the induction of apoptosis by AUY992 was enhanced (Fig. 6B).

Because of the increased phosphorylation of Met in DR6 cells, the interaction between Met and HSP90 was increased, leading to Met stabilization in these cells (Fig. 6C); this complex was dissociated by AUY992 treatment (Fig. 6D), an effect that was blocked by the proteasome inhibitor MG132, which preserved Met expression in a dose-dependent manner in the presence of AUY992 (Fig. 6E). The association between the CBL ubiquitin ligase and Met was also preserved by MG132 treatment, indicating that AUY992 enhances Met degradation via CBL by disrupting the HSP90–Met complex (Fig. 6F).

In addition to its role in Met stabilization, HSP90 promotes SMYD3 histone H3-lysine 4 methyltransferase activity and plays an important role in transcriptional regulation as a constituent of the RNA polymerase complex (34). SMYD3-binding sites are present in the *Met* promoter region (35). We found that AUY992 inhibited *Met* gene promoter activity in DR6 cells, although the activity was maintained up to the concentrations of 0.1 μmol/L AUY992 in MET1000 cells (Fig. 6G and Supplementary Fig. S5B). Basal SMYD3 expression

Figure 6.

HSP90 protects against Met degradation by CBL and enhances transcriptional regulation by SMYD3, leading to increased Met expression in DR6 cells. **A,** MET1000 and DR6 cells were seeded into 96-well plates at 5×10^3 cells/50-μL growth media/well, then preincubated overnight and treated with AUY992 at the indicated concentrations under 1 μmol/L gefitinib and/or 1 μmol/L PHA665752 exposure for 72 hours. An MTT assay was performed and the OD570 measured. Data are the means ± SEM for 6–12 wells. **B,** DR6 cells were exposed to graded concentrations of AUY992 in the presence or absence of gefitinib and/or PHA665752 for 24 hours and cell lysates were immunoblotted (IB) for the indicated primary antibodies. β-Actin was included as a loading control. **C,** interaction between Met and HSP90. MET1000 and DR6 cells were lysed and subjected to immunoprecipitation (IP) with an anti-Met antibody followed by IB with anti-HSP90, anti-Met, and anti-phosphorylated Met (P-Met) antibodies. **D,** HSP90 inhibitor disrupts Met-HSP90 interactions. DR6 cells were incubated with increasing concentrations of AUY992 for 24 hours, lysed, and subjected to IP with an anti-Met antibody followed by IB with anti-HSP90 and anti-Met antibodies. **E,** AUY992-stimulated Met degradation is mediated by the proteasome. DR6 cells were treated with the proteasome inhibitor MG132 1 hour before treatment with 0.1 μmol/L AUY992 for an additional 24 hours. Cells were collected, lysed, and subjected to immunoblotting with anti-Met antibodies. **F,** HSP90 inhibition results in enhanced Met ubiquitination. DR6 cells were treated with MG132 1 hour before treatment with 0.1 μmol/L AUY992 for an additional 6 hours. Cells were collected, lysed, and subjected to IP with an anti-Met antibody followed by immunoblotting with anti-CBL and anti-Met antibodies. **G,** *Met* promoter-luciferase (pGL4-phMET) and pRL-TK plasmids were cotransfected into DR6 cells and treated with AUY992 for 24 hours, and the luciferase activities were determined 48 hours after transfection. Firefly luciferase activity was normalized with that of *Renilla* luciferase and *Met* promoter activity was indicated as relative luciferase units (RLU; dual luciferase system, Promega). Data are the means ± SEM for 6 wells. *, $P < 0.01$ for comparison with the control value. Data are representative of three independent experiments. **H** and **I,** DR6 cells were transfected with nontargeting (N/T) siRNA or siRNA directed against SMYD3. **H,** after 48 hours of transfection, DR6 cells were treated with the indicated concentrations of PHA665752 (PHA665) in the presence of 1 μmol/L gefitinib for 24 hours. SMYD3 knockdown was determined by Western blot analysis. Immunoblot analysis for the indicated primary antibodies is shown. β-Actin was included as a loading control. **I,** transfected cells were reseeded in the presence or absence of the indicated inhibitors, then after 72-hour incubation, an MTT assay was performed. Data are the means ± SEM for 6 wells. *, $P < 0.01$ for comparison with the control value.

Published OnlineFirst September 9, 2016; DOI: 10.1158/1535-7163.MCT-16-0313

level was markedly higher in DR6 than in MET1000 cells (Supplementary Fig. S5C). siRNA-mediated knockdown of SMYD3 attenuated basal Met expression and phosphorylation. Furthermore, treatment with PHA665752 and/or gefitinib suppressed AKT and ERK1/2 activation and induction of apoptosis, whereas in MET1000 cells, there was no inhibition of Met or induction of apoptosis even in the presence of gefitinib (Fig. 6H and Supplementary Fig. S5D). SMYD3 knockdown partly restored the sensitivity of DR6 cells to the combination of gefitinib and PHA665762 but not that of MET1000 cells to gefitinib (Fig. 6I and Supplementary Fig. S5E). These results demonstrate that Met overexpression was induced by HSP90 via inhibition of CBL degradation and by transcriptional regulation via SMYD3.

Discussion

The results of this study demonstrate the mechanisms of dual resistance to the Met-TKI PHA665752 and the EGFR-TKI gefitinib in cells previously treated with EGFR-TKI. We identified two distinct resistance mechanisms, namely, the activation of IGF/IGF1R as bypass signals in DR2 and DR4 cells and the overamplification of Met caused by HSP90 activity in DR6 cells. It is unclear how the presence of an activating EGFR mutation predisposes to this dual resistance. Nonetheless, these findings indicate the existence of IGF/IGF1R bypass signaling through either an increase or decrease of IGFBPs and of Met amplification through protection from CBL-mediated degradation or transcriptional regulation by SMYD3 as underlying resistance mechanisms. Our results thus provide evidence for heterogeneity among drug-resistant cell lines that reflects the variable nature of clinical drug resistance.

Decreased IGFBP3 production led to increased IGF/IGF1R activation as a bypass signal in some EGFR-TKI resistant cancer models such as A431GR (36), PC-9WZR, and PC-9PFR (3) cells. These reports support our finding that IGFBP attenuation leads to IGF/IGF1R activation in response to TKI, indicating that IGF1R activation is ligand-dependent (Fig. 3A and C). Therefore, treatment with BI836845, a humanized antibody for IGF1 and IGF2, might be effective in inhibiting the bypass signaling of IGF/IGF1R. BI836845 along with the EGFR-TKI afatinib is presently under evaluation in a clinical trial for patients with EGFR-mutant NSCLC who exhibit cancer progression following EGFR-TKI treatment (ClinicalTrials.gov identifier NCT02191891). We demonstrate that increased IGFBP3 production also resulted in bypass IGF/IGF1R activation and promoted the expression of Met via Smad2/3 in DR4 cells (Fig. 4D and E). It is important to note that either increased or decreased IGFBP production results in the activation of IGF/IGF1R signaling as a bypass mechanism. Further studies on the events leading to IGF/IGF1R activation are required to further confirm the role of IGFBP3 in TKI resistance.

We observed in this study that Met overexpression requires HSP90 activity (Fig. 6A). The HSP90 inhibitor ganetespib shows synergy with the Met-TKI crizotinib in cells overexpressing wild-type Met (37). This is consistent with our finding that the HSP90 inhibitor AUY992 combined with gefitinib/PHA665752 had a greater inhibitory effect than AUY992 treatment alone in DR6 cells (Fig. 6A). Clarifying the mechanism of Met overamplification might provide more detailed insight into the development of Met-TKI resistance. This is the first report demonstrating the role of SMYD3 in the acquisition of resistance to Met-TKI and EGFR-TKI treatment. HSP90 enhanced the activity of SMYD3, a histone lysine methyltransferase that functions in transcriptional activation as part of the RNA polymerase complex and is implicated in different types of cancer including hepatocellular carcinoma and colorectal cancer (34). There are two SMYD3 binding sites in the *Met* promoter region (35). Silencing of the *SMYD3* gene decreased Met expression, whereas application of PHA665752/gefitinib induced apoptosis and suppressed cell proliferation (Fig. 6H and I). HSP90 is a molecular chaperone that stabilizes and activates many mutated or overexpressed oncoproteins (38), and HSP90 inhibitors have been reported to destabilize Met (39) as well as mutated EGFR (40). This is in agreement with our finding that treatment with the HSP90 inhibitor AUY992 reduced the expression of Met and of mutated EGFR in DR6 cells (Fig. 6B).

This is also the first report to demonstrate that activation of IGF/IGF1R-IRS1-AKT signaling contributes to the acquired resistance to both Met-TKI and EGFR-TKI (Fig. 2C and D and Supplementary Fig. S2A and S2B). Previous studies have shown that PI3K-AKT signaling must be suppressed for TKIs to work effectively (36, 41, 42). For example, loss of *PTEN* contributes to erlotinib resistance in EGFR-mutant lung cancer via Akt activation (41). Furthermore, gefitinib-resistant EGFR-overexpressing A431GR cells show resistance to EGFR inhibitors via IGF1R activation, even when ERK1/2 activation is inhibited by gefitinib (36). The GAB2 adaptor protein couples Met to the RAS-MAPK pathway, while the scaffold protein GAB1 indirectly links Met to PI3K-AKT signaling (43). Consistent with these observations, Met signaling was transduced via GAB2 to activate RAS-MAPK signaling in DR2 cells.

ERK1/2 activation through the reduction of DUSP4 expression was observed upon partial Met dephosphorylation following treatment with low-dose Met-TKIs, with concomitant enhancement of cell proliferation at specific concentrations in DR6 cells (Fig. 5B and D). DUSP4 dephosphorylates ERK1/2 in the nucleus. Its expression is downstream of growth factor stimulation and is thought to be stimulated via MAPK signaling as part of a negative feedback loop (44). Our results show that ERK1/2 phosphorylation increased in association with decreased DUSP4 abundance resulting from treatment with the Met-TKI crizotinib or GSK1363089 plus gefitinib (Fig. 5D and E). Furthermore, application of the MEK1/2 inhibitor U0126 or *DUSP4* knockdown suppressed this negative feedback-regulated phosphorylation of ERK1/2 (Fig. 5F and Supplementary Fig. S6). Consistent with this finding, DUSP4 protein decrease in gastric cancer cell lines has been shown to be primarily dependent on MEK-ERK signaling (31). Therefore, complete inhibition of Met phosphorylation leads to dephosphorylation of MEK-ERK upon downregulation of DUSP4 protein levels. Resistance to Met-TKIs in GLT-16 gastric cancer cells can occur via formation of a BRAF fusion protein or KRAS amplification promoting ERK signaling (13, 45). Thus, MEK-ERK activation can induce resistance to Met inhibitors.

In summary, we elucidated an important mechanism of dual resistance to Met-TKI PHA665752 and EGFR-TKI gefitinib in the context of sequential drug treatment; that is, gefitinib

treatment in PC-9 cells with an activating EGFR mutation followed by PHA665752 plus gefitinib for Met-amplified gefitinib-resistant MET1000 cells. In addition, three DR cell lines showed variable mechanisms of acquired resistance. These novel observations provide insight into the basis of tumor recurrence through development of resistance to TKIs.

Disclosure of Potential Conflicts of Interest

T. Ohmori reports receiving commercial research support from Boehringer Ingelheim. Y. Sasaki reports receiving commercial research grants from Eisai, Bristol Myers Squibb, Taiho Pharmaceuticals, and Chugai-Roche and has received speakers' bureau honoraria from Taiho Pharmaceuticals. No potential conflicts of interest were disclosed by the others.

Authors' Contributions

Conception and design: T. Yamaoka, T. Ohmori, S. Kusumoto
Development of methodology: T. Yamaoka, S. Arata, S. Kusumoto
Acquisition of data (provided animals, acquired and managed patients, provided facilities, etc.): T. Yamaoka, S. Arata, Y. Murata, S. Kusumoto
Analysis and interpretation of data (e.g., statistical analysis, biostatistics, computational analysis): T. Yamaoka, S. Kusumoto
Writing, review, and/or revision of the manuscript: T. Yamaoka, T. Ohmori, M. Ohba, S. Kusumoto, H. Ishida, T. Hirose, T. Ohnishi
Administrative, technical, or material support (i.e., reporting or organizing data, constructing databases): T. Yamaoka, M. Ohba, T. Shirai, Y. Sasaki
Study supervision: T. Yamaoka, T. Ohmori, Y. Kishino, T. Hirose, Y. Sasaki

Acknowledgments

We thank the members of the Institute of Molecular Oncology for thoughtful discussions and helpful advice, and Ms. Yoshie Akaji for technical assistance and English language editing.

Grant Support

This work was supported by the MEXT-Supported Program for the Strategic Research Foundation at Private Universities (2012–2016) from the Ministry of Education, Culture, Sports, Science, and Technology of Japan (to T. Yamaoka, T. Ohmori, M. Ohba).

The costs of publication of this article were defrayed in part by the payment of page charges. This article must therefore be hereby marked *advertisement* in accordance with 18 U.S.C. Section 1734 solely to indicate this fact.

Received May 17, 2016; revised August 3, 2016; accepted August 6, 2016; published OnlineFirst September 9, 2016.

References

1. Kuan FC, Kuo LT, Chen MC, Yang CT, Shi CS, Teng D, et al. Overall survival benefits of first-line EGFR tyrosine kinase inhibitors in EGFR-mutated non-small-cell lung cancers: a systematic review and meta-analysis. Br J Cancer 2015;113:1519–28.
2. Yu HA, Arcila ME, Rekhtman N, Sima CS, Zakowski MF, Pao W, et al. Analysis of tumor specimens at the time of acquired resistance to EGFR-TKI therapy in 155 patients with EGFR-mutant lung cancers. Clin Cancer Res 2013;19:2240–7.
3. Cortot AB, Repellin CE, Shimamura T, Capelletti M, Zejnullahu K, Ercan D, et al. Resistance to irreversible EGF receptor tyrosine kinase inhibitors through a multistep mechanism involving the IGF1R pathway. Cancer Res 2013;73:834–43.
4. Zhang Z, Lee JC, Lin L, Olivas V, Au V, LaFramboise T, et al. Activation of the AXL kinase causes resistance to EGFR-targeted therapy in lung cancer. Nat Genet 2012;44:852–60.
5. Sequist LV, Soria JC, Goldman JW, Wakelee HA, Gadgeel SM, Varga A, et al. Rociletinib in EGFR-mutated non-small-cell lung cancer. N Engl J Med 2015;372:1700–9.
6. Janne PA, Yang JC, Kim DW, Planchard D, Ohe Y, Ramalingam SS, et al. AZD9291 in EGFR inhibitor-resistant non-small-cell lung cancer. N Engl J Med 2015;372:1689–99.
7. Sierra JR, Tsao MS. c-MET as a potential therapeutic target and biomarker in cancer. Ther Adv Med Oncol 2011;3:S21–35.
8. Lutterbach B, Zeng Q, Davis LJ, Hatch H, Hang G, Kohl NE, et al. Lung cancer cell lines harboring MET gene amplification are dependent on Met for growth and survival. Cancer Res 2007;67:2081–8.
9. McDermott U, Sharma SV, Dowell L, Greninger P, Montagut C, Lamb J, et al. Identification of genotype-correlated sensitivity to selective kinase inhibitors by using high-throughput tumor cell line profiling. Proc Natl Acad Sci U S A 2007;104:19936–41.
10. Smolen GA, Sordella R, Muir B, Mohapatra G, Barmettler A, Archibald H, et al. Amplification of MET may identify a subset of cancers with extreme sensitivity to the selective tyrosine kinase inhibitor PHA-665752. Proc Natl Acad Sci U S A 2006;103:2316–21.
11. Christensen JG, Schreck R, Burrows J, Kuruganti P, Chan E, Le P, et al. A selective small molecule inhibitor of c-Met kinase inhibits c-Met-dependent phenotypes *in vitro* and exhibits cytoreductive antitumor activity *in vivo*. Cancer Res 2003;63:7345–55.
12. Qi J, McTigue MA, Rogers A, Lifshits E, Christensen JG, Janne PA, et al. Multiple mutations and bypass mechanisms can contribute to development of acquired resistance to MET inhibitors. Cancer Res 2011;71:1081–91.
13. Cepero V, Sierra JR, Corso S, Ghiso E, Casorzo L, Perera T, et al. MET and KRAS gene amplification mediates acquired resistance to MET tyrosine kinase inhibitors. Cancer Res 2010;70:7580–90.
14. Engelman JA, Zejnullahu K, Mitsudomi T, Song Y, Hyland C, Park JO, et al. MET amplification leads to gefitinib resistance in lung cancer by activating ERBB3 signaling. Science 2007;316:1039–43.
15. Turke AB, Zejnullahu K, Wu YL, Song Y, Dias-Santagata D, Lifshits E, et al. Preexistence and clonal selection of MET amplification in EGFR mutant NSCLC. Cancer Cell 2010;17:77–88.
16. Suda K, Murakami I, Katayama T, Tomizawa K, Osada H, Sekido Y, et al. Reciprocal and complementary role of MET amplification and EGFR T790M mutation in acquired resistance to kinase inhibitors in lung cancer. Clin Cancer Res 2010;16:5489–98.
17. Ando K, Ohmori T, Inoue F, Kadofuku T, Hosaka T, Ishida H, et al. Enhancement of sensitivity to tumor necrosis factor alpha in non-small cell lung cancer cells with acquired resistance to gefitinib. Clin Cancer Res 2005;11:8872–9.
18. Frasca F, Pandini G, Scalia P, Sciacca L, Mineo R, Costantino A, et al. Insulin receptor isoform A, a newly recognized, high-affinity insulin-like growth factor II receptor in fetal and cancer cells. Mol Cell Biol 1999;19:3278–88.
19. Yatabe Y, Hida T, Horio Y, Kosaka T, Takahashi T, Mitsudomi T. A rapid, sensitive assay to detect EGFR mutation in small biopsy specimens from lung cancer. J Mol Diagn 2006;8:335–41.
20. Yoshida T, Zhang G, Smith MA, Lopez AS, Bai Y, Li J, et al. Tyrosine phosphoproteomics identifies both codrivers and cotargeting strategies for T790M-related EGFR-TKI resistance in non-small cell lung cancer. Clin Cancer Res 2014;20:4059–74.
21. Ercan D, Zejnullahu K, Yonesaka K, Xiao Y, Capelletti M, Rogers A, et al. Amplification of EGFR T790M causes resistance to an irreversible EGFR inhibitor. Oncogene 2010;29:2346–56.
22. Ohashi K, Sequist LV, Arcila ME, Moran T, Chmielecki J, Lin YL, et al. Lung cancers with acquired resistance to EGFR inhibitors occasionally harbor BRAF gene mutations but lack mutations in KRAS, NRAS, or MEK1. Proc Natl Acad Sci U S A 2012;109:E2127–33.
23. Koizumi F, Shimoyama T, Taguchi F, Saijo N, Nishio K. Establishment of a human non-small cell lung cancer cell line resistant to gefitinib. Int J Cancer 2005;116:36–44.
24. Ogino A, Kitao H, Hirano S, Uchida A, Ishiai M, Kozuki T, et al. Emergence of epidermal growth factor receptor T790M mutation during chronic exposure to gefitinib in a non small cell lung cancer cell line. Cancer Res 2007;67:7807–14.

Published OnlineFirst September 9, 2016; DOI: 10.1158/1535-7163.MCT-16-0313

25. Ding CB, Yu WN, Feng JH, Luo JM. Structure and function of Gab2 and its role in cancer (Review). Mol Med Rep 2015;12:4007–14.
26. Friedbichler K, Hofmann MH, Kroez M, Ostermann E, Lamche HR, Koessl C, et al. Pharmacodynamic and antineoplastic activity of BI 836845, a fully human IGF ligand-neutralizing antibody, and mechanistic rationale for combination with rapamycin. Mol Cancer Ther 2014;13:399–409.
27. Baxter RC. IGF binding proteins in cancer: mechanistic and clinical insights. Nat Rev Cancer 2014;14:329–41.
28. Fanayan S, Firth SM, Baxter RC. Signaling through the Smad pathway by insulin-like growth factor-binding protein-3 in breast cancer cells. Relationship to transforming growth factor-beta 1 signaling. J Biol Chem 2002;277:7255–61.
29. Kajihara I, Jinnin M, Makino T, Masuguchi S, Sakai K, Fukushima S, et al. Overexpression of hepatocyte growth factor receptor in scleroderma dermal fibroblasts is caused by autocrine transforming growth factor beta signaling. Biosci Trends 2012;6:136–42.
30. Amit I, Wides R, Yarden Y. Evolvable signaling networks of receptor tyrosine kinases: relevance of robustness to malignancy and to cancer therapy. Mol Syst Biol 2007;3:151.
31. Lai AZ, Cory S, Zhao H, Gigoux M, Monast A, Guiot MC, et al. Dynamic reprogramming of signaling upon met inhibition reveals a mechanism of drug resistance in gastric cancer. Sci Signal 2014;7:ra38.
32. Funakoshi Y, Mukohara T, Tomioka H, Ekyalongo RC, Kataoka Y, Inui Y, et al. Excessive MET signaling causes acquired resistance and addiction to MET inhibitors in the MKN45 gastric cancer cell line. Invest New Drugs 2013;31:1158–68.
33. Neckers L, Mollapour M, Tsutsumi S. The complex dance of the molecular chaperone Hsp90. Trends Biochem Sci 2009;34:223–6.
34. Hamamoto R, Furukawa Y, Morita M, Iimura Y, Silva FP, Li M, et al. SMYD3 encodes a histone methyltransferase involved in the proliferation of cancer cells. Nat Cell Biol 2004;6:731–40.
35. Zou JN, Wang SZ, Yang JS, Luo XG, Xie JH, Xi T. Knockdown of SMYD3 by RNA interference down-regulates c-Met expression and inhibits cells migration and invasion induced by HGF. Cancer Lett 2009;280:78–85.
36. Guix M, Faber AC, Wang SE, Olivares MG, Song Y, Qu S, et al. Acquired resistance to EGFR tyrosine kinase inhibitors in cancer cells is mediated by loss of IGF-binding proteins. J Clin Invest 2008;118:2609–19.
37. Miyajima N, Tsutsumi S, Sourbier C, Beebe K, Mollapour M, Rivas C, et al. The HSP90 inhibitor ganetespib synergizes with the MET kinase inhibitor crizotinib in both crizotinib-sensitive and -resistant MET-driven tumor models. Cancer Res 2013;73:7022–33.
38. Wandinger SK, Richter K, Buchner J. The Hsp90 chaperone machinery. J Biol Chem 2008;283:18473–7.
39. Maulik G, Kijima T, Ma PC, Ghosh SK, Lin J, Shapiro GI, et al. Modulation of the c-Met/hepatocyte growth factor pathway in small cell lung cancer. Clin Cancer Res 2002;8:620–7.
40. Yang S, Qu S, Perez-Tores M, Sawai A, Rosen N, Solit DB, et al. Association with HSP90 inhibits Cbl-mediated down-regulation of mutant epidermal growth factor receptors. Cancer Res 2006;66:6990–7.
41. Sos ML, Koker M, Weir BA, Heynck S, Rabinovsky R, Zander T, et al. PTEN loss contributes to erlotinib resistance in EGFR-mutant lung cancer by activation of Akt and EGFR. Cancer Res 2009;69:3256–61.
42. Engelman JA, Janne PA, Mermel C, Pearlberg J, Mukohara T, Fleet C, et al. ErbB-3 mediates phosphoinositide 3-kinase activity in gefitinib-sensitive non-small cell lung cancer cell lines. Proc Natl Acad Sci U S A 2005;102:3788–93.
43. Birchmeier C, Birchmeier W, Gherardi E, Vande Woude GF. Met, metastasis, motility and more. Nat Rev Mol Cell Biol 2003;4:915–25.
44. Patterson KI, Brummer T, O'Brien PM, Daly RJ. Dual-specificity phosphatases: critical regulators with diverse cellular targets. Biochem J 2009;418:475–89.
45. Dillon R, Nilsson CL, Shi SD, Lee NV, Krastins B, Greig MJ. Discovery of a novel B-Raf fusion protein related to c-Met drug resistance. J Proteome Res 2011;10:5084–94.

Published OnlineFirst September 9, 2016; DOI: 10.1158/1535-7163.MCT-16-0313

Molecular Cancer Therapeutics

Acquired Resistance Mechanisms to Combination Met-TKI/EGFR-TKI Exposure in Met-Amplified EGFR-TKI–Resistant Lung Adenocarcinoma Harboring an Activating EGFR Mutation

Toshimitsu Yamaoka, Tohru Ohmori, Motoi Ohba, et al.

Mol Cancer Ther 2016;15:3040-3054. Published OnlineFirst September 9, 2016.

Biochemistry and Biophysics Reports 5 (2016) 1–7

Contents lists available at ScienceDirect

Biochemistry and Biophysics Reports

journal homepage: www.elsevier.com/locate/bbrep

Up-regulation of Syndecan-4 contributes to TGF-β1-induced epithelial to mesenchymal transition in lung adenocarcinoma A549 cells

Yoko Toba-Ichihashi, Toshimitsu Yamaoka *, Tohru Ohmori, Motoi Ohba

Institute of Molecular Oncology, Showa University, 1-5-8 Hatanodai, Shinagawa-ku, Tokyo 142-8555, Japan

ARTICLE INFO

Article history:
Received 9 May 2015
Received in revised form
2 November 2015
Accepted 19 November 2015
Available online 27 November 2015

Keywords:
Syndecan-4
Transforming growth factor-β 1
Epithelial to mesenchymal transition
Snail
Slug

ABSTRACT

Syndecan-4 (SDC4) is a cell-surface proteoglycan associated with cell adhesion, motility, and intracellular signaling. Here, we present that SDC4 functions as a positive regulator of the transforming growth factor (TGF)-β1-induced epithelial to mesenchymal transition (EMT) via Snail in lung adenocarcinoma, A549 cells. TGF-β1 up-regulated the expression of SDC4, accompanied by the induction of EMT. Wound-healing and transwell chemotaxis assay revealed that SDC4 promoted cell migration and invasion. SDC4 knockdown recovered the E-cadherin and decreased vimentin and Snail expression in EMT-induced A549 cells. However, depletion of SDC4 resulted in little change of the Slug protein expression and mesenchymal cell morphology induced by TGF-β1. The double knockdown of SDC-4 and Slug was required for reversal of epithelial morphology; it did not occur from the SDC4 single knockdown. These findings suggest that Snail is a transcriptional factor downstream of SDC4, and SDC4 regulates TGF-β1-induced EMT by cooperating with Slug. Our data provide a novel insight into cellular mechanisms, whereby the cell-surface proteoglycan modulated TGF-β1-induced EMT in lung adenocarcinoma, A549 cells.

1. Introduction

Lung cancer is one of the most commonly diagnosed cancers, and the leading cause of death worldwide. Of these deaths, nearly 60% of patients progress into advanced stages with metastasis [1]. Chemotherapy is an important therapeutic strategy for advanced non-small cell lung cancer (NSCLC). However, most patients treated with chemotherapy frequently acquire the resistance to anti-cancer drugs [2]. Therefore, the mechanisms of the biologic processes that drive metastasis and drug resistance need to be elucidated.

Accumulating evidence suggests that the acquisition of epithelial-to-mesenchymal transition (EMT) is one of the cause of chemo-resistance of NSCLC [3]. Furthermore, EMT is associated with the invasiveness and metastasis [3]. EMT is a complex process, which involves cytoskeletal remodeling and cell–cell and cell–matrix adhesion, leading to the transition from a polarized, epithelial phenotype to a highly motile mesenchymal phenotype [4]. A major hallmark of EMT is the down-regulation of cell–cell adhesion molecule, E-cadherin [5], and the up-regulation of several transcriptional factors such as Snail, Slug and Twist, which repress the transcription of E-cadherin [5].

In particular, it has been well documented that Snail and Slug (a closely related member of the Snail family) regulate several genes involved in cell adhesion and cell junctions [6]. Despite many similarities between Snail and Slug, they have different biological functions via their target genes in cancer cells [7,8]. However, little is known about the upstream molecules that modulate the expression of Snail and Slug, which is a cause of subsequent occurrence of EMT.

Syndecans (SDCs) are evolutionary conserved transmembrane heparan sulfate proteoglycan. They are composed of four genes (*SDC1-4*), and act as receptors and co-receptors of cytokines, growth factors and extracellular matrix components. They participate in regulation of cell–cell and cell–extracellular matrix (ECM) adhesion, cell migration, and growth factor activity. Among them, SDC4 is concentrated into focal adhesions together with integrins, which cooperate in generating the signals for the formation of focal adhesion and actin-stress fibers, resulting in the organization of both morphology and cell migration [9]. To date, up-regulation of SDC4 has been identified in the hepatocellular carcinomas and malignant mesotheliomas [10,11]. Nevertheless, it is not clear whether SDC4 play a role in tumor progression and metastasis including EMT.

In the present study, we investigated the role of SDC4 in the control of EMT elicited by transforming growth factor (TGF)-β1 in human lung adenocarcinoma, A549 cells. We found that SDC4 is implicated in the regulation of TGF-β1-induced EMT via Snail. In

Abbreviations: EMT, epithelial to mesenchymal transition; TGF-β, transforming growth factor-β; SDC4, Syndecan-4

* Corresponding author.
E-mail address: yamaoka.t@med.showa-u.ac.jp (T. Yamaoka).

http://dx.doi.org/10.1016/j.bbrep.2015.11.021

addition, both SDC4 and Slug is required for completion of TGF-β1-induced EMT in A549 cells.

2. Materials and methods

2.1. Cell culture and reagents

The human lung adenocarcinoma A549 cell line was obtained from Riken Gene Bank (Tsukuba, Japan) and NCI-H292 cell line was purchased from ATCC. A549 cells were maintained in Dulbecco's modified Eagle's medium (DMEM), and NCI-H292 cells were cultured in RPMI-1640 medium supplemented with 10% fetal bovine serum (FBS) in a humidified atmosphere of 5% CO_2 at 37 °C. TGF-β1 was purchased from R&D Systems (Minneapolis, MN, USA).

2.2. RNA interference

Small interfering (si) RNAs for SDC4, Snail, Slug and control scramble siRNA were obtained from Sigma-Aldrich (MISSION® siRNA, St. Louis, MO, USA). siRNAs with the following sense and antisense sequences were used: SDC4, 5′-GUAUCUCCAGCUCUGAUUATT-3′ (sense), 5′-UAAUCAGAGCUGGAGAUACTT-3′ (antisense); SNAIL, 5′-GCCUUCAACUGCAAAUACUTT-3′ (sense), 5′-AGUAUUUGCAGUUGAAGGCTT-3′ (antisense); SLUG, 5′-GCAUUUGCAGACAGGUCAATT-3′ (sense), 5′-UUGACCUGUCUGCAAAUGCTT-3′ (antisense); control scramble, 5′-CAGUGAAAUUUAUCCACAATT-3′ (sense), 5′-UUGUGGAUAAAUUUCACUGTT-3′ (antisense). For transient RNA interference, the siRNA were transfected at a concentration of 100 pmol per well with Lipofectamine RNAi MAX (Life Technologies Inc., Carlsbad, CA, USA) according to the manufacturer's protocol. Depletion of the targeted genes was confirmed with Western blot, Dot blot analysis, or the real-time reverse transcriptase PCR (RT-PCR).

2.3. RNA purification and real-time RT-PCR analysis

RNA was isolated with the RNeasy Mini Kit (Qiagen, Valencia, CA, USA). First-strand cDNA was synthesized with the Prime Script RT reagent kit (Takara Bio Inc., Otsu, Japan), and gene expression was quantified with the SYBR Green method of real-time PCR with the StepOne Real-Time PCR System (Life Technologies Inc.). Primer sequences are provided in Supplementary Table S1. Relative messenger (m) RNA levels, after normalization with GAPDH, were assessed with the $2-\Delta\Delta Ct$ method. The experiments were performed in triplicate.

2.4. Western blot and dot blot analysis

Whole cell lysates were prepared by lysing the cells in a buffer containing 50 mM Tris–HCl (pH 7.5), 0.15 M NaCl, 0.1% sodium dodecylsulfate, 1% sodium deoxycholate, 1% Triton X-100, and proteinase and phosphatase inhibitor cocktails (Sigma-Aldrich). Lysates were centrifuged for 10 min at 4 °C and an equal amount of protein 25–50 μg from the supernatants was used for SDS-PAGE and immunoblotting.

For Western blot analysis, the primary antibodies were as follows: E-cadherin (BD Biosciences, San Jose, CA, USA); N-cadherin, Snail and Slug (Cell Signaling Technology); integrin α5, β1, and β3 (BD Biosciences); GAPDH (EMD Millipore, Bedford, MA, USA) and SDC4 (Sigma-Aldrich). For Dot blot analysis, the conditioned medium from A549 cells was collected after 24 h of TGF-β1 stimulation, and blotted onto PVDF membranes. Then the membrane was probed with SDC4-specific antibody and visualized with ECL detection reagent.

2.5. Immunofluorescent staining

Cells grown on a glass slide (Poly-D-Lysine 8-well Culture Slides, BD Biosciences) were fixed in 4% paraformaldehyde and permeabilized with 0.1% Triton X-100. After washing with PBS, the cells were blocked with 1% bovine serum albumin in PBS, and incubated with primary antibodies against SDC4 (1:50) overnight. The cells were then incubated in Alexa Fluor 488-conjugated anti-rabbit IgG (Life Technologies Inc.). For phalloidin staining, the cells were incubated for 20 min at room temperature with Alexa Fluor 594 Phalloidin (Life Technologies Inc.) diluted with PBS and 0.1% BSA. After immunostaining, the slides were stained with 4', 6-diamidino-2-phenylindole (DAPI) and mounted.

2.6. Wound-healing assay

Cells were seeded in triplicate on 24-well culture plates at 2×10^4 cells/well. A scratch through the central axis of the plate was gently made using 200-μl micropipette tip 48 h after the cells had been transfected with control non-specific, SDC4 or Slug siRNA. The cells were washed with PBS to remove any loose cells, and fresh media were added with or without TGF-β1 (5 ng/ml). The images were obtained immediately after wounding and after 20 h of incubation. The percentage (%) change in restitution was determined by comparing the difference in wound width ($n=3$).

2.7. Transwell chemotaxis assay

The chemotactic response was assessed with the BD Falcon FluoroBlok system (BD Biosciences) with pore sizes of 8.0 μm in 24-well inserts. Cells (2×10^4 cells) transfected with control, SDC4 or Slug siRNA were loaded into the inserts in 200 μl of DMEM medium containing 0.5% FBS in the presence or absence of TGF-β1 (5 ng/ml). Lower wells of the plate were filled with 800 μl of DMEM supplemented with 10% FBS as an attractant. After 24 h, the lower side of the membrane were fixed with methanol and mounted on glass slides for DAPI staining. DAPI-positive migrated cells were counted with a fluorescent microscope. Assays were performed in triplicate with 3 separate microscope fields per membrane.

2.8. Cell proliferation assay

Cells were transfected with control or SDC4 siRNA at a concentration of 100 pmol per well. After transfection for 48 h, cells (5×10^3 cells/well) were detached and re-seeded in a 96-well plate in the presence or absence of TGF-β1. After 72 h incubation, the MTT (Cell Titer 96 assay kit, Promega, Madison, WI) assay was performed following the manufacturer's instruction. All experimental points were set up in 6–12 wells and all experiments were repeated at least 3 times.

3. Statistical analysis

Statistical analysis was carried out using a two-tailed Student's *t*-Test. *P* values < 0.05 were considered significant.

4. Results

4.1. Up-regulation of SDC4 expression in TGF-β1-induced EMT

A549 cells have been frequently used as a model of inducible TGF-β1-mediated EMT in lung cancer. As shown in Fig. 1A, treatment with TGF-β1 induced a spindle-like mesenchymal morphology characteristic of EMT in A549 cells. This morphological

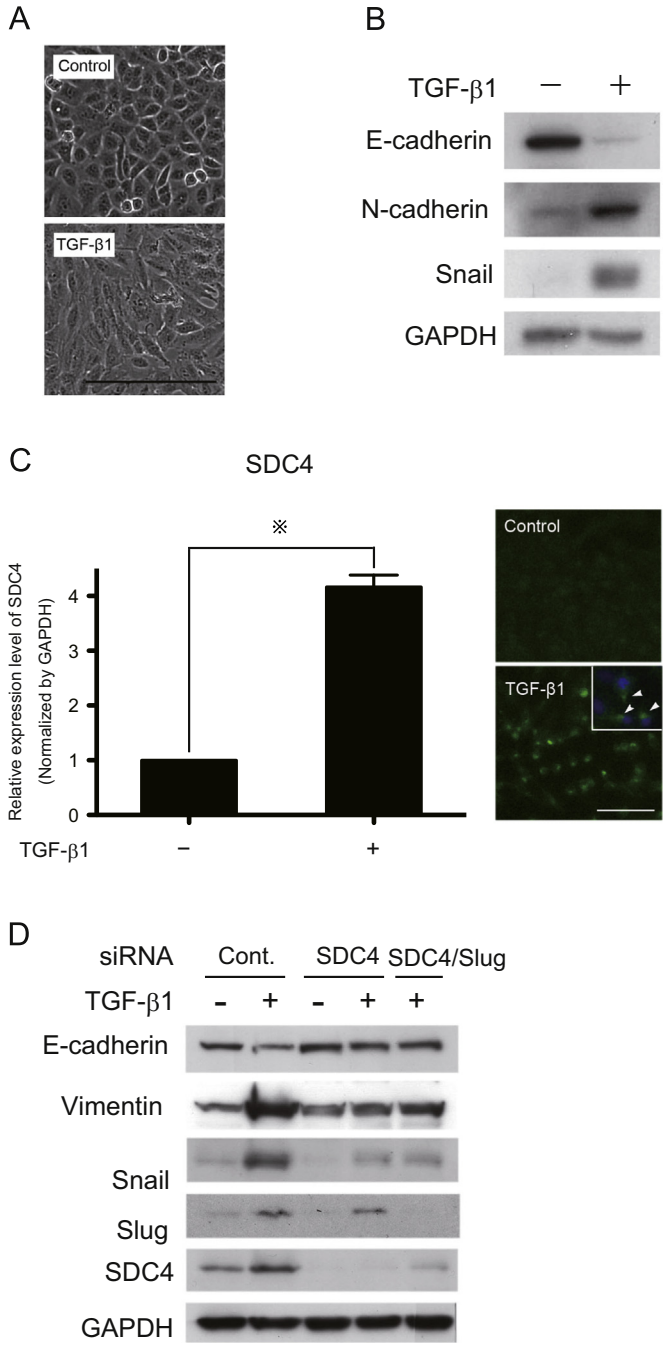

Fig. 1. SDC4 is significantly increased in TGF-β1-induced EMT. A, The images of TGF-β1-induced EMT. Scale bar: 200 μm. A549 cells were exposed in the presence or absence of TGF-β1 (5 ng/ml) for 48 h then images were obtained. B, E-cadherin, N-cadherin and Snail protein expression were determined by Western blot analysis. GAPDH was used as loading control. C, Left: SDC4 mRNA expression was analyzed by real-time RT-PCR using specific primers for SDC4 (Supplementary Table S1). The data were normalized to GAPDH. Each bar represents means ± SEM ($n=3$). "※" indicates statistically significant ($P<0.05$). Right: the images of SDC4 expression by immunofluorescent staining. The arrows indicate SDC4 positive cells. Scale bar: 100 μm. D, The effects of SDC4 siRNA on E-cadherin, Vimentin, Snail and Slug expression were determined by Western blot analysis. Cells were seeded in 6-well culture plates at 1×10^5 cells/well, 48 h after transfection with indicated siRNA(s), then harvest protein samples. GAPDH was used as loading control.

change was accompanied by decrease of E-cadherin expression and increased expression of mesenchymal marker, N-cadherin and EMT-related transcriptional factor, Snail and Slug (Fig. 1B, Fig. 1D). These data indicated that A549 cells exhibit phenotype consistent with EMT. In parallel with the occurrence of EMT, TGF-β1 significantly induced the expression of SDC4 at both protein and mRNA levels (Fig. 1C, left panel, Fig. 1D). Immunofluorescence analysis revealed the punctate localization of SDC4 in the TGF-β1–treated A549 cells (Fig. 1C, right panel). Similar results were obtained from the experiments in another human lung adenocarcinoma cell lines, NCI-H292. SDC4 was induced in NCI-H292 cells by the treatment of TGF-β1, accompanied by the changed expression of some of EMT-related genes including E-cadherin, vimentin and Snail (Fig. S4).

4.2. SDC4 partially contributes to TGF-β1-induced EMT via the up-regulation of Snail

To clarify the role of SDC4 in TGF-β1-induced EMT, we examined the effects of SDC4 siRNA on the EMT phenotype. As shown in Fig. 1D, SDC4 knockdown partially restored the protein expression of E-cadherin, and decreased vimentin. RT-PCR analysis also showed that SDC4 knockdown upregulated the expression of E-cadherin, regardless of whether or not TGF-β1 was present (Fig. 2C). mRNA induction of mesenchymal markers, vimentin and N-cadherin, by TGF-β1 treatment was reduced in the SDC4-siRNA expressed A549 cells (Fig. S6). Furthermore, SDC4 overexpression enhanced the induction of EMT-related genes by the stimulation of TGF-β1 in the both A549 and NCI-H292 cells (Fig. S5). These data show that SDC4 up-regulates the process of TGF-β1-induced EMT. However, the spindle-shaped mesenchymal morphology evoked by TGF-β1 remained in SDC4-knocked down A549 cells (Fig. 2D), indicating that the SDC4 knockdown is insufficient to restore the epithelial morphology. In addition, the SDC4-overexpressing A549 and NCI-H292 cells remained the cobblestone appearance, a characteristic epithelial morphology (Fig. S5A). These results suggest that SDC4 is not involved in the morphological changes accompanied by EMT. Therefore, we investigated how SDC4 knockdown affected the expression of Snail and Slug. The knockdown of SDC4 repressed the expression of Snail at both mRNA and protein levels (Fig. 1D and 2A). In contrast, the expression of Slug protein was not significantly changed by SDC4 knockdown (Fig.1D). Rather, Slug mRNA was increased by SDC4 depletion, as opposed to Snail expression (Fig. 2A and B). In addition, we further addressed the effects of Snail-forced expression in A549 cells (Fig. S2). Single overexpression of Snail, however, did not induce the EMT phenotype. Above findings raise the possibility that SDC4 partially contributes to TGF-β1-induced EMT via the up-regulation of Snail, but additional molecules including Slug is necessary for the completion of EMT in A549 cells.

4.3. Double knockdown of SDC4 and Slug restores epithelial morphology of A549 cells

This notion mentioned above is supported by the experiments using double knockdown of SDC4 and Slug. In the double-knockdown A549 cells, E-cadherin mRNA increased approximately twice as high as those with either SDC4 or Slug single-knockdown (Fig. 2C). Knockdown of both SDC4 and Slug genes restored the epithelial morphology from spindle shape of A549 elicited by TGF-β1 (Fig. 2D). Moreover, phalloidin staining showed TGF-β1 induced the actin stress fibers formation, a feature of EMT. Single knockdown of SDC4 did not affect this actin remodeling. However, when both SDC4 and Slug were silenced, actin filaments organization completely restored the epithelial morphology (Fig. 2E). These results indicated that the expression of both SDC4 and Slug is necessary for TGF-β1-induced EMT.

4.4. SDC-4 enhances TGF-β1-stimulated cell migration and proliferation

The acquisition of more motile phenotype is important consequences of EMT. In response to TGF-β1, A549 cells exhibited

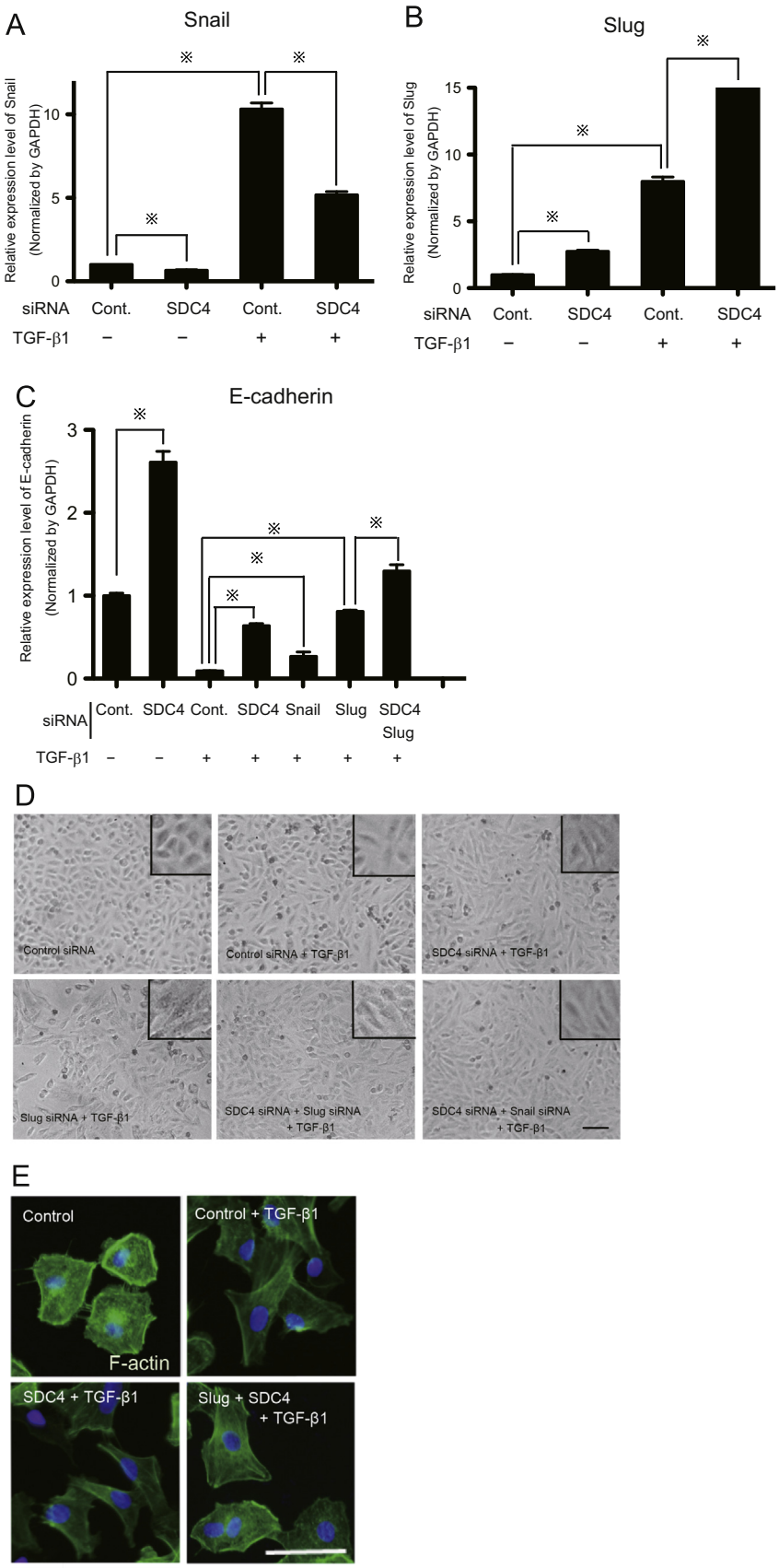

Fig. 2. Effects of SDC4 knockdown on the expression of EMT-related genes and cell morphology. A, B, C, Cells were transfected with indicated siRNAs and after 48 h mRNA was isolated with the RNeasy Mini Kit (Qiagen), then real-time RT-PCR for Snail, Slug and E-cadherin was performed by indicated primers in Supplemental Table S1. Each bar represents means ± SEM ($n=3$). "※" indicates statistically significant ($p<0.05$). D, The cellular morphological images were observed by optical microscope. A549 cells were transfected by indicated siRNA(s), then exposed TGF-β1 for 48 h. Scale bar: 100 μm. E, Representative cellular images of A549 cells subjected to immunofluorescent staining. F-actin was stained with phalloidin. Images of fluorescent staining were obtained for each field and merged by fluorescent microscope (Nikon Eclipse Ni-E). A549 cells were transfected by indicated siRNA(s), then exposed TGF-β1 for 48 h. The blue color indicates nuclei, stained with DAPI. Scale bar: 50 μm.

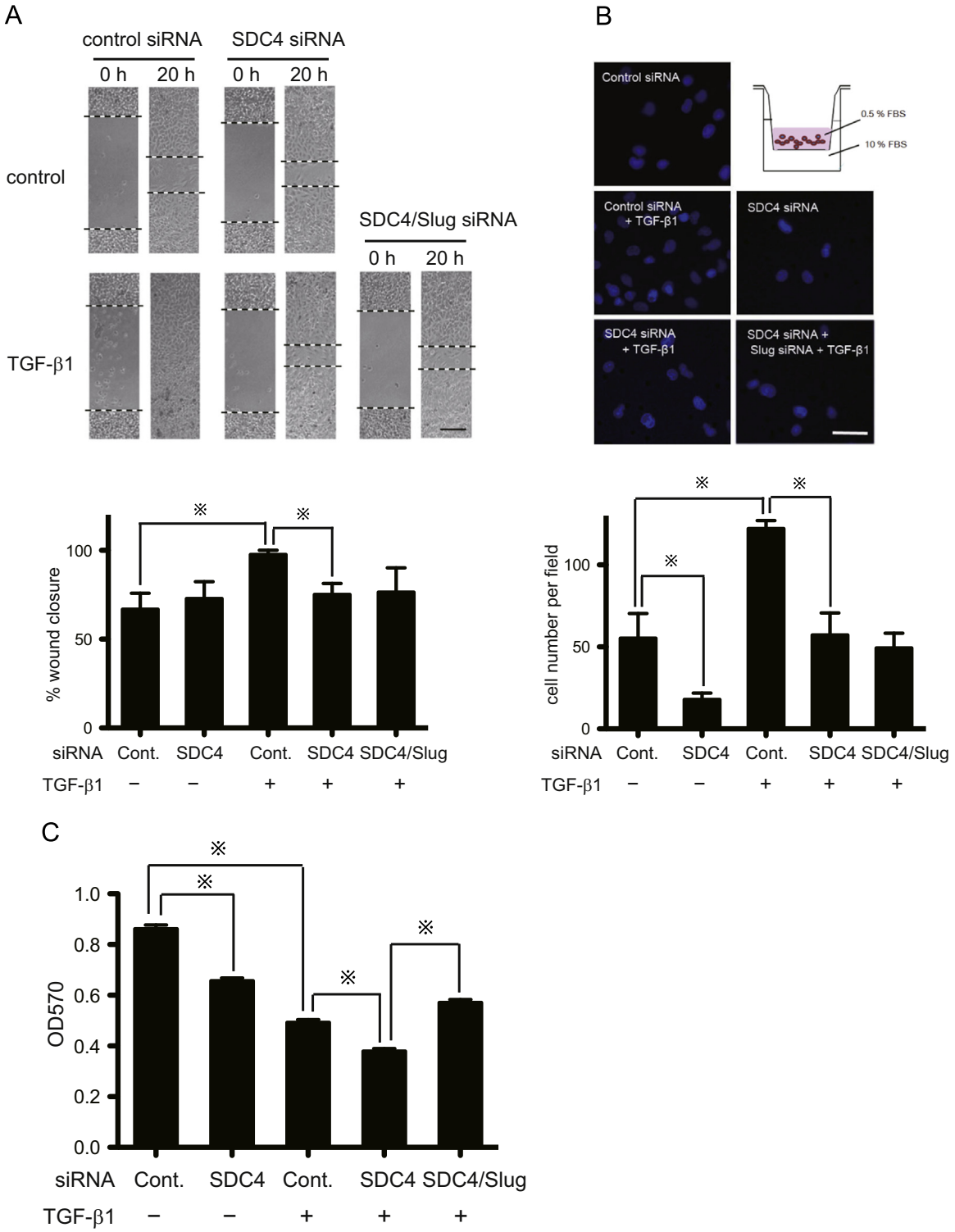

Fig. 3. SDC4 enhances TGF-β1 stimulated cellular restitution, chemotaxis and proliferation. A, Scratched restitution assay. Cells were seeded in 24-well culture plates at 2×10^4 cells/well. Forty-eight hours after transfection with indicated siRNA, a scratch was made using 200-μl micropipette tip. Upper: 0 and 20 h after wounding. Black dotted lines indicate the wound edge. Lower: Percentage (%) change in migration as determined by comparing the difference in wound width ($n=3$). Each bar represents means ± SEM; ※, $p < 0.05$. Scale bars: 100 μm. B, Transwell chemotaxis assay: The transfected A549 cells (2×10^4 cells) were loaded into 24-well inserts (8.0 μm-pore size) with DMEM medium containing 0.5% FBS in the presence or absence of TGF-β1 (5 ng/ml). Lower wells of the plate were filled with DMEM with 10% FBS. After 24 h, remove A549 cell on upper-side, then lower side of membrane were stained with DAPI. DAPI-positive migrated cells were counted with a fluorescent microscope. Each bar represents means ± SEM; ※, $p < 0.05$. Scale bars: 50 μm. C, Cellular proliferation assay: The cellular proliferation was assessed with MTT assay. A549 cells were transfected with indicated siRNAs and reseeded into 96-well plate (5×10^3 cells/well) in the presence or absence of TGF-β1 (5 ng/ml), then after 72 h incubation, MTT assay was performed. Data represent means ± SEM; ※, $p < 0.05$.

enhanced migratory ability, as shown by the wound-healing and transwell chemotaxis assays (Fig. 3A and B). Knockdown of SDC4 resulted in a decreased migration ability with wound-closure rate of 75.1% compared to control siRNA-transfected cells (97.6% wound closure) in the presence of TGF-β1 (Fig. 3A, lane3, 4). A similar result was observed in the transwell chemotaxis assay. SDC4

knockdown significantly blocked the cellular chemotaxis compared with the control siRNA-treated cells, regardless of whether or not TGF-β1 was present (Fig. 3B). However, we didn't find a synergistic effect of the combination of Slug and SDC4 siRNA on cell motility (Fig. 3A and B). Moreover, SDC4 increased the proliferation of A549 cells as shown in Fig. 3C. These results indicate that SDC4 accelerates the cell migration in the context of EMT.

4.5. Ectodomain shedding of SDC4 does not affect TGF-β1-induced EMT

SDC4 is known to be shed by proteolytic cleavage, yielding a variety of physiological reactions including cancer progression. Therefore, we examined the effects of the shed SDC4 on EMT. However, the quantity of shed SDC4 was not changed after exposure of TGF-β1 (Fig. S1A). The addition of cell culture supernatant from A549 cells didn't compensate for the decrease of E-cadherin and Snail mRNA expression by SDC4 siRNA (Fig. S1B). These indicate that the SDC4 ectodomain is not functional for TGF-β1-induced EMT.

4.6. SDC4 is required for retaining the inherent β1 and β3 integrin expression pattern

SDC4 acts cooperatively with integrins in the processes of cell spreading, focal adhesion formation and actin stress fiber assembly. Therefore, we investigated the relationship between the expression of SDC4 and integrin in the process of EMT. By treatment with TGF-β1, the expression of α5 integrin was significantly upregulated, whereas both β1 and β3 integrin expression were down-regulated (Fig. 4A). When SDC4 was knocked down, α5 integrin expression was slightly decreased, while the expression of β1 and β3 integrin was increased (Fig. 4A), suggesting partial reverse to the inherent phenotype of A549 cells. In addition, double knockdown of SDC4 and Slug induced the decreased β1 integrin expression and a further increase of β3 integrin expression (Fig. 4A). These results suggest that the expression of β1 and β3 integrin are independently regulated by SDC4 and Slug, agreeing with the results of actin filaments remodeling shown in Fig. 2E.

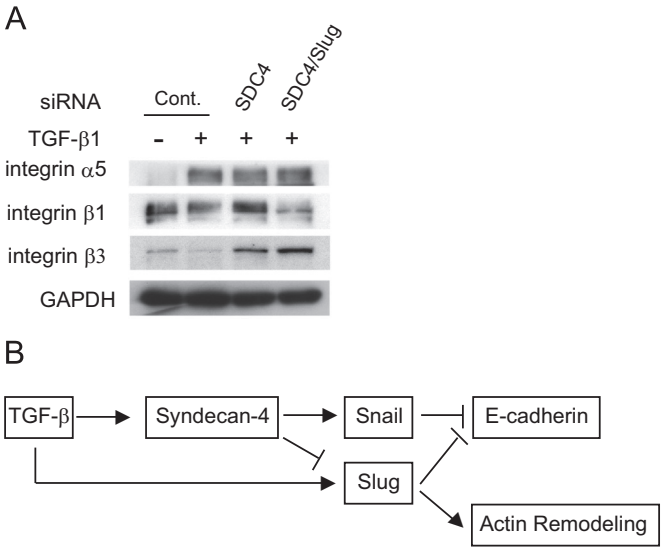

Fig. 4. SDC4 are required for retaining the inherent β1 and β3 integrin expression pattern. A, α5, β1, and β3 integrin expressions were determined by Western-blot analysis. Forty-eight hours after transfection with indicated siRNA, A549 cells were exposed with or without TGF-β1 (5 ng/ml) for 48 h. GAPDH was used as loading control. B, Schema of simplified signal transduction pathways, regulating E-cadherin expression via SDC4, Snail and Slug, and consequent actin remodeling.

5. Discussion

In this study, we demonstrated a correlation between the upregulation of SDC4 expression and TGF-β1-induced EMT in human lung adenocarcinoma, A549 cells. SDC4 is an upstream molecule of Snail, and subsequently modulates the expression of EMT-related genes and promotes cell migration. However, SDC4 didn't upregulate Slug expression in EMT. Both SDC4 and Slug expression are required for the TGF-β-induced EMT in A549 cells.

SDC4 is a focal adhesion component in a range of cell types, adherent to several different matrix molecules, activating protein kinase C-alpha, focal adhesion kinase (FAK), and small GTPase Rho to promote cell adhesion and motility. The SDC4 overexpressing cells showed larger and denser focal adhesions, and correlated to stronger attachment and decreased cell motility [12], whereas SDC4 null cells are deficient in phosphorylated FAK and show impaired cell motility [13,14]. E-cadherin is a mediator cell–cell adhesion in epithelial tissue, and loss of E-cadherin can promote invasive and metastatic behavior in many epithelial tumors [15]. Our study revealed that the SDC4 knockdown significantly inhibited Snail expression and induced E-cadherin. Conversely, Kato et al. reported that loss of syndecan-1 resulted in the mesenchymal phenotype accompanied by the decrease of E-cadherin [16]. Therefore, this is the first report that SDC4 is involved in TGF-β1-induced EMT via Snail signaling.

Snail and Slug are key regulators of TGF-β1-induced EMT in a variety of cancers. Several studies have shown that the induction of both Snail and Slug in the response to TGF-β is mediated by common transcriptional factor, Smad3, which binds to the promoter and activates its transcription of these genes [17–19]. In our study, however, SDC4 raised the expression of Snail and repressed Slug (Fig. 1D, 2A and B). Similar results have been reported in estradiol/estrogen α-induced EMT in breast cancer cell lines [20]. In that paper, the transcription of Slug gene was modulated by the epigenetic histone modification or phosphoinositide 3-kinase/protein kinase B signaling [20]. Furthermore, in pancreatic cancer, Snail and Slug have different functions on cell motility and Rho signaling [21]. Snail, but not Slug, promotes cell migration by β1 integrin [21]. Thus, molecular mechanisms by which the transcription of Snail and Slug is inversely regulated in TGF-β-induced EMT in A549 cells need further elucidation.

Silencing of SDC4 upregulated the E-cadherin expression even in the absence of TGF-β1 (Fig. 2C), though the Snail level was not changed significantly (Fig. 2A). One interpretation of these results is that SDC4 regulates E-cadherin expression via other repressors of E-cadherin expression (e.g. ZEB1/2, Twist1/2 and E47/TCF3 etc) than Snail under the condition without TGF-β1. SDC4 is a multifunctional proteoglycan, which functions as a co-receptor for several growth factors, an independent receptor for FGF or PDGF, a physical connector to extra cellular matrix, and a regulator of Wnt signaling. Therefore, SDC4 might control the expression of E-cadherin through the various and complex signaling in basal condition.

The shed SDC4 ectodomain by proteolytic cleavage is also an important regulatory mechanism for altering pathophysiological conditions, including the processes of tumor development, progression, and metastasis [25–29]. Our study shows that exposure to the conditioned media from A549 cells, including the shed SDC4 ectodomain, is insufficient to disrupt expression of the EMT markers E-cadherin and Snail in response to TGF-β1 in SDC4-attenuated A549 cells (Fig. S1). These findings suggest that the cytoplasmic domain of SDC4 is required for TGF-β–induced EMT.

SDC4 functions as a co-receptor for chemokine and growth factor including TGF-β, vascular endothelial growth factor and fibroblast growth factors [22,23]. SDC4 facilitates binding of such growth factors to their receptors through the heparan sulfate

chains, and enhances the signal evoked by these receptors [24]. Our data showed that TGF-β induced SDC4 expression, followed by the progression of EMT. Possibly, the induced SDC4 protein might further promote EMT by the acceleration of binding TGF-β to the receptor in a positive feedback manner.

In addition, SDC4 is involved in focal adhesion formation and actin stress fibers by cooperating with integrins in a Rho– and protein kinase Cα–dependent manner [25]. A recent study showed that TGF-β signaling enhances Smad3 binding to the β1 integrin promoter, triggering an up-regulation of β1 integrin gene expression [26]. Another study also reported that TGF-β induced to increase both mRNA and protein of β3 integrin subunit in human lung fibroblasts via Src-, and p38 MAPK-dependent pathway [27]. Generally, raised expression of α5β1 and αvβ3 integrin is favorable for cell movement via the attachment to extracellular matrix (ECM) such as fibronectin and vitronectin. However, in human lung adenocarcinoma, A549 cells, TGF-β induced the α5 integrin, but reduced β1/β3 integrin slightly (Fig. 4A). Additionally, SDC4 knockdown led to further increase of both β1 and β3 integrin, although its knockdown inhibited EMT (Fig. 1 and 4). This finding is contrary to previous reports described above [24, 25]. SDC4 is known to interact with ECM identically to integrins and a full cell-adhesion to ECM requires engagement of both types of receptors. Therefore, the increased expression of β1/β3 integrin by SDC4 knockdown may have resulted from a compensation for the attenuated binding between SDC4 and ECM.

SDC4 knockdown could not change the mesenchymal morphology associated with TGF-β1-induced EMT (Fig. 2D and E). Double knockdown of SDC4 and Slug make it possible to revert to the epithelial morphology. Furthermore, single knockdown of SDC4 repressed the cellular restitution and chemotaxis, while double knockdown of SDC4 and Snail exhibited no synergistic effects on the cell migration (Fig. 3). These data suggest that Snail is a regulator of cell motility downstream of SDC4, and Slug is a modulator of the cytoskeletal changes and actin remodeling in TGF-β1-induced EMT in A549 cells. Moreover, single overexpression of Snail could not induce any EMT phenotypes in A549 cells (Fig. S2), suggesting that the progression of TGF-β1-induced EMT is required for more additional factors, e.g. Zeb and Twist family genes.

In conclusion, we have identified a novel role for SDC4 and a new regulatory mechanism during TGF-β1-mediated EMT in lung adenocarcinoma, A549 cells. A549 cells are the typical model of TGF-β-induced EMT. It is necessary to generalize the involvement of SDC4 in EMT using other NSCLC cell lines. Further studies about the regulatory mechanisms of TGF-β-induced EMT via SDC4 should be carried out, thereby disclosing the aspects of cell motility, cell adhesion, and actin filament remodeling in cancer cell invasion and metastasis.

Acknowledgments

This work was supported in part by MEXT-Supported Program for the Strategic Research Foundation at Private Universities, 2012–2014, from the Ministry of Education, Culture, Sports, Science and Technology of Japan. We would like to thank the members of the institute of molecular oncology and Dr. Stephanie Constantin for helpful discussions, and Mr. Andrew Bourger and Gerald O'rourke for correction of the English.

Appendix A. Supplementary material

Supplementary data associated with this article can be found in the online version at http://dx.doi.org/10.1016/j.bbrep.2015.11.021.

References

[1] C.F. Mountain, C.M. Dresler, Regional lymph node classification for lung cancer staging, Chest 111 (1997) 1718–1723.
[2] T.S. Mok, S.S. Ramalingam, Maintenance therapy in nonsmall-cell lung cancer: a new treatment paradigm, Cancer 115 (2009) 5143–5154.
[3] J. Massague, TGFβ in Cancer, Cell 134 (2008) 215–230.
[4] M.A. Huber, N. Kraut, H. Beug, Molecular requirements for epithelial-mesenchymal transition during tumor progression, Curr. Opin. Cell. Biol. 17 (2005) 548–558.
[5] J.P. Thiery, H. Acloque, R.Y. Huang, M.A. Nieto, Epithelial–mesenchymal transitions in development and disease, Cell 139 (2009) 871–890.
[6] K.M. Hajra, D.Y. Chen, E.R. Fearon, The SLUG zinc-finger protein represses E-cadherin in breast cancer, Cancer Res. 62 (2002) 1613–1618.
[7] J.Y. Shih, P.C. Yang, The EMT regulator slug and lung carcinogenesis, Carcinogenesis 32 (2011) 1299–1304.
[8] M. Bernfield, R. Kokenyesi, M. Kato, M.T. Hinkes, J. Spring, R.L. Gallo, E.J. Lose, Biology of the syndecans: a family of transmembrane heparan sulfate proteoglycans, Annu. Rev. Cell. Biol. 8 (1992) 365–393.
[9] A. Woods, J.R. Couchman, Syndecan-4 and focal adhesion function, Curr. Opin. Cell. Biol. 13 (2001) 578–583.
[10] M. Gulyas, A. Hjerpe, Proteoglycans and WT1 as markers for distinguishing adenocarcinoma, epithelioid mesothelioma, and benign mesothelium, J. Pathol. 199 (2003) 479–487.
[11] T. Roskams, R. De Vos, G. David, B. Van Damme, V. Desmet, Heparan sulphate proteoglycan expression in human primary liver tumours, J. Pathol. 185 (1998) 290–297.
[12] R.L. Longley, A. Woods, A. Fleetwood, G.J. Cowling, J.T. Gallagher, J.R. Couchman, Control of morphology, cytoskeleton and migration by syndecan-4, J. Cell. Sci. 112 (Pt 20) (1999) 3421–3431.
[13] A. Woods, Syndecans: transmembrane modulators of adhesion and matrix assembly, J. Clin. Invest. 107 (2001) 935–941.
[14] L.A. Cary, J.F. Chang, J.L. Guan, Stimulation of cell migration by overexpression of focal adhesion kinase and its association with Src and Fyn, J. Cell. Sci. 109 (1996) 1787–1794.
[15] W. Birchmeier, J. Behrens, Cadherin expression in carcinomas: role in the formation of cell junctions and the prevention of invasiveness, Biochim. Et. Biophys. acta 1198 (1994) 11–26.
[16] M. Kato, S. Saunders, H. Nguyen, M. Bernfield, Loss of cell surface syndecan-1 causes epithelia to transform into anchorage-independent mesenchyme-like cells, Mol. Biol. Cell. 6 (1995) 559–576.
[17] K.E. Hoot, J. Lighthall, G. Han, S.L. Lu, A. Li, W. Ju, M. Kulesz-Martin, E. Bottinger, X. J. Wang, Keratinocyte-specific Smad2 ablation results in increased epithelial–mesenchymal transition during skin cancer formation and progression, J. Clin. Invest 118 (2008) 2722–2732.
[18] H.J. Cho, K.E. Baek, S. Saika, M.J. Jeong, J. Yoo, Snail is required for transforming growth factor-β-induced epithelial-mesenchymal transition by activating PI3 kinase/Akt signal pathway, Biochem. Biophys. Res. Commun. 353 (2007) 337–343.
[19] T. Morita, T. Mayanagi, K. Sobue, Dual roles of myocardin-related transcription factors in epithelial mesenchymal transition via slug induction and actin remodeling, J. Cell. Biol. 179 (2007) 1027–1042.
[20] Y. Ye, Y. Xiao, W. Wang, K. Yearsley, J.X. Gao, B. Shetuni, S.H. Barsky, ERalpha signaling through slug regulates E-cadherin and EMT, Oncogene 29 (2010) 1451–1462.
[21] M.A. Shields, S.B. Krantz, D.J. Bentrem, S. Dangi-Garimella, H.G. Munshi, Interplay between β1-integrin and Rho signaling regulates differential scattering and motility of pancreatic cancer cells by snail and Slug proteins, J. Biol. Chem. 287 (2012) 6218–6229.
[22] D. Jiang, J. Liang, G.S. Campanella, R. Guo, S. Yu, T. Xie, N. Liu, Y. Jung, R. Homer, E. B. Meltzer, Y. Li, A.M. Tager, P.F. Goetinck, A.D. Luster, P.W. Noble, Inhibition of pulmonary fibrosis in mice by CXCL10 requires glycosaminoglycan binding and syndecan-4, J. Clin. Invest 120 (2010) 2049–2057.
[23] K. Ishiguro, T. Kojima, T. Muramatsu, Syndecan-4 as a molecule involved in defense mechanisms, Glycoconj. J. 19 (2002) 315–318.
[24] E. Tkachenko, J.M. Rhodes, M. Simons, Syndecans: new kids on the signaling block, Circ. Res. 96 (2005) 488–500.
[25] S. Saoncella, F. Echtermeyer, F. Denhez, J.K. Nowlen, D.F. Mosher, S.D. Robinson, R. O. Hynes, P.F. Goetinck, Syndecan-4 signals cooperatively with integrins in a Rho-dependent manner in the assembly of focal adhesions and actin stress fibers, Proc. Natl. Acad. Sci. USA 96 (1999) 2805–2810.
[26] Y.C. Yeh, W.C. Wei, Y.K. Wang, S.C. Lin, J.M. Sung, M.J. Tang, Transforming growth factor-β1 induces Smad3-dependent β1 integrin gene expression in epithelial-to-mesenchymal transition during chronic tubulointerstitial fibrosis, Am. J. Pathol. 177 (2010) 1743–1754.
[27] D.V. Pechkovsky, A.K. Scaffidi, T.L. Hackett, J. Ballard, F. Shaheen, P.J. Thompson, V. J. Thannickal, D.A. Knight, Transforming growth factor β1 induces αvβ3 integrin expression in human lung fibroblasts via a beta3 integrin-, c-Src-, and p38 MAPK-dependent pathway, J. Biol. Chem. 283 (2008) 12898–12908.

Evaluation of the Safety and Efficacy of Combination Chemotherapy with Vinorelbine and Platinum Agents for Patients with Non-small Cell Lung Cancer with Interstitial Lung Disease

KENTARO OKUDA[1], TAKASHI HIROSE[1], YASUNARI OKI[1], YASUNORI MURATA[1], SOJIRO KUSUMOTO[1], TOMOHIDE SUGIYAMA[1], HIROO ISHIDA[1], TAKAO SHIRAI[1], MASANAO NAKASHIMA[1], TOSHIMITSU YAMAOKA[2], TSUKASA OHNISHI[1] and TOHRU OHMORI[2]

[1]*Division of Respiratory Medicine and Allergology, Department of Internal Medicine,*
[2]*Institute of Molecular Oncology, Showa University School of Medicine, Shinagawa, Tokyo, Japan*

Abstract. *Background: Acute chemotherapy-associated exacerbation of interstitial lung disease (ILD) can occur in patients with non-small cell lung cancer (NSCLC). The safety and efficacy of cytotoxic chemotherapy has not yet been established for NSCLC with ILD. Thus, patients with advanced NSCLC with ILD usually receive only best supportive care. The aim of this study was to assess the safety and efficacy profiles of the combination chemotherapy of vinorelbine and a platinum agent in patients with advanced NSCLC with ILD. Patients and Methods: Nineteen patients with advanced NSCLC with ILD treated with vinorelbine and a platinum agent, either cisplatin or carboplatin, were retrospectively reviewed to examine acute exacerbation of ILD, toxicity, response rate, and survival time. Additionally, possible predictive factors for acute chemotherapy-associated exacerbation of ILD were analyzed. Results: The response rate was 42.1%, the progression-free survival time was 4.4 months, the median survival time was 7.4 months, and the one-year survival rate was 36.8%. Neutropenia was the most frequent grade 3 to 4 toxicity and it occurred in 63.2% of patients. Acute chemotherapy-associated exacerbation of ILD occurred in three patients (15.8%) and caused the death of one of these patients (5.3%). No variables were identified as being predictive factors for acute chemotherapy-associated exacerbation of ILD. Conclusion: The combination chemotherapy with vinorelbine and a platinum agent can be considered as a treatment option for patients with advanced NSCLC with ILD, with careful management after sufficient evaluation of the risks and the benefits.*

Correspondence to: Takashi Hirose, MD, Ph.D., Division of Respiratory Medicine and Allergology, Department of Internal Medicine, Showa University School of Medicine, 1-5-8 Hatanodai, Shinagawa, Tokyo 142-8666, Japan. Tel: +81 337848532, Fax: +81 337848742, e-mail: thirose-shw@umin.ac.jp

Key Words: Acute exacerbation, interstitial lung disease, lung cancer, vinorelbine, platinum agent.

Various interstitial lung diseases (ILDs) have been reported to be risk factors for lung cancer (1). In particular, the incidence of lung cancer in patients with idiopathic pulmonary fibrosis (IPF) has been reported to be high and ranges from 4.4 to 38% (1-3). In patients with lung cancer, the prevalence of IPF is 2% to 8% (3). ILDs are typically chronic conditions and gradually cause respiratory insufficiency. However, some patients with ILD have acute exacerbations characterized by acute progressive and severe respiratory failure, with newly-appearing ground-glass opacity or consolidation on computed tomography (CT) of the chest (4-9). Acute exacerbation of ILD can cause death in weeks to months.

Acute exacerbation of ILD can occur with surgery, chemotherapy, or thoracic radiotherapy in patients with lung cancer with ILD (10-14). Retrospective studies have found rates of acute chemotherapy-associated exacerbation of ILD in patients with lung cancer with ILD to be 20.0% to 37.9% (12-15). However, few studies have evaluated the safety, efficacy, and rate of acute exacerbation of ILD associated with specific chemotherapy regimens in patients with lung cancer with ILD. Recently, in a retrospective study, the combination chemotherapy of monthly or weekly carboplatin and weekly paclitaxel was reported to have caused grade 3 or greater pneumonitis in four out of 15 patients (27%) with advanced non-small cell lung cancer (NSCLC) with ILD (15). On the other hand, Minegishi *et al.* reported that combination chemotherapy of carboplatin and weekly paclitaxel caused acute exacerbation of ILD in only one out of 18 patients (5.6%) with advanced NSCLC with ILD (16).

For patients with advanced NSCLC with ILD, the indication for chemotherapy has not yet been evaluated and a standard regimen has not been established because such patients have been excluded from almost all clinical trials. Thus, patients with advanced NSCLC with ILD usually receive only best supportive care, which is comfort-oriented.

The combination chemotherapy of vinorelbine and a platinum agent, either cisplatin or carboplatin, is a standard chemotherapy regimen for patients with advanced NSCLC. Several studies have shown that this regimen achieves promising survival times and response rates in these patients (17-19). However, to our knowledge, combination chemotherapy of vinorelbine and a platinum agent has not been evaluated in patients with advanced NSCLC with ILD. Therefore, the aims of the present study were to examine the safety, efficacy, and associated rate of acute exacerbation of ILD of the combination chemotherapy of vinorelbine and a platinum agent, either cisplatin or carboplarin, in patients with advanced NSCLC with ILD and to identify factors predicting acute chemotherapy-associated exacerbation of ILD.

Patients and Methods

Patients. From July 2000 through April 2009, 28 patients with advanced NSCLC with ILD were examined at our institution. Out of these 28 patients, 19 (67.9%) met the criteria mentioned below and underwent combination chemotherapy with vinorelbine and cisplatin or carboplatin. Data of these 19 patients were retrospectively analyzed. Out of another 9 patients, 6 received only best supportive care, 2 received single-agent chemotherapy, and 1 received other combination chemotherapy. The criteria for treatment with this regimen were as follows: histologically- or cytologically-proven NSCLC, unresectable stage III or IV disease, a measurable lesion, and adequate bone marrow function (neutrophil count of 1,500/μl or more, platelet count of 100,000/μl or more, and hemoglobin level of 9.0 g/dl or more), renal function (serum creatinine levels less than 1.5 mg/dl and creatinine clearance rate of 50 ml/min or more), and hepatic function (total serum bilirubin level less than the upper limit of the normal range, aspartate aminotransferase and alanine aminotransferase levels less than or equal to twice the upper limits of the normal ranges). Patients who had ILD-related collagen vascular disease were included. Patients who had unstable or acute ILD were excluded. In addition, patients were excluded if they had active infections, severe heart disease, pleural effusion or pericardial effusion that required drainage, or symptomatic brain metastasis. This study protocol for retrospective analysis was approved by the Ethics Committee of Showa University School of Medicine.

Treatment. The treatment regimen consisted of vinorelbine at a dose of 20 or 25 mg/m^2 and of cisplatin at a dose of 80 mg/m^2 or carboplatin with a target area under the plasma concentration *versus* time curve of (AUC) of 5 mg min/ml using the Calvert formula. Cisplatin or carboplatin was administered on day 1, and vinorelbine was administered on days 1 and 8. These agents were administered every three weeks. Chemotherapy was discontinued for grade 3 or higher non-hematological toxicity, except for nausea/vomiting, anorexia, constipation, diarrhea, alopecia, and fatigue; serum creatinine levels greater than 2.0 mg/dl; or a treatment outcome of progressive disease at any time. Vinorelbine was not given on day 8 of treatment if the neutrophil count was less than 1,000/μl or if the platelet count was less than 75,000/μl. Full doses of vinorelbine were then given on day 15 of treatment. If the serum creatinine level was 1.5 to 2.0 mg/dl, cisplatin or carboplatin was withheld. The doses of these agents during the next course were reduced by 20% of the previous doses for grade 4 neutropenia lasting three days or longer, grade 3 or 4 neutropenia associated with a fever greater than 38˚C, or grade 4 thrombocytopenia.

Definition of ILD and acute exacerbation. ILD was classified as showing an IPF pattern and a non-IPF pattern. Diagnosis of the IPF pattern was made with high-resolution CT of the chest and clinical features according to the American Thoracic Society/European Respiratory Society criteria (20). Typical chest CT findings of the IPF pattern were as follows: basal predominant, sub-pleural reticular abnormality with traction bronchiectasis, honeycomb cysts, and no atypical features of IPF (21, 22). The CT scans were reviewed by two physicians. Acute exacerbation of ILD was diagnosed when the following criteria had been fulfilled within one month; i) exacerbation of dyspnea; ii) decline in arterial oxygen tension (PaO_2) of 10 mmHg or more under the same conditions; iii) exacerbation of consolidation or ground-glass opacity on CT scan; and iv) heart failure, pulmonary infection, pulmonary embolism, or pneumothorax had been excluded (4-6).

Clinical evaluation. Evaluation for staging before treatment included chest radiography, CT of the chest and abdomen, magnetic resonance imaging or CT of the brain, and radionucleotide bone scanning. During chemotherapy, complete blood cell counts with differential and routine chemistry profiles were determined at least once a week, and chest radiography was performed once per week. In 15 patients, the percent age vital capacity (%VC) and percent age diffusing capacity for carbon monoxide (%DLCO) were evaluated before chemotherapy.

We investigated serum C-reactive protein (CRP), lactate dehydroxygenase (LDH), Klebs von den Lungen (KL)-6, surfactant protein D (SP-D), and PaO_2, arterial carbon oxygen tension (PaCO2), and alveolar-arterial PaO_2 difference (AaDO2) in arterial blood while the patient breathed room air before chemotherapy. We compared these variables between patients with and without acute exacerbation of ILD.

Tumor response was classified according to the Response Evaluation Criteria in Solid Tumors criteria version 1.0 (23). The toxicity was evaluated according to the National Cancer Institute Common Terminology Criteria for adverse events 3.0 (24).

Statistical methods. Overall survival time was measured from the start of the present treatment until death or last follow-up. Progression-free survival (PFS) time was measured from the start of treatment to the identifiable time of progression. The Kaplan-Meier method was used to construct survival curves. Survival differences between subgroups were compared by means of the log-rank test. The chi-square test was used to determine the significance of differences of laboratory variables between patients with and without acute exacerbation of ILD. Differences with a p-value <0.05 were considered statistically significant. Statistical analyses were performed using the Stat View 5.0 software package (SAS Inc., Chicago, IL, USA).

Table I. *Patients' characteristics*.

Total numbers of patients	19
Gender (male/female)	16/3
Median age in years (range)	69 (52-79)
Smoking status	
Current	13
Former	5
Never	1
Performance status (0/1/2/3)	2/12/4/1
Stage (IIIA/IIIB/IV)	4/6/9
Histological type	
Squamous cell carcinoma	7
Adenocarcinoma	10
Other	2
ILD pattern	
IPF pattern	16
Non-IPF pattern	3
Combined with emphysema (yes/no)	6/13
Treatment before chemotherapy	
Surgery	1
Thoracic radiotherapy	5
None	13
Treatment regimen	
Carboplatin+vinorelbine	9
Cisplatin+vinorelbine	10

ILD: Interstitial lung disease; IPF: idiopathic pulmonary fibrosis.

Results

Patients' characteristics. Of the 19 patients, 16 were men and three were women, with a mean age of 69 years (range=52-79 years; Table I). Sixteen patients had a IPF pattern and three patients a non-IPF pattern. Five patients underwent chemotherapy to treat recurrent disease after surgery (one patient) or thoracic radiotherapy (four patients). Additionally, one patient underwent chemotherapy after palliative thoracic radiotherapy because of stenosis of a main bronchus. The median number of cycles of chemotherapy was 2 (range=1-4).

The mean serum levels of CRP, LDH, KL-6, and SP-D were 2.9 mg/dl, 292.7 IU/l, 912.8 U/ml, and 101.5 ng/ml, respectively. Mean PaO_2, $PaCO_2$, and AaDO2 were 81.1 mmHg, 38.5 mmHg, and 20.7 mmHg, respectively. Mean %VC and %DLCO were 89.6% and 64.5%, respectively.

Treatment response and survival. Out of the 19 patients, none achieved a complete response, eight achieved a partial response, six had stable disease, four had progressive disease, and one was not evaluable: the overall response rate was 42.1% (95% confidence interval=20.3%-66.5%) and the disease control rate was 73.7% (95% confidence interval=48.8%-90.9%).

Survival analysis was performed when the median follow-up time of all patients was 7 months. At the time of analysis, two patients (10.5%) were alive, and one patient had been lost to follow-up. The median PFS time was 4.4 months (range=1-44 months; Figure 1). The median survival time (MST) was 7.4 months (range=1-44 months), and the one-year survival rate was 36.8% (Figure 2).

At the time of evaluation, one patient was alive without recurrence, and three patients had died without cancer recurrence. Out of the 15 other patients who had recurrence, six (40%) received second-line chemotherapy: five (33.3%) received cytotoxic chemotherapy-alone, one (6.7%) received both cytotoxic chemotherapy and an epidermal growth factor receptor (EGFR) tyrosine kinase inhibitor. The other nine patients received only best supportive care.

Acute exacerbation of ILD and other toxicities. Acute chemotherapy-associated exacerbation of ILD occurred in three patients (15.8%) and caused the death of one of these patients (5.3%). The patient who died of acute exacerbation of ILD was a 56-year-old man with adenocarcinoma and an IPF-pattern ILD. He underwent three cycles of chemotherapy with cisplatin and vinorelbine and achieved a partial response. However, he had high fever 21 days after the completion of the third cycle of chemotherapy and consequently had dyspnea. A CT scan of the chest showed newly-diffuse ground-glass opacity in both lungs. Although corticosteroid pulse therapy (1000 mg of methylprednisolone per day for three days) was administered, the respiratory failure did not resolve, and the patient died of acute exacerbation of ILD. Another patient with IPF-pattern ILD had acute exacerbation of ILD unrelated to chemotherapy 30 months after the completion of chemotherapy. Although she received corticosteroids and immunosuppresive therapy, respiratory function worsened, and she died of her respiratory failure 45 months after the completion of chemotherapy without cancer recurrence.

Of the toxicities other than acute exacerbation of ILD, neutropenia was the most frequent grade 3 to 4 toxicity and occurred in 63.2% of patients (Table II). Infection was the most frequent grade 3 to 4 non-hematological toxicity and occurred in 21.1% of patients. There was one treatment-related death due to enterocolitis accompanied by severe diarrhea.

Markers for predicting acute exacerbation of ILD. We evaluated possible markers (CRP, LDH, KL-6, SP-D, PaO_2, and AaDO2) for predicting acute chemotherapy-associated exacerbation of ILD (Table III). However, none were significantly correlated with chemotherapy-associated exacerbation of ILD.

Discussion

Acute exacerbation of various types of ILD has been reported to occur in patients without lung cancer (4-9). Acute exacerbation of IPF, non-specific interstitial pneumonia, and

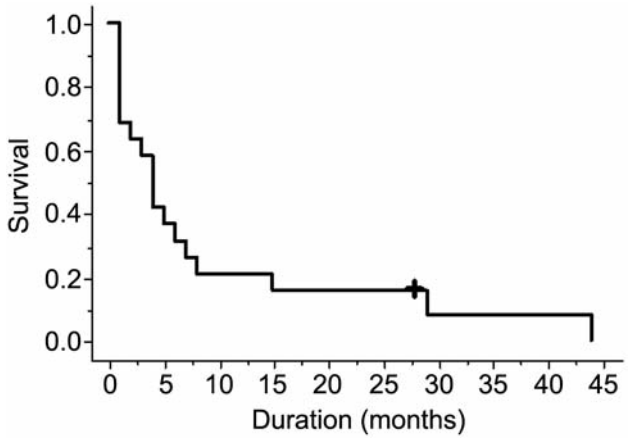

Figure 1. *Progression-free survival (PFS) time estimated with the Kaplan-Meier method. The median PFS time was 4.4 months (range=1-44 months).*

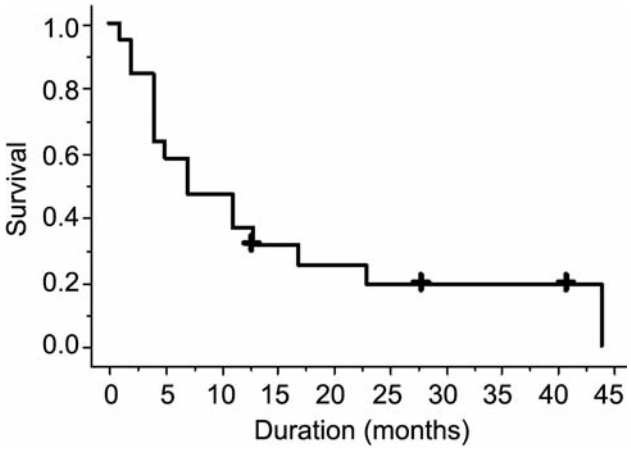

Figure 2. *Overall survival estimated with the Kaplan-Meier method. The median survival time was 7.4 months (range=1-44 months).*

Table II. *Toxicity according to the National Cancer Institute-Common Terminology Criteria (ref. 24)*

Toxicity	Grade					
	1	2	3	4	5	3-5 (%)
Neutropenia	1	4	3	9	0	63.2
Thrombocytopenia	4	6	4	3	0	36.8
Anemia	5	0	1	0	0	5.3
Infection	0	2	3	0	1	21.1
Renal dysfunction	1	0	0	0	0	0
Elevation of aminotransferase	1	2	0	0	0	0
Nausea	7	2	0	0	0	0
Diarrehea	0	0	0	0	1	5.5
Peripheral neuropathy	5	0	0	0	0	0
Arthralgia	2	0	0	0	0	0
Shortness of breath	3	1	1	0	0	0
Pneumonitis	0	0	1	1	1	15.8
Hypoxia	0	1	4	1	0	26.3

Table III. *Variables before chemotherapy associated with acute exacerbation of interstitial lung disease.*

Laboratory data	Cut-off value	Acute exacerbation		*p*-Value
		Yes	No	
CRP (mg/dl)	>1	3	9	0.15
	<1	0	7	
KL-6 (U/ml)	>500	2	13	0.57
	<500	1	3	
SP-D (ng/ml)	>120	0	8	0.11
	<120	3	8	
LDH (IU/l)	>350	1	2	0.36
	<350	2	14	
PaO_2 (mmHg)	>70	2	16	0.46
	<70	1	3	
$AaDO_2$ (mmHg)	>20	3	8	0.11
	<20	0	8	

CRP: C-Reactive protein; LDH: lactate dehydroxygenase; KL-6: Klebs von den Lungen; SP-D: surfactant protein D; PaO_2: arterial oxygen tension; $AaDO_2$: alveolar-arterial PaO_2 difference.

ILD related to collagen vascular disease in the year after diagnosis have been reported to occur at rates of 5% to 19%, 4.2%, and 1.3% to 3.3%, respectively (4, 7-9). On the other hand, in patients who have lung cancer without ILD, lung injury associated with anticancer chemotherapy has been reported to occur at rates of 0.5% to 2.5% (25, 26). Such lung injury is more common in patients with ILD than in those without (25). Additionally, the frequency of acute exacerbation of ILD is higher in Japanese patients than in patients from other countries, due, perhaps, to a genetic difference (25).

Retrospective studies in patients with lung cancer with ILD have found acute chemotherapy-associated exacerbation of ILD at rates of 20.0% to 37.9% (12-15). Recent prospective or retrospective Japanese studies have reported that combination chemotherapy of carboplatin and weekly paclitaxel causes acute exacerbation of ILD in 5.6% to 27% of patients with advanced NSCLC with ILD (15, 16). In the present study, combination chemotherapy of vinorelbine and a platinum agent caused acute exacerbation of ILD in three of 19 patients (15.8%) with advanced NSCLC with ILD. This rate was equivalent to or lower than rates in previous retrospective and prospective studies in Japan (12-16).

Considering that acute exacerbation of ILD can occur without chemotherapy, the combination chemotherapy of vinorelbine and a platinum agent could be administered to patients with advanced NSCLC with ILD, with careful management after sufficient evaluation of the risks and the benefits.

In recent Japanese studies, the response rate with combination chemotherapy of carboplatin and weekly paclitaxel for patients with advanced NSCLC with ILD was 33% to 61%, the median PFS time was 2.5 to 5.3 months, and the MST was 7.0 to 10.6 months (15, 16). In the present study, the response rate was 42.1%, the PFS time was 4.4 months, and the MST was 7.4 months. Response rates and PFS times in patients with advanced NSCLC with ILD in these two earlier studies and the present study were equivalent to those in previous randomized phase III studies of patients with advanced NSCLC without ILD, but the MSTs were inferior (19, 27, 28). The inferior MSTs despite equivalent response rates and PFS times in patients with advanced NSCLC with ILD could be due to some patients having acute exacerbation of ILD both associated and not associated with chemotherapy. In addition, such patients were less likely to receive second-line chemotherapy than patients without ILD, despite the fact that docetaxel, pemetrexed, or EGFR tyrosine kinase inhibitor is recommended as a second-line therapy for relapsed or refractory advanced NSCLC (29). Although patients with advanced NSCLC with ILD have usually received best supportive care because a standard chemotherapy regimen has not been established, our present results and the results of previous studies suggest that chemotherapy would be beneficial for patients with advanced NSCLC with ILD.

Markers have not been established for predicting acute chemotherapy-associated exacerbation of ILD in patients with NSCLC with ILD. Isobe *et al*. reported that smoking index, but not LDH, KL-6, SP-D, PaO_2, %VC, or %DLCO, is the only predictive marker for acute exacerbation of IPF associated with cancer therapy (13). Minegishi *et al*. reported that CRP, but not KL-6, SP-D, PaO_2, or %VC, is the only predictive marker for acute exacerbation of ILD associated with chemotherapy (12). In the present study, none of the evaluated markers, including CRP, LDH, KL-6, SP-D, PaO_2, and AaDO2, was identified as a predictive marker for acute chemotherapy- associated exacerbation of ILD.

Our study has several limitations. Firstly, patient characteristics were heterogeneous, because this study was retrospective. This study included five patients who underwent chemotherapy when they had recurrences after surgery or thoracic radiotherapy and one patient who underwent chemotherapy after palliative thoracic radiotherapy. Previous therapies could have affected the development of acute chemotherapy-associated exacerbation of ILD. Secondly, the number of patients was too small to precisely determine the safety and efficacy of chemotherapy and to identify predictive markers for acute chemotherapy-associated exacerbation of ILD. Performing a large prospective study of specific chemotherapy regimens in patients with advanced NSCLC with ILD is difficult because few patients have both these conditions.

In conclusion, to our knowledge, the present study is the first to evaluate platinum doublet chemotherapy with vinorelbine in patients with advanced NSCLC with ILD. In this study, the efficacy and the rate of acute exacerbation of ILD compared favorably with those of other platinum doublet regimens for patients with advanced NSCLC with ILD. Therefore, combination chemotherapy with a platinum agent and vinorelbine can be considered as a treatment option for patients with advanced NSCLC with ILD, with careful management after sufficient evaluation of the risks and the benefits. Large prospective studies are warranted to evaluate the safety and efficacy of chemotherapy in patients with advanced NSCLC with ILD.

References

1 Bouros D, Hatzakis K, Labrakis H and Zeibecoglou K: Association of malignancy with diseases causing interstitial pulmonary changes. Chest *121*: 1278-1289, 2002.

2 Hubbard R, Venn A, Lewis S and Britton J: Lung cancer and cryptogenic fibrosing alveolitis: A population-based cohort study. Am J Respir Crit Care Med *161*: 5-8, 2000.

3 Raghu G, Nyberg F and Morgan G: The epidemiology of interstitial lung disease and its association with lung cancer. Br J Cancer *91*: S3-S10, 2004.

4 Hyzy R, Huang S, Myers J, Flaherty K and Martinez F: Acute exacerbation of idiopathic pulmonary fibrosis. Chest *132*: 1652-1658, 2007.

5 Kondoh Y, Taniguchi H, Kawabata Y, Yokoi T, Suzuki K and Takagi K: Acute exacerbation in idiopathic pulmonary fibrosis. Analysis of clinical and pathologic findings in three cases. Chest *103*: 1808-1812, 1993.

6 Akira M, Hamada H, Sakatani M, Kobayashi C, Nishioka M and Yamamoto S: CT findings during phase of accelerated deterioration in patients with idiopathic pulmonary fibrosis. Am J Roentgenol *168*: 79-93, 1997.

7 Suda T, Kaida Y, Nakamura Y, Enomoto N, Fujisawa T, Imokawa S, Hashizume H, Naito T, Hashimoto T, Takehara Y, Inui N, Nakamura H, Colby TV and Chida K: Acute exacerbation of interstitial pneumonia associated with collagen vascular diseases. Respir Med *103*: 846-853, 2009.

8 Kim DS, Park JH, Park BK, Lee JS, Nicholson AG and Colby TV: Acute exacerbation of idiopathic pulmonary fibrosis: Frequency and clinical features. Eur Respir J *27*: 143-150, 2006.

9 Park IN, Kim DS, Shim TS, Lim CM, Lee SD, Koh Y, Kim WS, Kim WD, Jang SJ and Colby TV: Acute exacerbation of interstitial pneumonia other than idiopathic pulmonary fibrosis. Chest *132*: 214-220, 2007.

10 Chiyo M, Sekine Y, Iwata T, Tatsumi K, Yasufuku K, Iyoda A, Otsuji M, Yoshida S, Shibuya K, Iizasa T, Saitoh Y and Fujisawa T: Impact of interstitial lung disease on surgical morbidity and mortality for lung cancer: Analyses of short-term and long-term outcomes. J Thorac Cardiovasc Surg *126*: 1141-1146, 2003.

11 Kushibe K, Kawaguchi T, Takahama M, Kimura M, Tojo T and Taniguchi S: Operative indications for lung cancer with idiopathic pulmonary fibrosis. Thorac Cardiovasc Surg *55*: 505-508, 2007.
12 Minegishi Y, Takenaka K, Mizutani H, Sudoh J, Noro R, Okano T, Azuma A, Yoshimura A, Ando M, Tsuboi E, Kudoh S and Gemma A: Excerbation of idiopathic interstitial pneumonias associated with lung cancer therapy. Intern Med *48*: 665-672, 2009.
13 Isobe K, Hata Y, Sakamoto S, Takai Y, Shibuya K and Homma S: Clinical characteristics of acute respiratory deterioration in pulmonary fibrosis associated with lung cancer following anticancer therapy. Respirology *15*: 88-92, 2010.
14 Watanabe N, Taniguchi H, Kondoh Y, Kimura T and Kataoka K: Clinical characteristics of advanced non-small cell lung cancer patients with interstitial pneumonia. Japanese Journal of Lung Cancer *51*: 171-176, 2011 (in Japanese).
15 Shukuya T, Ishiwata T, Hara M, Muraki K, Shibayama R, Koyama R and Takahashi K: Carboplatin plus weekly paclitaxel treatment in non-small cell lung cancer patients with interstitial lung disease. Anticancer Res *30*: 4357-4361, 2010.
16 Minegishi Y, Sudoh J, Kuribayasi H, Mizutani H, Seike M, Azuma A, Yoshimura A, Kudoh S and Gemma A: The safety and efficacy of weekly paclitaxel in combination with carboplatin for advanced non-small cell lung cancer with idiopathic interstitial pneumonias. Lung Cancer *71*: 70-74, 2011.
17 Bretti S, Manzin E, Celano A, Ritorto G, Loddo C and Berruti A: Low dose carboplatin (AUC 4.5) combined with vinorelbine in the treatment of advanced non-small cell lung cancer: A single institution phase II study. Oncol Rep *8*: 381-385, 2001.
18 Cremonesi M, Mandala M, Cazzaniga M, Rezzani C, Gambera M and Barni S: Vinorelbine and carboplatin in inoperable non-small cell lung cancer: A monoinstitutional phase II study. Oncology *64*: 97-101, 2003.
19 Ohe Y, Ohashi Y, Kubota K, Tamura T, Nakagawa K, Negoro S, Nishiwaki Y, Saijo N, Ariyoshi Y and Fukuoka M: Randomized phase III study of cisplatin plus irinotecan *versus* carboplatin plus paclitaxel, cisplatin plus gemcitabine, and cisplatin plus vinorelbine for advanced non-small cell lung cancer: Four-Arm Cooperative Study in Japan. Ann Oncol *18*: 317-323, 2007.
20 Demedts M and Costabel U: ATS/ERS International Multidisciplinary Consensus Classification of the idiopathic interstitial pneumonias. Am J Respir Crit Care Med *165*: 277-304, 2002.
21 Raghu G, Mageto YN, Lockhart D, Schmidt RA, Wood DE and Godwin JD: The accuracy of the clinical diagnosis of new-onset idiopathic pulmonary fibrosis and other interstitial lung disease: A prospective study. Chest *116*: 1168-1174, 1999.
22 Johkoh T, Muller NL, Cartier Y, Kavanagh PV, Akira M, Ichikado K, Ando M and Nakamura H: Idiopathic interstitial pneumonias: Diagnostic accuracy of thin-section CT in 129 patients. Radiology *211*: 555-560, 1999.
23 Therasse P, Arbuck SG, Eisenhauer EA, Wanders J, Kaplan RS, Rubinstein L, Verweij J, van Glabbeke M, van Oosterom AT, Christian MC and Gwyther SG: New guidelines to evaluate the response to treatment in solid tumors, European Organization for Research and Treatment of Cancer, National Cancer Institute of the United States, National Cancer Institute of Canada. J Natl Cancer Inst *92*: 205-216, 2000.
24 National Cancer Institute of the United States: Common Terminology Criteria for Adverse Events (CTCAE) version 3.0. http://ctep.cancer.gov/reporting/ctc.html.
25 Kudoh S, Kato H, Nishiwaki Y, Fukuoka M, Nakata K, Ichinose Y, Tsuboi M, Yokota S, Nakagawa K, Suga M, Japan Thoracic Radiology Group, Jiang H, Itoh Y, Armour A, Watkins C, Higenbottam T and Nyberg F: Interstitial lung disease in Japanese patients with lung cancer: A cohort and nested case control study. Am J Respir Crit Care Med *177*: 1348-1357, 2008.
26 Camus P, Fanton A, Bonniaud P, Camus C and Foucher P: Interstitial lung disease induced by drugs and radiation. Respiration *71*: 301-326, 2004.
27 Sandler A, Gray R, Perry MC, Brahmer J, Schiller JH, Dowlati A, Lilenbaum R and Johnson DH: Paclitaxel-carboplatin alone or with bevacizumab for non-small cell lung cancer. N Engl J Med *355*: 2542-2550, 2006.
28 Scagliotti GV, Parikh P, von Pawel J, Biesma B, Vansteenkiste J, Manegold C, Serwatowski P, Gatzemeier U, Digumarti R, Zukin M, Lee JS, Mellemgaard A, Park K, Patil S, Rolski J, Goksel T, de Marinis F, Simms L, Sugarman KP and Gandara D: Phase III study comparing cisplatin plus gemcitabine with cisplatin plus pemetrexed in chemotherapy-naive patients with advanced-stage non-small-cell lung cancer. J Clin Oncol *26*: 3543-3551, 2008.
29 Azzoli CG, Baker Jr S, Temin S, Pao W, Aliff T, Brahmer J, Johnson DH, Laskin JL, Masters G, Milton D, Nordquist L, Pfister DG, Piantadosi S, Schiller JH, Smith R, Smith TJ, Strawn JR, Trent D and Giaccone G: American Society of Clinical Oncology Clinical Practice Guideline Update on chemotherapy for stage IV non-small cell lung cancer. J Clin Oncol *27*: 6251-6266, 2009.

Received September 25, 2012
Revised October 26, 2012
Accepted October 29, 2012

Published OnlineFirst October 19, 2016; DOI: 10.1158/1078-0432.CCR-16-1779

Personalized Medicine and Imaging

Clinical Cancer Research

Significant Effect of Polymorphisms in *CYP2D6* on Response to Tamoxifen Therapy for Breast Cancer: A Prospective Multicenter Study

Hitoshi Zembutsu[1], Seigo Nakamura[2], Sadako Akashi-Tanaka[2], Takashi Kuwayama[2], Chie Watanabe[2], Tomoko Takamaru[2], Hiroyuki Takei[3], Takashi Ishikawa[4], Kana Miyahara[4], Hiroshi Matsumoto[5], Yoshie Hasegawa[6], Goro Kutomi[7], Hiroaki Shima[7], Fukino Satomi[7], Minoru Okazaki[8], Hisamitsu Zaha[9], Mai Onomura[9], Ayami Matsukata[10], Yasuaki Sagara[10], Shinichi Baba[10], Akimitsu Yamada[11], Kazuhiro Shimada[11], Daisuke Shimizu[12], Koichiro Tsugawa[13], Arata Shimo[13], Ern Yu Tan[14], Mikael Hartman[15], Ching-Wan Chan[15], Soo Chin Lee[16], and Yusuke Nakamura[17]

Abstract

Purpose: CYP2D6 is the key enzyme responsible for the generation of the potent active metabolite of tamoxifen, "endoxifen." There are still controversial reports questioning the association between *CYP2D6* genotype and tamoxifen efficacy. Hence, we performed a prospective multicenter study to evaluate the clinical effect of *CYP2D6* genotype on tamoxifen therapy.

Experimental Design: We enrolled 279 patients with hormone receptor–positive and human epidermal growth factor receptor 2-negative, invasive breast cancer receiving preoperative tamoxifen monotherapy for 14 to 28 days. Ki-67 response in breast cancer tissues after tamoxifen therapy was used as a surrogate marker for response to tamoxifen. We prospectively investigated the effects of allelic variants of *CYP2D6* on Ki-67 response, pathological response, and hot flushes.

Results: Ki-67 labeling index in breast cancer tissues significantly decreased after preoperative tamoxifen monotherapy ($P = 0.0000000000000013$). Moreover, proportion and Allred scores of estrogen receptor–positive cells in breast cancer tissues were significantly associated with Ki-67 response ($P = 0.0076$ and 0.0023, respectively). Although *CYP2D6* variants were not associated with pathologic response nor hot flushes, they showed significant association with Ki-67 response after preoperative tamoxifen therapy ($P = 0.018$; between two groups, one with at least one wild-type allele and the other without a wild-type allele).

Conclusions: This is the first prospective study evaluating the relationship between *CYP2D6* variants and Ki-67 response after tamoxifen therapy. Our results suggest that genetic variation in *CYP2D6* is a key predictor for the response to tamoxifen in patients with breast cancer. *Clin Cancer Res; 23(8); 2019–26. ©2016 AACR.*

Introduction

Tamoxifen has been mainly used for the treatment or prevention of recurrence in patients with estrogen receptor (ER)–positive breast cancers. Five-year tamoxifen therapy was reported to improve the risk of its relapse at least for 15 years, particularly for estrogen receptor–positive invasive tumors in premenopausal women (1). However, in the result of the ATLAS trial (Adjuvant Tamoxifen Longer Against the Shorter), the risk of recurrence during years 5 to 14 was >20% in the patients treated with adjuvant tamoxifen therapy (2). Despite many studies being conducted, the mechanisms underlying the response to this drug in a subset of the patients are not fully identified. 4-Hydroxytamoxifen and endoxifen (4-hydroxy-N-desmethyltamoxifen), which are representative metabolites of tamoxifen, are known to be active therapeutic moieties (3, 4). These two metabolites have 100- fold greater affinity to ER and 30- to 100-fold greater potency

[1]Division of Genetics, National Cancer Center Research Institute, Tokyo, Japan. [2]Department of Breast Surgery, Showa University, Tokyo, Japan. [3]Department of Breast Surgery, Nippon Medical School, Tokyo, Japan. [4]Department of Breast Surgery, Tokyo Medical University, Tokyo, Japan. [5]Department of Breast Surgery, Saitama Cancer Center, Saitama, Japan. [6]Department of Breast Surgery, Hirosaki Municipal Hospital, Hirosaki, Japan. [7]1st Department of Surgery, Sapporo Medical University, Sapporo, Japan. [8]Department of Breast Surgery, Sapporo Breast Surgical Clinic, Sapporo, Japan. [9]Department of Breast Surgery, Nakagami Hospital, Okinawa, Japan. [10]Department of Breast Surgery, Sagara Hospital, Kagoshima, Japan. [11]Department of Breast and Thyroid Surgery, Yokohama City University Medical Center, Yokohama, Japan. [12]Department of Breast Surgery, Yokohama Minato Red Cross Hospital, Yokohama, Japan. [13]Department of Breast and Endocrine Surgery, St. Marianna University School of Medicine Hospital, Kawasaki, Japan. [14]Department of General Surgery, Tan Tock Seng Hospital, Singapore. [15]Department of Surgery, Yong Loo Lin School of Medicine, National University of Singapore and National University Health System, Singapore. [16]Department of Hematology Oncology, National University Cancer Institute, National University Health System, Singapore. [17]Section of Hematology/Oncology, Department of Medicine, The University of Chicago, Chicago, Illinois.

Note: Supplementary data for this article are available at Clinical Cancer Research Online (http://clincancerres.aacrjournals.org/).

Corresponding Author: Hitoshi Zembutsu, Division of Genetics, National Cancer Center, Research Institute, 5-1-1 Tsukiji, Chuou-ku, Tokyo 104-0045, Japan. Phone: 81-3-3542-2511; Fax: 81-3-6737-1221; E-mail: hzenbuts@ncc.go.jp

doi: 10.1158/1078-0432.CCR-16-1779

Published OnlineFirst October 19, 2016; DOI: 10.1158/1078-0432.CCR-16-1779

Translational Relevance

Although many investigations on tamoxifen pharmacogenomics have been performed, there are still inconsistencies with regard to the association results between efficacy of tamoxifen and genetic polymorphism of CYP2D6, which is the rate-limiting enzyme responsible for the metabolism of tamoxifen to its active metabolite, endoxifen. The data from our first prospective tamoxifen-CYP2D6 study show that CYP2D6 variants are significantly associated with Ki-67 response, a surrogate marker for efficacy of tamoxifen, after tamoxifen therapy. Integration of genotypes of CYP2D6 and the other genes, which are identified as novel predictors for efficacy of tamoxifen, could be the future approach to improve the ability of physicians to select the right drug for the estrogen receptor–positive breast cancer and provide a better quality of life to patients with breast cancer.

in inhibiting estrogen-dependent cell growth compared with a parent compound, tamoxifen (3–5). Hence, it has been considered that the differences in the formation of these active metabolites could affect the interindividual variability in the response to tamoxifen. Cytochrome P450 2D6 (CYP2D6) is one of the key enzymes for the generation of the potent active metabolites of tamoxifen, "4-hydroxytamoxifen" and "endoxifen" (6). Many studies indicated that decreased—or null-function—alleles of *CYP2D6* were associated with poor clinical outcome of breast cancer patients treated with tamoxifen (7–12). Genotype-guided dose-adjustment study of tamoxifen provides the evidence that dose adjustment is useful for the patients carrying the reduced or null allele of *CYP2D6* to maintain the effective endoxifen level (13, 14). However, there are several reports claiming the lack of association between *CYP2D6* genotypes and tamoxifen efficacy (15–19), although these studies have been criticized for multiple issues as the cause of false-negative results, including inappropriate patients population, inappropriate DNA sources, and incomplete genotyping analysis (20). Hence, it is critically important to perform prospective studies to clarify the clinical significance of *CYP2D6* genotypes in tamoxifen therapy (21, 22).

Expression levels of Ki-67 protein, a proliferation biomarker, have been known as a predictive marker for the prognosis of cancer patients (23–25). Although clinicopathologic factors such as baseline Ki-67 and tumor size are unlikely to be associated with clinical response to tamoxifen (1, 25), higher Ki-67 expression after short-term (2 weeks) endocrine therapy is suggested to be significantly associated with lower recurrence-free survival in patients with breast cancer (24, 25). Hence, a change in the expression of Ki-67 after short-term tamoxifen therapy could be a promising surrogate biomarker of tamoxifen efficacy (24, 25). Here, we conducted the first prospective association study between Ki-67 response after short-term (14–28 days) preoperative tamoxifen therapy and *CYP2D6* variants in breast cancer patients and evaluated the effect of *CYP2D6* genotypes on tamoxifen therapy.

Materials and Methods

Patients

The primary objective of this study was to examine the association between *CYP2D6* genotypes and clinical response measured by Ki-67 expression levels in breast cancer tissues in patients who are treated with tamoxifen preoperatively. The secondary objective was to determine the effect of *CYP2D6* genotype on pathologic response and adverse event (hot flushes). According to the previous report (26), Ki-67 labeling index decreased by 59.5% and 76.0% after 2 weeks of preoperative tamoxifen and aromatase inhibitor treatment, respectively. Suppose Ki-67 response after tamoxifen therapy in patients with *CYP2D6 wt/wt* correspond to those after aromatase inhibitor therapy, sample size required in this study is approximately 280 patients under the following conditions; statistical power >80%, significance level $P < 0.05$, standard deviation $(\delta) = 50$. Two hundred seventy nine patients with primary breast cancer were prospectively recruited from July 2012 to July 2014 at Showa University, Nippon Medical School, Tokyo Medical University, Saitama Cancer Center, Hirosaki Municipal Hospital, Sapporo Medical University, Sapporo Breast Surgical Clinic, Nakagami Hospital, Sagara Hospital, Yokohama City University Medical Center, Yokohama Minato Red Cross Hospital, St. Marianna University School of Medicine Hospital, Tan Tock Seng Hospital, and National University Cancer Institute, Singapore. All patients were women who were pathologically diagnosed with ER-positive (>10%), human epidermal growth factor receptor 2 (HER2)-negative, invasive breast cancer without distant spread. ER status was evaluated by immunohistochemistry at each site. HER2 negativity was defined as <2+ immunohistochemical staining or 2+ immunohistochemical staining without gene amplification by FISH test. After the definitive diagnosis of breast cancer, all patients received 20 mg/day of tamoxifen for 14 to 28 days (in the waiting period for radical operation) until the day before the operation for the primary breast cancer.

Core-needle biopsy samples for diagnosis of the primary tumor were obtained before the first dose of tamoxifen, and tumor tissues after tamoxifen treatment were obtained at the time of surgery. Tissue samples were fixed in 10% neutral-buffered formalin for <48 hours before being embedded in paraffin. Serial sections (4 μm) were cut and immunostained with mouse monoclonal antibody to Ki-67 (clone Mib-1, 1/200 dilution; Dako) for 30 minutes at room temperature with an automatic immunostainer (Autostainer; Dako). Ki-67 labeling index was recorded as the percentage of immunoreactive cells over the total number of invasive neoplastic cells or over at least 2,000 tumor cells in hotspot of each of the invasive carcinoma in the core-needle biopsy and surgical specimen. Automated recognition and counting of the tumor and immunoreactive cells were carried out using the Pathology Decision Support System "e-Pathologist" (NEC Corporation, Tokyo). Pathologic response to tamoxifen was assessed by using a 6-grade scale as follows: grade 0, no response; grade 1a, mild response; grade 1b, mild to moderate response; grade 2a, moderate to marked response; grade 2b, marked to almost complete response; grade 3, almost complete response.

International Union Against Cancer TNM classification was used to determine the tumor and nodal status. This study was approved by the Institutional Review Boards of the National Cancer Center (Tokyo, Japan) and each participating institution. Written informed consent was obtained from all patients.

Genotyping

Genomic DNA was extracted from peripheral blood using a Qiagen DNA extraction kit (Qiagen). Genotyping for key polymorphisms for *CYP2D6*4* (1846G>A), *CYP2D6*6* (1707delT), *CYP2D6*10* (100C>T), *CYP2D6*14* (1758G>A), *CYP2D6*18*

Published OnlineFirst October 19, 2016; DOI: 10.1158/1078-0432.CCR-16-1779

(4125_4133dupGTGCCCACT), *CYP2D6*21* (2573_2574insC), *CYP2D6*36* (gene conversion to *CYP2D7* in exon 9), and *CYP2D6*41* (2988G>A) was performed using Taqman Drug Metabolism Genotyping Assays (Thermo Fisher Scientific) according to the manufacturer's instructions. Determination of copy number of the *CYP2D6* gene was performed using TaqMan Copy Number Assays (Thermo Fisher Scientific). The whole-gene deletion (*CYP2D6*5*) was detected following reported protocols (27, 28). Multiplication alleles, which consisted of *CYP2D6*10* and *CYP2D6*36* (i.e., *CYP2D6*10-*36* and *CYP2D6*10-*36-*36*), were defined as *CYP2D6*10* because the enzymatic activity of protein encoded by *CYP2D6*36* has been reported to be negligible (29, 30). To evaluate the effects of all *CYP2D6* alleles tested in this study, we defined all decreased and null alleles (**4*, **5*, **10*, **10-*10*, **14*, **10-*18*, **18*, **21*, and **41*) as allele *V*, and **1* and **1-*1* alleles as allele *wt*.

Statistical analysis

All polymorphisms evaluated in this study were tested for deviation from Hardy–Weinberg equilibrium with the use of a χ^2 test. The differences in the Ki-67 labeling index among *CYP2D6* genotypes were evaluated by the Kruskal–Wallis test. The Mann–Whitney *U* test was used for the evaluation of the differences in the Ki-67 labeling index before and after preoperative tamoxifen therapy, and in change of Ki-67 among the proportion of ER-positive cells. We investigated the association of the *CYP2D6* allele with pathologic response and adverse event using the Fisher exact test under allelic, dominant-inheritance, and recessive inheritance models. Statistical tests provided two-sided *P* values, and a significance level of $P < 0.05$ was used. Statistical analyses were carried out using SPSS (version 17.0; SPSS) and the Ekuseru-Toukei 2015 (Social Survey Research Information Co., Ltd.).

Results

Patient characteristics

To examine the effect of tamoxifen on change in the Ki-67 labeling index in breast cancer tissues, we recruited 279 patients receiving preoperative tamoxifen monotherapy for 14 to 28 days. Table 1 shows the characteristics of these 279 patients who were pathologically diagnosed to have an ER-positive, HER2-negative, invasive breast cancer. Their median age at the time of surgery was 56 years old (range, 25–91 years). Among the characteristics listed in Table 1, the proportion of ER-positive cells and the Allred score of ER, which is a semi-quantitative system that takes into consideration the proportion of positive cells and staining intensity, showed significant association with Ki-67 response after preoperative tamoxifen therapy in the Mann–Whitney *U* test ($P = 0.0076$ and 0.0023, respectively, Supplementary Fig. S1).

Table 1. Patient demographics and clinical characteristics

Characteristic	Total ($N = 279$) No. of patients (%)
Age at registration, years	
Median	56
Range	25–91
Menopausal status	
Premenopausal	121 (43.4)
Postmenopausal	156 (55.9)
Unknown	2 (0.7)
Tumor size, cm	
≤2	163 (58.4)
>2	108 (38.7)
Unknown	8 (2.9)
Nodal status	
Negative	238 (85.3)
Positive	36 (12.9)
Unknown	5 (1.8)
ER status	
<1%	0 (0)
1%–10%	0 (0)
10%–32%	6 (2.1)
33%–67%	15 (5.4)
>67%	258 (92.5)
Allred score (ER)[a]	
<8	16 (5.8)
8	129 (46.2)
Unknown	134 (48.0)
PR status	
<1%	30 (10.8)
1%–10%	21 (7.5)
11%–32%	34 (12.2)
33%–67%	26 (9.3)
>67%	160 (57.3)
Unknown	8 (2.9)
Her-2	
Negative	89 (31.9)
1+	146 (52.3)
2+ (without amplification)	44 (15.8)

[a]Composite of the percentage of cells that stained (scored on a scale of 0–5) and the intensity of their staining (scored on a scale of 0–3).

Associations of *CYP2D6* genotypes with pathological response and adverse events

We determined *CYP2D6* genotypes of these 279 patients (Table 2). The allele frequency of *CYP2D6*10*, which is considered to have decreased enzymatic activity and is known to be present at a relatively high frequency in Asian populations, was 32.3%. The frequencies of the alleles observed in this study were comparable to those reported previously (28, 30). We defined all of the *CYP2D6* decreased and null alleles as a "*V*" allele and **1* as a "*wt*" allele as described in "Materials and Methods." We then examined association of *CYP2D6* genotypes with pathologic response and hot flushes in breast cancer patients who received short-term (14–28 days) preoperative tamoxifen treatment (Table 3). We observed no significant association of *CYP2D6* genotypes with pathological response or hot flushes.

Associations between Ki-67 response and tumor response after preoperative tamoxifen therapy

As a primary endpoint of this study, we used Ki-67 response which could be a promising surrogate biomarker of tamoxifen efficacy because duration of the preoperative treatment is very short (14–28 days) for accurate evaluation of tamoxifen efficacy by the tumor size change by an ultrasound test. Ki-67 labeling index was measured by using an automated recognition and counting system as described in Materials and Methods," and representative Ki-67–stained images in patients with *CYP2D6 wt/wt* and *CYP2D6 V/V* are shown in Fig. 1. Ki-67 labeling index in post-treatment tissues (median, 4.6% (0–83.5%)) was significantly lower than that in baseline tissues (median: 9.9% (0.1-78.9%)) as shown in Fig. 2A ($P = 0.0000000000000013$). The changes in Ki-67 for patients with *wt/wt*, *wt/V*, and *V/V* of *CYP2D6* before and after preoperative tamoxifen treatment are shown in Fig. 2B, respectively. Of the 279 patients enrolled in this study, 224 patients showed a decrease of Ki-67 index, and 55 patients

Published OnlineFirst October 19, 2016; DOI: 10.1158/1078-0432.CCR-16-1779

Table 2. Genotype frequency of *CYP2D6*

CYP2D6 genotype	*N* (%)
**1/*1*	96 (34.4)
**1/*5*	24 (8.6)
**1/*10*	97 (34.8)
**1/*10-*10*	1 (0.4)
**1/*10-*18*	1 (0.4)
**1/*14*	2 (0.7)
**1/*18*	1 (0.4)
**1/*21*	1 (0.4)
**1/*41*	9 (3.2)
**5/*10*	7 (2.5)
**5/*21*	1 (0.4)
**41/*41*	1 (0.4)
**10/*10*	35 (12.5)
**10/*10-*10*	1 (0.4)
**10/*41*	2 (0.7)

Table 3. Association of *CYP2D6* variants with pathological response and hot flush after short-term tamoxifen therapy

	Pathologic response (+)[a]	Pathologic response (−)[a]	Hot flush (+)	Hot flush (−)
Number of patients				
wt/wt	36 (0.44)	32 (0.33)	12 (0.32)	78 (0.34)
wt/V	36 (0.44)	45 (0.47)	14 (0.38)	117 (0.51)
V/V	10 (0.12)	19 (0.20)	11 (0.30)	36 (0.15)
Fisher test *P* values				
wt/wt vs	0.170		1.000	
V/V vs	0.220		0.059	
wt vs *V*	0.080		0.250	
Odds ratio (95 % CI)[b]				
wt/wt vs	1.57 (0.85–2.88)		0.94 (0.45–1.97)	
V/V vs	1.78 (0.77–4.08)		0.44 (0.19–0.96)	

[a]Pathological response (+), grade 1a or more; pathological response (−), grade 0.

[b]Odds ratios and confidence intervals (CI) are calculated using the *CYP2D6 V/V* and *Wt/V* or CYP2D6 *V/V* as reference.

showed an increase. We investigated the association between Ki-67 response and tumor response measured by ultrasound. However, we could not observe a significant association between them (R = - 0.12; Supplementary Fig. S2). We also investigated the association between Ki-67 response and pathological response after pre-operative tamoxifen treatment. Patients without any pathological response (grade 0) showed significantly poorer Ki-67 response compared to those showing ≥ grade 1a pathological response ($P = 0.029$; Supplementary Fig. S3).

Associations between *CYP2D6* genotypes and Ki-67 response after pre-operative tamoxifen therapy

We compared the after/before ratio of the Ki-67 index (when it is below 1, the proportion of Ki-67–positive cells is decreased) in two groups, one treated for less than 21 days and the other treated for 21 days or more, but found no significant difference between these two groups ($P = 0.67$, data not shown). To prospectively analyze the effects of *CYP2D6* genotypes on response to tamoxifen, we conducted an association study between *CYP2D6* genotypes and the after/before ratio of the Ki-67 index. Using the Kruskal–Wallis test, *CYP2D6* genotypes were significantly associated with Ki-67 response after tamoxifen treatment (after/before ratio of the Ki-67 index) as shown in Fig. 3A ($P = 0.045$). The patients with homozygous variant alleles (*V*/*V*) showed a smaller decrease of Ki-67 positivity than those carrying at least one wild-type allele ($P = 0.018$; Fig. 3B), suggesting that tumors in the

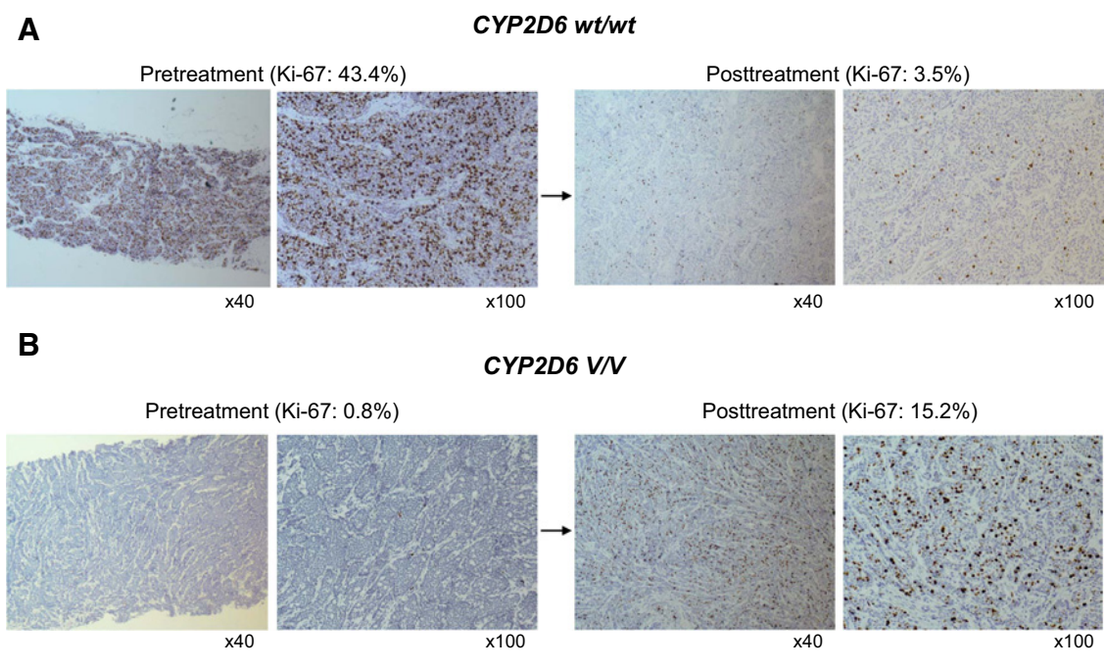

Figure 1.

Representative Ki-67–stained images in patients with *CYP2D6 wt/wt* and *CYP2D6 V/V*. **A,** Posttreatment tissues showed a lower Ki-67 labeling index (3.5%) than pretreatment tissues (43.4%) in patients with *CYP2D6 wt/wt*. **B,** Posttreatment tissues showed higher Ki-67 labeling index (15.2%) than pretreatment tissues (0.8%) in patients with *CYP2D6 V/V*.

Published OnlineFirst October 19, 2016; DOI: 10.1158/1078-0432.CCR-16-1779

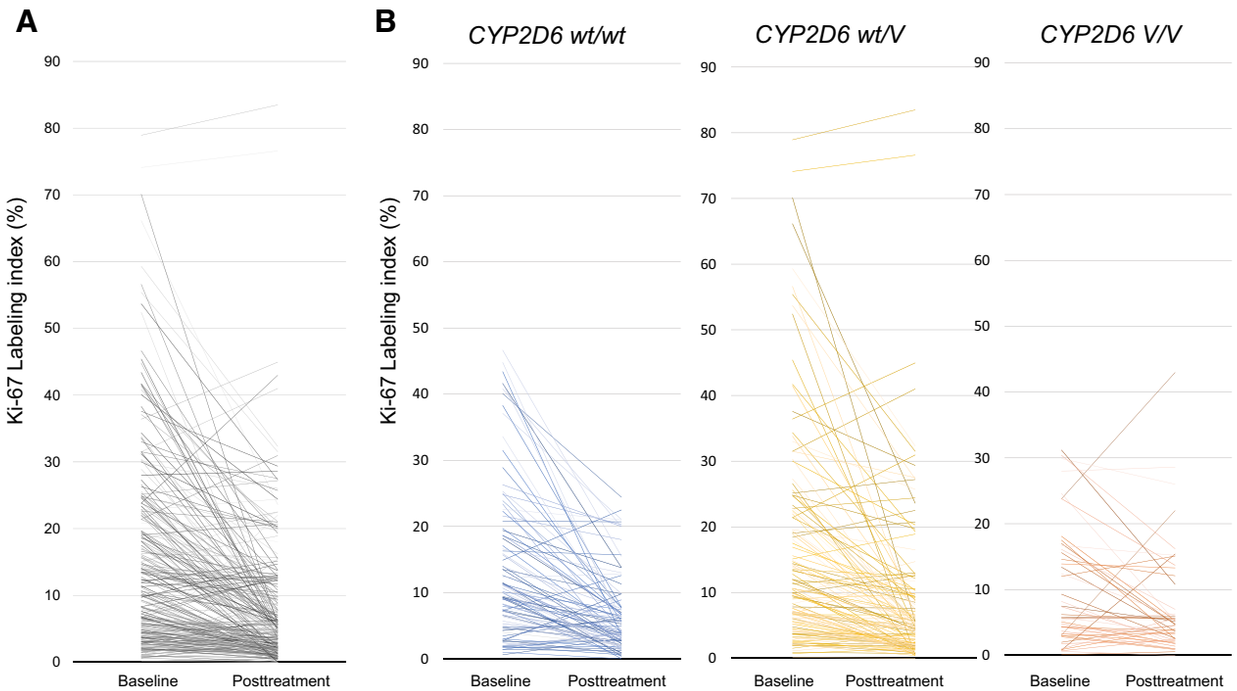

Figure 2.

The change in the Ki-67 labeling index in breast cancer tissues after short-term preoperative tamoxifen therapy. **A,** Of the 279 samples, most of the breast cancer tissues showed significant decrease of Ki-67 labeling index after short-term tamoxifen treatment ($P = 1.3 \times 10^{-15}$). **B,** Ki-67 labeling index of patients with each *CYP2D6* genotype before and after short-term preoperative tamoxifen treatment.

former patients had poorer response to tamoxifen treatment. We further investigated the association of all *CYP2D6* genotypes with Ki-67 and ER in pretreatment tissue, which might be confounding factors, but observed no significant association between them (Supplementary Fig. S4 and Supplementary Table S1).

Discussion

Tamoxifen treatment significantly improves survival in patients with ER-positive breast cancer (1, 2, 31, 32). Tamoxifen has revealed inferiority to aromatase inhibitors as an adjuvant therapy for breast cancer (33); however, some reports have indicated that the risk of certain adverse events including osteoporosis is higher in patients receiving aromatase inhibitors than tamoxifen. Hence, tamoxifen keeps being a key therapeutic drug for ER-positive breast cancer. We previously reported that *CYP2D6* variant alleles, which decrease or lose its enzymatic activity, such as **4*, **5*, **10*, **10-*10*, **14*, **21*, **36-*36*, *and *41*, were significantly associated with clinical outcome of patients with breast cancer receiving adjuvant tamoxifen monotherapy (30). Consistent with this previous report, many studies have reported a significant association between the *CYP2D6* genotypes and clinical outcome of breast cancer patients receiving the tamoxifen therapy in the adjuvant setting (7–12, 30, 34–41). However, discordant results have also been reported (15–19, 42, 43).

Although several critical issues or errors described below could explain these false-negative results (20, 44, 45), it is also quite obvious that the quality of genotyping could be one of the key issues in the pharmacogenomics study. The accuracy of genotyping methods, coverage of allele (genotype; ref. 46) and source of DNA have been reported to influence the quality of genotype data (20). The studies using low-quality genomic DNA extracted from formalin-fixed paraffin-embedded tumor tissues (in some cases, DNAs were extracted from cancer cells) without genotyping *CYP2D6*5* (deletion of the entire *CYP2D6* gene) are likely to lead to the misgenotyping results (20). Moreover, most of studies showing the null association included the patients who were treated with tamoxifen combined with anticancer drugs. To adapt these essential conditions and prospectively clarify the effect of *CYP2D6* as a pharmacogenomic predictor of tamoxifen efficacy, we genotyped wide coverage of *CYP2D6* alleles using high-quality genomic DNA extracted from blood samples of the patients receiving tamoxifen monotherapy, and obtained the results which could prove the clinical significance of *CYP2D6* genotyping in tamoxifen therapy.

In this study, we observed significant decreases in the Ki-67 labeling index with short-term preoperative tamoxifen treatment. The Ki-67 response was significantly associated with the expression level of ER (Supplementary Fig. S1), which is the established target of tamoxifen and also a predictive marker for the response to tamoxifen (47). Moreover, Ki-67 response was also associated with a pathologic response in breast cancer tissues after tamoxifen treatment (Supplementary Fig. S3). Although Ki-67 response after tamoxifen treatment has not yet been a well-established predictive marker for clinical response to tamoxifen, these lines of evidence support a possibility that Ki-67 response after short-term preoperative tamoxifen treatment could be a useful surrogate marker for clinical efficacy of tamoxifen. To prospectively investigate that

Published OnlineFirst October 19, 2016; DOI: 10.1158/1078-0432.CCR-16-1779

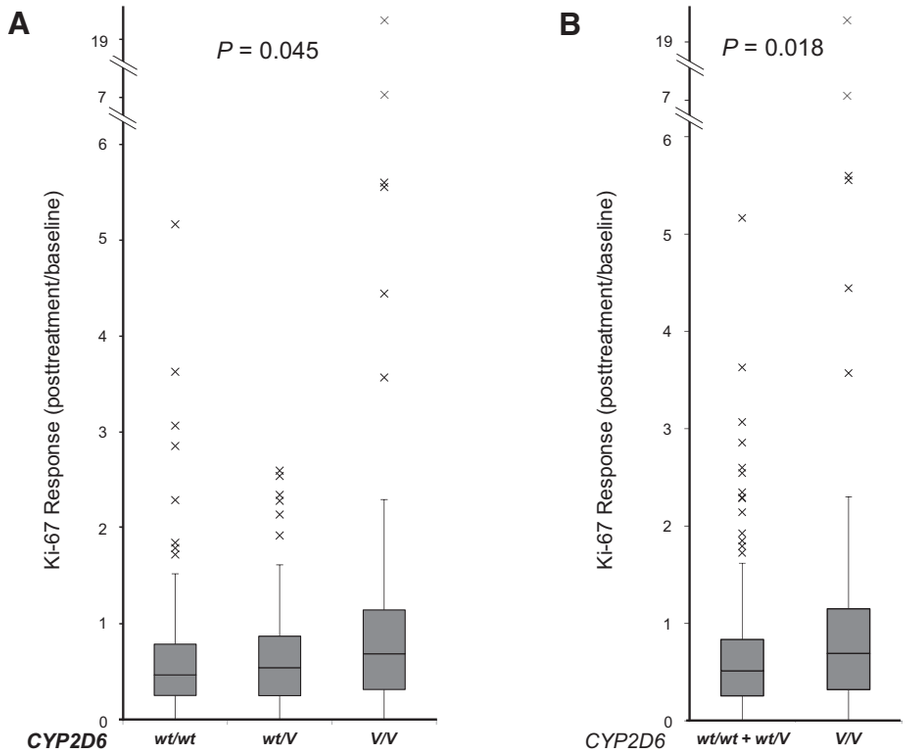

Figure 3.
The relationship between *CYP2D6* genotypes and Ki-67 response in 279 patients treated with pre-operative tamoxifen therapy. **A,** *CYP2D6* genotypes were significantly associated with the Ki-67 response in breast cancer tissues with tamoxifen therapy ($P = 0.045$). **B,** The patients with homozygous variant alleles (*V/V*) showed lower Ki-67 response than those carrying at least one wild-type allele (*wt/V* or *wt/wt*; $P = 0.018$).

CYP2D6 genotypes could be a useful marker for prediction of the response to tamoxifen treatment, we carried out the association study of *CYP2D6* genotypes with Ki-67 response after preoperative tamoxifen therapy. Although the association was not as strong as that observed in our previous retrospective studies in which endpoint were recurrence-free survival (30, 37), *CYP2D6* genotypes were significantly associated with the Ki-67 response ($P = 0.045$; Fig. 3A), which is the primary endpoint of this prospective study. In particular, patients with homozygous variant alleles (*V/V*) showed lower Ki-67 response than those carrying at least one wild-type allele (*wt/wt* or *wt/V*; $P = 0.018$; Fig. 3B). The difference of the significance level in the above studies might be caused by the difference in study endpoints (30, 37).

As secondary endpoints of this study, we investigated the association of *CYP2D6* genotypes with pathological response and hot flushes. Although we found no significant association between *CYP2D6* genotypes and pathological response or hot flushes, it is almost certain that our experimental design was not appropriate to evaluate these parameters, probably because the number of patients was too small, and the administration and observation periods were too short. Hence, further analysis using a larger number of patients treated with longer periods of tamoxifen is required for verification of the effect of *CYP2D6* variants on these endpoints.

The pharmacogenomic information is expected to contribute to establishment of the personalized medicine system in which each patient is provided a right amount of a right drug. To reduce the medical cost with maintaining the quality of medical care, it is of special importance to use effective drugs such as tamoxifen at the lower cost on the basis of individual germline and/or somatic genetic information. In this prospective study, we concluded that the accurate genotyping of *CYP2D6* could become an important predictor for the efficacy of tamoxifen for individual patients with breast cancer. Because novel genetic variants associated with efficacy of tamoxifen have been identified (30, 48), integration of genotypes of *CYP2D6* and other associated genes could be the future approach to improve the ability of physicians to select optimal hormonal therapy for the treatment of ER-positive breast cancer and provide better quality of lives to patients with breast cancer.

Disclosure of Potential Conflicts of Interest

No potential conflicts of interest were disclosed.

Authors' Contributions

Conception and design: H. Zembutsu, S. Nakamura, H. Takei, H. Matsumoto, F. Satomi, Y. Sagara, S. Baba, K. Tsugawa, Y. Nakamura

Development of methodology: H. Zembutsu, S. Nakamura, H. Matsumoto, F. Satomi

Acquisition of data (provided animals, acquired and managed patients, provided facilities, etc.): S. Nakamura, S. Akashi-Tanaka, T. Kuwayama, C. Watanabe, T. Takamaru, T. Ishikawa, H. Matsumoto, Y. Hasegawa, G. Kutomi, F. Satomi, M. Okazaki, H. Zaha, M. Onomura, A. Matsukata, Y. Sagara, S. Baba, A. Yamada, K. Shimada, D. Shimizu, K. Tsugawa, E.Y. Tan, M. Hartman, C.-W. Chan, S.C. Lee

Analysis and interpretation of data (e.g., statistical analysis, biostatistics, computational analysis): H. Zembutsu, S. Nakamura, T. Kuwayama, T. Ishikawa, H. Matsumoto, Y. Hasegawa, G. Kutomi, F. Satomi, M. Okazaki, H. Zaha, M. Onomura, A. Matsukata, S. Baba, A. Yamada, K. Shimada, K. Tsugawa, M. Hartman, S.C. Lee

Writing, review, and/or revision of the manuscript: H. Zembutsu, F. Satomi, E.Y. Tan, M. Hartman, C.-W. Chan, S.C. Lee, Y. Nakamura

Administrative, technical, or material support (i.e., reporting or organizing data, constructing databases): S. Nakamura, T. Kuwayama, T. Takamaru,

K. Miyahara, H. Matsumoto, Y. Hasegawa, H. Shima, F. Satomi, M. Okazaki, H. Zaha, M. Onomura, A. Matsukata, Y. Sagara, S. Baba, A. Yamada, K. Shimada, A. Shimo

Study supervision: H. Zembutsu, T. Ishikawa, F. Satomi, Y. Nakamura

Acknowledgments

We express our heartfelt gratitude to all the study participants. We thank Ms. Hitomi Gunji for technical assistance, and Tatsu Kimura and Ayaka Tomohisa for Ki-67 counting using the Pathology Decision Support System "e-Pathologist." We thank all other members and staffs for their contribution to the sample collection and the completion of our study.

Grant Support

This work was supported in part by Health Labor Sciences Research Grant, the third-term comprehensive control research for cancer (H. Zembutsu), Princess Takamatsu Cancer Research Fund (H. Zembutsu), National Medical Research Council Centre Grant (CG12Aug17; E.Y. Tan), and Japan Research Foundation for Clinical Pharmacology (H. Zembutsu).

The costs of publication of this article were defrayed in part by the payment of page charges. This article must therefore be hereby marked *advertisement* in accordance with 18 U.S.C. Section 1734 solely to indicate this fact.

Received July 14, 2016; revised September 9, 2016; accepted September 28, 2016; published OnlineFirst October 19, 2016.

References

1. Davies C, Godwin J, Gray R, Clarke M, Cutter D, Darby S, et al. Relevance of breast cancer hormone receptors and other factors to the efficacy of adjuvant tamoxifen: patient-level meta-analysis of randomised trials. Lancet 2011;378:771–84.
2. Davies C, Pan H, Godwin J, Gray R, Arriagada R, Raina V, et al. Long-term effects of continuing adjuvant tamoxifen to 10 years versus stopping at 5 years after diagnosis of oestrogen receptor-positive breast cancer: ATLAS, a randomised trial. Lancet 2013;381:805–16.
3. Borgna JL, Rochefort H. Hydroxylated metabolites of tamoxifen are formed in vivo and bound to estrogen receptor in target tissues. J Biol Chem 1981;256:859–68.
4. Lien EA, Solheim E, Lea OA, Lundgren S, Kvinnsland S, Ueland PM. Distribution of 4-hydroxy-N-desmethyltamoxifen and other tamoxifen metabolites in human biological fluids during tamoxifen treatment. Cancer Res 1989;49:2175–83.
5. Johnson MD, Zuo H, Lee KH, Trebley JP, Rae JM, Weatherman RV, et al. Pharmacological characterization of 4-hydroxy-N-desmethyl tamoxifen, a novel active metabolite of tamoxifen. Breast Cancer Res Treat 2004;85: 151–9.
6. Desta Z, Ward BA, Soukhova NV, Flockhart DA. Comprehensive evaluation of tamoxifen sequential biotransformation by the human cytochrome P450 system in vitro: prominent roles for CYP3A and CYP2D6. J Pharmacol Exp Ther 2004;310:1062–75.
7. Goetz MP, Rae JM, Suman VJ, Safgren SL, Ames MM, Visscher DW, et al. Pharmacogenetics of tamoxifen biotransformation is associated with clinical outcomes of efficacy and hot flashes. J Clin Oncol 2005;23:9312–8.
8. Goetz MP, Knox SK, Suman VJ, Rae JM, Safgren SL, Ames MM, et al. The impact of cytochrome P450 2D6 metabolism in women receiving adjuvant tamoxifen. Breast Cancer Res Treat 2007;101:113–21.
9. Schroth W, Goetz MP, Hamann U, Fasching PA, Schmidt M, Winter S, et al. Association between CYP2D6 polymorphisms and outcomes among women with early stage breast cancer treated with tamoxifen. Jama 2009;302:1429–36.
10. Schroth W, Antoniadou L, Fritz P, Schwab M, Muerdter T, Zanger UM, et al. Breast cancer treatment outcome with adjuvant tamoxifen relative to patient CYP2D6 and CYP2C19 genotypes. J Clin Oncol 2007;25:5187–93.
11. Newman WG, Hadfield KD, Latif A, Roberts SA, Shenton A, McHague C, et al. Impaired tamoxifen metabolism reduces survival in familial breast cancer patients. Clin Cancer Res 2008;14:5913–8.
12. Ramon y Cajal T, Altes A, Pare L, del Rio E, Alonso C, Barnadas A, et al. Impact of CYP2D6 polymorphisms in tamoxifen adjuvant breast cancer treatment. Breast Cancer Res Treat 2010;119:33–8.
13. Kiyotani K, Mushiroda T, Imamura CK, Tanigawara Y, Hosono N, Kubo M, et al. Dose-adjustment study of tamoxifen based on CYP2D6 genotypes in Japanese breast cancer patients. Breast Cancer Res Treat 2012;131:137–45.
14. Irvin WJJr, Walko CM, Weck KE, Ibrahim JG, Chiu WK, Dees EC, et al. Genotype-guided tamoxifen dosing increases active metabolite exposure in women with reduced CYP2D6 metabolism: a multicenter study. J Clin Oncol 2011;29:3232–9.
15. Wegman P, Elingarami S, Carstensen J, Stal O, Nordenskjold B, Wingren S. Genetic variants of CYP3A5, CYP2D6, SULT1A1, UGT2B15 and tamoxifen response in postmenopausal patients with breast cancer. Breast Cancer Res 2007;9:R7.
16. Wegman P, Vainikka L, Stal O, Nordenskjold B, Skoog L, Rutqvist LE, et al. Genotype of metabolic enzymes and the benefit of tamoxifen in postmenopausal breast cancer patients. Breast Cancer Res 2005;7: R284–90.
17. Okishiro M, Taguchi T, Jin Kim S, Shimazu K, Tamaki Y, Noguchi S. Genetic polymorphisms of CYP2D6 10 and CYP2C19 2, 3 are not associated with prognosis, endometrial thickness, or bone mineral density in Japanese breast cancer patients treated with adjuvant tamoxifen. Cancer 2009;115: 952–61.
18. Abraham JE, Maranian MJ, Driver KE, Platte R, Kalmyrzaev B, Baynes C, et al. CYP2D6 gene variants: association with breast cancer specific survival in a cohort of breast cancer patients from the United Kingdom treated with adjuvant tamoxifen. Breast Cancer Res 2010;12:R64.
19. Regan MM, Leyland-Jones B, Bouzyk M, Pagani O, Tang W, Kammler R, et al. CYP2D6 genotype and tamoxifen response in postmenopausal women with endocrine-responsive breast cancer: the breast international group 1–98 trial. J Natl Cancer Inst 2012;104:441–51.
20. Kiyotani K, Mushiroda T, Zembutsu H, Nakamura Y. Important and critical scientific aspects in pharmacogenomics analysis: lessons from controversial results of tamoxifen and CYP2D6 studies. J Hum Genet 2013;58: 327–33.
21. Hertz DL, McLeod HL, Irvin WJJr. Tamoxifen and CYP2D6: a contradiction of data. Oncologist 2012;17:620–30.
22. Province MA, Goetz MP, Brauch H, Flockhart DA, Hebert JM, Whaley R, et al. CYP2D6 genotype and adjuvant tamoxifen: meta-analysis of heterogeneous study populations. Clin Pharmacol Ther 2014;95:216–27.
23. Viale G, Giobbie-Hurder A, Regan MM, Coates AS, Mastropasqua MG, Dell'Orto P, et al. Prognostic and predictive value of centrally reviewed Ki-67 labeling index in postmenopausal women with endocrine-responsive breast cancer: results from Breast International Group Trial 1–98 comparing adjuvant tamoxifen with letrozole. J Clin Oncol 2008;26:5569–75.
24. DeCensi A, Guerrieri-Gonzaga A, Gandini S, Serrano D, Cazzaniga M, Mora S, et al. Prognostic significance of Ki-67 labeling index after short-term presurgical tamoxifen in women with ER-positive breast cancer. Ann Oncol 2011;22:582–7.
25. Dowsett M, Smith IE, Ebbs SR, Dixon JM, Skene A, A'Hern R, et al. Prognostic value of Ki67 expression after short-term presurgical endocrine therapy for primary breast cancer. J Natl Cancer Inst 2007;99:167–70.
26. Dowsett M, Smith IE, Ebbs SR, Dixon JM, Skene A, Griffith C, et al. Short-term changes in Ki-67 during neoadjuvant treatment of primary breast cancer with anastrozole or tamoxifen alone or combined correlate with recurrence-free survival. Clin Cancer Res 2005;11:951s–8s.
27. Fukuda T, Maune H, Ikenaga Y, Naohara M, Fukuda K, Azuma J. Novel structure of the CYP2D6 gene that confuses genotyping for the CYP2D6*5 allele. Drug Metab Pharmacokinet 2005;20:345–50.
28. Hosono N, Kato M, Kiyotani K, Mushiroda T, Takata S, Sato H, et al. CYP2D6 genotyping for functional-gene dosage analysis by allele copy number detection. Clin Chem 2009;55:1546–54.
29. Johansson I, Oscarson M, Yue QY, Bertilsson L, Sjoqvist F, Ingelman-Sundberg M. Genetic analysis of the Chinese cytochrome P4502D locus: characterization of variant CYP2D6 genes present in subjects with diminished capacity for debrisoquine hydroxylation. Mol Pharmacol 1994; 46:452–9.

Published OnlineFirst October 19, 2016; DOI: 10.1158/1078-0432.CCR-16-1779

30. Kiyotani K, Mushiroda T, Imamura CK, Hosono N, Tsunoda T, Kubo M, et al. Significant effect of polymorphisms in CYP2D6 and ABCC2 on clinical outcomes of adjuvant tamoxifen therapy for breast cancer patients. J Clin Oncol 2010;28:1287–93.
31. Effects of chemotherapy and hormonal therapy for early breast cancer on recurrence and 15-year survival: an overview of the randomised trials. Lancet 2005;365:1687–717.
32. Tamoxifen for early breast cancer: an overview of the randomised trials. Early breast cancer trialists' collaborative group. Lancet 1998;351: 1451–67.
33. Cuzick J, Sestak I, Baum M, Buzdar A, Howell A, Dowsett M, et al. Effect of anastrozole and tamoxifen as adjuvant treatment for early-stage breast cancer: 10-year analysis of the ATAC trial. Lancet Oncol 2010;11:1135–41.
34. Bijl MJ, van Schaik RH, Lammers LA, Hofman A, Vulto AG, van Gelder T, et al. The CYP2D6*4 polymorphism affects breast cancer survival in tamoxifen users. Breast Cancer Res Treat 2009;118:125–30.
35. Damodaran SE, Pradhan SC, Umamaheswaran G, Kadambari D, Reddy KS, Adithan C. Genetic polymorphisms of CYP2D6 increase the risk for recurrence of breast cancer in patients receiving tamoxifen as an adjuvant therapy. Cancer Chemother Pharmacol 2012;70:75–81.
36. Goetz MP, Suman VJ, Hoskin TL, Gnant M, Filipits M, Safgren SL, et al. CYP2D6 metabolism and patient outcome in the Austrian Breast and Colorectal Cancer Study Group trial (ABCSG) 8. Clin Cancer Res 2013; 19:500–7.
37. Kiyotani K, Mushiroda T, Sasa M, Bando Y, Sumitomo I, Hosono N, et al. Impact of CYP2D6*10 on recurrence-free survival in breast cancer patients receiving adjuvant tamoxifen therapy. Cancer Sci 2008;99:995–9.
38. Xu Y, Sun Y, Yao L, Shi L, Wu Y, Ouyang T, et al. Association between CYP2D6*10 genotype and survival of breast cancer patients receiving tamoxifen treatment. Ann Oncol 2008;19:1423–9.
39. Park HS, Choi JY, Lee MJ, Park S, Yeo CW, Lee SS, et al. Association between genetic polymorphisms of CYP2D6 and outcomes in breast cancer patients with tamoxifen treatment. J Korean Med Sci 2011;26:1007–13.
40. Teh LK, Mohamed NI, Salleh MZ, Rohaizak M, Shahrun NS, Saladina JJ, et al. The risk of recurrence in breast cancer patients treated with tamoxifen: polymorphisms of CYP2D6 and ABCB1. AAPS J 2012;14:52–9.
41. Sukasem C, Sirachainan E, Chamnanphon M, Pechatanan K, Sirisinha T, Ativitavas T, et al. Impact of CYP2D6 polymorphisms on tamoxifen responses of women with breast cancer: a microarray-based study in Thailand. Asian Pac J Cancer Prev 2012;13:4549–53.
42. Park IH, Ro J, Park S, Lim HS, Lee KS, Kang HS, et al. Lack of any association between functionally significant CYP2D6 polymorphisms and clinical outcomes in early breast cancer patients receiving adjuvant tamoxifen treatment. Breast Cancer Res Treat 2012;131:455–61.
43. Rae JM, Drury S, Hayes DF, Stearns V, Thibert JN, Haynes BP, et al. CYP2D6 and UGT2B7 genotype and risk of recurrence in tamoxifen-treated breast cancer patients. J Natl Cancer Inst 2012;104:452–60.
44. Nakamura Y, Ratain MJ, Cox NJ, McLeod HL, Kroetz DL, Flockhart DA. Re: CYP2D6 genotype and tamoxifen response in postmenopausal women with endocrine-responsive breast cancer: the Breast International Group 1–98 trial. J Natl Cancer Inst 2012;104:1264; author reply 6–8.
45. Goetz MP, Sun JX, Suman VJ, Silva GO, Perou CM, Nakamura Y, et al. Loss of heterozygosity at the CYP2D6 locus in breast cancer: implications for germline pharmacogenetic studies. J Natl Cancer Inst 2015;107.
46. Schroth W, Hamann U, Fasching PA, Dauser S, Winter S, Eichelbaum M, et al. CYP2D6 polymorphisms as predictors of outcome in breast cancer patients treated with tamoxifen: expanded polymorphism coverage improves risk stratification. Clin Cancer Res 2010;16:4468–77.
47. Vinayagam R, Sibson DR, Holcombe C, Aachi V, Davies MP. Association of oestrogen receptor beta 2 (ER beta 2/ER beta cx) with outcome of adjuvant endocrine treatment for primary breast cancer–a retrospective study. BMC Cancer 2007;7:131.
48. Kiyotani K, Mushiroda T, Tsunoda T, Morizono T, Hosono N, Kubo M, et al. A genome-wide association study identifies locus at 10q22 associated with clinical outcomes of adjuvant tamoxifen therapy for breast cancer patients in Japanese. Hum Mol Genet 2012;21:1665–72.

Published OnlineFirst October 19, 2016; DOI: 10.1158/1078-0432.CCR-16-1779

Clinical Cancer Research

Significant Effect of Polymorphisms in *CYP2D6* on Response to Tamoxifen Therapy for Breast Cancer: A Prospective Multicenter Study

Hitoshi Zembutsu, Seigo Nakamura, Sadako Akashi-Tanaka, et al.

Clin Cancer Res 2017;23:2019-2026. Published OnlineFirst October 19, 2016.

Original Study

BRCAness Predicts Resistance to Taxane-Containing Regimens in Triple Negative Breast Cancer During Neoadjuvant Chemotherapy☆

Sadako Akashi-Tanaka,[1] Chie Watanabe,[1] Tomoko Takamaru,[1] Takashi Kuwayama,[1] Murasaki Ikeda,[1] Hiroto Ohyama,[1] Miki Mori,[1] Reiko Yoshida,[1] Rikako Hashimoto,[1] Sawada Terumasa,[1] Katsutoshi Enokido,[1] Yuko Hirota,[2] Hiromi Okuyama,[3] Seigo Nakamura[1]

Abstract

We investigated BRCAness in the biopsy and surgical specimens from 73 patients with breast cancer, taken before and after taxane-containing neoadjuvant chemotherapy. All tumors that progressed on taxane-containing regimens had a poor prognosis; all had BRCAness and most were triple negative. Identifying BRCAness can help predict the response to taxane-containing regimens.

Background: To provide optimal treatment of heterogeneous triple negative breast cancer (TNBC), we need biomarkers that can predict the chemotherapy response. **Patients and Methods:** We retrospectively investigated BRCAness in 73 patients with breast cancer who had been treated with taxane- and/or anthracycline-based neoadjuvant chemotherapy (NAC). Using multiplex, ligation-dependent probe amplification on formalin-fixed core needle biopsy (CNB) specimens before NAC and surgical specimens after NAC. BRCAness status was assessed with the assessor unaware of the clinical information. **Results:** We obtained 45 CNB and 60 surgical specimens from the 73 patients. Of the 45 CNB specimens, 17 had BRCAness (38.6% of all subtypes). Of the 23 TNBC CNB specimens, 14 had BRCAness (61% of TNBC cases). The clinical response rates were significantly lower for BRCAness than for non-BRCAness tumors, both for all tumors (58.8% vs. 89.3%, $P = .03$) and for TNBC (50% vs. 100%, $P = .02$). All tumors that progressed with taxane therapy had BRCAness. Of the patients with TNBC, those with non-BRCAness cancer had pathologic complete responses significantly more often than did those with BRCAness tumors (77.8% vs. 14.3%, $P = .007$). After NAC, the clinical response rates were significant lower for BRCAness than for non-BRCAness tumors in all subtypes ($P = .002$) and in TNBC cases ($P = .008$). After a median follow-up of 26.4 months, 6 patients—all with BRCAness—had developed recurrence. Patients with BRCAness had shorter progression-free survival than did those with non- BRCAness ($P = .049$). **Conclusion:** Identifying BRCAness can help predict the response to taxane, and changing regimens for BRCAness TNBC might improve patient survival. A larger prospective study is needed to further clarify this issue.

Clinical Breast Cancer, Vol. 15, No. 1, 80-5 © 2015 The Authors. Published by Elsevier Inc. All rights reserved.
Keywords: Multiplex ligation-dependent probe amplification, Platinum salts, Predictive marker, Prognostic marker, Taxane resistance

Introduction

Triple negative breast cancer (TNBC) includes diverse histologic phenotypes and molecular profiles, with varying responses to therapy.[1] Approximately one third of patients with high-grade TNBC respond well to neoadjuvant chemotherapy (NAC) containing anthracycline and taxane and achieve a pathologic complete

[1]Department of Breast Surgical Oncology, Showa University School of Medicine, Tokyo, Japan
[2]Department of Pathology, Showa University School of Medicine, Tokyo, Japan
[3]Department of Pharmacy, Showa University School of Medicine, Tokyo, Japan

Submitted: May 3, 2014; Revised: Aug 12, 2014; Accepted: Aug 25, 2014; Epub: Sep 28, 2014

Address for correspondence: Sadako Akashi-Tanaka, MD, PhD, Department of Breast Surgical Oncology, Showa University School of Medicine, 1-5-8, Hatanodai, Shinagawa-ku, Tokyo 142-8666 Japan
E-mail contact: sakashi@med.showa-u.ac.jp

1526-8209/$ - see frontmatter © 2015 The Authors. Published by Elsevier Inc. All rights reserved.
http://dx.doi.org/10.1016/j.clbc.2014.08.003

response (pCR), which is reportedly a surrogate marker for overall survival in TNBC.[2,3] However, approximately 20% of patients with TNBC will develop progression during NAC, especially those receiving taxane regimens, and have a very poor prognoses.[4,5] Diagnostic imaging studies and immunohistochemical and histologic studies cannot distinguish between resistant and sensitive TNBC tumors. Therefore, quick, accessible, and reproducible biomarkers are needed to identify the optimal chemotherapeutic regimens for patients with this heterogeneous disease.

Recent randomized trials have shown that adding carboplatin to anthracycline and taxane for NAC improves the pCR rates for TNBC; 2 meta-analyses found similar effects from adding platinum agents to NAC regimens.[6-9] However, adding carboplatin to standard NAC increases the incidence of adverse events, leading to greater rates of discontinuation and dose modification. Whether carboplatin should be added to, or substituted for, standard NAC regimens is unclear; thus, markers that can predict the response to standard NAC are needed.

"BRCAness" refers to some sporadic cancers that share phenotypic characteristics with tumors that carry BRCA1/2 mutations (BRCAMut), such as methylation of BRCA1/2 promoters and low BRCA1 gene expression.[10] Double-strand DNA breaks (DSBs) are repaired by homologous recombination, mediated by the products of BRCA1 and BRCA2 and by nonhomologous end-joining. Single-strand breaks are repaired by the base-excision repair pathway, which is regulated by poly-ADP ribose polymerase (PARP) 1 and by nucleotide exon repair mechanisms. Therefore, because BRCAMut tumors cannot repair DSBs induced by agents such as bifunctional alkylators and platinum salts, they are hypersensitive to DSB-inducing agents and probably to PARP inhibitors.[11-14] Assessment of BRCAness using array comparative genomic hybridization (aCGH) or multiplex ligation-dependent probe amplification (MLPA) has recently been described.[15] Patients with BRCAness tumors survive longer when treated intensively with alkylating agents as adjuvant chemotherapy.[15] Although germline mutations in BRCA1 and BRCA2 genes have been associated with $\leq$ 15% of TNBC cases,[16,17] MLPA assessments of BRCA status have indicated that these mutations are seen in approximately two thirds of TNBC cases.[18] The number of those who will benefit from targeted chemotherapy regimens and/or PARP inhibitors might be larger when using BRCAness, rather than BRCA1/2 mutation status, as the determinant.

Emerging preclinical and some clinical studies have indicated that BRCA-associated tumors tend to be resistant to taxanes.[16,17] Mammary tumors of BRCAMut$^+$ mice are resistant to doxorubicin and docetaxel but not to cisplatin.[16] An in vitro study has shown a BRCAMut$^+$ breast cancer cell line to be resistant to taxane.[1] BRCAMut$^+$ hormone receptor–positive metastatic breast cancer has been shown to be less sensitive to taxane.[17] However, to our knowledge, the association between taxane response and BRCAness has not been previously reported.

The present study investigated whether BRCAness can predict the response to taxane treatment in patients with breast cancer treated with NAC.

Patients and Methods

Patients

All the patients who received NAC with either taxane and/or anthracycline for primary breast cancer from October 2010 to March 2013 at Showa University Hospital Breast Center were included in the present retrospective study. Most of these patients had been in randomized controlled trials comparing the efficacy and feasibility of docetaxel followed by 5-fluorouracil, epirubicin, and cyclophosphamide (FEC) every 3 weeks or weekly albumin-bound paclitaxel (nab-paclitaxel) followed by FEC as NAC for patients with human epidermal growth factor receptor 2 (HER2)–negative breast cancer. Before these trials had started, the regimen administered was docetaxel and cyclophosphamide every 3 weeks.

For HER2$^+$ tumors, the regimen was FEC followed by docetaxel and trastuzumab. Relevant clinicopathologic information was collected from our database and medical records. Clinical responses were determined by ultrasonography and magnetic resonance imaging using the Response Evaluation Criteria in Solid Tumors,[19] with imaging performed before NAC and at the end of the first and second cycles. The clinical response rate (cRR) was defined as the sum of the clinical complete and partial responses (PRs). In patients whose tumors progressed, the regimen was stopped, and either surgery performed or a second-line regimen substituted.

The patients underwent surgery approximately 1 month after completing the last NAC cycle. The surgical procedures were determined according to the diagnostic imaging findings after NAC completion. Sentinel lymph node biopsy was performed in patients whose lymph nodes had been clinically negative before NAC.

The institutional review board of our university approved present the study.

Pathology

The tumor subtypes were routinely determined immunohistochemically before NAC, using core needle biopsy (CNB) specimens. The cancer specimens were defined as HER2$^+$ when HER2 immunohistochemical staining was 3+ or fluorescence in situ hybridization (FISH) showed HER2 gene amplification. Estrogen receptor (ER) and progesterone receptor (PgR) positivity was defined as $\geq$ 1% of tumor cells staining positive for ER or PgR. A pCR was defined as complete remission of the invasive components of cancer in the breast.[20]

MLPA Method

BRCAness was determined by examination of formalin-fixed, paraffin-embedded (FFPE) CNB specimens taken before NAC and surgical specimens taken after NAC. DNA was isolated from the tumor tissue using the QIAamp DNA FFPE Tissue Kit (Qiagen, Hilden, Germany) after macrodissection. Classification of BRCAness was performed using MLPA with the Probemix P376-B2 BRCA1ness (MRC-Holland, Amsterdam, The Netherlands), as previously reported by Oonk et al.[13] MLPA was performed at Falco Biosystems (Kyoto, Japan) as a part of collaborative research and according to the manufacturer's instructions. For each sample, the relative copy number ratios for the 38 target-specific probes, compared with the reference samples of human genomic DNA (Promega, Madison, WI), were calculated using the Coffalyser.Net software and were used for the prediction analysis for microarrays, with the training set generated by MRC-Holland. Each sample was analyzed twice. The average scores were used for this analysis. BRCAness status was analyzed by experienced laboratory scientists who were unaware of the

patients' clinical information. The cutoff ratio for BRCAness positivity was 0.4.

BRCA1/2 Germline Mutation

Genetic counseling was recommended for patients suspected of having BRCA germline mutations, in accordance with the National Comprehensive Cancer Network guidelines. One half of them underwent genetic testing. BRCA1/2 mutation analysis was performed at Falco Biosystems (Kyoto, Japan) using the direct sequencing method on patient blood samples. If this initial analysis did not detect a mutation, the sample was checked again for BRCA1/2 genetic rearrangements using MLPA.

Statistical Analysis

Fisher's exact test was used to assess the differences between the BRCAness and non-BRCAness groups. Student's *t* test was used to assess the differences between the BRCAness and non-BRCAness groups for the Ki-67 index. The log-rank test was used to evaluate the differences in relapse-free survival. The software used was EZR on R[21] for Fisher's exact test and SPSS for the log-rank test.

Results

Of the 73 patients who underwent NAC, surgical specimens were available from 60 patients and CNB specimens from 45 patients for BRCAness analysis (Table 1). In 13 patients who had a pCR, BRCAness could not be measured on the surgical specimens. Also, 28 CNB specimens were not available, because the CNBs had been performed by the patients' family doctor. The patients' overall mean age at the diagnosis of breast cancer was 42.0 years (range, 27-75 years). Nine patients underwent genetic testing for BRCA1/2 germline mutation after genetic counseling; 5 patients carrying the BRCA1 germline mutation and 2 with the BRCA2 mutation were identified among the 73 patients. Of these 5 patients, 4 with the BRCA1 germline mutation and 1 with the BRCA2 mutation were BRCAness positive.

Of the 45 CNB specimens of all tumor subtypes, 17 (23.3%) were BRCAness positive. Of the 23 CNB specimens with TNBC, 14 (60.9%) were BRCAness positive. The other 3 BRCAness tumors without TNBC included 2 HER2-enriched tumors and 1 ER^+ tumor. One tumor that was $HER2^+$ before NAC had changed to TNBC after NAC. Another $HER2^+$ tumor was immunohistochemically 3+ but had been FISH-negative before NAC. The tumor tested positive after NAC. The only ER^+ tumor remained ER^+ after NAC.

We analyzed the association between BRCAness found in the CNB specimen and the cRR for taxane-containing regimens (Table 2). The cRR was significantly lower for BRCAness tumors of all subtypes (58.8%) than for non-BRCAness tumors (89.3%; $P = .027$) and, more strikingly so, for BRCAness TNBC (50%) than for non-BRCAness TNBC (100%; $P = .019$). All the non-BRCAness TNBC cases responded well to taxane regimens.

Five patients experienced progressive disease (PD) during taxane-containing NAC (Table 3), including 4 with BRCAness TNBC and 1 with a mucinous ER^+/PgR^+ carcinoma. CK5/6 and epidermal growth factor receptor were not effective in predicting the response to taxane.

Table 1 Relevant Patient and Tumor Characteristics

Variable	All NAC Patients (n = 73)	CNB Available (n = 45)
Age (years)	42.0 (27-75)	42.3 (27-73)
Tumor size before NAC		
T1	10 (13.7)	5 (11.1)
T2	43 (58.9)	28 (62.2)
T3	15 (20.5)	9 (20.0)
T4b	5 (6.8)	3 (6.7)
Histologic type before NAC		
IDC	68 (93.2)	40 (88.9)
ILC	2 (2.7)	2 (4.4)
Apocrine	1 (1.4)	1 (2.2)
Mucinous	2 (2.7)	2 (4.4)
Subtype before NAC		
Triple negative	26 (35.6)	23 (51.1)
$ER^-/HER2^+$	13 (17.8)	7 (15.6)
$ER^+/HER2^+$	7 (9.6)	2 (4.4)
$ER^+/HER2^-$	27 (37.0)	13 (28.9)
Regimen		
Taxane + anthracycline	48 (65.8)	32 (72.7)
Taxane	12 (16.4)	10 (22.7)
Taxane + anthracycline + trastuzumab	13 (17.8)	3 (4.5)
Clinical response		
CR	7 (9.6)	7 (15.9)
PR	47 (64.4)	28 (61.4)
SD	14 (19.2)	5 (11.4)
PD	5 (6.8)	5 (11.4)
Pathologic response		
pCR	11 (15.1)	11 (25.0)
Other	62 (84.9)	34 (75.0)
Pathologic nodal status		
N0	46 (61.3)	32 (71.1)
N1-N3	18 (24.7)	8 (17.8)
N4 or greater	9 (12.3)	5 (11.1)

Data presented as mean (range) or n (%).
Abbreviations: CNB = core needle biopsy; CR = complete response; ER = estrogen receptor; HER2 = human epidermal growth factor receptor 2; IDC = invasive ductal carcinoma; ILC = invasive lobular carcinoma; NAC = neoadjuvant chemotherapy; pCR = pathologic complete response; PD = progressive disease; PR = partial response; SD = stable disease.

Patients with non-BRCAness TNBC achieved pCRs significantly more often (77.8%) than did those with BRCAness TNBC (14.3%; $P = .0066$; Table 4). Before NAC, the patients with BRCAness or non-BRCAness TNBC did not differ significantly in any other clinicopathologic factor.

Of the 60 surgical specimens taken after NAC, 9 (15.0%) were BRCAness positive. Analysis of the association between BRCAness subtype and the cRR after taxane-containing regimens showed that, for all subtypes, the cRR was significantly lower for BRCAness tumors (22.2%) than for non-BRCAness tumors (78.4%; $P = .002$) and more so for BRCAness TNBC tumors (14.3%) than for non-BRCAness TNBC tumors (88.9%; $P = .008$).

Table 2 Relationships Between BRCAness Before Neoadjuvant Chemotherapy and Clinical Responses to Taxane for All Subtypes and for Triple Negative Breast Cancer

Clinical Response	BRCAness (%)	Non-BRCAness (%)	*P* Value (Fisher's Exact Test)
All			.027
CR+PR	10 (58.8)	25 (89.3)	
SD+PD	7 (41.2)	3 (10.7%)	
TNBC			.019
CR+PR	7 (50)	9 (100)	
SD+PD	7 (50)	0 (0)	

Abbreviations: CR = complete response; PD = progressive disease; PR = partial response; SD = stable disease; TNBC = triple negative breast cancer.

The median follow-up duration from the initiation of NAC was 26.4 months. Of the 26 patients with TNBC before NAC, 6 developed a recurrence, including 3 with locoregional recurrence and 3 with distant metastases (1 patient each with brain, lung, or liver metastases). All 3 locoregional recurrences had developed after radical mastectomy for BRCAness TNBC. The patients with BRCAness had worse progression-free survival than those with non-BRCAness (58% vs. 100%, $P = .049$).

Figure 1 shows the BRCAness changes in TNBC after NAC. Of the 14 BRCAness TNBC tumors before NAC, 5 remained BRCAness positive after NAC. Of these 5 patients, 3 had PD and 2 stable disease; 3 developed a recurrence. Of the 14 BRCAness TNBCs before NAC, 7 tested negative after NAC. Their responses to taxane varied from a PR to PD. In contrast, of 9 tumors that were non-BRCAness before NAC, 7 (77.8%) had achieved a pCR and 2 had a clinical PR.

Discussion

The results of the present study indicate that BRCAness tumors have a significantly poorer response to taxane regimens than do non-BRCAness tumors. Originally, BRCAness was identified by comparing BRCAMut tumors with sporadic TNBC tumors using the aCGH method. However, MLPA probes are now commercially available. Adjuvant therapy with high-dose, platinum-based, alkylating agents is reportedly more effective for BRCAness tumors (according to aCGH) than conventional chemotherapy; this has not been true for non-BRCAness tumors.[11] The assessment of BRCAness using MLPA and aCGH is reportedly concordant (accuracy 94%) and also predicts similar survival benefits with intensive alkylating agent chemotherapy.[15] However, with conventional dose anthracycline chemotherapy, the prognoses of BRCAness and non-BRCAness tumors are similar.[13] Patients with BRCAness tumors have substantially better outcomes after adjuvant DSB-inducing chemotherapy.[11] Together with our findings, these results imply that administering platinum salts according to BRCAness status in patients with TNBC will be preferable to administering them to all TNBC patients. Our recommended treatment strategy is that patients with BRCAness tumors receive platinum- and anthracycline-based chemotherapy and that patients with non-BRCAness TNBC receive standard taxane- and

Table 4 Relationships Between BRCAness Before, and Pathologic Responses to, Neoadjuvant Chemotherapy for Triple Negative Breast Cancer

Variable	BRCAness (n = 14)	Non-BRCAness (n = 9)	*P* Value
Average age (years)	46 (27-62)	48 (37-59)	NS
Tumor size before NAC			NS
T1	1 (7.1)	2 (22.2)	
T2	11 (78.6)	7 (77.8)	
T3	1 (7.1)	0 (0)	
T4b	1 (7.1)	0 (0)	
Histologic grade			NS
1-2	5 (35.7)	3 (33.3)	
3	8 (57.1)	5 (55.6)	
ND	1	2	
Pathologic response			.0066
pCR	2 (14.3)	7 (77.8)	
Other	12 (85.7)	2 (22.2)	
Pathologic nodal status			NS
N0	9 (64.3)	7 (77.8)	
N+	5 (35.7)	2 (22.2)	
Average Ki-67 (%)	66.0	58.1	NS
Recurrence			NS
Yes	5 (35.7)	0 (0)	
No	9 (64.3)	9 (100)	

Data presented as average (range) or n (%).
Abbreviations: NAC = neoadjuvant chemotherapy; ND = not determined; NS = not significant; pCR = pathologic complete response.

Table 3 Characteristics of Tumors That Developed Progressive Disease During Taxane-Based Neoadjuvant Chemotherapy

Pt. No.	NAC Response	Germline Mutation	BRCAness	ER	PgR	HER2	Ki-67	EGFR	CK-56	Pathologic Response
1	PD @ Doce 1 cycle (FEC)	BRCA2	+	−	−	1	80-90	+	+	Poor response
2	PD @ Doce 1 cycle	NP	+	−	−	0	60-70	+	−	No response
3	PD @ Doce 2 cycle (FEC)	NP	+	−	−	0	60-70	+	−	No response
4	PD @ nabPTX 7 cycle (FEC)	BRCA1	+	−	−	0	50-60	−	−	Poor response
5	PD @ TC 3 cycle	NP	−	+	+	1	5	NP	NP	No response

Abbreviations: + = positive; − = negative; Doce = docetaxel; EGFR = epidermal growth factor receptor; ER = estrogen receptor; FEC = 5-fluorouracil, epirubicin, cyclophosphamide; HER2 = human epidermal growth factor receptor 2; nabPTX = albumin-bound paclitaxel; NAC = neoadjuvant chemotherapy; NP = not performed; PD = progressive disease; PgR = progesterone receptor; Pt. No. = patient number; TC = docetaxel, cyclophosphamide.

Figure 1 Changes in BRCAness Status After Neoadjuvant Chemotherapy in Triple Negative Breast Cancer and Relationship to Clinical Response

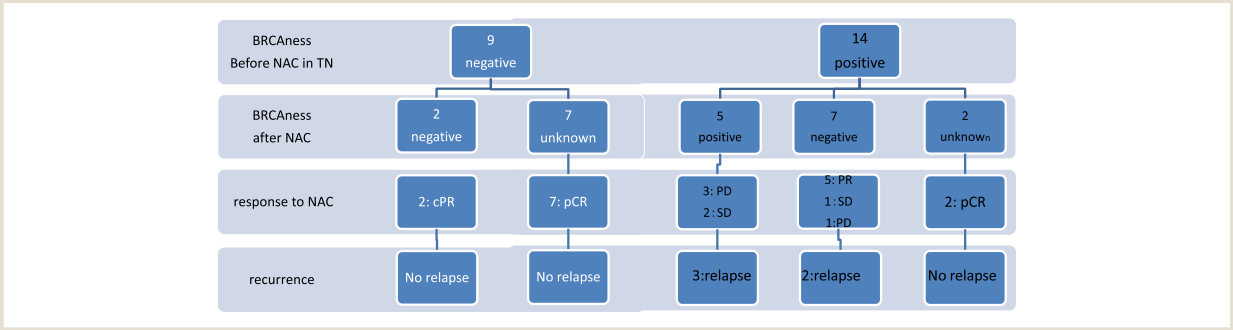

Abbreviations: CR = complete response; NAC = neoadjuvant chemotherapy; ND = no data; NS = not significant.

anthracycline-based chemotherapy. Adding a PARP inhibitor, for both patients with BRCA1 germline mutations and those with BRCAness, might improve survival[12] and warrants additional study.

The ability to predict resistance to taxane treatment by BRCAness status was shown in all our patients, regardless of subtype, but especially in the TNBC subgroup. The reported rates of BRCAness assessed using the aCGH and MLPA methods were 18% for all subtypes and 69% for TNBC.[11,22] Approximately two thirds of TNBC tumors in the present study were BRCAness positive, but only a few non-TNBC tumors were BRCAness positive, corresponding with the results from previous reports. Therefore, we recommend assessing BRCAness status only for patients with TNBC.

The mechanisms for resistance to taxane by BRCAness tumors have not yet been established. Intact BRCA1 function might play an important role in the optimal response to taxane-based therapy.[23] A BRCA1-induced increase in the c-Jun N-terminal kinase pathway causes apoptosis in BRCA1-expressing cells treated with paclitaxel.[24,25]

Tumors with low BRCA1 expression, demonstrated by immunohistochemistry, have had shorter times to progression when treated with taxane-containing regimens.[26] However, this finding has not been confirmed by other investigators, possibly because of the poor reproducibility of the BRCA1 antibody assays. A homologous recombination deficiency assay reported in 2013,[27] which performs genome-wide, single-nucleotide polymorphism analysis using Affymetrix molecular inversion probe arrays of DNA sequencing, is also effective for selecting likely responders to neoadjuvant carboplatin, gemcitabine, and iniparib.

Reportedly, the pCR rate after a NAC regimen of dose-dense cyclophosphamide and doxorubicin was significantly greater in BRCA1-mutated tumors (63%) than in non-BRCA1–mutated tumors (33%). The pCR rate also tended to be greater in BRCAness than in non-BRCAness tumors (35% vs. 21%).[22] However, these investigators also reported that the recurrence rates after adjuvant chemotherapy with anthracycline-based regimens did not differ between these groups. In our study, patients with BRCAness tumors treated with taxane and/or anthracycline had a poor prognosis, developing both PD and PRs. These discrepancies in outcomes likely reflect the different regimens used.

Paluch-Shimon et al[28] reported that BRCA1/2-associated TNBC had a better pCR rate than TNBC in noncarriers (61% vs. 39%; $P = .007$) after dose-dense NAC with an anthracycline and a taxane, opposite the results in our study. They also reported that the pCR was not associated with the long-term outcome in BRCA1/2-associated TNBC, unlike non-BRCA–associated TNBC, probably owing to enrichment of the cancer stem cells in BRCA1/2 tumors.[28] In our study, all 6 patients with tumor relapse had BRCAness-positive tumors and no pCR response. In contrast, patients with a pCR had a better prognosis. Only 7 of our patients who had BRCA1/2 germline mutations, 4 of whom (57%) achieved a pCR, and none of whom relapsed. Two of the patients with BRCA1/2-associated breast cancer who did not achieve a pCR developed a relapse. In our small series, a pCR also seemed to be associated with better long-term outcomes in patients with BRCA1/2-associated breast cancer. The characteristic differences in terms of chemosensitivity and cancer stem cells among BRCA1/2-associated TNBC cases and BRCAness cases should be investigated further.

In the present study, we used a cutoff ratio for BRCAness of 0.4. However, in the original report, the cutoff point was 0.5.[11] The scores in about 75% of the BRCAness tumors were > 0.7, but approximately 80% of the non-BRCAness tumors scored < 0.2. Thus, these 2 categories are easy to differentiate. The score of 1 patient with PD after 2 cycles of docetaxel was 0.42 before NAC and 0.86 after NAC. In no other patient did the BRCAness status change from negative to positive after NAC. Therefore, we applied this cutoff point. A larger scale study is needed to clarify the appropriate cutoff point.

The present study had some limitations. The first was that it was a small retrospective analysis. Retrospective validation studies using NAC cohorts from other hospitals are ongoing. A larger prospective study is needed to validate our findings. Second, some data concerning BRCAness before NAC were unavailable, because we did not perform new biopsies in patients who had been already diagnosed with breast cancer at other hospitals.

Conclusion

Identifying the BRCAness status can help predict the response to taxane, and changing regimens for BRCAness TNBC might improve patient survival. A larger prospective study is needed to further clarify this issue.

Clinical Practice Points

- Approximately one fifth of TNBC tumors progress during NAC, especially those treated with taxane-containing regimens.
- Adding platinum salts to standard NAC regimens significantly improves the pCR rate in patients with TNBC. Although whether platinum salts should be added to, or substituted for, the standard regimen is controversial.
- We found that most patients with non-BRCAness TNBC achieved a pCR rate using the standard regimen; however, patients with BRCAness TNBC were more likely to develop PD and have a worse prognosis.
- Adjuvant therapy with high-dose, platinum-based alkylating agents is reportedly more effective than conventional chemotherapy for BRCAness tumors but not for non-BRCAness tumors. Therefore, platinum salts for TNBC should be selected according to the BRCAness status rather than adding it to the regimens of all patients with TNBC.
- The method we used is clinically feasible and requires only commercially available MLPA probes.
- In the future, this biomarker might also assist in the selection of patients with TNBC to receive a PARP inhibitor.

Acknowledgments

The assays for BRCAness were performed by Falco Biosystems (Kyoto, Japan) at no cost under a collaborative study contract. The present study was partly supported by a grant for the Third Comprehensive Strategy for Cancer from the Ministry of Health, Labour and Welfare, H23-cancer-004, Japan.

Disclosure

The authors have stated that they have no conflicts of interest.

References

1. Lehmann BD, Bauer JA, Chen X, et al. Identification of human triple-negative breast cancer subtypes and preclinical models for selection of targeted therapies. *J Clin Invest* 2011; 121:2750-67.
2. Cortazar P, Zhang L, Untch M, et al. Pathological complete response and long-term clinical benefit in breast cancer: the CTNeoBC pooled analysis. *Lancet* 2014; 384:164-72.
3. von Minckwitz G, Untch M, Blohmer JU, et al. Definition and impact of pathologic complete response on prognosis after neoadjuvant chemotherapy in various intrinsic breast cancer subtypes. *J Clin Oncol* 2012; 30:1796-804.
4. Iwata H, Sato N, Masuda N, et al. Docetaxel followed by fluorouracil/epirubicin/cyclophosphamide as neoadjuvant chemotherapy for patients with primary breast cancer. *Jpn J Clin Oncol* 2011; 41:867-75.
5. Shien T, Yoshida M, Hojo T, et al. Clinicopathologic features of primary breast cancer resisting primary systemic therapy. *Jpn J Breast Cancer* 2008; 23:49-53.
6. Von Minckwitz G, Schneeweiss A, Salat C, et al. Addition of Carboplatin Beneficial in Neoadjuvant Treatment of Triple-NegativeBreast Cancer. *J Clin Oncol (Proc ASCO)* 2014, 1004.
7. Sikov WN, Berry DA, Perou CM, et al. The impact of addition of carboplatin and/or bevacizumab to neoadjuvant weekly paclitaxel followed by dose-dense AC on pathologic complete response rate in triple -negative breast cancer: CALGB 40603 (Alliance). *J Clin Oncol* Published Ahead of Print on August 4, 2014 as http://dx.doi.org/10.1200/JCO.2014.57.0572.
8. Petrelli F, Coinu A, Borgonovo K, et al. The value of platinum agents as neoadjuvant chemotherapy in triple-negative breast cancers: a systematic review and meta-analysis. *Breast Cancer Res Treat* 2014; 144:223-32.
9. Liu M, Mo QG, Wei CY, et al. Platinum-based chemotherapy in triple-negative breast cancer: a meta-analysis. *Oncol Lett* 2013; 5:983-91.
10. Turner N, Tutt A, Ashworth A. Hallmarks of "BRCAness" in sporadic cancers. *Nat Rev Cancer* 2004; 4:814-9.
11. Vollebergh MA, Lips EH, Nederlof PM, et al. An aCGH classifier derived from BRCA1-mutated breast cancer and benefit of high-dose platinum-based chemotherapy in HER2-negative breast cancer patients. *Ann Oncol* 2011; 22:1561-70.
12. Lee JM, Ledermann JA, Kohn EC. PARP Inhibitors for BRCA1/2 mutation-associated and BRCA-like malignancies. *Ann Oncol* 2014; 25:32-40.
13. Oonk AM, van Rijn C, Smits MM, et al. Clinical correlates of "BRCAness" in triple-negative breast cancer of patients receiving adjuvant chemotherapy. *Ann Oncol* 2012; 23:2301-5.
14. Chalasani P, Livingston R. Differential chemotherapeutic sensitivity for breast tumors with "BRCAness": a review. *Oncologist* 2013; 18:909-16.
15. Lips EH, Laddach N, Savola SP, et al. Quantitative copy number analysis by multiplex ligation-dependent probe amplification (MLPA) of BRCA1-associated breast cancer regions identifies BRCAness. *Breast Cancer Res* 2011; 13:R107.
16. Rottenberg S, Nygren AO, Pajic M, et al. Selective induction of chemotherapy resistance of mammary tumors in a conditional mouse model for hereditary breast cancer. *Proc Natl Acad Sci U S A* 2007; 104:12117-22.
17. Kriege M, Jager A, Hooning MJ, et al. The efficacy of taxane chemotherapy for metastatic breast cancer in BRCA1 and BRCA2 mutation carriers. *Cancer* 2012; 118:899-907.
18. Rummel S, Varner E, Shriver CD, et al. Evaluation of BRCA1 mutations in an unselected patient population with triple-negative breast cancer. *Breast Cancer Res Treat* 2013; 137:119-25.
19. Eisenhauer EA, Bogaerts J, Schwartz LH, et al. New response evaluation criteria in solid tumours: Revised RECIST guideline (version 1.1). *Eur J Cancer* 2009; 45:228-47.
20. Shigenaga R, Akashi-Tanaka S. [Comparison among Japanese general rules for clinical and pathological recording of breast cancer, 16th ed and UICC TNM classification, 7th ed]. *Nihon Rinsho* 2012; 70(suppl 7):191-4.
21. Kanda Y. Investigation of the freely available easy-to-use software "EZR" for medical statistics. *Bone Marrow Transplant* 2013; 48:452-8.
22. Lips EH, Mulder L, Oonk A, et al. Triple-negative breast cancer: BRCAness and concordance of clinical features with BRCA1-mutation carriers. *Br J Cancer* 2013; 108:2172-7.
23. Sung M, Giannakakou P. BRCA1 regulates microtubule dynamics and taxane-induced apoptotic cell signaling. *Oncogene* 2014; 33:1418-28.
24. Lafarge S, Sylvain V, Ferrara M, et al. Inhibition of BRCA1 leads to increased chemoresistance to microtubule-interfering agents, an effect that involves the JNK pathway. *Oncogene* 2001; 20:6597-606.
25. Chabalier C, Lamare C, Racca C, et al. BRCA1 downregulation leads to premature inactivation of spindle checkpoint and confers paclitaxel resistance. *Cell Cycle* 2006; 5:1001-7.
26. Kurebayashi J, Yamamoto Y, Kurosumi M, et al. Loss of BRCA1 expression may predict shorter time-to-progression in metastatic breast cancer patients treated with taxanes. *Anticancer Res* 2006; 26:695-701.
27. Telli M, Jensen KC, Kurian AW, et al. PrECOG 0105: Final efficacy results from a phase II study of gemcitabine (G) and carboplatin (C) plus iniparib (BSI-201) as neoadjuvant therapy for triple-negative (TN) and BRCA1/2 mutation-associated breast cancer ASCO proceedings. 2013, Abstract PD 09-04.
28. Paluch-Shimon S, Friedman E, Berger R, et al. Does pathologic complete response predict for outcome in BRCA mutation carriers with triple-negative breast cancer? *J Clin Oncol* 2014; 32(suppl):5s (abstract 1023).

Lung Cancer 93 (2016) 69–76

Contents lists available at ScienceDirect

Lung Cancer

journal homepage: www.elsevier.com/locate/lungcan

Association of pharmacokinetics and pharmacogenomics with safety and efficacy of gefitinib in patients with *EGFR* mutation positive advanced non-small cell lung cancer

Takashi Hirose[a,b,*], Ken-ichi Fujita[c], Sojiro Kusumoto[b], Yasunari Oki[b], Yasunori Murata[b], Tomohide Sugiyama[b], Hiroo Ishida[d], Takao Shirai[b], Masanao Nakashima[b], Toshimitsu Yamaoka[c], Kentaro Okuda[b], Tohru Ohmori[c], Yasutsuna Sasaki[d]

[a] *Depatment of Respirology, National Hospital Organization, Tokyo National Hospital, Kiyose, Tokyo, Japan*
[b] *Division of Respiratory Medicine and Allergology, Showa University School of Medicine, Kiyose, Tokyo, Japan*
[c] *Institute of Molecular Oncology, Showa University, Kiyose, Tokyo, Japan*
[d] *Division of Medical Oncology, Showa University School of Medicine, Shinagawa, Tokyo, Japan*

ARTICLE INFO

Article history:
Received 21 August 2015
Received in revised form 4 December 2015
Accepted 6 January 2016

Keywords:
Pharmacokinetics
Pharmacogenomics
Gefitinib
Interstitial lung disease

ABSTRACT

Objectives: Gefitinib is a potent epidermal growth factor receptor (EGFR) tyrosine kinase inhibitor and is a key drug for patients with *EGFR* mutation-positive advanced non-small cell lung cancer (NSCLC). The pharmacokinetics of orally administered gefitinib varies greatly among patients. We prospectively evaluated the association of pharmacokinetics and pharmacogenomics with the safety and efficacy of gefitinib in patients with *EGFR* mutation-positive advanced NSCLC.
Patients and methods: Pharmacokinetics was evaluated with samples of peripheral blood obtained on day 1 before treatment and 1, 3, 5, 8, and 24 h after gefitinib (250 mg per day) was administered and on days 8 and 15 as the trough values. The plasma concentration of gefitinib was analyzed with high-performance liquid chromatography. The genotypes of *ABCG2*, *ABCB1*, *CYP3A4*, *CYP3A5*, and *CYP2D6* genes were analyzed with direct sequencing.
Results: The subjects were 35 patients (21 women; median age, 72 years; range, 53 to 90 years) with stage IV adenocarcinoma harboring *EGFR* mutations. The median peak plasma concentration (C_{max}) was 377 (range, 168–781) ng/mL. The median area under the curve (AUC) of the plasma concentration of gefitinib from 0 to 24 h was 4893 (range, 698–13991) ng/mL h. The common adverse events were skin toxicity (68% of patients), diarrhea (46%), and liver injury (63%). One patient died of drug-induced interstitial lung disease (ILD). The overall response rate was 82.9% (95% confidence interval, 66.4%–93.4%). The median progression-free survival time was 10 months, and the median survival time was 25 months. The pharmacokinetics and pharmacogenomics were not associated with significantly different toxicities, response rates, or survival times with gefitinib. However, the AUC and C_{max} were highest and the trough value on day 8 was the second highest in one patient who died of drug-induced ILD.
Conclusion: Elevated gefitinib exposure might be associated with drug-induced ILD.

1. Introduction

Somatic mutations of the epidermal growth factor receptor (EGFR) gene, *EGFR*, were first discovered in 2004 as a predictive marker for treatment with EGFR tyrosine kinase inhibitor (TKI) in patients with advanced non-small cell lung cancer (NSCLC) [1,2]. Phase III trials in patients with *EGFR* mutation-positive advanced NSCLC have found that EGFR-TKI is superior to platinum doublet cytotoxic chemotherapy [3–6]. Thus, for such patients EGFR-TKI is now globally considered the standard first-line treatment.

Gefitinib is a potent EGFR-TKI that is metabolized in the liver, mainly by cytochrome P450 (CYP) 3A4/3A5, and, to lesser extent, by CYP2D6 and CYP1A1. After being metabolized, gefitinib is transported by the active efflux pumps *P*-glycoprotein (ATP-binding cassette [ABC], sub-family B, member 1 [ABCB1]) and breast cancer resistance protein (BCRP, ABC, sub-family G, member 2 [ABCG2])

* Corresponding author at: Depatment of Respirology, National Hospital Organization Tokyo National Hospital, 3-1-1 Takeoka Kiyose, Tokyo 204-8585, Japan. Fax: +81 42 494 2168.
E-mail address: thirose-shw@umin.ac.jp (T. Hirose).

http://dx.doi.org/10.1016/j.lungcan.2016.01.005
0169-5002/

[7–9]. After oral absorption of gefitinib, its pharmacokinetics shows large variability among patients [10]. These pharmacokinetics differences might be attributed to polymorphisms of the genes of CYPs, ABCB1, and ABCG2.

After being administered for treatment, gefitinib causes numerous toxicities, the most common of which are skin toxicity, diarrhea, and liver injury [3,4]. The most severe, yet rare, toxicity is a drug-induced interstitial lung disease (ILD) [11]. Such toxicities sometimes cause gefitinib therapy to be discontinued. The severity of these toxicities is different in each patient. The most common toxicities have been suggested, by several previous studies, to be related to the plasma concentration of gefitinib [10,12–14]. However, it remains unclear whether common toxicities are related to the plasma concentration of gefitinib when it has been administration at a dose of 250 mg because large studies have not been reported [10,14]. Additionally, the relationship of the plasma concentration of gefitinib to gefitinib-related ILD has not, to our knowledge, been previously reported.

The association between the toxicity of gefitinib and pharmacogenomics has been controversial. Polymorphism of *ABCG2* is reportedly associated with the occurrence of diarrhea due to gefitinib [15]. On the other hand, other studies have reported no associated between gefitinib-induced toxicities and genetic polymorphisms including those of *ABCG2* [14,16].

Of patients with *EGFR* mutation-positive advanced NSCLC, 20%–30% show intrinsic resistance to EGFR-TKI [3,4]. The mechanisms of intrinsic resistance are poorly understood, despite various mechanisms for acquired resistance having been identified [17,18]. In one study a ratio of plasma trough levels of gefitinib on day 8 and day 3 of administration of gefitinib was reportedly associated with a progression-free survival (PFS) time; however, the results are inconclusive because the study included patients with advanced NSCLC either negative or positive for *EGFR* mutation [19]. Until now, the relationship between the efficacy of gefitinib and its pharmacokinetics and pharmacogenomics in patients with *EGFR* mutation-positive advanced NSCLC has been unclear. The pharmacokinetics and pharmacogenomics might possibly be mechanisms of the intrinsic resistance to EGFR-TKI.

Therefore, clarifing the association of pharmacokinetics and pharmacogenomics with the toxicity and efficacy of gefitinib is important. In the present study, we aimed to clarify (1) the association of pharmacokinetics with pharmacogenomics, (2) the association of pharmacokinetics and pharmacogenomics with toxicity of gefitinib, and (3) the association of pharmacokinetics and pharmacogenomics with efficacy of gefitinib in patients with *EGFR* mutation-positive advanced NSCLC.

2. Patients and methods

2.1. Study participants and treatment

From October 2009 through December 2012, 35 patients with *EGFR* mutation-positive advanced NSCLC were prospectively enrolled in this study. The eligibility criteria were as follows: histologically or cytologically proven *EGFR* mutation-positive NSCLC, unresectable and ineligible for thoracic radiotherapy, stage IIIB or IV disease, 20 years or older, no prior treatment of EGFR-TKI, Eastern Cooperative Oncology Group performance status of 0–3, a measurable lesion, and adequate bone marrow function (neutrophil count of 1500/μl or more, platelet count of 100,000/μl or more, and hemoglobin level of 8.0 g/dl or more), renal function (serum creatinine levels less than 1.5 mg/dl), and hepatic function (total serum bilirubin level less than 2.0 mg/dl, aspartate aminotransferase and alanine aminotransferase levels less than or equal to 2.5 times the upper limits of the normal ranges). Patients were excluded if they had ILD, active infections, severe heart disease, uncontrolled diabetes mellitus, second malignancy, or taken a medicine that affected CYP3A4, a proton-pump inhibitor, or a histamine H2 receptor antagonists. Gefitinib was administered orally once daily at a dose of 250 mg until disease progressed or severe adverse events occurred. This study protocol was approved by the Ethics Committee of Showa University School of Medicine. We obtained written informed consent from all patients.

2.2. Pharmacokinetics and pharmacogenomics analysis

The evaluation of pharmacokinetics was performed with samples of peripheral blood obtained on day 1 before treatment and 1, 3, 5, 8, and 24 h after the first administration of 250 mg of gefitinib. Additionally, the samples of peripheral blood were obtained before administration of gefitinib on days 8 and 15 to determine the trough value. The samples were centrifuged immediately, and the plasma was stored at −80°C until analysis. The plasma concentration of gefitinib was analyzed with high-performance liquid chromatography following the method of Faivre et al [20]. We determined the plasma concentration-time profiles from 0 to 24 h on day 1 of the first administration of gefitinib. The peak plasma concentrations (C_{max}) and the interval required to reach the peak concentration (Tmax) were obtained directly from the profile. The median area under curve (AUC) of the plasma concentration of gefitinib from 0 to 24 h was calculated with the linear trapezoidal rule.

Genomic DNA was extracted from 200 μL of peripheral blood, which had been stored at −80°C until analysis. The genotypes of *ABCB1 1236C>T, ABCB1 2677G>T or A, ABCB1 3435C>T,* and *ABCG2* 421C>A were analyzed with direct sequencing following the method by Akiyama et al. [21]. The genotypes of *CYP3A4 20230G>A, CYP3A4 15603C>G, CYP3A4 20070T>C, and CYP3A4 20148A>G* were analyzed with direct sequencing following the method by Eiselt et al. [22]. The genotype of *CYP3A5 6986A>G* was analyzed with direct sequencing following the method by Saeki et al. [23]. The genotype of *CYP2D6 *1/*1, 10, or 36* was analyzed with direct sequencing following the method by Soyama et al. [24].

2.3. Clinical evaluation

The evaluation before treatment with gefitinib included a baseline history, physical examination, complete blood count with differential, routine chemistry profiles, chest radiography, computed tomography (CT) of the chest and abdomen, magnetic resonance imaging or CT of the brain, and a radionucleotide bone scan or positron-emission tomography. Tumor response was classified according to the Response Evaluation Criteria in Solid Tumors criteria version 1.1. The toxicity of gefitinib was evaluated according to the National Cancer Institute Common Terminology Criteria for adverse events 4.0.

The association between the pharmacokinetics of gefitinib and the pharmacogenomics was prospectively evaluated in patients with *EGFR* mutation-positive advanced NSCLC. Also evaluated in these patients were the associations of pharmacokinetics and pharmacogenomics with skin toxicity, mucosal toxicity, diarrhea, nausea, liver injury, and the pulmonary toxicity and efficacy of gefitinib.

2.4. Statistical methods

Overall survival time was measured from the start of the present treatment until death or the last follow-up examination. The PFS time was measured from the start of treatment to the identifiable time of progression. The Kaplan–Meier method was used to construct survival curves. Survival differences between patients with lower than median AUC, $_{C}$max, or trough values and higher than

Table 1
Patient characteristics.

Total number of patients	35
Sex (M/F)	14/21
Age, years (range)	72 (53–90)
Performance status (0/1/2/3)	5/20/7/3
Stage (IIIB/IV)	0/35
Histologic type	
Adenocarcinoma	35
EGFR mutation status	
exon 19 deletion	18
exon 21 L858R	16
exon 18 G719A	1
Number of previous chemotherapy regimens (median)	
0/1/2	19/14/2

median AUC, C_{max}, or trough values were compared by means of the log-rank test. The chi-square test was used to determine the significance of differences between patients with toxicities of grade 0 and those with toxicities of grade 1 or higher. Differences with a p-value <0.05 were considered statistically significant. Statistical analyses were performed with the software package Stat View 5.0 (SAS Institute Inc., Cary, NC, USA).

3. Results

3.1. Patient characteristics

The subjects were 35 patients with stage IV adenocarcinoma (14 men and 21 women; mean age, 72 years; age range, 53–90 years; Table 1). The types of *EGFR* mutations were as follows: exon 19 deletions in 18 patients, exon 21 L858R in 16 patients, and exon 18 G719A in 1 patient.

3.2. Pharmacokinetics and pharmacogenomics analysis

Pharmacokinetics was evaluated in all 35 patients, and pharmacogenomics was evaluated in 33 patients. The C_{max} was achieved 5 h after dosing, and the median value was 377 (range, 168–781) ng/mL. The median AUC of the plasma concentration of gefitinib from 0 to 24 h on day 1 of the administration of gefitinib was 4893 (range, 698–13991) ng/mL h (Fig. 1). The trough values on day 8 and 15 were almost identical, and the median trough values on day 8 and 15 were 431 (range, 140–928) ng/mL and 390 (range, 115–1021) ng/mL, respectively.

The associations of AUC, C_{max}, and trough values on day 8 with pharmacogenomics analysis are shown in Table 2. There were no statistically significant associations between AUC and the genotypes of *ABCG2, ABCB1, CYP3A4, CYP3A5,* and *CYP2D6*. Additionally, there were no statistically significant associations between C_{max} and the genotypes of *ABCG2, ABCB1, CYP3A4, CYP3A5,* and *CYP2D6*. Moreover, there were no statistically significant associations between the trough values and the genotypes of *ABCG2, ABCB1, CYP3A4, CYP3A5,* and *CYP2D6*.

3.3. Toxicity

The most common adverse events were skin toxicity (69% of patients), liver injury (63% of patients), and diarrhea (46% of patients) (Table 3). One patient who died of gefitinib-related ILD was a 78-year-old woman who had had no ILD before she received gefitinib. A CT scan of the chest 1 month after administration of gefitinib showed diffuse ground–glass opacity throughout both lungs. Although gefitinib was immediately discontinued and treatment was started with corticosteroid pulse therapy (1000 mg of methylprednisolone per day for 3 days) and supplemental oxygen, there was no improvement in respiratory function. The patient died of gefitinib-related ILD 21 days later.

Table 2
Association between pharmacogenomic analysis and pharmacokinetic data.

Genotype (N = 33)	Number	%	AUC	p score	C_{max}	p score	Trough	p score
ABCB1 1236C>T								
C/C	5	15	5364		335		604	
C/T	16	48	5185		398		304	
T/T	12	36	5409	0.71	380	0.99	429	0.64
ABCB1 2677G>T or A								
G/G	7	21	4694		335		431	
G/T or A	17	52	5096		380		440	
T or A/Tor A	9	27	5990	0.75	416	0.63	309	0.46
ABCB1 3435C>T								
C/C	5	15	4694		322		492	
C/T	17	52	5945		438		383	
T/T	11	33	4381	0.27	317	0.16	308	0.20
ABCG2 421C>A								
C/C	18	55	5856		416		435	
A/C	11	33	4962		375		306	
A/A	4	12	3621	0.98	241	0.02	243	0.15
CYP3A4 20230G>A								
G/G	17	52	5453		416		434	
G/A	15	46	4872		335		296	
A/A	1	3	8180	0.19	541	0.28	529	0.41
CYP3A5 6986A>G								
A/A	4	12	6616		465		434	
G/A	17	52	5409		362		433	
G/G	12	36	4872	0.88	393	0.43	433	0.77
CYP2D6								
*1/*1	12	36	4738		362		371	
*1/*10 or 36	16	48	5409		380		431	
*10 or 36/*10 or 36	5	15	6169	0.16	443	0.16	612	0.10

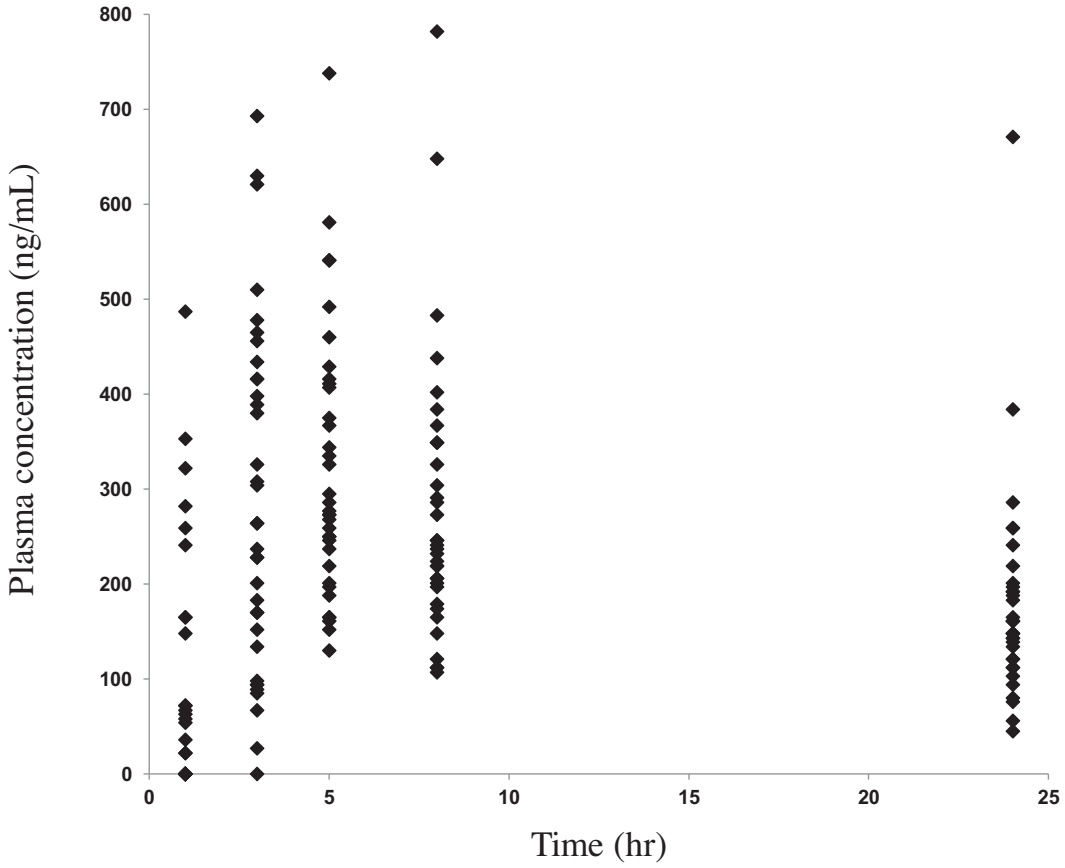

Fig 1. The observed plasma data of concentrations versus time of the first administration of 250 mg of gefitinib are shown.

Table 3
Toxicity.

	National cancer institute-common terminology criteria grade						
Toxicity	1	2	3	4	5	all	3–5 (%)
Skin toxicity	19	5	0	0	0	68	0
Mucosal toxicity	2	1	0	0	0	9	0
Diarrhea	14	2	0	0	0	46	0
Nausea	6	1	0	0	0	20	0
Anorexia	15	1	0	0	0	46	0
Elevation of aminotransferase	12	2	8	0	0	63	23
Pulmonary toxicity	0	0	0	0	1	3	3
Fatigue	8	2	0	0	0	29	0

The AUC, C_{max}, and trough values were not significantly associated with skin toxicity (Fig. 2A, B), diarrhea (Fig. 2C, D), or liver injury (Fig. 2E, F) due to gefitinib (trough level data not shown). However, the AUC and C_{max} were the highest and the trough value on day 8 was the second highest in the patient who died of gefitinib-related ILD, had no homozygous genotype was present (Fig. 2G, H, I).

3.4. Treatment response and survival

The response to treatment in the 35 patients was a complete response in 1 patient, a partial response in 28 patients, stable disease in 2 patients, progressive disease in 2 patients, and unable to be evaluated in 2 patients. The overall response rate was 82.9% (29 of 35 patients; 95% confidence interval: 66.4–93.4%) and the disease control rate was 88.6% (31 of 35 patients; 95% confidence interval: 73.3–96.8%). Neither the C_{max} ($p = 0.08$), the AUC ($p = 0.31$), nor the trough value on day 8 ($p = 0.96$) differed significantly between responders and nonresponders.

Survival was analyzed when the median follow-up time was 24 months for all 35 patients. At the time of analysis, 4 patients (11%) were alive and no patients had been lost to follow-up. The median PFS time was 10 months (range: 0–28 months; Fig. 3A), and the median survival time was 25 months (range: 2–108 months; Fig. 3B). The PFS time did not differ significantly between patients with lower than median AUC (11 months) and patients with higher than median AUC (9 months) ($p = 0.21$) (Fig. 3C), between patients with lower than median C_{max} (11 months) and patients with higher than median C_{max} (9 months) ($p = 0.28$) (Fig. 3D), or between patients with lower than median trough value on day 8 (12 months) and patients with higher than median trough value on day 8 (9 months) ($p = 0.76$) (Fig. 3E).

4. Discussion

To our knowledge, the present study is the first to evaluate the associations of pharmacokinetics and pharmacogenomics with gefitinib-related ILD and efficacy of gefitinib in patients with EGFR mutation-positive advanced NSCLC. In the present study no significant associations was found between the pharmacokinetics of gefitinib and pharmacogenomics in patients with *EGFR* mutation-positive advanced NSCLC. Furthermore, neither the pharmacokinetics of gefitinib nor pharmacogenomics was found to be statistically associated with the toxicity or efficacy of gefitinib.

Although several previous studies have revealed a correlation between pharmacokinetics and pharmacogenomics of another EGFR-TKI, erlotinib, and the development of toxicity, the results were controversial [25,26]. In one study, *ABCG2* polymorphism was

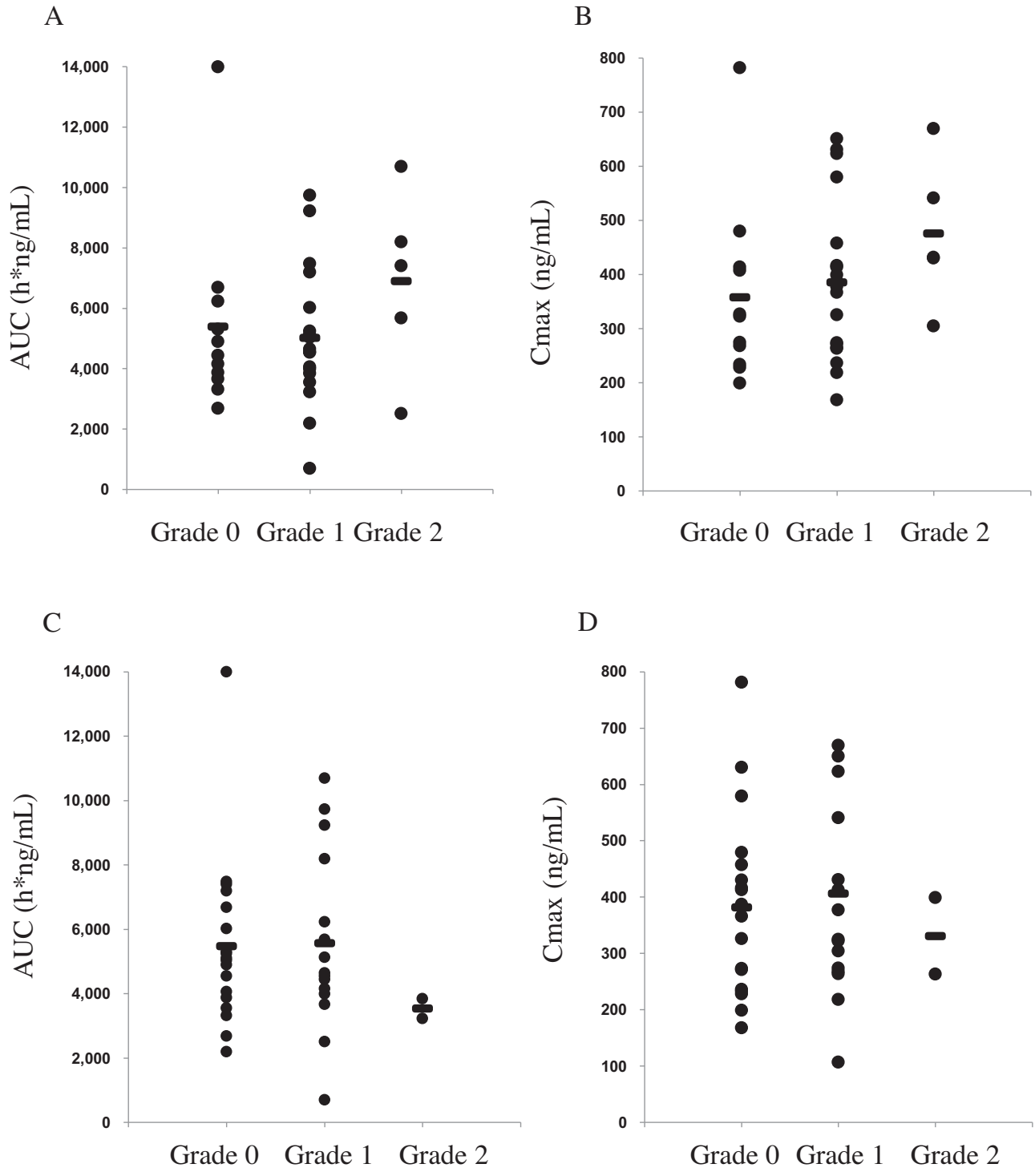

Fig. 2. (A) The association of AUC with the skin toxicity of gefitinib is shown. There was no significant association of AUC and the skin toxicity of gefitinib ($p = 0.62$). (B) The association of C_{max} with the skin toxicity of gefitinib is shown. There was no significant association of C_{max} and the skin toxicity of gefitinib ($p = 0.29$). (C) The association of AUC with diarrhea from gefitinib is shown. There was no significant association of AUC and diarrhea from gefitinib ($p = 0.77$). (D) The association of C_{max} with diarrhea from gefitinib is shown. There was no significant association of C_{max} and diarrhea from gefitinib ($p = 0.75$). (E) The association of AUC with liver injury from gefitinib is shown. There was no significant association of AUC and liver injury from gefitinib ($p = 0.15$). (F) The association of C_{max} with liver injury from gefitinib is shown. There was no significant association of C_{max} and liver injury from gefitinib ($p = 0.22$). (G) The association of AUC with interstitial lung disease (ILD) from gefitinib is shown. One patient who died of gefitinib-related ILD showed the highest AUC of all patients. (H) The association of C_{max} with interstitial lung disease (ILD) of gefitinib is shown. One patient who died of gefitinib-related ILD showed the highest C_{max} of all patients. (I) The association of trough value on day 8 with interstitial lung disease (ILD) of gefitinib is shown. One patient who died of gefitinib-related ILD showed the second highest trough value of all patients.

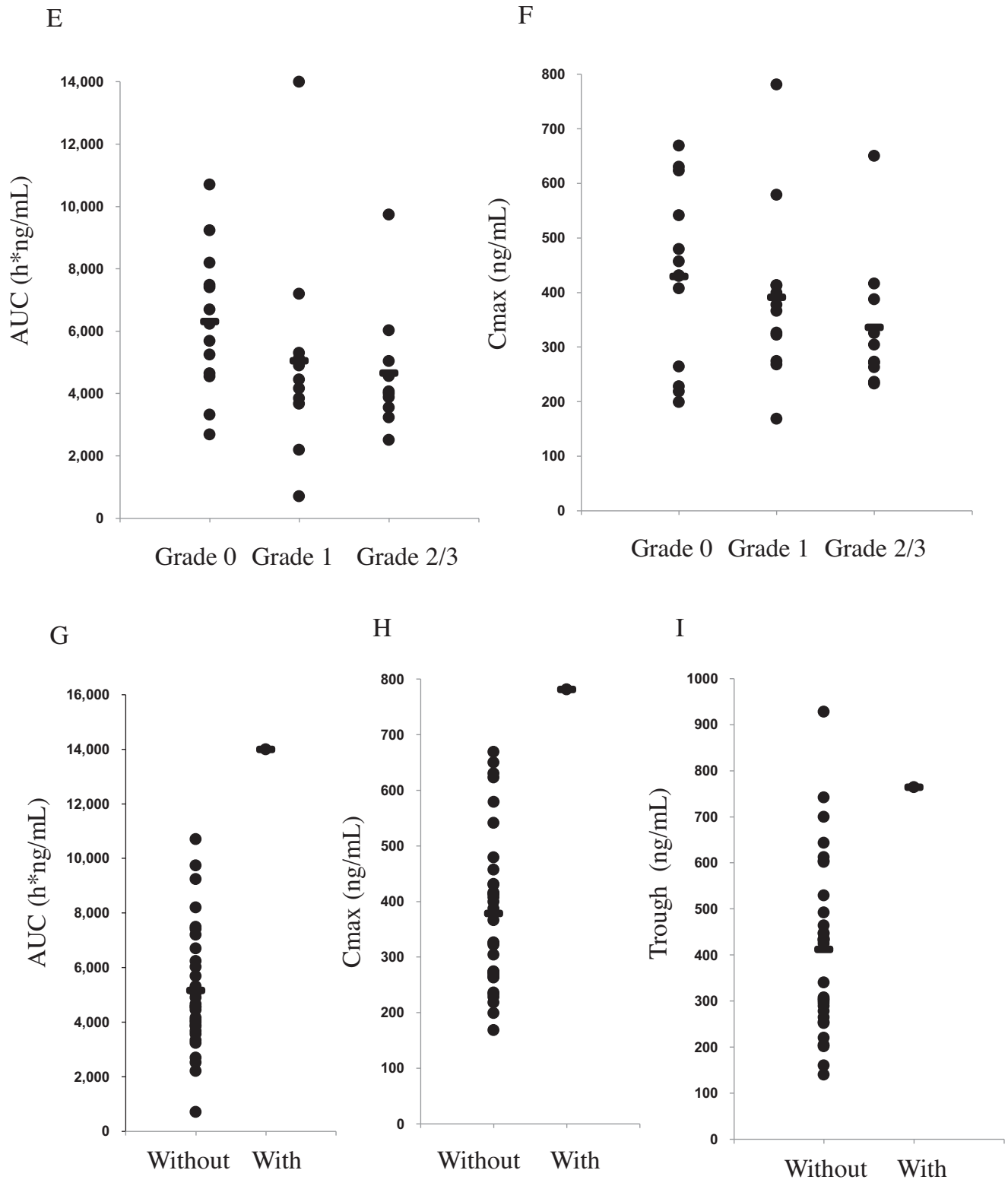

Fig. 2. (*Continued*).

found to influence the apparent clearance of erlotinib, whereas *ABCB1* and *CYP3A5* polymorphism were not [25]. In another study *ABCB1* polymorphism was found to be associated with higher plasma concentration of erlotinib and the risk of toxicity [27]. Although other previous studies in patients with advanced NSCLC have suggested a relationship of the plasma concentration of gefitinib with skin toxicity, diarrhea, and liver injury, it remains unclear whether common toxicities are related to the plasma concentration of gefitinib when it is administered at a dose of 250 mg [12–14]. Moreover, whether an association exists between genetic polymorphisms and the toxicity of gefitinib in patients with advanced NSCLC is controversial [15,16]. In the present study in patients with

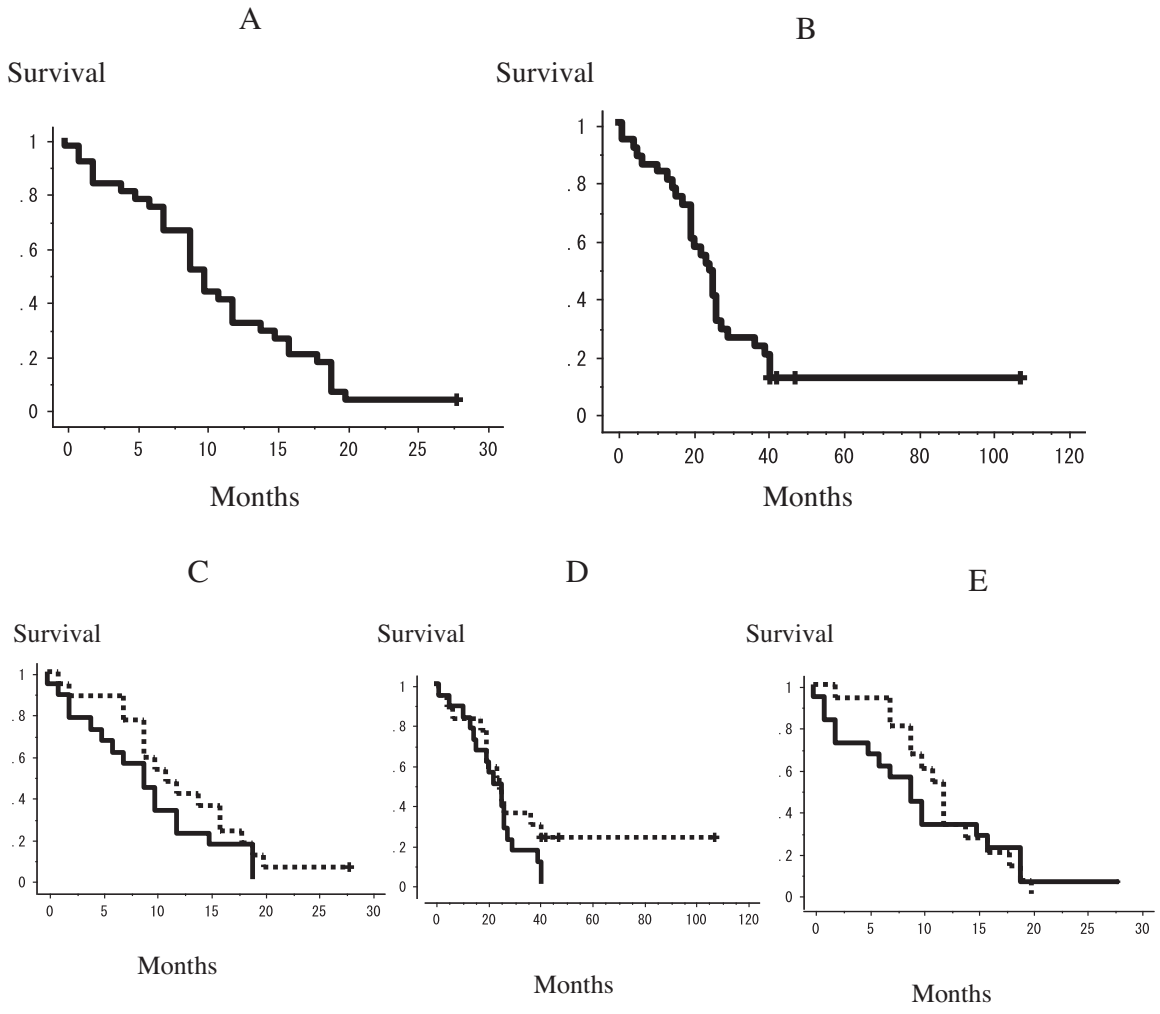

Fig. 3. (A) Progression-free survival (PFS) time estimated with the Kaplan–Meier method. The median PFS time was 10 months (range = 0–28 months). (B) Overall survival estimated with the Kaplan–Meier method. The median survival time was 25 months (range = 2–108 months). (C) Progression-free survival (PFS) time estimated with the Kaplan–Meier method according to AUC. There was no significant difference in PFS time between patients with lower than median AUC (dashed line: 11 months) and patients with higher than median AUC (solid line: 9 months) ($p = 0.21$). (D) Progression-free survival (PFS) time estimated with the Kaplan–Meier method according to C_{max}. There was no statistically significant difference in PFS time between patients with lower than median C_{max} (dashed line: 11 months) and patients with higher than median C_{max} (solid line: 9 months) ($p = 0.28$). (E) Progression-free survival (PFS) time estimated with the Kaplan–Meier method according to trough value on day 8. There was no statistically significant difference in PFS time between patients with lower than median trough value (dashed line: 12 months) and patients with higher than median trough value (solid line: 9 months) ($p = 0.76$).

EGFR mutation-positive advanced NSCLC, the pharmacokinetics of gefitinib and pharmacogenomics were no found to be significantly associated with the toxicity of gefitinib.

Although rare, ILD is a potentially fatal adverse event. The frequency of EGFR-TKI-related ILD is higher in patients in Japan than in other countries [11] but the reason for the difference in frequency is unknown. Two large, multi-institutional studies have found that ILD has an incidence in Japan of 3.5% to 4.0% [11]. With respect to erlotinib, a relationship between a high plasma concentration and related ILD has been suggested [25,28]. However, to our knowledge, no relationship between the plasma concentration of gefitinib and gefitinib-related ILD has been reported. Of the patients of the present study, the one who died of gefitinib-related ILD had the highest AUC and C_{max} and the second highest trough value on day 8 of all patients. The present study suggests that the elevated gefitinib exposure is associated with gefitinib-related ILD. Further studies are needed of how pharmacokinetics or pharmacogenomics is associated with the toxicity of EGFR-TKI.

Of patients with *EGFR* mutation-positive advanced NSCLC, intrinsic resistance to EGFR-TKI is shown by 20% to 30% [3,4]. However, the mechanisms of intrinsic resistance have been poorly understood. A phase III study of erlotinib has demonstrated a correlation between the development of rash of grade 2 or greater and the efficacy of erlotinib in patients with previously treated advanced NSCLC [29]; this study suggests that individual variations in pharmacokinetics might be related to the efficacy of erlotinib. On the other hand, neither the severity of rash nor the efficacy of erlotinib has been reported to correlate with exposure to erlotinib [30]. Furthermore, the response to erlotinib was not higher with a higher trough level of erlotinb in patients with *EGFR* mutation-positive advanced NSCLC; however, the response rate was higher with a higher trough level in patients with *EGFR* mutation-negative advanced NSCLC [25]. Although the association of pharmacokinetics with the efficacy of erlotinib remains controversial, it might not exist in patients with *EGFR* mutation-positive advanced NSCLC because *EGFR* mutation is the strongest biomarker for the efficacy of EGFR-TKI [1,2]. Body surface area has been reported to affect the PFS time of patients with *EGFR* mutation-positive advanced NSCLC who are treated with gefitinib; a higher body surface area was associated with a shorter PFS time [31]. Authors have speculated

about the association between the efficacy and the blood concentration of gefitinib because physical size has been noted to affect pharmacokinetics of most cytotoxic agents. To our knowledge, relationships of the pharmacokinetics and pharmacogenomics to the efficacy of gefitinib in patients with *EGFR* mutation-positive advanced NSCLC have not previously been reported. In the present study, we found no significant association of pharmacokinetics or pharmacogenomics with the efficacy of gefitinib in these patients.

Our study has several limitations. One limitation is that the number of patients was too small for the association of pharmacokinetics and pharmacogenomics with the toxicity and efficacy of gefitinib to be precisely determined. Additionally, gefitinib-related ILD occurred in only 1 patient. Second limitation is that because some gene polymorphisms were of low frequency, the association might possibly be accidental. Third limitation is blood sampling time. Ranson et al. have reported that the steady-state plasma concentrations were achieved by day 7 to 10 [13]. Additionally, they have reported that the C_{max} at steady-state increased by a mean of 2.5-fold and the AUC at steady-state increased by a mean of 3-fold compared with single administration [13]. Therefore, the C_{max} and AUC on day 1 of gefitinib administration are less accurately reflected than at steady-state. However, associations of the trough value on day 8 with toxicity and efficacy of gefitinib were almost identical to associations of the C_{max} and AUC on day 1 with toxicity and efficacy of gefitinib.

In conclusion, the present study found no significant associations of pharmacokinetics and pharmacogenomics with the toxicity and efficacy of gefitinib in patients with *EGFR* mutation-positive advanced NSCLC. However, the one patient who died of gefitinib-related ILD had the highest AUC and C_{max} and the second highest trough value. Thus, the elevated gefitinib exposure might be associated with gefitinib-related ILD. Further studies are needed to assess the association of pharmacokinetics or pharmacogenomics with the toxicity of EGFR-TKI.

Conflict of interest

None declared.

References

[1] T.J. Lynch, D.W. Bell, R. Sordella, et al., Activating mutations in the epidermal growth factor receptor underlying responsiveness of non-small-cell lung cancer to gefitinib, N. Engl. J. Med. 350 (2004) 2129–2139.
[2] J.G. Paez, P.A. Janne, J.C. Lee, et al., EGFR mutations in lung cancer: correlation with clinical response to gefitinib therapy, Science 304 (2004) 1497–1500.
[3] M. Maemondo, A. Inoue, K. Kobayashi, et al., Gefitinib or chemotherapy for non-small-cell lung cancer with mutated EGFR, N. Engl. J. Med. 362 (2010) 2380–2388.
[4] T. Mitsudomi, S. Morita, Y. Yatabe, et al., Gefitinib versus cisplatin plus docetaxel in patients with non-small-cell lung cancer harbouring mutations of the epidermal growth factor receptor (WJTOG3405): an open label, randomised phase 3 trial, Lancet Oncol. 11 (2010) 121–128.
[5] R. Rosell, C. Carcereny, R. Gervais, et al., Erlotinib versus standard chemotherapy as first-line treatment for European patients with advanced EGFR mutation-positive non-small-cell lung cancer (EURTAC): a multicentre, open-label, randomised phase 3 trial, Lancet Oncol. 13 (2012) 239–246.
[6] J.C.H. Yang, Y.L. Wu, M. Schuler, et al., Afatinib versus cisplatin-based chemotherapy for EGFR mutation-positive lung adenocarcinoma (LUX-Lung 3 and LUX-Lung 6): analysis of overall survival data from two randomised, phase 3 trials, Lancet Oncol. 16 (2015) 141–151.
[7] J. Li, M. Zhao, P. He, et al., Differential metabolism of gefitinib and erlotinib by human cytochrome P450 enzymes, Clin. Cancer Res. 13 (2007) 3731–3737.
[8] M. Leggas, J.C. Panetta, Y. Zhuang, et al., Gefitinib modulates the function of multiple ATP-binding cassette transporters *in vivo*, Cancer Res. 66 (2006) 4802–4807.
[9] D. McKillop, A.D. McCormick, A. Millar, et al., Cytochrome P450-dependent metabolism of gefitinib, Xenobiotica 35 (2005) 39–50.
[10] J. Li, M.O. Karlsson, J. Brahmer, et al., CYP3A4 phenotyping approach to predict systemic exposure to EGFR tyrosine kinase inhibitors, J. Natl. Cancer Inst. 98 (2006) 1714–1723.
[11] S. Kudoh, H. Kato, Y. Nishiwaki, et al., Interstitial lung disease in Japanese patients with lung cancer: a cohort and nested case-control study, Am. J. Respir. Crit. Care Med. 177 (2008) 1348–1357.
[12] K. Nakagawa, T. Tamura, S. Negoro, et al., Phase I pharmacokinetic trial of the selective oral epidermal growth factor receptor tyrosine kinase inhibitor gefitinib ('Iressa', ZD1839) in Japanese patients with solid malignant tumors, Ann. Oncol. 14 (2003) 922–930.
[13] M. Ranson, L.A. Hammond, D. Ferry, et al., ZD1839, a selective oral epidermal growth factor receptor-tyrosine kinase inhibitor, is well tolerated and active in patients with solid, malignant tumors: results of a phase I trial, J. Clin. Oncol. 20 (2002) 2240–2250.
[14] H. Kobayashi, K. Sato, T. Niioka, et al., Relationship among gefitinib exposure, polymorphisms of its metabolizing enzymes and transporters, and side effects in Japanese patients with non-small-cell lung cancer, Clin. Lung Cancer 16 (2015) 274–281.
[15] G. Cusatis, V. Gregorc, J. Li, et al., Pharmacogenetics of ABCG2 and adverse reactions to gefitinib, J. Natl. Cancer Inst. 98 (2006) 1739–1742.
[16] K. Akasaka, T. Kaburagi, S. Yasuda, et al., Impact of functional *ABCG2* polymorphisms on the adverse effects of gefitinib in Japanese patients with non-small-cell lung cancer, Cancer Chemother. Pharmacol. 66 (2010) 691–698.
[17] S. Kobayashi, T.J. Boggon, T. Dayaram, et al., EGFR mutation and resistance of non-small-cell lung cancer to gefitinib, N. Engl. J. Med. 352 (2005) 786–792.
[18] J.A. Engelman, K. Zeinullahu, T. Mitsudomi, et al., MET amplification leads to gefitinib resistance in lung cancer by activating ERBB3 signaling, Science 316 (2007) 1039–1043.
[19] Y. Nakamura, K. Sano, H. Soda, et al., Pharmacokinetics of gefitinib predicts antitumor activity for advanced non-small cell lung cancer, J. Thorac. Oncol. 5 (2010) 1404–1409.
[20] L. Faivre, C. Gomo, O. Mir, et al., A simple HPLC–UV method for the simultaneous quantification of gefitinib and erlotinib in human plasma, J. Chromatogr. B Anal. Technol. Biomed. Life Sci. 879 (2011) 2345–2350.
[21] Y. Akiyama, K. Fujita, H. Ishida, et al., Association of ABCC genotype with efficacy of first-line FOLFIRI in Japanese patients with advanced colorectal cancer, Drug Metab. Pharmacokinet. 27 (2012) 325–335.
[22] R. Eiselt, T.L. Domanski, A. Zibat, et al., Identification and functional characterization of eight CYP3A4 protein variants, Pharmacogenetics 11 (2001) 447–458.
[23] M. Saeki, Y. Saito, T. Nakamura, et al., Single nucleotide polymorphisms and haplotype frequencies of CYP3A5 in a Japanese population, Hum. Mutat. 21 (2003) 653.
[24] A. Soyama, Y. Saito, K. Komamura, et al., Novel single nucleotide polymorphisms in the CYP2D6 gene associated with CYP2D6*2 and/or CYP2D6*10 alleles, Drug Metab. Pharmacokinet. 17 (2002) 475–478.
[25] M. Fukudo, Y. Ikemi, Y. Togashi, et al., Population pharmacokinetics/pharmacodynamics of erlotinib and pharmacogenomic analysis of plasma and cerebrospinal fluid drug concentrations in Japanese patients with non-small cell lung cancer, Clin. Pharmacokinet. 52 (2013) 593–609.
[26] J.F. Lu, S.M. Eppler, J. Wolf, et al., Clinical pharmacokinetics of erlotinib in patients with solid tumors and exposure-safety relationship in patients with non-small cell lung cancer, Clin. Pharmacol. Ther. 80 (2006) 136–145.
[27] A. Hamada, J.I. Sasaki, S. Saeki, et al., Association of *ABCB1* polymorphisms with erlotinib pharmacokinetics and toxicity in Japanese patients with non-small-cell lung cancer, Pharmacogenomics 13 (2012) 615–624.
[28] R. ter Heine, R.T. van den Bosch, C.M. Schaefer-Prokop, et al., Fatal interstitial lung disease associated with high erlotinib and metabolite levels: a case report and a review of the literature, Lung Cancer 75 (2012) 391–397.
[29] B. Wacker, T. Nagrani, J. Weinberg, et al., Correlation between development of rash and efficacy in patients treated with the epidermal growth factor receptor tyrosine kinase inhibitor erlotinib in two large Phase III studies, Clin. Cancer Res. 13 (2007) 3913–3921.
[30] A.C. Mita, K. Papadopoulos, M.J.A. de Jonge, et al., Erlotinib 'dosing-to-rash': a phase II intrapatient dose escalation and pharmacologic study of erlotinib in previously treated advanced non-small cell lung cancer, Br. J. Cancer 105 (2011) 938–944.
[31] E. Ichihara, K. Hotta, N. Takigawa, et al., Impact of physical size on gefitinib efficacy in patients with non-small cell lung cancer harboring EGFR mutations, Lung Cancer 81 (2013) 435–439.

ANTICANCER RESEARCH *36*: 5957-5964 (2016)
doi:10.21873/anticanres.11183

Investigation of Bioequivalence Between Brand-name and Generic Irinotecan Products

KEN-ICHI SAITO[1,2], YUTAKA INOUE[2], YOJI IKEGAMI[2], IZUMI NANBO[2], MARI ONOZUKA[2], KAZUMI SANO[2], HISAHIRO YOSHIDA[2], TOSHIHIRO SAKAMOTO[3], EMI TATEBAYASHI[3], KEN-ICHI FUJITA[4], YASUTSUNA SASAKI[5] and TAKAKI KITAZAWA[3,6]

[1]*Department of Pharmacy Services, Saitama Medical Center, Saitama Medical University, Saitama, Japan;*
[2]*Department of Drug Metabolism and Disposition, Meiji Pharmaceutical University, Kiyose, Japan;*
[3]*Department of Pharmacy Services, Saitama Medical University International Medical Center, Saitama, Japan;*
[4]*Institute of Molecular Oncology, Showa University, Tokyo, Japan;*
[5]*Division of Medical Oncology, Department of Medicine, Showa University School of Medicine, Tokyo, Japan;*
[6]*Department of Pharmacy Services, Saitama Medical University, Moroyama, Japan*

Abstract. *Background/Aim: To investigate bioequivalence among generic and brand-name irinotecan products. Materials and Methods: Products of Yakult and Daiichi-Sankyo (brand-name products), Sandoz, Nippon Kayaku, Taiho, and Sawai were compared with respect to their composition and antitumor activity. Results: High-performance liquid chromatography demonstrated that related substances were within the acceptable range. The 3-(4,5-dimethylthiazol-2-yl)-2,5-diphenyltetrazolium bromide assay revealed significant differences in cytotoxicity for four cancer cell lines among the products. The concentration of the active compound SN-38 was highest in Yakult's product (23.82 ng/ml) and lowest in Daiichi-Sankyo's product (8.96 ng/ml). MTT assay data were correlated with the SN-38 concentration, suggesting that it influenced differences in cytocidal activity among products. However, the SN-38 concentration was far lower than that of irinotecan (20 mg/ml), suggesting a negligible clinical effect. Metabolism of irinotecan to SN-38 or open-ring forms did not differ significantly among the products. Conclusion: The generic products showed equivalent efficacy and safety to the brand-name products.*

Generic products are expected to show equivalence to brand-name products with respect to the dosage form, safety, efficacy and quality, while reducing medical expenses due to their lower cost. For oral drugs, equivalence between generic and brand-name products must be demonstrated by dissolution and bioequivalence tests. On the other hand, while quality assurance tests, such as purity tests, are required for injectable products, bioequivalence tests are not compulsory. Therefore, only certain companies voluntarily perform bioequivalence tests of injectable products. For anticancer agents, excluding some hormonal agents, bioequivalence studies in healthy volunteers are prohibited. However, some reports have been published comparing safety and pharmacokinetics between brand-name and generic injectable products. For example, the safety and pharmacokinetics of paclitaxel were reported to be similar between brand-name and generic products in patients with cancer (1-4). In contrast, it has been reported that generic forms of docetaxel, another taxane anticancer agent, cause more serious febrile neutropenia than the brand-name product (5). Moreover, cisplatin generics were found to cause more severe nephropathy and hematological toxicity than the brand-name product (6-8).

Irinotecan is a DNA topoisomerase I inhibitor derived from camptothecin that shows broad-spectrum strong antitumor activity (9). It is a prodrug, and carboxylesterases in the liver and other tissues convert it to the active metabolite, 7-ethyl-10-hydroxy-camptothecin (SN-38) (10), which has 1000-fold stronger pharmacological activity than the parent compound (11). Irinotecan is a key drug for treating various cancer types, including colorectal (12), lung (13), gastric cancer (14), breast (15), cervical (16), and ovarian (17). Generic products for irinotecan were released in Japan in May 2009.

Irinotecan is a semisynthetic derivative of camptothecin extracted from *Camptotheca acuminata* or *Nothapodytes foetida*, which are native to China (18, 19). It has been

Correspondence to: Yoji Ikegami, Department of Drug Metabolism and Disposition, Meiji Pharmaceutical University, 2-522-1 Noshio, Kiyose-shi, Tokyo 204-8588, Japan. Tel: +81 424958470, e-mail: yoji@my-pharm.ac.jp

Key Words: Cytotoxicity, chemotherapy, generic, irinotecan, bioequivalence.

Table I. *List of irinotecan products and manufacturers.*

Type of product	Name	Manufacturer
Brand name	Campto for *i.v.* infusion	Yakult Honsha
Generic	Irinotecan Hydrochloride Intravenous Infusion [SANDOZ]	Sandoz
Generic	Irinotecan for *i.v.* infusion [NK]	Nippon Kayaku Co., Ltd
Generic	Irinotecan Hydrochloride *i.v.* infusion「TAIHO」	Taiho Pharmaceutical Co., Ltd.
Generic	Irinotecan Hydrochloride	Sawai Pharmaceutical Co., Ltd.
Brand name	Topotecin Intravenous Drip Infusion	Daiichi-Sankyo Co., Ltd.

reported that the plant used as a source material differs among pharmaceutical companies and that levels of contaminants vary as a consequence (20). Antitumor activity is also influenced by pH-related lactone ring opening, since the lactone form shows higher antitumor activity than the carboxylate form. These features of irinotecan suggest the potential for safety and pharmacokinetics to differ between the brand-name and generic products, but there have been no reports about this issue.

Accordingly, the present study was performed to investigate *in vitro* bioequivalence among the irinotecan products of various pharmaceutical companies by performing various tests, including assessment of purity, cytocidal activity, pH-dependent lactone ring opening, cytotoxicity of Y3 (a related substance), and formation of active metabolites by human hepatic microsomes. Our findings suggest that the brand-name and generic products would be expected to have equivalent efficacy and safety.

Materials and Methods

Anticancer agents. The reference formulation (brand-name product) was Campto® (Yakult Honsha,Tokyo, Japan), while the other products studied were Topotecin® (brand-name product) and four generic products (Table I). Authentic specimens of the following potential contaminants were supplied by Yakult Honsha: 3,10-diethyl-8-[(4-piperidinopiperidino)carbonyloxy]furo [3',4':6,7] indolizino-[1,2-b]quinoline-1,13(3*H*,11*H*)-dione (D1); 10-ethyl-2-methyl-3-propionyl-8-[(4-piperidinopiperidino)carbonyloxy] indolizino[1,2-b]-quinoline-1(11*H*)-one (D3); (4*S*)-4,11-diethyl-4,12-dihydroxy-9-[(4-piperidinopiperidino)carbonyloxy-1*H*-pyrano[3',4':6,7]-indolizino[1,2-b]quinoline-3,14(4*H*,12*H*)-dione (Y1); (4*S*)-4,11-diethyl-4,9,12-trihydroxy-1*H*-pyrano[3',4':6,7] indolizino[1,2-b]quinoline-3,14(4*H*,12*H*)-dione (Y3), and 4-ethyl-2-[6-(4-ethyl-4-hydroxy-3,8(1*H*,7*H*)-dioxopyrano[3,4-c]pyridyl)]-6-(piperidinopiperidino)-carbonyloxyquinoline-3-carboxylic acid (U1) (Figure 1).

Cell lines and culture. A small cell lung cancer cell line (PC-6) was obtained from the Second Department of Internal Medicine of Nagasaki University (Nagasaki, Japan), a non-small cell lung cancer cell line (PC-9) was from Kinki University (Higasiosaka-shi, Japan), and another non-small cell lung cancer cell line (A549) and an ovarian cancer cell line (NIH:OVCAR-3) were from the Riken Cell Bank, Tsukuba, Ibaraki, Japan.

A549 cells were incubated in Dulbecco's modified Eagle's medium (DMEM) (Wako, Osaka, Japan), while PC-6, PC-9, and NIH:OVCAR-3 cells were incubated in RPMI-1640 medium (Sigma-Aldrich, Tokyo, Japan). Both media contained 10% fetal bovine serum and incubation was at 37˚C under 5% CO_2.

Assessment of purity. High-performance liquid chromatography (HPLC) was performed using a Hitachi Detector L-2400 and a Hitachi Pump L-2130 (Hitachi, Tokyo, Japan). The detection wavelength was 254 nm. The analytical column was a Capcell Pak C18 MG (5 μ, 3.0 Φ×150 mm) from Shiseido (Tokyo, Japan). Mobile phase A was a mixture of 50 mM formic acid buffer (pH 5.1), acetonitrile and MeOH at 75:10:15 (v/v/v), while mobile phase B was a mixture of 50 mM formic acid buffer (pH 5.1), acetonitrile and MeOH at 55:30:15 (v/v/v). Elution was performed at a flow rate of 1.0 ml/min and a temperature of 50˚C using the following protocol: gradient elution from A to B (30 min)→A (1 min)→ equilibration (5 min).

Cytotoxicity test. Small cell lung cancer cells (PC-6), non-small cell lung cancer cells (PC-9, A549) and ovarian cancer cells (NIH:OVCAR-3) were used to evaluate cytotoxicity by the 3-(4,5-dimethylthiazol-2-yl)-2,5-diphenyltetrazolium bromide (MTT) assay. Cells in the logarithmic growth phase were suspended in 0.05% trypsin-EDTA (Nacalai Tesque, Kyoto, Japan) and adjusted to 5.6×10^3 cells/ml in irinotecan-free medium. This suspension was inoculated at a volume of 1,800 μl/well (1,000 cells/well) into a 96-well microplate, and serial dilutions of each product in medium were added to the wells. After 72 h of incubation, 5 mg/ml MTT (Nacalai Tesque) was added at 20 μl/well and incubation was continued for 4 h. Then centrifugation (400 × *g* at 4˚C) was performed for 10 min. After the medium was discarded, dimethyl sulfoxide was added at a volume of 200 μg/well, and the absorbance was measured at 570 nm using a microplate reader (reference wavelength of 650 nm).

Formation of open-ring irinotecan. Irinotecan adopts closed- and open-ring forms under acidic and basic conditions, respectively (21). Because opening the lactone ring alters the antitumor activity of irinotecan, the extent of formation of its open-ring form was compared among the products. During incubation of each product in human plasma (pH 7.4±0.05) at 37˚C, samples were collected over time and deproteinized for analysis by HPLC (fluorescence detector: excitation at 380 nm and emission at 550 nm). The concentration of the closed-ring form relative to the total irinotecan

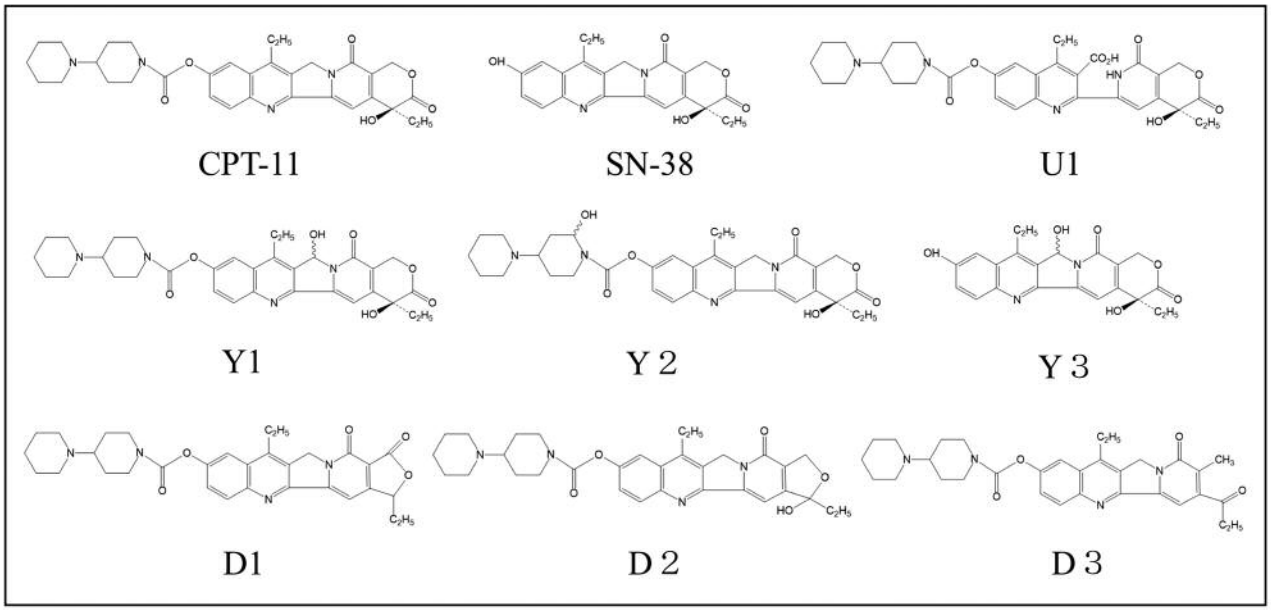

Figure 1. *Structure of irinotecan and related substances.*

concentration was determined over time, with the concentration of the closed-ring form at the start of incubation being set at 100%.

SN-38 formation by human hepatic microsomes. An aliquot (30 μl) of 25 mg/ml human hepatic microsomes (Biopredic, Saint-Grégoire, France) was solubilized by adding 6 μl of 1% Triton X-100. The solubilized microsomes were added to 60 μl of NaH_2PO_4 (0.1 mol/l pH 7.4) together with 51 μl of water and 3 μl of irinotecan (0.8 mg/ml) for incubation at 37˚C. Samples were collected after 2, 4, and 6 min and were immediately added to acetonitrile on ice (0˚C) for deproteinization. After centrifugation for 5 min at 21,000 × g and 4˚C, 10 μl of the supernatant was injected into the HPLC system by an autosampler for analysis (fluorescence detector: excitation at 380 nm and emission at 550 nm).

Cytotoxicity of Y3 and SN-38. Because the potential contaminant Y3 has a similar structure to SN-38, even a low content of Y3 can influence a product's cytocidal activity. Therefore, the cytotoxicity of Y3 for small-cell lung cancer cell line PC-6 and non-small cell lung cancer cell line PC-9 was evaluated by the MTT assay and the Y3 content of each product was measured by HPLC.

Results

Comparison of impurities among the products. When impurities were measured by HPLC and compared among the products, peaks of related substances with known structures (such as D1, D3, Y1, and U1) were detected in addition to the peaks of irinotecan and SN-38 (Table II). While the peak area of each related substance varied among the products, it was always less than 0.2%, which is the threshold specified by "Impurities in New Drug Products" in the International Conference on Harmonisation (ICH) guidelines (22). Peaks of unknown contaminants were also noted, but the peak area of each contaminant was less than 0.1%. These results suggest that the products were equivalent with respect to their impurities.

Cytotoxicity. When *in vitro* cytocidal activity was compared between the products by the MTT assay (Table III), the 50% inhibitory concentration (IC_{50}) for PC-6 showed a significant difference between the reference formulation and three other products.In addition, the IC_{50} values for PC9 and NIH:OVCAR-3 cells were significantly different between the reference formulation and four or five other products, respectively. When the SN-38 content was measured in the impurity test, it was significantly lower in the products of Sandoz, Sawai, and Daiichi-Sankyo than in the reference formulation (Table IV). The difference of IC_{50} against PC-6 cells among the products was significantly related to the SN-38 content (r^2=0.813, p<0.05) as it was against PC-9 cells (r^2=0.951, p<0.01), but not A549 cells (r^2=0.326, p>0.05) nor NIH:OVCA R-3 cells (r^2=0.123, p>0.05). Yakult's product had the highest SN-38 content (23.82±3.55 ng/ml) and the strongest cytotoxicity, while the product of Daiichi-Sankyo had the lowest SN-38 content (8.96±0.62 ng/ml) and tended to exhibit weaker cytotoxicity than the other products against all cell lines.

Open-ring form. When each product was incubated in human plasma, the decrease in the lactone (closed-ring) form of irinotecan over time did not significantly differ among the

Table II. *Peak area ratios of irinotecan and contaminants. High-performance liquid chromatography peak area (%) profiles of the reference formulation and other products are shown. The peak area ratio of each contaminant was <0.2% and was acceptable by International Conference on Harmonisation guidelines.*

	Product manufacturer					
Compound	Yakult	Sandoz	Nippon Kayaku	Taiho	Sawai	Daiichi-Sankyo
Irinotecan (closed)	99.56	99.52	99.60	99.46	99.52	99.47
Irinotecan (open)	0.14	0.18	0.20	0.22	0.11	0.14
D1	0.05	0.01	0.02	0.01	0.01	0.01
D3	0.10	0.08	0.06	0.11	0.09	0.11
Y1	0.04	0.06	0.01	0.06	0.08	0.06
U1	0.06	0.02	0.06	0.02	0.05	0.07
Unknown 1	n.d.	n.d.	0.01	0.01	0.01	0.04
Unknown 2	n.d.	0.06	0.01	0.04	0.05	0.01
Other	0.05	0.07	0.03	0.07	0.08	0.09
Total	100.00	100.00	100.00	100.00	100.00	100.00

Table III. *Cytotoxicity of each product. The 50% inhibitory concentration (IC_{50}) of each product was determined by the 3-(4,5-dimethylthiazol-2-yl)-2,5-diphenyltetrazolium bromide assay. The cytotoxicity of the other products was weaker than that of the Yakult reference formulation.*

	IC_{50} (μM)					
	Product manufacturer					
Cell line	Yakult	Sandoz	Nippon Kayaku	Taiho	Sawai	Daiichi-Sankyo
PC-6	1.37±0.05	1.86±0.06**	1.38±0.08	1.59±0.09**	1.39±0.05	2.03±0.07**
PC-9	7.46±0.68	12.36±0.47**	8.01±0.51	9.07±0.48**	9.14±0.29**	16.70±0.56**
A549	44.99±6.90	77.09±8.89**	64.07±10.21**	75.17±7.95**	61.61±7.63**	72.32±6.89**
NIH:OVCAR-3	16.66±0.71	20.85±1.37**	23.08±3.44**	24.70±2.26**	24.63±0.95**	24.08±2.13**

Data are the mean±SD. **Significantly different at $p<0.005$ *vs.* Yakult by Student's *t*-test.

products (Figure 2), and the formation rate of the open-ring form was considered to be equivalent among the products.

Metabolism to SN-38. When the conversion rate of irinotecan to SN-38 by human hepatic microsomes was investigated, there were no significant differences among the products (Table V).

Cytotoxicity of Y3 and SN-38. The IC_{50} of Y3 for PC-6 and PC-9 cells was 24-fold and 64-fold higher than that of SN-38, respectively (Table VI). The Y3 content of each product was similar to or significantly lower than that of the reference formulation (Table IV). In addition, the Y3 content was approximately 45, 20, 11, 8, 23 and 109 times higher than the SN-38 content in the products of Yakult, Sandoz, Nippon Kayaku, Taiho, Sawai, and Daiichi-Sankyo, respectively (Table IV). Even though Y3 was less toxic than SN-38, these differences in Y3 content might have influenced the cytotoxicity of the products. In fact, Yakult's

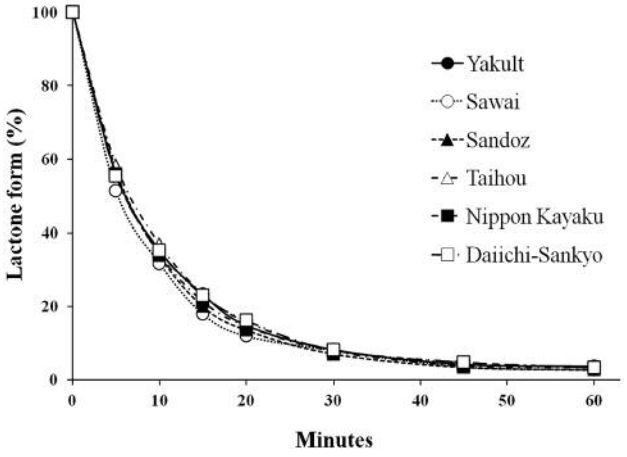

Figure 2. *Elimination rate of the lactone form of irinotecan. Each irinotecan product was incubated in human blood plasma in vitro. The lactone form was changed to carboxylate form with increasing pH over time. There were no significant differences between products at each time point.*

Table IV. *SN-38 and Y3 concentration in each product. High-performance liquid chromatography showed that the reference formulation had the highest concentration of SN-38.*

	Product manufacturer					
Compound	Yakult	Sandoz	Nippon Kayaku	Taiho	Sawai	Daiichi-Sankyo
SN-38 (ng/ml)	23.82±3.55	14.59±2.14**	22.91±4.20	21.56±0.57	18.16±0.86*	8.96±0.62**
Y3 (ng/mI)	1069.7±64.7	293.3±91.1**	243.8±74.3**	168.4±45.5**	413.3±67.1**	974.0±166.9

Data are the mean±SD. Significantly different at *$p<0.05$ and **$p<0.005$ *vs*. Yakult by Student's *t*-test.

Table V. *Formation of SN-38 by human hepatic microsomes. There were no appreciable differences in metabolism to SN-38 among the products by Student's t-test.*

	Product manufacturer					
	Yakult	Sandoz	Nippon Kayaku	Taiho	Sawai	Daiichi-Sankyo
ng/min/mgP	1.21±0.14	1.15±0.07	1.33±0.04	1.38±0.06	1.40±0.14	1.40±0.07

Data are the mean±SD.

product, with the highest content of SN-38 and Y3, had the strongest cytotoxicity (Table III).

Discussion

In this study, we evaluated the *in vitro* bioequivalence of various irinotecan products and we clarified the following points. Firstly, levels of contaminants differed among the products, but were always within the acceptable range specified by the guidelines. Secondly, cytotoxicity differed significantly among the products, and these differences probably reflected differences of the SN-38 content. Finally, there were no significant differences of pH-dependent ring-opening or metabolism to SN-38. Because irinotecan is a semisynthetic derivative of camptothecin, each product was subjected to HPLC to determine the levels of active ingredients and contaminants, and we also compared cytotoxicity, metabolism, and pH-dependent ring opening.

Various contaminants (D1, D3, Y1, U1, *etc*.) were detected in addition to irinotecan and its active metabolite SN-38. The content of each related substance differed among the products, presumably due to differences in the raw materials and manufacturing methods, but this was considered to be of no clinical relevance because the content of each substance was always within the acceptable range according to the ICH guidelines. Comparison of pH-dependent irinotecan ring opening also did not significantly differ among the products. However, the MTT assay revealed significant differences of cytotoxicity among the products. Formulations of irinotecan contain trace levels of various decomposition products and contaminants, including the active metabolite SN-38, with far stronger antitumor activity than irinotecan (100 to several thousand times higher) (23, 24). This study showed that the SN-38 concentration of each product (8.96-23.82 ng/ml) was far lower than the irinotecan concentration (20 mg/ml). If irinotecan was partially metabolized to SN-38 during the MTT assay, the amount of SN-38 produced would be far higher than the initial content in each product, which might suggest there was little likelihood of the differences in the baseline concentration of SN-38 causing the differences in cytotoxicity among the products. However, there was no significant difference in the metabolism of irinotecan to SN-38 by hepatic microsomes among the products and cytotoxicity in the MTT assay was related to the concentration of SN-38 in each product, suggesting that the differences in cytotoxicity among the products were actually related to differences of the baseline SN-38 concentration.

Table VI. *Cytotoxicity of Y3 and SN-38. The 50% inhibitory concentration (IC_{50}) values of Y3 and SN-38 were measured by the 3-(4,5-dimethylthiazol-2-yl)-2,5-diphenyltetrazolium bromide assay using cancer cell lines (PC-6 and PC-9). The cytotoxicity of Y3 was much weaker than that of SN-38.*

	Mean IC_{50}±S.E. (nM) Cell line	
Compound	PC-6	PC-9
SN-38	39.7±3.2	45.2±3.3
Y3	933.5±40.2	2898.4±154.8

We also compared cytotoxicity between SN-38 and Y3, a related substance with a similar structure to SN-38. Although the cytotoxicity of Y3 was lower than that of SN-38, the Y3 content of each product was 8-109 times higher, suggesting that Y3 was likely to influence the results of the MTT assay. In fact, Yakult's product, with the highest SN-38 and Y3 content, had the strongest cytotoxicity and the product of Daiichi-Sankyo with a Y3 content 109-fold higher than that of SN-38 (8.96±0.62 ng/ml *vs*. 974.0±166.9 ng/ml) exhibited relatively strong cytotoxicity against A549 and NIH:OVCAR-3 cells.

However, it must also be considered whether such *in vitro* differences among the products could lead to clinical differences in safety and pharmacokinetics. The concentration of irinotecan in each product was 20 mg/ml, which was many times higher than that of SN-38 (8.96-23.82 ng/ml) and Y3 (168.4-1,069.7 ng/ml). Moreover, the area under the plasma concentration–time curve for plasma SN-38 was found to be approximately 0.03-0.08 times that of irinotecan in clinical studies (25-27). The SN-38 concentrations of the products were much lower than that generated from irinotecan in plasma. Hence, the differences of SN-38 concentrations of the products would have little influence on *in vivo* cytotoxicity, indicating that each product is considered to be equivalent. The SN-38 concentrations of the generic products were similar to or lower than that of reference formulation, indicating that there is little likelihood of the generic products having stronger clinical cytotoxicity.

In summary, based on the results of the present study, we concluded that each irinotecan product tested was equivalent to the reference formulation.

Irinotecan causes various adverse reactions, including myelosuppression and diarrhea (28, 29). We consider that bioequivalence should be investigated for injectable drugs with strong toxicities such as anticancer agents. If possible, clinical studies should be performed to assess the safety and efficacy of generic products before their approval. Although large-scale clinical studies are undoubtedly expensive, *in vitro* studies such as the present investigation can provide an indication of bioequivalence. In the future, it would seem necessary to conduct further studies to determine whether the differences among products that we identified influence the efficacy and adverse reactions of these products in clinical practice.

References

1 Sagara Y, Rai Y, Sagara Y, Matsuyama Y, Baba S, Tamada S, Sagara Y and Ando M: Comparison of the pharmacokinetics and safety of a paclitaxel injection NK and Taxol injection in breast cancer patients. Gan To Kagaku Ryoho *36*: 247-250, 2009.

2 Takahara S, Yamamoto H, Tokushima Y and Shiba E: Safety evaluation of paclitaxel injection NK in adjuvant therapy for breast cancer. Gan To Kagaku Ryoho *36*: 1851-1856, 2009.

3 Tsukiyama I, Hotta K, Takeuchi M, Onishi M, Toyama Y, Saito H, Sai Y, Miyamoto K and Hasegawa T: Evaluation of safety in clinical use of generic paclitaxel [NK] for injection. Gan To Kagaku Ryoho *39*: 613-617, 2012.

4 Yamamoto D, Tsubota Y, Sueoka N, Yokoi T, Inoue K, Ohira M and Muranaka T: Comparison of a safety evaluation between paclitaxel injection NK and Taxol. Gan To Kagaku Ryoho *40*: 959-961, 2013.

5 Poirier E, Desbiens C, Poirier B, Hogue JC, Lemieux J, Doyle C, Leblond AF, Cote I, Cantin G and Provencher L: Comparison of serious adverse events between the original and a generic docetaxel in breast cancer patients. Ann Pharmacother *48*: 447-455, 2014.

6 Ochi N, Yamane H, Hotta K, Fujii H, Isozaki H, Honda Y, Yamagishi T, Kubo T, Tanimoto M, Kiura K and Takigawa N: Cisplatin-induced hyponatremia in malignancy: comparison between brand-name and generic formulation. Drug Design Deve Ther *8*: 2401-2408, 2014.

7 Oike T, Ohno T, Noda S-e, Sato H, Tamaki T, Kiyohara H, Ando K and Nakano T: Comparison of hematological toxicities between innovator and generic cisplatin formulations in cervical cancer patients treated with concurrent chemoradiotherapy. J Radiat Res (Tokyo) *54*: 474-478, 2013.

8 Sekine I, Kubota K, Tamura Y, Asahina H, Yamada K, Horinouchi H, Nokihara H, Yamamoto N and Tamura T: Innovator and generic cisplatin formulations: comparison of renal toxicity. Cancer Sci *102*: 162-165, 2011.

9 Hsiang YH, Hertzberg R, Hecht S and Liu LF: Camptothecin induces protein-linked DNA breaks *via* mammalian DNA topoisomerase I. J Biol Chem *260*: 14873-14878, 1985.

10 Satoh T, Hosokawa M, Atsumi R, Suzuki W, Hakusui H and Nagai E: Metabolic activation of CPT-11, 7-ethyl-10-[4-(1-piperidino)-1- piperidino]carbonyloxycamptothecin, a novel antitumor agent, by carboxylesterase. Biol Pharm Bull *17*: 662-664, 1994.

11 Kawato Y, Aonuma M, Hirota Y, Kuga H and Sato K: Intracellular roles of SN-38, a metabolite of the camptothecin derivative CPT-11, in the antitumor effect of CPT-11. Cancer Res *51*: 4187-4191, 1991.

12 Douillard JY, Cunningham D, Roth AD, Navarro M, James RD, Karasek P, Jandik P, Iveson T, Carmichael J, Alakl M, Gruia G, Awad L and Rougier P: Irinotecan combined with fluorouracil compared with fluorouracil alone as first-line treatment for metastatic colorectal cancer: a multicentre randomised trial. Lancet *355*: 1041-1047, 2000.

13 Sanchez R, Esteban E, Palacio I, Fernandez Y, Muniz I, Vieitez JM, Fra J, Blay P, Villanueva N, Una E, Mareque B, Estrada E, Buesa JM and Lacave AJ: Activity of weekly irinotecan (CPT-11) in patients with advanced non-small cell lung cancer pretreated with platinum and taxanes. Invest New Drugs *21*: 459-463, 2003.

14 Kohne CH, Catane R, Klein B, Ducreux M, Thuss-Patience P, Niederle N, Gips M, Preusser P, Knuth A, Clemens M, Bugat R, Figer I, Shani A, Fages B, Di Betta D, Jacques C and Wilke HJ: Irinotecan is active in chemonaive patients with metastatic gastric cancer: a phase II multicentric trial. Br J Cancer *89*: 997-1001, 2003.

15 Xu L, Wu X, Hu C, Zhang Z, Zhang L, Liang S, Xu Y and Zhang F: A meta-analysis of combination therapy *versus* single-agent therapy in anthracycline- and taxane-pretreated metastatic breast cancer: results from nine randomized Phase III trials. OncoTargets Ther *9*: 4061-4074, 2016.

16 Sugiyama T, Yakushiji M, Noda K, Ikeda M, Kudoh R, Yajima A, Tomoda Y, Terashima Y, Takeuchi S, Hiura M, Saji F, Takahashi T, Umesaki N, Sato S, Hatae M and Ohashi Y: Phase II study of irinotecan and cisplatin as first-line chemotherapy in advanced or recurrent cervical cancer. Oncology *58*: 31-37, 2000.
17 Shoji T, Takatori E, Omi H, Kumagai S, Yoshizaki A, Yokoyama Y, Mizunuma H, Fujimoto T, Takano T, Yaegashi N, Tase T, Nakahara K, Kurachi H, Nishiyama H and Sugiyama T: Phase II clinical study of the combination chemotherapy regimen of irinotecan plus oral etoposide for the treatment of recurrent ovarian cancer (Tohoku Gynecologic Cancer Unit 101 Group Study). Int J Gynecol Cancer *21*: 44-50, 2011.
18 Gallo RC, Whang-Peng J and Adamson RH: Studies on the antitumor activity, mechanism of action, and cell cycle effects of camptothecin. J Natl Cancer Inst *46*: 789-795, 1971.
19 Wall ME, Wani MC, Cook CE, Palmer KH, McPhail AT and Sim GA: Plant Antitumor Agents. I. The Isolation and Structure of Camptothecin, a Novel Alkaloidal Leukemia and Tumor Inhibitor from *Camptotheca acuminata*. J AM Chem Soc *88*: 3888-3890, 1966.
20 Akimoto K, Kawai A and Kazumi O: Simultaneous determination of a camptothecin derivative, used as an anticancer drug, and its photodegradation products by high-performance liquid chromatography. J Chromatogr A *734*: 401-404, 1996.
21 Sano K, Yoshikawa M, Hayasaka S, Satake K, Ikegami Y, Yoshida H, Ishikawa T, Sawada S and Tanabe S: Simple non-ion-paired high-performance liquid chromatographic method for simultaneous quantitation of carboxylate and lactone forms of 14 new camptothecin derivatives. J Chromatogr B Analyt Technol Biomed Life Sci *795*: 25-34, 2003.
22 International Conference on Harmonisation (ICH) Guidline Q3B (R2): impurities in new drug products, 2006.
23 Jansen WJ, Zwart B, Hulscher ST, Giaccone G, Pinedo HM and Boven E: CPT-11 in human colon-cancer cell lines and xenografts: characterization of cellular sensitivity determinants. Int J Cancer *70*: 335-340, 1997.
24 van Ark-Otte J, Kedde MA, van der Vijgh WJ, Dingemans AM, Jansen WJ, Pinedo HM, Boven E and Giaccone G: Determinants of CPT-11 and SN-38 activities in human lung cancer cells. Br J Cancer *77*: 2171-2176, 1998.
25 Crews KR, Stewart CF, Jones-Wallace D, Thompson SJ, Houghton PJ, Heideman RL, Fouladi M, Bowers DC, Chintagumpala MM and Gajjar A: Altered irinotecan pharmacokinetics in pediatric high-grade glioma patients receiving enzyme-inducing anticonvulsant therapy. Clin Cancer Res *8*: 2202-2209, 2002.
26 Pitot HC, Goldberg RM, Reid JM, Sloan JA, Skaff PA, Erlichman C, Rubin J, Burch PA, Adjei AA, Alberts SA, Schaaf LJ, Elfring G and Miller LL: Phase I dose-finding and pharmacokinetic trial of irinotecan hydrochloride (CPT-11) using a once-every-three-week dosing schedule for patients with advanced solid tumor malignancy. Clin Cancer Res *6*: 2236-2244, 2000.
27 Stewart CF, Panetta JC, O'Shaughnessy MA, Throm SL, Fraga CH, Owens T, Liu T, Billups C, Rodriguez-Galindo C, Gajjar A, Furman WLand McGregor LM: UGT1A1 promoter genotype correlates with SN-38 pharmacokinetics, but not severe toxicity in patients receiving low-dose irinotecan. J Clin Oncol *25*: 2594-2600, 2007.
28 Rothenberg ML, Eckardt JR, Kuhn JG, Burris HA, 3rd, Nelson J, Hilsenbeck SG, Rodriguez GI, Thurman AM, Smith LS, Eckhardt SG, Weiss GR, Elfring GL, Rinaldi DA, Schaaf LJand Von Hoff DD: Phase II trial of irinotecan in patients with progressive or rapidly recurrent colorectal cancer. J Clin Oncol *14*: 1128-1135, 1996.
29 Shimada Y, Yoshino M, Wakui A, Nakao I, Futatsuki K, Sakata Y, Kambe M, Taguchi T and Ogawa N: Phase II study of CPT-11, a new camptothecin derivative, in metastatic colorectal cancer. CPT-11 Gastrointestinal Cancer Study Group. J Clin Oncol *11*: 909-913, 1993

Received August 9, 2016
Revised September 5, 2016
Accepted September 12, 2016

Takata et al. Journal of Pharmaceutical Health Care and Sciences (2016) 2:30
DOI 10.1186/s40780-016-0064-5

Journal of Pharmaceutical Health Care and Sciences

RESEARCH ARTICLE Open Access

Cost-minimization analysis of adjuvant chemotherapy regimens given to patients with colorectal cancer in Japan

Kosuke Takata[1], Ken-ichi Fujita[2*], Yutaro Kubota[3], Hiroo Ishida[3], Wataru Ichikawa[4], Ken Shimada[5], Takashi Sekikawa[6,4], Iori Taki-Takemoto[1], Daisuke Kamei[1], Shinichi Iwai[1] and Yasutsuna Sasaki[2,3]

Abstract

Background: Consideration of medical costs as well as effectiveness and adverse events is rapidly been becoming an important factor in the selection of chemotherapy regimens. However, practical data on the costs of chemotherapy are scarce. We clinically estimated the medical costs of 6 adjuvant chemotherapy regimens for colorectal cancer on the basis of clinical and cost-related data and compared their cost-effectiveness by cost-minimization analyses.

Methods: All patients who received adjuvant chemotherapy for colorectal cancer between April 2012 and May 2015 at four hospitals affiliated with Showa University were studied retrospectively. Clinical and cost data related to adjuvant chemotherapy were collected from medical records and medical fee receipt data, respectively. Six adjuvant chemotherapy regimens were studied: capecitabine and oxaliplatin (CapeOX); 5-fluorouracil (5-FU), ℓ-leucovorin (LV), and oxaliplatin (modified FOLFOX6 [mFOLFOX6]); 5-FU and LV (5-FU/LV); tegafur and uracil (UFT), and LV (UFT/LV); capecitabine; and tegafur, gimeracil and oteracil (S-1). The regimens were divided into 2 groups according to whether or not they contained oxaliplatin because of the difference in effectiveness. Cost-minimization analyses, where relative costs of regimens showing equivalent effectiveness were simply compared, were performed to evaluate the cost-effectiveness of the regimens in each group.

Results: A total of 154 patients with colorectal cancer received adjuvant chemotherapy during the study period. Fifty-seven patients were treated with CapeOX, 10 with mFOLFOX6, 38 with UFT/LV, 20 with capecitabine, and 29 with S-1. No patient received 5-FU/LV. The total costs of oxaliplatin-containing regimens were significantly higher than those of oxaliplatin non-containing regimens. The high cost of oxaliplatin, but not the costs of drugs or various tests for the treatment of adverse events, was the primary reason for the higher costs of the oxaliplatin-containing regimens. The cost-effectiveness of the oxaliplatin-containing regimens CapeOX and mFOLFOX6 were comparable. Among the oxaliplatin non-containing regimens, the cost-effectiveness of S-1 and capecitabine was superior to that of UFT/LV.

Conclusion: Thus, we provided the cost-effectiveness data of 5 adjuvant chemotherapy regimens for colorectal cancer based on practical clinical and cost data from Japanese patients. The results can be included as a factor in regimen selection because these results would represent the real world.

Trial registration: This study is a retrospective observational study and does not include any health care interventions. Therefore, we did not register the protocol of this study.

Keywords: Cost-minimization analysis, Cost-effectiveness, Colorectal cancer, Adjuvant chemotherapy, Regimen selection

* Correspondence: k.fujita@med.showa-u.ac.jp
[2]Institute of Molecular Oncology, Showa University, 1-5-8, Hatanodai, Shinagawa-ku, Tokyo 142-8555, Japan
Full list of author information is available at the end of the article

Background

Cancer therapy has rapidly evolved over the past two decades, contributing to improvements in the survival and quality of life of cancer patients. However, the costs of the cancer therapy have also rapidly increased in parallel to progress in cancer therapy [1]. A previous study reported that 30.6 % or more of patients with cancer are complaining about the rising costs of cancer therapy [2]. Another study found that the frequency of bankruptcy was 2.65-fold higher among patients with cancer than those without the disease [3]. Many highly effective anticancer drugs have recently been developed and are now used in clinical practice. However, the costs of these drugs are generally high. For example, the cost of one intravenous dose of the cytotoxic anticancer drug oxaliplatin is higher than 80,000 yen (800 US dollars, assuming that 100 yen is equivalent to 1 dollar) when the drug is given to a Japanese patient with an average body surface area (BSA) of 1.69 m^2 [4]. As for molecularly targeted drugs, the cost of one dose of bevacizumab or cetuximab is higher than 100,000 yen (1000 dollars). In the case of the immune checkpoint inhibitor nivolumab, which was very recently launched, the cost of a single intravenous dose of the drug exceeds 1,000,000 yen (10,000 dollars). Given the remarkable increase in the costs of anticancer drug therapies, oncologists can no longer ignore or blindly accept that costs have no place in medical decision making [5]. Therefore, it has been widely recommended that costs related to cancer chemotherapy should be considered in addition to effectiveness and adverse events in the selection of treatment regimens [5, 6]. However, cost data on cancer medications in Japan are extremely limited; patients and oncologists generally choose treatment regimens on the basis of only effectiveness and adverse events, without considering costs.

For patients who have pathological stage II colorectal cancer with a high risk of recurrence or patients who have stage III disease, adjuvant chemotherapy is recommended after potentially curative resection [7]. Six adjuvant chemotherapy regimens are used to treat colorectal cancer in Japan: 1) CapeOX, consisting of capecitabine and oxaliplatin [8]; 2) FOLFOX4, comprising 5-fluorouracil (5-FU), ℓ-leucovorin (LV), and oxaliplatin [9], which is usually replaced by modified FOLFOX6 (mFOLFOX6), comprising the same agents as FOLFOX4, in Japan, because mFLOFOX6 is simpler to handle than FOLFOX4, while the effectiveness and safety of these regimens are nearly equivalent [10]; 3) 5-FU/LV, consisting of 5-FU plus LV [11]; 4) UFT/LV, comprising UFT (a fixed combination of tegafur and uracil) and oral LV [12]; 5) capecitabine [13]; and 6) S-1 (tegafur, gimeracil, and oteracil) [14].

Several economic studies have examined the cost-effectiveness of adjuvant chemotherapy for colorectal cancer in Japan [15–17]. The clinical data used in these studies were derived from international phase 3 trials, but not based on clinical practice. The cost of a drug or a test was calculated by multiplying the pre-determined numbers of drug doses or tests by their respective unit prices. These methods have the advantage that cost calculation is straightforward and simple. However, the costs related to adjuvant chemotherapy thus obtained might differ from those obtained by using patient data in the real world, because patients' backgrounds are different between international phase 3 trials and clinical practice. In clinical practice, subpopulations of patients with advanced age, comorbidities, organ dysfunctions, or lower performance status who generally cannot participate in international phase 3 trials are given adjuvant chemotherapy. Given that patients who receive adjuvant chemotherapy in clinical practice might receive a lower dose intensity and suffer more severe adverse events than patients enrolled in international phase 3 trials, considerable differences in the medical costs from the phase 3-based approach are plausible. When selecting regimens for patients in clinical practice, the use of the medical costs reflecting the actual situation is desirable.

Based on these backgrounds, we calculated the total costs of 6 regimens of adjuvant chemotherapy for colorectal cancer by using data from Japanese patients treated in clinical practice. Based on the costs thus obtained, we compared the cost-effectiveness of these regimens.

Methods

This was a retrospective study of all patients who received adjuvant chemotherapy for colorectal cancer in Showa University Hospital, Showa University Fujigaoka Hospital, Showa University Koto Toyosu Hospital, or Showa University Northern Yokohama Hospital between April 2012 and May 2015. The present study was approved by the Institutional Review Board of Showa University (approved number; Showa University Hospital, 1824; Showa University Fujigaoka Hospital, 2015023; Showa University Koto Toyosu Hospital, 15T7006; Showa University Northern Yokohama Hospital, 1505-07).

Selection of patients

All patients who received either CapeOX, mFOLFOX6, 5-FU/LV, UFT/LV, capecitabine, or S-1 at the aforementioned hospitals and completed all scheduled cycles were studied. Patients were required to undergo potentially curative resection for colorectal cancer before receiving adjuvant chemotherapy.

Chemotherapeutic regimens

CapeOX consisted of a 2-h intravenous infusion of oxaliplatin (130 mg/m^2) on day 1 and oral capecitabine (1000 mg/m^2) twice daily on days 1 to 14, repeated every 3 weeks for 8 cycles [8]. mFOLFOX6 consisted of LV (200 mg/m^2) given as a 2-h infusion and oxaliplatin (85 mg/m^2) given as a 2-h infusion, followed by a bolus infusion of 5-FU (400 mg/m^2) and a 46-h continuous infusion of 5-FU (2400 mg/m^2). This regimen was repeated every 2 weeks for 12 cycles [10]. Brand-name oxaliplatin was used in CapeOX and mFOLFOX6. 5-FU/LV comprised a 2-h infusion of LV (250 mg/m^2) and a bolus infusion of 5-FU (500 mg/m^2) given 1 h after starting the LV infusion, repeated weekly for 6 weeks followed by a 2-week rest [11]. This regimen was given for 3 cycles. UFT/LV consisted of oral UFT (300 mg/m^2) and LV (75 mg/patient) given 3 times daily on days 1 to 28 followed by a 7-day rest, repeated for 5 cycles [12]. Capecitabine was given orally in a dose of 1250 mg/m^2 twice daily on days 1 to 14, followed by a 7-day rest, repeated for 8 cycles [13]. S-1 was administered orally twice daily for 28 consecutive days, followed by a 2-week rest. S-1 was given in a fixed dose based on the patient's BSA according to the dose recommendations of the manufacturer's package insert in Japan. The dose was 80 mg/day for patients with a BSA of less than 1.25 m^2, 100 mg/day for those with a BSA of 1.25 to 1.5 m^2, and 120 mg/day for those with a BSA of more than 1.5 m^2. This regimen was given for 4 cycles [14].

Data collection

Patient background data, such as age and disease stage, as well as data during adjuvant chemotherapy, including laboratory tests, prescribed drugs, and adverse events, were collected from the patients' medical records.

Cost data related to adjuvant chemotherapy were extracted from medical fee receipt data. Costs for outpatient visits, laboratory tests, imaging tests for tumor diagnosis, and prescription fees for administered drugs were collected. The cost of each administered drug was calculated by multiplying the drug dose prescribed by its unit price according to the Japanese National Health Insurance fee-for-service system in 2014. The summation of these costs was defined as total cost. Since all hospitals in Showa University have adopted the diagnosis procedure combination (DPC) system [18], hospitalization costs were constant regardless of the number of drugs administered and laboratory tests performed. When the total hospitalization costs calculated by the DPC included the cost of drugs related to adjuvant chemotherapy, the drug costs were calculated by the method described above (the drug dose prescribed x its unit price), and the hospitalization cost was calculated by subtracting the cost of chemotherapy-related drugs from the hospitalization cost according to the DPC. This analysis was performed from the perspective of the health care payer. We described the unit of all costs by Japanese yen and US dollars, assuming that 1 US dollar was equivalent to 100 Japanese yen.

Cost-minimization analyses

Cost-minimization analysis is one of methods to evaluate cost-effectiveness of therapeutic options [19], in which relative costs of therapeutic options showing equivalent outcomes of interventions are simply compared. We performed cost-minimization analyses for the oxaliplatin-containing regimens (CapeOX and mFOLFOX6) and the oxaliplatin non-containing regimens (5-FU/LV, UFT/LV, capecitabine, and S-1) because of the following reasons:

1) Because there was no direct comparison between CapeOX and mFOLFOX6, we compared the effectiveness of these regimens based on the following considerations. As demonstrated by 2 international phase 3 trials, 16968 [8] and MOSAIC [9], the effectiveness of CapeOX and FOLFOX4 was significantly superior to that of 5-FU/LV and LV5FU2, respectively (Table 1 and Fig. 1a)). Because the effectiveness of LV5FU2 and 5-FU/LV [20, 21] and that of FOLFOX4 and mFOLFOX6 were comparable [10] (Table 1), the 3-year disease-free survival (DFS) rates of both CapeOX and mFOLFOX6 were comparable and approximately 5 % higher than that of 5-FU/LV. 2) Two international phase 3 trials, NSABP C-06 [12] and X-ACT [13] (Table 1), showed that UFT/LV and capecitabine were noninferior to 5-FU/LV in terms of 5-year overall survival (OS). In addition, the ACTS-CC international phase 3 trial demonstrated that S-1 was noninferior to UFT/LV with respect to the 3-year DFS rate [14] (Table 1 and Fig. 1a)). On the basis of these results, we assumed that the effectiveness of these 3 regimens was comparable and nearly equivalent to the effectiveness of 5-FU/LV.

Statistical analyses

Differences in quantitative variables, including cost data, were tested using the nonparametric Wilcoxon rank-sum test. Differences in qualitative variables were tested using the χ^2 test. Two-tailed P values of less than 0.05 were considered to indicate statistical significance. All analyses were carried out with the use of JMP version 12.0 software (SAS Institute, Cary, NC).

Results

Patient characteristics

From April 2012 through May 2015, a total of 154 patients with colorectal cancer received adjuvant chemotherapy in hospitals affiliated with Showa University. Fifty-seven patients were treated with CapeOX, 10 with

Table 1 Phase 3 trials of adjuvant chemotherapy for colorectal cancer

Trials	Race	Regimens	Primary endpoint	Result of the trials	Conclusion of the trials	Reference
16968	Whites	5-FU/LV vs. CapeOX	3-Year DFS rate	66.5 vs. 70.9 %	Superiority of CapeOX to 5-FU/LV	[8]
MOSAIC	Whites	LV5FU2 vs. FOLFOX4	3-Year DFS rate	65.3 vs. 72.2 %	Superiority of FOLFOX4 to LV5FU2	[9]
INT 0089	Whites	5-FU/LV (RPMI) vs. 5-FU/LV (Mayo)	5-Year OS rate	66.0 vs. 66.0 %	Non-inferiority of 5-FU/LV (RPMI) to 5-FU/LV (Mayo)	[20]
GERCOR C96.1	Whites	5-FU/LV (Mayo) vs. LV5FU2	6-Year DFS rate	65.0 vs. 66.0 %	Non-inferiority of 5-FU/LV (Mayo) to LV5FU2	[21]
	Japanese	FOLFOX4 vs. mFOLFOX6	Response rate	53.7 vs. 46.6 %	Non-inferiority of mFOLFOX6 to FOLFOX4	[10][a]
NSABP C-06	Whites	5-FU/LV vs. UFT/LV	5-Year OS rate	71.5 vs. 69.6 %	Non-inferiority of UFT/LV to 5-FU/LV	[12]
X-ACT	Whites	5-FU/LV vs. capecitabine	3-Year DFS rate	60.6 vs. 64.2 %	Non-inferiority of capecitabine to 5-FU/LV	[13]
ACTS-CC	Japanese	UFT/LV vs. S-1	3-Year DFS rate	72.5 vs. 75.5 %	Non-inferiority of S-1 to UFT/LV	[14]

RPMI Roswell Park Memorial Institute regimen
[a]Phase 2 trial

mFOLFOX6, 38 with UFT/LV, 20 with capecitabine, and 29 with S-1 (Table 2). No patient was given 5-FU/LV during the study period. The distributions of gender, age, site of cancer, and performance status were similar among the 5 regimens. The stage of cancer significantly differed among these regimens ($P < 0.001$). Ratios of patients with stage III in CapeOX and mFOLFOX6 were higher than those in UFT/LV, capecitabine, and S-1.

Cost analyses

Total costs calculated for each regimen are shown in Fig. 1b). The costs of oxaliplatin-containing regimens were approximately 1,860,000 yen (18,600 dollars) for CapeOX and 1,970,000 yen (19,700 dollars) for mFOLFOX6. The total costs of oxaliplatin-containing regimens were significantly higher than those of oxaliplatin non-containing regimens ($P < 0.001$) (CapeOX vs. UFT/LV, $P < 0.001$; CapeOX vs. capecitabine, $P < 0.001$; CapeOX vs.

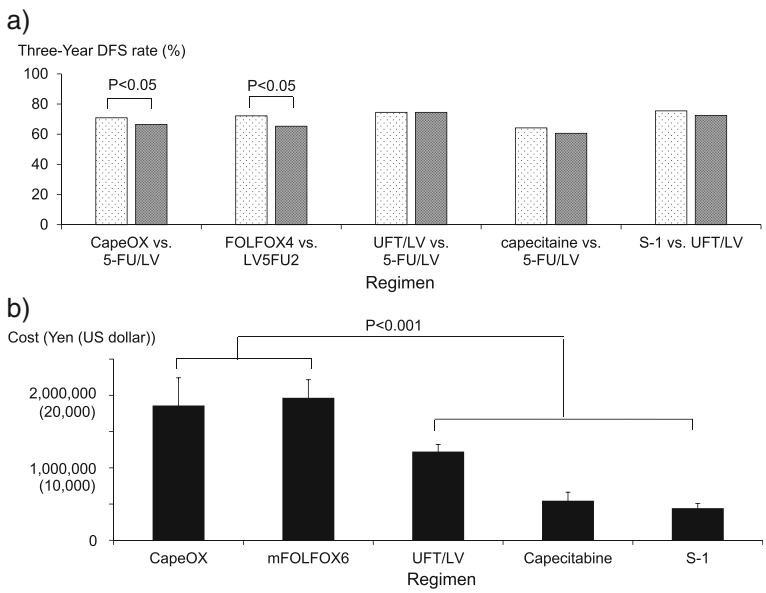

Fig. 1 Comparisons of **a**) effectiveness and **b**) total costs among adjuvant chemotherapy regimens for colorectal cancer. **a** Three-year DFS rates of CapeOX and FOLFOX4 were superior to that of 5-FU containing regimens [8, 9], whereas those of UFT/LV and capecitabine showed non-inferiority to 5-FU containing regimens [12, 13] (see Methods session). S-1 was non-inferior to UFT/LV [14] (see Methods session). **b** The total costs included anticancer drug costs, hospitalization costs, laboratory and imaging test costs, prescription fees for administered drugs, supportive care drug costs, and other costs. The total costs of oxaliplatin-containing regimens were significantly higher than those of oxaliplatin non-containing regimens ($P < 0.001$). Mean ± standard deviation, $n = 57$ for CapeOX, $n = 10$ for mFOLFOX6, $n = 38$ for UFT/LV, $n = 20$ for capecitabine, $n = 29$ for S-1

Table 2 Patient characteristics

	CapeOX	mFOLFOX6	UFT/LV	Capecitabine	S-1	*P*
Gender†						
Male/female	32/25	5/5	20/18	10/10	18/11	0.909[a]
Age‡	65.0 (79-40)	55.5 (73-41)	67.0 (79-40)	60.0 (78-40)	63.0 (80-42)	0.309[b]
Tumor type						
Colon cancer/rectal cancer†	35/22	9/1	27/11	15/5	17/12	0.372[a]
Stage†						
Ⅰ / Ⅱ / Ⅲ	0/3/54	0/0/10	0/11/27	0/2/18	4/11/14	<0.001[a]
Performance status†						
0/1	57/0	10/0	35/3	18/2	29/0	0.0680[a]

†Number; ‡Median (range)
[a]χ^2 test; [b]Analysis of variance

S-1, $P < 0.001$; mFOLFOX6 vs. UFT/LV, $P < 0.001$; mFOLFOX6 vs. capecitabine, $P < 0.001$; mFOLFOX6 vs. S-1, $P < 0.001$) (Fig. 1b). The total costs of CapeOX and mFOLFOX6 did not differ significantly ($P = 0.374$).

Among the oxaliplatin non-containing regimens, the total cost of UFT/LV was significantly higher than that of capecitabine ($P < 0.001$). The cost of capecitabine was significantly higher than that of S-1 ($P = 0.003$).

Factors causing the higher costs of oxaliplatin-containing regimens

To address the causes of the higher total costs of oxaliplatin-containing regimens, the breakdown of the costs for each regimen was calculated (Fig. 2). The cost of oxaliplatin in CapeOX was about 1,150,000 yen (11,500 dollars), which was equivalent to approximately 60 % of the total cost. In the case of mFOLFOX6, the cost of oxaliplatin was about 900,000 yen (9000 dollars), which was equivalent to approximately 40 % of the total cost. The total cost of mFOLFOX6 also included hospitalization costs (400,000 yen [4000 dollars]), such as the fee required to prepare a central venous port for administration of 5-FU, LV, and oxaliplatin. Thus, the hospitalization costs required for mFOLFOX6 increased the total cost of this regimen to a level comparable to the cost of CapeOX. The costs of drugs for supportive care required to administer CapeOX and mFOLFOX6 were approximately equivalent to 10 % of the total costs. The breakdown of the costs of supportive care drugs is shown in Fig. 3. The costs of the drugs prescribed to treat peripheral sensory neuropathy, which is frequently associated with oxaliplatin-related chemotherapy, were approximately 7500 yen (75 dollars) for CapeOX and 4300 yen (43 dollars) for mFOLFOX6, which comprised

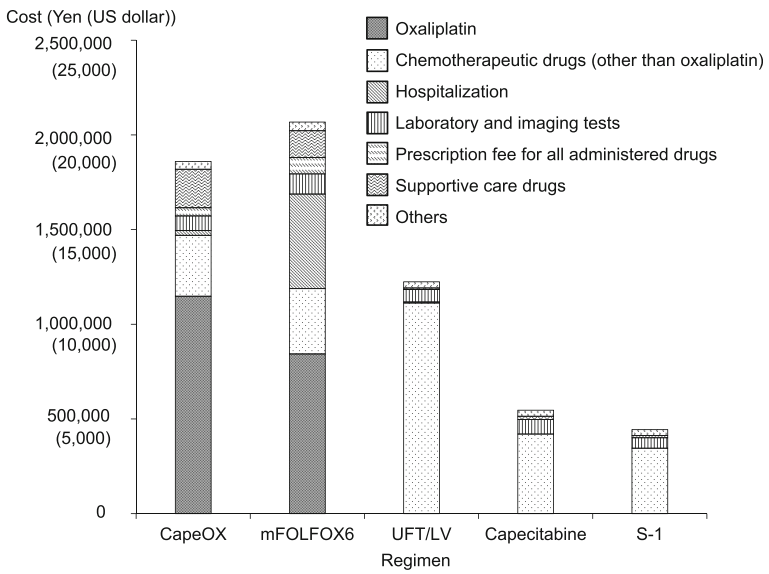

Fig. 2 Breakdown of the total costs for each regimen. Supportive care drugs included drugs used as premedication to prevent nausea and vomiting, drugs used to treat adverse events, and infusion solutions (see Fig. 3)

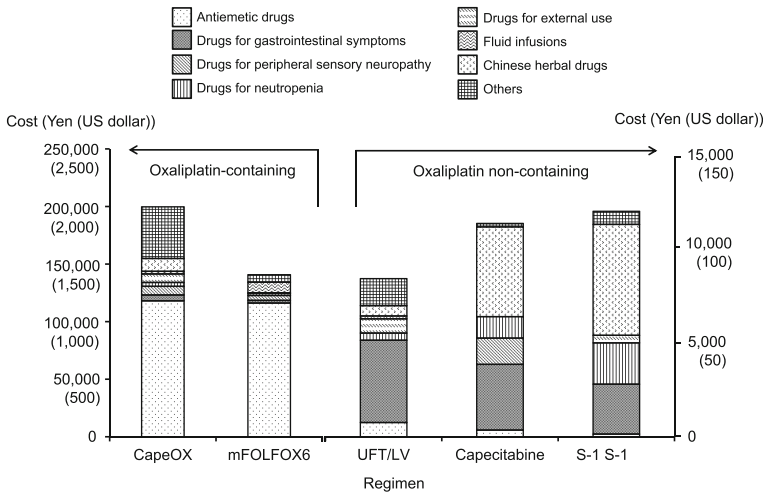

Fig. 3 Breakdown of the costs for drugs prescribed for supportive care in each regimen. Representative therapeutic drugs included in Others for CapeOX were ELENTAL®, KRESTIN®, levofloxacin, loxoprofen, and Posterisan® forte

only 0.4 and 0.2 % of the total costs of CapeOX and mFOLFOX6, respectively. We considered the possibility that a lower frequency of peripheral sensory neuropathy in the present study than in previous studies led to the lower cost of prescriptions for this adverse event. The frequency of peripheral sensory neuropathy of CapeOX in the present study was lower than the results of previous study (Table 3). However, in the case of mFOLFOX6, the frequency and grade of peripheral sensory neuropathy in the present study were not necessarily lower than those of previous studies (Table 3). On the other hand, the costs of antiemetics were approximately 118,000 yen (1180 dollars) for CapeOX and 116,000 yen (1160 dollars) for mFOLFOX6, accounting for about 6 % of the total costs. Antiemetics such as aprepitant, azasetron, domperidone, granisetron, metoclopramide, ondansetron, palonosetron, prochlorperazine and ramosetron were prescribed in CapeOX and mFOLFOX6 regimens. The parentages of patients who used palonosetron and aprepitant were 100 and 26 % in CapeOX, and 60 and 40 % in mFOLFOX6, respectively.

Table 3 Comparison of the frequency of peripheral sensory neuropathy between present study and phase 3 trials

Regimen	Grade	Present study	Phase 3 trials
CapeOX	All Grade	54.4 %	78.0 %[a]
	≥ Grade 3	1.80 %	11.0 %[a]
mFOLFOX6	All Grade	90.0 %	92.0 %[b]
	≥ Grade 3	40.0 %	12.5 %[b]

Grade of neuropathy was evaluated according to the Common Terminology Criteria for Adverse Events version 3.0.
[a]Data from reference [8]; [b]Result of FOLFOX4 [9]. Effectiveness and safety of mFOLFOX6 were comparable to those of FOLFOX4 [10].

Cost-minimization analyses

Because the effectiveness (Methods session and Fig. 1a)) and the total costs (Fig. 1b)) of CapeOX and mFOLFOX6 were comparable, the cost-effectiveness of these regimens was judged to be similar (Table 4). As described in the Methods session and Fig. 1a), the effectiveness of the oxaliplatin non-containing regimens was comparable. Therefore, on the basis of the total costs of these regimens (Fig. 1b)), the cost-effectiveness of S-1 was superior to that of UFT/LV, and the cost-effectiveness of capecitabine was superior to that of UFT/LV, which were caused by the high cost of LV.

Discussion

The present study compared the cost effectiveness of 5 regimens of adjuvant chemotherapy given to patients with colorectal cancer. The total costs were calculated with the use of clinical and cost data obtained from Japanese patients who received each regimen of adjuvant chemotherapy in clinical practice. This is in contrast to most previous studies assessing the costs of adjuvant chemotherapy for colorectal cancer in Japan, which based the costs of treatment on clinical data obtained from large phase 3 clinical trials [15–17].

To date, three studies of cost-effectiveness employing clinical data from phase 3 clinical trials have been performed: Hisashige et al. [15] analyzed the cost-effectiveness of UFT by comparing clinical and cost data between patients who received or did not receive UFT in the NSAS CC trial [22]. In other Japanese studies, the cost-effectiveness of 5-FU/LV and capecitabine [16] was evaluated with the use of clinical data from X-ACT trial [13], and that of 5-FU/LV and FOLFOX4 [17] was evaluated with the use of data from the

Table 4 Cost-minimization analyses

Regimen	Comparison of cost	Comparison of effectiveness	Cost-minimization analyses
CapeOX vs. mFOLFOX6	Comparable	Comparable	Comparable
UFT/LV vs. S-1	Higher in UFT/LV than S-1	Comparable	S-1 superior to UFT/LV
UFT/LV vs. capecitabine	Higher in UFT/LV than capecitabine	Comparable	Capecitabine superior to UFT/LV

MOSAIC trial [9]. We compared the costs required for the following 3 categories between the present study and previous studies based on large international phase 3 trials: 1) anticancer drugs, 2) drugs used for supportive care, and 3) laboratory tests. 1) The previously estimated cost of 1 year of treatment with UFT (about 393,700 yen [3937 dollars]) [15] was generally similar to the cost calculated by us (i.e., about 360,200 yen [3602 dollars], equivalent to twice the cost of 6 months' treatment with UFT in our study). However, the cost of capecitabine calculated in a previous study (540,000 yen [5400 dollars]) [16] was higher than that estimated by us (about 420,500 yen [4205 dollars]). The reason for the higher cost of capecitabine in the previous study is considered to be the difference in relative dose intensity (RDI) of capecitabine between the two studies. The previous study used a theoretical RDI of 100.0 %, whereas our study used the clinically observed RDI of 75.4 %. The cost of capecitabine estimated by Shiroiwa et al. [16] would have been about 407,200 yen (4072 dollars) if an RDI of 75.4 % had been adopted, which is nearly comparable to our estimated cost. 2) The costs of agents prescribed for supportive care in previous studies of UFT and capecitabine [15, 16] were about 300 yen (3 dollars) and 7000 yen (70 dollars), respectively, while those in the present study were about 8400 yen (84 dollars) for UFT/LV and about 17,500 yen (175 dollars) for capecitabine, demonstrating clearly higher costs for supportive care in our study. The primary reason first considered for the higher supportive care costs in our study was a higher incidence of adverse events in the present study than in previous studies. However, the incidence of bilirubin increase in the NSAS CC trial was 60.0 % [22], as compared with 10.5 % in the present study. The incidence of hand-foot syndrome associated with capecitabine regimens was 60.0 % in the X-ACT trial [13] and 30.0 % in our study. Thus, the incidences of adverse events were not necessarily higher in our study as compared with previous phase 3 trials. As shown in Fig. 3, patients given UFT/LV were mainly prescribed drugs to manage gastrointestinal symptoms, such as proton pump inhibitors and histamine-2 blockers. In patients who received capecitabine, Chinese herbal drugs such as Juzentaihoto and Hochuekkito were predominantly prescribed. The costs of these drugs might have contributed to the higher costs for supportive care drugs in our study. 3) The estimated cost of laboratory tests for UFT regimens in a previous study (about 180,100 yen [1801 dollars]) [15] was approximately 3 times higher than that calculated in our practical study (about 65,500 yen [655 dollars]). On the other hand, the laboratory test costs in patients who received FOLFOX4 regimens in a previously reported study (76,800 yen [768 dollars]) [17] was lower than that in our present study (about 106,500 yen [1065 dollars]). These findings indicate that the costs of 1) anticancer drugs, 2) drugs prescribed for supportive care, and 3) laboratory tests calculated on the basis of clinical data from phase 3 trials differ from those calculated on the basis of data from actual clinical practice. Because the costs calculated from patient data in clinical practice would precisely represent the actual situation, cost-effectiveness data thus obtained can be used for regimen selection.

In Japan, a system of the public health insurance for the entire nation has been adopted. Patients have to pay for medical costs according to their age and income. The cost borne by the patient ranges from 10.0 to 30.0 % of total medical costs. In addition, the patient's financial burden is maintained below specified limits under the high-cost medical care benefit system. The specified limits are determined by the patient's income. If this system is applied, the costs for adjuvant chemotherapy that would be actually paid by the patient could be lower. Data from Showa University Hospital indicate when the public health insurance was applied to a patient, the cost of oxaliplatin-containing regimens was approximately 550,000 yen (5500 dollars), and that of UFT/LV was 263,000 yen (2630 dollars). The difference was 287,000 yen (2870 dollars). However, when the specified limits were applied, the cost of oxaliplatin-containing regimens was approximately 448,000 yen (4480 dollars), and that of UFT/LV was approximately 262,000 yen (2620 dollars), leading to a difference of 186,000 yen (1860 dollars). Thus, the specified limits might lower the medical costs of oxaliplatin-containing regimens to a greater extent than the costs of UFT/LV, although the specified limits system is not necessarily applicable to all patients because application of this system depends on the income of each patient. It is plausible that patients who derive an economic benefit tend to select oxaliplatin-containing regimens over other regimens. The medical costs are supplemented with taxes from Japanese citizens. To maintain the patient's financial

burden below specified limits, Japanese citizens have to pay higher taxes. This is an important issue to be discussed by health care payer.

An analysis of patient characteristics showed the stage of cancer significantly differed among the regimens (Table 2). However, the total costs of the CapeOX, UFT/LV, and S-1 regimens did not differ significantly between stage II and stage III. ($P = 0.668$, $P = 0.711$, and $P = 0.743$, respectively). Therefore, there might be no relation between the stage of cancer and total costs.

Our study had several limitations. 1) Direct comparisons of effectiveness are not available for some of the regimens. For example, no phase 3 trials have compared effectiveness between CapeOX and mFOLFOX6 or between UFT/LV and capecitabine. We therefore compared the effectiveness of CapeOX and mFOLFOX6 by the indirect comparisons of independent phase 3 trials (see Methods session). 2) The phase 3 trials that we referred to when comparing the effectiveness of the regimens were not necessarily performed in Japan. Theoretically, the effectiveness of the regimens should have been compared on the basis of data from phase 3 trials performed in Japan; however, we used data from clinical trials performed in whites because suitable Japanese trials were unavailable. It is well known that the survival advantage of a specific regimen in Japanese trials is generally better than that in clinical trials performed in other countries. For example, trials conducted in only Japanese patients tend to have better 3-year DFS rates and 5-year OS rates than those performed in whites [23]. One of the reasons is thought to be the better operation quality in Japan. For example, the extent of lymph-node resection during cancer surgery is greater in Japan than in other countries. 3) Some of the phase 3 trials that we referred to when comparing the effectiveness of the regimens included patients with stage III, but others included those with stage II and stage III. The effectiveness of these phase 3 trials might be affected by the difference in stage of patients enrolled. Taken together, our comparisons of the effectiveness of different regimens might have been biased by such factors.

Conclusions

Costs of oxaliplatin-containing regimens were significantly higher than those of oxaliplatin non-containing regimens, but the cost-effectiveness of the oxaliplatin-containing regimens CapeOX and mFOLFOX6 were judged to be comparable. Among the oxaliplatin non-containing regimens, the cost-effectiveness of S-1 and capecitabine were superior to that of UFT/LV. Costs based on clinical data from phase 3 trials were shown to differ from costs based on data from actual clinical practice. Because costs based on patient data in clinical practice would more precisely represent the actual situation, the resulting cost-effectiveness data can be used for regimen selection.

Abbreviations

5-FU: 5-Fluorouracil; 5-FU/LV: 5-FU and LV; BSA: Body surface area; CapeOX: Capecitabine and oxaliplatin; DFS: Disease-free survival; DPC: Diagnosis procedure combination; FOLFOX4 or FOLFOX6: 5-FU, LV, and oxaliplatin; LV: ℓ-Leucovorin; mFOLFOX6: Modified FOLFOX6; OS: Overall survival; RDI: Relative dose intensity; S-1: Tegafur, gimeracil, and oteracil; UFT: Tegafur and uracil; UFT/LV: UFT, and oral LV

Acknowledgements

The authors thank the staffs of the patient billing offices of Showa University Hospital, Showa University Fujigaoka Hospital, Showa University Koto Toyosu Hospital, and Showa University Northern Yokohama Hospital for providing the patient billing data.

Funding

This study was supported by a research grant in Department of Healthcare and Regulatory Sciences, School of Pharmacy, Showa University.

Availability of data and materials

All data generated or analyzed during this study are included in this published article.

Authors' contributions

KT, KF, and YS contributed to the study conception and design. KT, WI, KS, and TS were involved in data acquisition. KT, and KF were involved in data analyses, interpretation, and manuscript writing. YK, HI, ITT, DK, SI, and YS revised the drafted manuscript critically. All authors have read and approved the final manuscript.

Competing interests

The authors declare that they have no competing interests.

Consent for publication

Not applicable.

Ethics approval and consent to participate

The present study was approved by the Institutional Review Board of Showa University.

Author details

[1]Department of Healthcare and Regulatory Sciences, School of Pharmacy, Showa University, 1-5-8, Hatanodai, Shinagawa-ku, Tokyo 142-8555, Japan. [2]Institute of Molecular Oncology, Showa University, 1-5-8, Hatanodai, Shinagawa-ku, Tokyo 142-8555, Japan. [3]Division of Medical Oncology, Department of Internal Medicine, School of Medicine, Showa University, 1-5-8 Hatanodai, Shinagawa-ku, Tokyo 142-8555, Japan. [4]Division of Medical Oncology, Department of Internal Medicine, Showa University Fujigaoka Hospital, 1-30 Fujigaoka, Aoba-ku, Yokohama, Kanagawa 227-8501, Japan. [5]Department of Internal Medicine, Showa University Koto Toyosu Hospital, 5-1-38 Toyosu, Koto-ku, Tokyo 135-8577, Japan. [6]Department of Internal Medicine, Showa University Yokohama Northern Hospital, 35-1 Chigasakichuo, Tsuzuki-ku, Yokohama, Kanagawa 224-8503, Japan.

Received: 14 September 2016 Accepted: 2 November 2016
Published online: 09 November 2016

References

1. Meropol NJ, Schulman KA. Cost of cancer care: issues and implications. J Clin Oncol. 2007;25:180–6.
2. Fenn KM, Evans SB, McCorkle R, DiGiovanna MP, Pusztai L, Sanft T, et al. Impact of financial burden of cancer on survivors' quality of life. J Oncol Pract. 2014;10:332–8.
3. Ramsey S, Blough D, Kirchhoff A, Kreizenbeck K, Fedorenko C, Snell K, et al. Washington State cancer patients found to be at greater risk for bankruptcy than people without a cancer diagnosis. Health Aff (Millwood). 2011;32:1143–52.
4. National health insurance drug price standard [in Japanese]. Tokyo: Jiho, 2014
5. Saltz LB. The value of considering cost, and the cost of not considering value. J Clin Oncol. 2016;34:659–60.
6. ASCO value framework: fact sheet. 2014. http://www.canceradvocacy.org/wp-content/uploads/2014/10/ASCO-Value-Framework-Fact-Sheet.pdf. Accessed 13 Sep 2016

7. Watanabe T, Itabashi M, Shimada Y, Tanaka S, Ito Y, Ajioka Y, et al. Japanese Society for Cancer of the Colon and Rectum. Japanese Society for Cancer of the Colon and Rectum (JSCCR) Guidelines 2014 for treatment of colorectal cancer. Int J Clin Oncol. 2015;20:207–39.
8. Haller DG, Tabernero J, Maroun J, de Braud F, Price T, Van Cutsem E, et al. Capecitabine plus oxaliplatin compared with fluorouracil and folinic acid as adjuvant therapy for stage III colon cancer. J Clin Oncol. 2011;29:1465–71.
9. André T, Boni C, Navarro M, Tabernero J, Hickish T, Topham C, et al. Improved overall survival with oxaliplatin, fluorouracil, and leucovorin as adjuvant treatment in stage II or III colon cancer in the MOSAIC trial. J Clin Oncol. 2009;27:3109–16.
10. Nagata N, Kondo K, Kato T, Shibata Y, Okuyama Y, Ikenaga M, et al. Multicenter Phase II study of FOLFOX for Metastatic Colorectal Cancer (mCRC) in Japan; SWIFT-1 and 2 study. Hepatogastroenterology. 2009;56:1346–53.
11. Wolmark N, Rockette H, Mamounas E, Jones J, Wieand S, Wickerham DL, et al. Clinical trial to assess the relative efficacy of fluorouracil and leucovorin, fluorouracil and levamisole, and fluorouracil, leucovorin, and levamisole in patients with Dukes' B and C carcinoma of the colon: results from National Surgical Adjuvant Breast and Bowel Project C-04. J Clin Oncol. 1999;17:3553–9.
12. Lembersky BC, Wieand HS, Petrelli NJ, O'Connell MJ, Colangelo LH, Smith RE, et al. Oral uracil and tegafur plus leucovorin compared with intravenous fluorouracil and leucovorin in stage II and III carcinoma of the colon: results from National Surgical Adjuvant Breast and Bowel Project Protocol C-06. J Clin Oncol. 2006;24:2059–64.
13. Twelves C, Wong A, Nowacki MP, Abt M, Burris 3rd H, Carrato A, et al. Capecitabine as adjuvant treatment for stage III colon cancer. N Engl J Med. 2005;352:2696–704.
14. Mochizuki I, Takiuchi H, Ikejiri K, Nakamoto Y, Kinugasa Y, Takagane A, et al. Safety of UFT/LV and S-1 as adjuvant therapy for stage III colon cancer in phase III trial: ACTS-CC trial. Br J Cancer. 2012;106:1268–73.
15. Hisashige A, Yoshida S, Kodaira S. Cost-effectiveness of adjuvant chemotherapy with uracil-tegafur for curatively resected stage III rectal cancer. Br J Cancer. 2008;99:1232–8.
16. Shiroiwa T, Fukuda T, Shimozuma K. Cost-effectiveness analysis of capecitabine compared with bolus 5-fluorouracil/l-leucovorin for the adjuvant treatment of colon cancer in Japan. Pharmacoeconomics. 2009;27:597–608.
17. Shiroiwa T, Takeuchi T, Fukuda T, Shimozuma K, Ohashi Y. Cost-effectiveness of adjuvant FOLFOX therapy for stage III colon cancer in Japan based on the MOSAIC trial. Value Health. 2012;15:255–60.
18. Ministry of Health, Labour and Welfare Central Social Insurance Medical Council. http://www.mhlw.go.jp/stf/shingi/shingi-chuo.html?tid=128164 Accessed 13 Sep 2016
19. Husereau D, Drummond M, Petrou S, Carswell C, Moher D, Greenberg D, et al. Consolidated Health Economic Evaluation Reporting Standards (CHEERS) statement. BJOG. 2013;120:765–70.
20. Haller DG, Catalano PJ, Macdonald JS, O'Rourke MA, Frontiera MS, Jackson DV, et al. Phase III study of fluorouracil, leucovorin, and levamisole in high-risk stage II and III colon cancer: final report of Intergroup 0089. J Clin Oncol. 2005;23:8671–8.
21. Baumgaertner I, Quinaux E, Khalil A, Louvet C, Buyse M, de Gramont A, et al. Comparison of the levogyre and dextro-levogyre forms of leucovorin in a phase III trial of bimonthly LV5FU2 versus monthly 5-fluorouracil and high-dose leucovorin for patients with stage II and III colon cancer (GERCOR C96.1). Clin Colorectal Cancer. 2010;9:E5–E10.
22. Akasu T, Moriya Y, Ohashi Y, Yoshida S, Shirao K, Kodaira S. Adjuvant chemotherapy with uracil-tegafur for pathological stage III rectal cancer after mesorectal excision with selective lateral pelvic lymphadenectomy: a multicenter randomized controlled trial. Jpn J Clin Oncol. 2006;36:237–44.
23. West NP, Kobayashi H, Takahashi K, Perrakis A, Weber K, Hohenberger W, et al. Understanding optimal colonic cancer surgery: comparison of Japanese D3 resection and European complete mesocolic excision with central vascular ligation. J Clin Oncol. 2012;30:1763–9.

A comparison of four methods for detecting *KRAS* mutations in formalin-fixed specimens from metastatic colorectal cancer patients

MOTOTSUGU MATSUNAGA[1], TOSHIKADO KANETA[2], KEISUKE MIWA[1], WATARU ICHIKAWA[2], KEN-ICHI FUJITA[2], FUMIO NAGASHIMA[3], JUNJI FURUSE[3], MASAYOSHI KAGE[4], YOSHITO AKAGI[5] and YASUTSUNA SASAKI[2]

[1]Multidisciplinary Treatment Cancer Center, Kurume University Hospital, Kurume, Fukuoka 830-0011; [2]Division of Medical Oncology, Department of Internal Medicine, Showa University Hospital, Hatanodai, Shinagawa, Tokyo 142-8666; [3]Department of Medical Oncology, Kyorin University School of Medicine, Hinkawa, Mitaka, Tokyo 181-8611; Departments of [4]Diagnostic Pathology and [5]Surgery, Kurume University Hospital, Kurume, Fukuoka 830-0011, Japan

Received April 2, 2015; Accepted April 29, 2016

DOI: 10.3892/ol.2016.4576

Abstract. There is currently no standard method for the detection of Kirsten rat sarcoma viral oncogene homolog (*KRAS*) mutation status in colorectal tumors. In the present study, we compared the *KRAS* mutation detection ability of four methods: direct sequencing, Scorpion-ARMS assaying, pyrosequencing and multi-analyte profiling (Luminex xMAP). We evaluated 73 cases of metastatic colorectal cancer (mCRC) resistant to irinotecan, oxaliplatin and fluoropyrimidine that were enrolled in an all-case study of cetuximab. The *KRAS* mutation detection capacity of the four analytical methods was compared using DNA samples extracted from tumor tissue, and the detection success rate and concordance of the detection results were evaluated. *KRAS* mutations were detected by direct sequencing, Scorpion-ARMS assays, pyrosequencing and Luminex xMAP at success rates of 93.2%, 97.3%, 95.9% and 94.5%, respectively. The concordance rates of the detection results by Scorpion-ARMS, pyrosequencing and Luminex xMAP with those of direct sequencing were 0.897, 0.923 and 0.900 (κ statistics), respectively. The direct sequencing method could not determine *KRAS* mutation status in five DNA samples. Of these, Scorpion-ARMS, pyrosequencing and Luminex xMAP successfully detected three, two and one *KRAS* mutation statuses, respectively. Three cases demonstrated inconsistent results, whereby Luminex xMAP detected mutated *KRAS* in two samples while wild-type *KRAS* was detected by the other methods. In the remaining case, direct sequencing detected wild-type *KRAS,* which was identified as mutated *KRAS* by the other methods. In conclusion, we confirmed that Scorpion-ARMS, pyrosequencing and Luminex xMAP were equally reliable in detecting *KRAS* mutation status in mCRC. However, in rare cases, the *KRAS* status was differentially diagnosed using these methods.

Correspondence to: Dr Keisuke Miwa, Multidisciplinary Treatment Cancer Center, Kurume University Hospital, 67 Asahi-Machi, Kurume, Fukuoka 830-0011, Japan
E-mail: miwakeisuke@gmail.com

Key words: colorectal cancer, *KRAS* mutation, direct sequencing, Scorpion-ARMS, pyrosequencing, Luminex xMAP

Introduction

Cetuximab is a monoclonal antibody that targets the extracellular domain of the epidermal growth factor receptor (EGFR), and is an essential treatment option in patients with metastatic colorectal cancer (mCRC). Numerous researchers have reported that anti-EGFR agents have extremely poor antitumor effects in chemotherapy for mCRC with mutated Kirsten rat sarcoma viral oncogene homolog (*KRAS*) (1-5), providing clear evidence that administration of anti-EGFR agents is recommended only for mCRC with wild-type *KRAS*. However, although a number of methods may be used for *KRAS* mutation testing with varying sensitivity and specificity levels, no standard method has yet been recommended for clinical practice. Therefore, the use of these detection assays is somewhat erratic worldwide.

In Japan, cetuximab was administered for ~18 months following its launch in September 2009 without determination of *KRAS* mutation status, since the above-mentioned analytical methods were not covered by health insurance. The direct sequencing method (6) was covered in April 2010, followed by multi-analyte profiling (Luminex xMAP) technology (7) in March 2011 and Scorpion-ARMS assays (8) in May 2011. Pyrosequencing analysis methods (9) have also been evaluated and are already on the market in other countries. All four methods use the polymerase chain reaction (PCR) method but have different assay techniques. A number of sequencing- and PCR-based methods for detecting *KRAS* mutations

are currently in clinical use, although it is not clear which technique offers the best performance in terms of sensitivity, specificity, reproducibility and success rates (10). The aim of this retrospective study was to compare the analytical performances of the four methods (direct sequencing, Scorpion-ARMS assaying, pyrosequencing and Luminex xMAP) using extracted DNA from formalin-fixed paraffin-embedded (FFPE) tissues, and to clarify whether there are cases in which mutant *KRAS* status results differ among the examined methods.

Materials and methods

Patients. The eligibility criteria of patients enrolled in this study were as follows: Cases aged 20 years or over and less than 80 years who had been enrolled in an all-case study of cetuximab conducted between September 2008 and January 2010 following the Good Post-marketing Study Practice (GPSP) of the Japanese Pharmaceutical Affairs Act; diagnosis of mCRC with histological findings of primary colorectal adenocarcinoma; Eastern Cooperative Oncology Group performance status (ECOG PS) of grade 0-2; clinically unresponsive or intolerant to irinotecan, oxaliplatin and fluoropyrimidine; treated with cetuximab alone or cetuximab plus irinotecan; appropriate and usable FFPE sections available, consisting of ten undyed 10-μm-thick sections and two 4-μm-thick sections for hematoxylin and eosin (HE) staining. Cetuximab was administered to all subjects once a week according to the package insert. The initial dosage was 400 mg/m^2 and other dosages were 250 mg/m^2.

Four institutions in Japan participated in this study: Saitama Medical University International Medical Center (Hidaka, Saitama, Japan), the National Defense Medical College Hospital (Tokorozawa, Saitama, Japan), Kyorin University Hospital (Mitaka, Tokyo, Japan) and Showa University Hospital (Shinagawa, Tokyo, Japan). The protocol was reviewed and approved by the independent ethics committee or the institutional review board of each participating institution, and the study was conducted according to the Declaration of Helsinki alongside local ethical and legal requirements. The study was conducted between 1 July 2010 and 30 September 2011. Specific study termination criteria were not determined in advance, but a simple guideline was implemented to immediately halt the study should an ethically serious problem occur during the course of the study, such as in the event of a subject's personal information being compromised.

Pathological assessment and DNA extraction. All FFPE tissue blocks from the primary CRC site were prepared at each institution. First, 10 undyed 10-μm-thick serial sections were prepared from each FFPE tissue block, and two 4-μm-thick sections for HE staining were removed from either side of each prepared 10-μm-thick section. Then, microscopic examination was conducted at the Department of Diagnostic Pathology, Saitama Medical University International Medical Center, Japan. Pathologists marked areas where tumor tissue accounted for more than 50% of the prepared slides, and confirmed the results by observing tumor areas on two HE-stained sections sandwiching the marked slide between them. Following this, DNA extraction was performed after manual microdissection from five of the ten 10-μm-thick serial sections and without manual microdissection from the latter five, according to the manufacturer's instructions for DNA extraction using the QIAamp DNA FFPE tissue kit (Qiagen, Venlo, Netherlands). DNA concentrations were measured using a NanoDrop ND 1000 spectrophotometer (Thermo Fisher Scientific, Waltham, MA, USA).

Mutation testing methods. DNA extracted from serial sections by manual microdissection was used for direct sequencing. Based on the manufacturer's instructions, DNA extracted from serial sections by manual microdissection was used for Luminex xMAP, and DNA extracted without manual microdissection was used for Scorpion-ARMS assays and pyrosequencing. The four detection assays were conducted at the same institution under the same conditions. Direct sequencing for exon 2 of the *KRAS* gene was carried out using PCR and 2X bidirectional direct sequencing following previously described protocols (11,12). Tumor DNA for exon 3 was amplified using the following primers: forward, 5'-CACTGTAATAATCCA GACTGTG-3' and reverse, 5'-CCCACCTATAATGGTGAA TATC-3'. Sequencing reactions were performed in direct and reverse directions, and electropherograms were reviewed manually to detect any genetic alterations. All variants were confirmed by resequencing of independent PCR products. In the study, analyses were carried out using home-brew primers and the following *in vitro* research use only reagents: Expand High Fidelity PCR system (Roche Diagnostics, Basel, Switzerland), BigDye terminator Cycle Sequencing Ready Reaction (Life Technologies, Carlsbad, CA, USA) and BigDye XTerminator purification kit (Life Technologies). The other tests were performed according to each measurement manual. In this study, Scorpion-ARMS assays, pyrosequencing and Luminex xMAP were carried out using a TheraScreen kit (Qiagen), a *KRAS* Pyro kit (Qiagen) and a MEBGEN *KRAS*™ mutation detection kit (Medical and Biological Laboratories, Nagoya, Aichi, Japan) as *in vitro* diagnostic tests, respectively.

Statistical analyses. The significance of the concordance of mutation detection by the different methods for the two categories (wild type and mutated type) was assessed by κ statistics. We classified the κ values according to Landis and Koch (13): <0.00, poor; 0.00-0.20, slight; 0.21-0.40, fair; 0.41-0.60, moderate; 0.61-0.80, substantial; and 0.81-1.00, almost perfect.

Results

In this study, we recruited and analyzed 73 mCRC patients. All subjects had been enrolled in an all-case study of cetuximab, the results of which enabled us to calculate their progression-free survival (PFS) and overall survival (OS). Among these, 69 patients completed the study and could be followed up until mortality, while four cases dropped out. Of these 73 cases, 42 cases received cetuximab alone and 31 cases received cetuximab plus irinotecan. Patient characteristics are detailed in Table I. The objective response rate of cetuximab for all subjects was 15%. The median PFS and OS were 77 and 228 days, respectively. The median PFS of wild-type *KRAS* cases detected by direct sequencing was 112 days and that of

Table I. Characteristics of eligible patients.

Characteristic	No. of patients (n=73)
Age (range)	65 (39-80)
Gender	
Male	58 (79%)
Female	15 (21%)
ECOG performance status	
0	41 (56%)
1	29 (40%)
2	3 (4%)
No. of previous chemotherapy regimens	
2	40 (55%)
3	21 (29%)
≥4	12 (16%)
Objective response rate	
CR	0
PR	11 (15%)
SD	24 (33%)
PD	35 (48%)
NE	3 (4%)
Median progression-free survival (range), days	77 (8-682)
Median overall survival (range), days	228 (25-1058)

ECOG, Eastern Cooperative Oncology Group; CR, complete response; PR, partial response; SD, stable disease; PD, progression disease; NE, not evaluated.

mutated *KRAS* cases was 53 days [log-rank, P=0.001; hazard ratio (HR), 0.416; 95% confidence interval (CI), 0.244-0.718]. The median OS of wild-type *KRAS* cases detected by direct sequencing was 318 days and that of mutated *KRAS* cases was 196 days (log-rank, P=0.0149; HR, 0.523; 95% CI, 0.307-0.897).

The median concentrations of extracted DNA after and without manual microdissection were 119.5 ng/μl (range, 2.8-358.9 ng/μl) and 130.1 ng/μl (range, 2.1-500.4 ng/μl), respectively. The success rates of detection by direct sequencing, Scorpion-ARMS, pyrosequencing and Luminex xMAP were 93.2, 97.3, 95.9 and 94.5%, respectively. With respect to *KRAS* mutation, direct sequencing, Scorpion-ARMS, pyrosequencing and Luminex xMAP detected mutated *KRAS* in 28 (38.4%), 29 (39.7%), 29 (39.7%) and 31 (42.5%) subjects, respectively (Table II). All mutation sites in cases detected as mutated *KRAS* by the four methods were in complete accordance with each method.

Pairwise concordances between each method for *KRAS* status are shown in Table III. The concordance rates of direct sequencing with Scorpion-ARMS, pyrosequencing and Luminex xMAP were 0.897, 0.923 and 0.900 as the κ values, respectively. The κ value of Scorpion-ARMS with pyrosequencing and Luminex xMAP, and that of pyrosequencing with Luminex xMAP were sufficient to demonstrate good concordances.

The direct sequencing method could not detect *KRAS* mutations in five cases (Table IV). There was one case (case 3) in which *KRAS* mutation status was determined by all four methods. Notably, the remaining four cases were diagnosed as wild-type *KRAS* by all three methods. Scorpion-ARMS failed to detect two cases, pyrosequencing three and Luminex xMAP four. The cases that could not be detected by Scorpion-ARMS, pyrosequencing and Luminex xMAP were all included in the five cases that were undetectable by direct sequencing. Among those, Scorpion-ARMS, pyrosequencing and Luminex xMAP successfully detected three, two and one cases, respectively. All of these cases had wild-type *KRAS*. One case (case 2) was detected only by Scorpion-ARMS and had a PFS and OS of 383 days and 740 days, respectively, while another case (case 4) was detected only by Luminex xMAP, with a PFS and OS of 61 and 147 days, respectively.

There were three cases for which the *KRAS* mutation status was inconsistently detected by the different methods (Table V). In two of these three cases, only Luminex xMAP detected mutated *KRAS* (G12D for case 1 and G12S for case 2), whereas the other three methods detected wild-type *KRAS*. These two cases appeared to be clinically responsive to cetuximab therapy in terms of disease control and survival. The remaining case (case 3) with poor prognosis was diagnosed as mutated *KRAS* (G12C) by the other three methods, although direct sequencing revealed a wild-type *KRAS* status.

Discussion

Retrospective analyses of pivotal clinical trials for the anti-EGFR monoclonal antibodies cetuximab and panitumumab have revealed that patients with CRC-containing activating mutations in the downstream *KRAS* gene do not benefit from these therapies (14,15). The association between defined mutations and response to therapy provides a clear opportunity to increase response rates and reduce the likelihood of treating patients who are unlikely to respond to certain drugs, which is costly and unnecessarily exposes them to potential adverse effects. Therefore, mutant *KRAS* has been demonstrated to be a strong negative predictive biomarker to indicate whether a CRC patient is likely to respond to anti-EGFR treatment, and administration of cetuximab is recommended only for patients with a wild-type *KRAS* tumor. In addition, a previous study demonstrated that cetuximab is ineffective for tumors harboring any *RAS* mutations except in exon 2 of *KRAS* (16).

A number of sequencing- and PCR-based methods to detect *KRAS* mutations are currently in clinical use. At present, there are numerous ways of testing for *KRAS* mutations, and there have been comparative studies and analyses of the sensitivity of these assays in the clinical setting (16-19). However, it is not clear which technique offers the best performance in terms of sensitivity, specificity, reproducibility and success rates. We confirmed the high performance of more sensitive methods including Scorpion-ARMS, Luminex xMAP and pyrosequencing in analyzing *KRAS* mutation status in DNA extracted from FFPE tissues compared with the detection sensitivity of 20% by direct sequencing. Additionally, to our knowledge, this is the first study to report rare cases in which

Table II. *KRAS* mutation statuses detected by each analytical method (n=73).

Parameter	Direct sequencing	Scorpion-ARMS	Pyrosequencing	Luminex xMAP
Detected cases (%)	68 (93.2%)	71 (97.3%)	70 (95.9%)	69 (94.5%)
Wild-type *KRAS* (%)	40 (54.8%)	42 (57.5%)	41 (56.2%)	38 (52.1%)
Mutated *KRAS* (%)	28 (38.4%)	29 (39.7%)	29 (39.7%)	31 (42.5%)
Undetectable cases (%)	5 (6.8%)	2 (2.7%)	3 (4.1%)	4 (5.5%)

KRAS, Kirsten rat sarcoma viral oncogene homolog.

Table III. Pairwise concordance between methods of KRAS mutation detection.

Method	Scorpion-ARMS			Pyrosequencing			Luminex xMAP		
Direct sequencing	W	M	NE	W	M	NE	W	M	NE
W	39	1	0	39	1	0	37	3	0
M	0	28	0	0	28	0	0	28	0
NE	3	0	2	2	0	3	1	0	4
		κ=0.89672			κ=0.92347			κ=0.90004	
Scorpion-ARMS									
W				41	0	1	37	2	3
M				0	29	0	0	29	0
NE				0	0	2	1	0	1
					κ=0.97355			κ=0.84502	
Pyrosequencing									
W							37	2	2
M							0	29	0
NE							1	0	2
								κ=0.87238	

KRAS, Kirsten rat sarcoma viral oncogene homolog; W, wild-type *KRAS*; M, mutated *KRAS*; NE, not evaluated.

Table IV. Detection capability of each analytical method for undetectable cases.

Case	Direct sequencing	Scorpion-ARMS	Pyrosequencing	Luminex xMAP	DNA (ng/μl) without MD	DNA (ng/μl) with MD	ORR	PFS (days)	OS (days)
1	NE	Wild	Wild	NE	95.6	100.5	SD	83	157
2	NE	Wild	NE	NE	39.0	57.7	SD	383	740
3	NE	NE	NE	NE	26.6	56.2	PR	116	317
4	NE	NE	NE	Wild	2.1	4.3	SD	61	147
5	NE	Wild	Wild	NE	93.5	126.5	PD	17	95

NE, not evaluated; Wild, wild-type *KRAS*; ORR, objective response rate; PFS, progression-free survival; OS, overall survival; PR, partial response; SD, stable disease; PD, progression disease; MD, manual microdissection.

the status of *KRAS* was differentially diagnosed by the more sensitive methods.

All subjects in the study were enrolled in an all-case study of cetuximab following the GPSP of the Japanese Pharmaceutical Affairs Act, and the effects of cetuximab administration and prognoses of these patients were already described in specified studies, which enabled us to expect a small selection bias. Mutant *KRAS* is observed in ~35-45% of CRC (1,5,14,15,20-22), and codon 12 and 13 are two hotspots that account for ~95% of all mutation types (5,23,24); our results were within this range. Moreover, the results of *KRAS* analysis by direct sequencing demonstrated

Table V. Details of inconsistent results.

Case	Direct sequencing	Scorpion-ARMS	Pyro-sequencing	Luminex-xMAP	Mutation site	DNA (ng/μl) without MD	DNA (ng/μl) with MD	ORR	PFS (days)	OS (days)
1	Wild	Wild	Wild	Mutant	G12D	78.3	68.7	PR	287	344
2	Wild	Wild	Wild	Mutant	G12S	217.5	215.5	SD	108	208
3	Wild	Mutant[a]	Mutant[a]	Mutant[a]	G12C	138.7	182.5	PD	42	90

[a]All cases had *KRAS* G12C mutation. Wild, wild-type *KRAS*; mutant, mutated *KRAS*; ORR, objective response rate; PFS, progression-free survival; OS, overall survival; PR, partial response; SD, stable disease; PD, progression disease; MD, manual microdissection.

significant prolongation of PFS and OS in wild-type *KRAS* cases compared with mutated *KRAS* cases, consistent with the published data (4,25).

In this study, we evaluated the differences between four PCR-based analytical methods using the same DNA samples. The success rates in *KRAS* status detection ranged from 93.2% to 97.3% by the four methods (Table II) without statistical significance due to the small sample size. However, among the five cases in which the *KRAS* mutation was not detected by direct sequencing, the mutation status in four of these cases was detectable by the other more sensitive methods (Table IV). This might be simply explained by the differences in sensitivities to detect *KRAS* mutation status between direct sequencing and the other three methods. It has already been reported that direct sequencing has poor sensitivity for low levels of mutation (26). Thus, the direct sequencing method should not be applied to detect *KRAS* mutation status in clinical practice. The detection sensitivity by direct sequencing, Scorpion-ARMS, Pyrosequencing and Luminex xMAP is ~20%, 1%, 5-10% and 5-10%, respectively. Three cases were diagnosed as wild-type *KRAS* by Scorpion-ARMS among four cases in which the *KRAS* status could not be determined by Luminex xMAP. We were able to diagnose *KRAS* status by Scorpion-ARMS in one case among three in which *KRAS* status was not determined by pyrosequencing. These results may reflect the higher sensitivity in detecting *KRAS* mutation status in Scorpion-ARMS compared with pyrosequencing and Luminex xMAP.

Scorpion-ARMS is a real-time PCR-based assay that combines the amplified refractory mutation system (ARMS) with Scorpion probes (seven probes for seven different mutations in *KRAS*), eliminating the requirement for post-PCR confirmation by direct sequencing. Until recently, this was considered to be the most sensitive method, with a sensitivity of 1% compared with the other three methods (27). In this study, the concordance rates of Scorpion-ARMS with pyrosequencing and Luminex xMAP were κ=0.974 and κ=0.845, respectively. Since we classified the κ values according to the Landis and Koch methods (13), as previously mentioned, the comparison of κ values has no statistical significance if the values were over 0.80 in our analysis. Pairwise analysis results were almost perfect among the three sensitive methods, inferring that these methods are equally useful and reliable.

The median concentrations of extracted DNA with and without manual microdissection were 119.5 and 130.1 ng/μl, respectively. All analytical methods accurately detected DNA samples prepared at a concentration of 100 ng/μl or more. It is considered that while detectability depends on DNA concentrations of 100 ng/μl or more, it is reliant on the quality of DNA when the concentration is less than 100 ng/μl. Research has demonstrated that DNA quality is influenced by the concentration of formic acid used to fix tissues and the fixation time (28,29). In this study, among the five cases in which *KRAS* status could not detected by direct sequencing, there was one case (case 3) that could not be determined by all three sensitive methods (Table IV). This was due to the low concentration of extracted DNA. It was therefore notable that one case with 2.1 ng/μl DNA obtained without manual microdissection was diagnosed as wild-type *KRAS* only by Luminex xMAP and not by the other two sensitive methods. We do not have any explanation for this observed result. It may be that the fixation time was longer in the undetectable cases, or that the DNA sample contained excess fragmentation. However, we were unable to investigate these aspects due to the retrospective nature of this study.

There were three cases in which the status of *KRAS* was differentially diagnosed by the examined methods (Table V). One case (case 3) was judged to be *KRAS*-mutant (G12C) by the three sensitive methods, although the *KRAS* status was diagnosed as wild type by direct sequencing; this discordance is likely due to the levels of sensitivity. Two cases were judged to have *KRAS* mutations (G12D for case 1 and G12S for case 2) by Luminex xMAP, although Scorpion-ARMS and pyrosequencing diagnosed these cases to be wild type. These two cases clinically responded to cetuximab-alone therapy. Although patients with G13D mutations are reported to benefit more from cetuximab than patients with tumors harboring *KRAS* codon 12 mutations (30), these cases had mutations of G12D or G12S. If clinicians took account of the results of Luminex xMAP and did not use cetuximab, positive outcomes were not achieved. We assumed the *KRAS* status of these two cases to be wild type. These conflicting results might be explained by non-specific reactions of the primer probe used in Luminex xMAP.

Certain limitations exist in our study. One is the retrospective nature of the study, including the small number of patients treated by cetuximab alone or the combination therapy with irinotecan. Second, more sensitive and specific methods than those used in our study, including the BEAMing method (31) and WAVEbased Surveyor Scan kits (32), are available to detect *KRAS* mutation status. However, it was

technically difficult to apply these in this study. Third, our data were limited to *KRAS* mutations in exon 2, while we are now at the point where there is technology available to detect all *RAS* mutations beyond *KRAS* mutations. At the same time, considering those false results on exon 2 mutations, it is necessary to bear in mind that similar false-positive or false-negative test results may also be obtained for other mutation sites.

In conclusion, all three sensitive methods (Scorpion-ARMS, pyrosequencing and Luminex xMAP) were equally useful and reliable in detecting *KRAS* mutation status, with high success and concordance rates between each method. However, there were rare incidences in which the *KRAS* status was differentially diagnosed by the three methods, even though the same DNA samples were used. Further large prospective studies are necessary to clarify the clinical factors responsible for the discordant *KRAS* results between the different methods.

Acknowledgements

The authors thank Professor Michio Shimizu for his assistance at the Department of Diagnostic Pathology, Saitama Medical University International Medical Center, and also thank Ms. Kaori Kawara for her assistance at the Department of Medical Oncology, Saitama Medical University International Medical Center.

References

1. Bokemeyer C, Bondarenko I, Makhson A, Hartmann JT, Aparicio J, de Braud F, Donea S, Ludwig H, Schuch G, Stroh C, *et al*: Fluorouracil, leucovorin, and oxaliplatin with and without cetuximab in the first-line treatment of metastatic colorectal cancer. J Clin Oncol 27: 663-671, 2009.
2. Ciardiello F, Tejpar S and Papamichael D: Implications of KRAS mutation status for the treatment of metastatic colorectal cancer. Target Oncol 4: 311-322, 2009.
3. De Roock W, Piessevaux H, De Schutter J, Janssens M, De Hertogh G, Personeni N, Biesmans B, Van Laethem JL, Peeters M, Humblet Y, *et al*: KRAS wild-type state predicts survival and is associated to early radiological response in metastatic colorectal cancer treated with cetuximab. Ann Oncol 19: 508-515, 2008.
4. Harbison CT, Horak CE, Ledeine JM, Mukhopadhyay P, Malone DP, O'Callaghan C, Jonker DJ, Karapetis CS, Khambata-Ford S, Gustafson N, *et al*: Validation of companion diagnostic for detection of mutations in codons 12 and 13 of the KRAS gene in patients with metastatic colorectal cancer: analysis of the NCIC CTG CO.17 trial. Arch Pathol Lab Med 137: 820-827, 2013.
5. Van Cutsem E, Köhne CH, Hitre E, Zaluski J, Chang Chien CR, Makhson A, D'Haens G, Pintér T, Lim R, Bodoky G, *et al*: Cetuximab and chemotherapy as initial treatment for metastatic colorectal cancer. N Engl J Med 360: 1408-1417, 2009.
6. Jonker DJ, O'Callaghan CJ, Karapetis CS, Zalcberg JR, Tu D, Au HJ, Berry SR, Krahn M, Price T, Simes RJ, *et al*: Cetuximab for the treatment of colorectal cancer. N Engl J Med 357: 2040-2048, 2007.
7. Khan IH, Krishnan VV, Ziman M, Janatpour K, Wun T, Luciw PA and Tuscano J: A comparison of multiplex suspension array large-panel kits for profiling cytokines and chemokines in rheumatoid arthritis patients. Cytometry B Clin Cytom 76: 159-168, 2009.
8. Kimura H, Fujiwara Y, Sone T, Kunitoh H, Tamura T, Kasahara K and Nishio K: High sensitivity detection of epidermal growth factor receptor mutations in the pleural effusion of non-small cell lung cancer patients. Cancer Sci 97: 642-648, 2006.
9. Ahle JD, Barr S, Chin AM and Battersby TR: Sequence determination of nucleic acids containing 5-methylisocytosine and isoguanine: identification and insight into polymerase replication of the non-natural nucleobases. Nucleic Acids Res 33: 3176-3184, 2005.
10. Whitehall V, Tran K, Umapathy A, Grieu F, Hewitt C, Evans TJ, Ismail T, Li WQ, Collins P, Ravetto P, *et al*: A multicenter blinded study to evaluate KRAS mutation testing methodologies in the clinical setting. J Mol Diagn 11: 543-552, 2009.
11. Conde E, Angulo B, Tang M, Morente M, Torres-Lanzas J, Lopez-Encuentra A, Lopez-Rios F and Sanchez-Cespedes M: Molecular context of the EGFR mutations: evidence for the activation of mTOR/S6K signaling. Clin Cancer Res 12: 710-717, 2006.
12. Fernandez P, Carretero J, Medina PP, Jimenez AI, Rodriguez-Perales S, Paz MF, Cigudosa JC, Esteller M, Lombardia L, Morente M, *et al*: Distinctive gene expression of human lung adenocarcinomas carrying LKB1 mutations. Oncogene 23: 5084-5091, 2004.
13. Landis JR and Koch GG: The measurement of observer agreement for categorical data. Biometrics 33: 159-174, 1977.
14. Karapetis CS, Khambata-Ford S, Jonker DJ, O'Callaghan CJ, Tu D, Tebbutt NC, Simes RJ, Chalchal H, Shapiro JD, Robitaille S, *et al*: K-ras mutations and benefit from cetuximab in advanced colorectal cancer. N Engl J Med 359: 1757-1765, 2008.
15. Amado RG, Wolf M, Peeters M, Van Cutsem E, Siena S, Freeman DJ, Juan T, Sikorski R, Suggs S, Radinsky R, *et al*: Wild-type KRAS is required for panitumumab efficacy in patients with metastatic colorectal cancer. J Clin Oncol 26: 1626-1634, 2008.
16. Sorich MJ, Wiese MD, Rowland A, Kichenadasse G, McKinnon RA and Karapetis CS: Extended RAS mutations and anti-EGFR monoclonal antibody survival benefit in metastatic colorectal cancer: a meta-analysis of randomized, controlled trials. Ann Oncol 26: 13-21, 2015.
17. Angulo B, García-García E, Martínez R, Suárez-Gauthier A, Conde E, Hidalgo M and López-Ríos F: A commercial real-time PCR kit provides greater sensitivity than direct sequencing to detect KRAS mutations: a morphology-based approach in colorectal carcinoma. J Mol Diagn 12: 292-299, 2010.
18. Franklin WA, Haney J, Sugita M, Bemis L, Jimeno A and Messersmith WA: KRAS mutation: comparison of testing methods and tissue sampling techniques in colon cancer. J Mol Diagn 12: 43-50, 2010.
19. Tol J, Dijkstra JR, Vink-Börger ME, Nagtegaal ID, Punt CJ, Van Krieken JH and Ligtenberg MJ: High sensitivity of both sequencing and real-time PCR analysis of KRAS mutations in colorectal cancer tissue. J Cell Mol Med 14: 2122-2131, 2010.
20. Douillard JY, Siena S, Cassidy J, Tabernero J, Burkes R, Barugel M, Humblet Y, Bodoky G, Cunningham D, Jassem J, *et al*: Randomized, phase III trial of panitumumab with infusional fluorouracil, leucovorin, and oxaliplatin (FOLFOX4) versus FOLFOX4 alone as first-line treatment in patients with previously untreated metastatic colorectal cancer: the PRIME study. J Clin Oncol 28: 4697-4705, 2010.
21. Peeters M, Price TJ, Cervantes A, Sobrero AF, Ducreux M, Hotko Y, André T, Chan E, Lordick F, Punt CJ, *et al*: Randomized phase III study of panitumumab with fluorouracil, leucovorin, and irinotecan (FOLFIRI) compared with FOLFIRI alone as second-line treatment in patients with metastatic colorectal cancer. J Clin Oncol 28: 4706-4713, 2010.
22. Van Cutsem E, Köhne CH, Láng I, Folprecht G, Nowacki MP, Cascinu S, Shchepotin I, Maurel J, Cunningham D, Tejpar S, *et al*: Cetuximab plus irinotecan, fluorouracil, and leucovorin as first-line treatment for metastatic colorectal cancer: updated analysis of overall survival according to tumor KRAS and BRAF mutation status. J Clin Oncol 29: 2011-2019, 2011.
23. Asaka S, Arai Y, Nishimura Y, Yamaguchi K, Ishikubo T, Yatsuoka T, Tanaka Y and Akagi K: Microsatellite instability-low colorectal cancer acquires a KRAS mutation during the progression from Dukes' A to Dukes' B. Carcinogenesis 30: 494-499, 2009.
24. Russo A, Rizzo S, Bronte G, Silvestris N, Colucci G, Gebbia N, Bazan V and Fulfaro F: The long and winding road to useful predictive factors for anti-EGFR therapy in metastatic colorectal carcinoma: the KRAS/BRAF pathway. Oncology 77 (Suppl 1): S57-S68, 2009.
25. Li S, Schmitz KR, Jeffrey PD, Wiltzius JJ, Kussie P and Ferguson KM: Structural basis for inhibition of the epidermal growth factor receptor by cetuximab. Cancer Cell 7: 301-311, 2005.
26. Gonzalez de Castro D, Angulo B, Gomez B, Mair D, Martinez R, Suarez-Gauthier A, Shieh F, Velez M, Brophy VH, Lawrence HJ and Lopez-Rios F: A comparison of three methods for detecting KRAS mutations in formalin-fixed colorectal cancer specimens. Br J Cancer 107: 345-351, 2012.

27. Jimeno A, Messersmith WA, Hirsch FR, Franklin WA and Eckhardt SG: KRAS mutations and sensitivity to epidermal growth factor receptor inhibitors in colorectal cancer: practical application of patient selection. J Clin Oncol 27: 1130-1136, 2009.
28. Srinivasan M, Sedmak D and Jewell S: Effect of fixatives and tissue processing on the content and integrity of nucleic acids. Am J Pathol 161: 1961-1971, 2002.
29. Yokota T, Shibata N, Ura T, Takahari D, Shitara K, Muro K and Yatabe Y: Cycleave polymerase chain reaction method is practically applicable for V-Ki-ras2 Kirsten rat sarcoma viral oncogene homolog (KRAS)/V-raf murine sarcoma viral oncogene homolog B1 (BRAF) genotyping in colorectal cancer. Transl Res 156: 98-105, 2010.
30. De Roock W, Jonker DJ, Di Nicolantonio F, Sartore-Bianchi A, Tu D, Siena S, Lamba S, Arena S, Frattini M, Piessevaux H, *et al*: Association of KRAS p.G13D mutation with outcome in patients with chemotherapy-refractory metastatic colorectal cancer treated with cetuximab. JAMA 304: 1812-1820, 2010.
31. Bokemeyer C, Kohne C-H, Ciardiello F, *et al*: Treatment outcome according to tumor RAS mutation status in OPUS study patients with metastatic colorectal cancer (mCRC) randomized to FOLFOX4 with/without cetuximab. ASCO Meeting Abstracts 32: 3505, 2014.
32. Douillard JY, Oliner KS, Siena S, Tabernero J, Burkes R, Barugel M, Humblet Y, Bodoky G, Cunningham D, Jassem J, *et al*: Panitumumab-FOLFOX4 treatment and RAS mutations in colorectal cancer. N Engl J Med 369: 1023-1034, 2013.